Coal evaluation and reactivity for direct solid based pre-reduction of sponge iron

S van Wyk

22127054

Dissertation submitted in fulfilment of the requirements for the degree *Magister* in Chemical Engineering at the Potchefstroom Campus of the North-West University

Supervisor:	Prof HWJP Neomagus
Co-supervisor	Prof JR Bunt
Assistant-supervisor	Prof R Everson

May 2016

Declaration

I, Surika van Wyk, hereby declare that the dissertation entitled: "*Coal evaluation and reactivity for direct solid based pre-reduction of sponge iron*", submitted in fulfilment of the requirements for a Master's degree in Chemical Engineering (M. Eng), is my own work, except where acknowledged in the text and that this dissertation has not been submitted to any other tertiary institution either in or part or as a whole.

Signed at Potchefstroom, on the_____ day of _____, 2015.

_____

Surika van Wyk

Acknowledgements

I would like to acknowledge and thank the following institutions and persons that contributed to the completion of this research project.

- Firstly I would like to thank Our Heavenly Father for giving me guidance and strength to complete this project to the best of my abilities.
- Professor Hein Neomagus for his valuable advice, guidance, support and motivation during the project.
- Professors John Bunt and Ray Everson for their advice and support.
- EVRAZ Highveld Steel and Vanadium for their financial support and supplying the coal. Also Ms Jacoline Botha and Mr Wesley Teessen for their advice and support.
- Mr Jan Kroeze, Mr Adrian Brock and Mr Ted Paarlberg and everyone from the workshop for technical support.
- Dr Henry Matjie for his assistance with XRD analysis and interpretation.
- Mr Shawn Liebenberg from the Statistical Consultation Service for his assistance with the statistical analysis and interpretation.
- The coal research group at the North-West University for valuable advice and assistance with administrative tasks.
- The financial assistance of the National Research Foundation (NRF Grant UID: 94409) towards this research is hereby acknowledged. Opinions expressed and conclusions arrived at, are those of the author and are not necessarily to be attributed to the NRF.
- My friends for their advice, support and motivation.
- My family, especially my mother, for their love and support.
- The work presented in this paper is based on the research supported by the South African Research Chairs Initiative of the Department of Science and Technology and National Research Foundation of South Africa (Coal Research Chair Grant No. 86880). Any opinion, finding or conclusion or recommendation expressed in this material is that of the author(s) and the NRF does not accept any liability in this regard.

Abstract

Solid based direct reduction of iron ore requires the reductant coal to have a suitable CO_2 reactivity in order to achieve optimum pre-reduction within a rotary kiln. CO_2 reactivity is affected by numerous factors including coal properties and operating conditions. Relating CO_2 reactivity to coal/char properties will assist in proposing suitable coals/blends. The CO_2 gasification reactivity and coal/char characteristics of nine different coals originating from the Highveld, Witbank and Ermelo coalfields were determined and compared to a benchmark coal previously utilised for pre-reduction. The experiments were divided into two phases. The first was a screening process whereby the reactivity of all nine samples (20 mm particles) was measured and compared at both 950 and 1050 °C utilising a large particle thermo gravimetric analyser. From the results, two coals along with the benchmark coal were selected for further kinetic studies. For these coals, 6 mm and 212 µm char particles were gasified at 900, 950, 1000 and 1050 °C. The influence of particle size was investigated, and the activation energy was determined for the different samples and kinetic modelling of the conversion experiments was executed.

Statistical analysis of the phase one results showed that the coal volatile and vitrinite content had the most significant influence on reactivity at 1050 °C, while the fixed carbon and inertinite content had the greatest influence at 950 °C. For the char analysis it was observed that chemical and physical properties had the greatest influence on reactivity at both 950 and 1050 °C. Multiple linear regression was used to derive empirical equations that correlate the initial specific reaction rates at both 950 and 1050 °C as a function of coal/char properties. The equations derived for 1050 °C were able to more accurately predict the reactivity. The results of phase two indicated that increased particle sizes decreased CO_2 reactivity and that the rate of internal mass transfer was not negligible at the given experimental conditions. The apparent activation energies appeared to decrease with particles size and were estimated as 211 – 224 kJ/mol for 6 mm and 174 – 227 kJ/mol for 212 µm particles, which compared well with previous studies. Lastly, the Wen model showed accurate predictions of the rate of gasification.

The conclusion was made that CO_2 gasification reactivity is dependent on both internal (coal/char properties) and external (temperature and particles size) properties. Chemical and petrographic coal properties had the greatest influence, while for the char properties the chemical and structural properties had the greatest impact. From the results and conclusions it was recommended that the two coals (AC-5-72 & FC-2-21) selected for phase two are blended in order to achieve desired pre-reduction within the rotary kilns.

Keywords: Iron pre-reduction; CO_2 gasification; large particle TGA; Statistical analysis; empirical equations

Opsomming

Die pre-reduksie van ystererts, wat steenkool as ‘n reduksie medium gebruik, vereis dat steenkool ‘n geskikte CO_2 reaktiwiteit het om optimum pre-reduksie waardes binne-in ‘n roterende oond te verseker. Die reaktiwiteit van CO_2 vergassing word beïnvloed deur verskeie faktore insluitend steenkool eienskappe en omgewings toestande binne-in die roterende oond. ‘n Evaluasie van die invloed wat steenkool en sintel eienskappe op CO_2 vergassings reaktiwiteit het, sal daartoe bydra om steenkole met geskikte eienskappe en CO_2 reaktiwiteit te selekteer vir toekomstige gebruik.

Die CO_2 vergassings reaktiwiteit van nege verskillende steenkole, afkomstig vanaf die Hoëveld, Witbank and Ermelo steenkoolvelde, is bepaal en vergelyk met die maatstaf steenkool. Die maatstaf steenkool is voorheen gebruik vir die pre-reduksie van ystererts. Die eksperimente is in twee fases verdeel, naamlik fase een en fase twee. Vir fase een word die reaktiwiteit van al nege steenkole (20 mm) bepaal by beide 950 and 1050 °C en dan met mekaar vergelyk. Alle reaktiwiteits eksperimente is in ‘n termo gravimetriese analiseerder uitgevoer. Na aanleiding van die resultate van fase een, is twee steenkole vir fase twee geselekteer vir verdere kinetiese studie. Die reaktiwiteit van die twee steenkole en die maatstaf steenkool is bepaal by 900, 950, 1000 en 1050 °C onderskeidelik. Die partikel grootte vir fase twee was 212 µm en 6 mm. Die invloed van partikel grootte op die vergassings reaktiwiteit was geondersoek. Die aktiverings energieë was bepaal en kinetiese modelering was toegepas.

Die resultate van die statistiese analise vir fase een het getoon dat die steenkool se vlugtige stowwe en vitriniet inhoud die grootste impak gehad het op die reaktiwiteit by 1050 °C. Vir die reaktiwiteit by 950 °C, het die inertiniet en koolstof inhoud van die steenkool die grootste invloed gehad. Die resultate vir die sintel eienksappe het getoon dat die chemiese en strukturele eienskappe die grootste invloed gehad het vir ’n reaktiwiteit by beide 950 en 1050 °C. Empiriese vergelykings is afgelei deur van meervoudige lineêre regressie gebruik te maak. Vanaf die vergelykings kon die aanvanklike reaktiwiteits tempo as ‘n funksie van steenkool/sintel eienskappe bepaal word, vir beide 950 en 1050 °C. Die vergelykings vir 1050 °C, was meer akkuraat invergelyking met die wat vir die 950 °C afgelei is.

Die resultate van die tweede fase het getoon dat die reaktiwiteit afgeneem het met ‘n toename in partikel grootte. Dit is as gevolg van interne diffussie wat die reaktiwiteits tempo verhinder. Die berekende skynbare aktiverings energieë was 211 – 224 kJ/mol vir die 6 mm partikels en 174 – 227 kJ/mol vir 212 µm partikels. Die berekende waardes stem ooreen met die waardes

wat in literatuur aangeteken word. Die Wen model was die meeste geskik om die vergassings reaktiwiteit van die verskillende sintels te beskryf.

Die gevolgtrekkings wat gemaak is, is dat die CO_2 vergassings reaktiwiteit afhanklik is van beide steenkool en sintel eienskappe, asook omgewings toestande (temperatuur en partikel grootte). Vir steenkool eienskappe het die chemiese en petrografiese eienskappe die grootste invloed op reaktiwiteit gehad. Vir die sintel eienskappe het die chemiese en strukturele eienskappe die grootste invloed gehad. Na volledige analise van die bevindinge en gevolgtrekkings is die voorstel gemaak dat beide die steenkole (AC-5-72 & FC-2-21) wat vir fase twee geselekteer was, gemeng moet word sodat die optimum pre-reduksie waardes in die oond verseker kan word.

Sleutelwoorde: Ystererts pre-reduksie; CO_2 vergassing; groot partikel TGA; statistiese analise; empiriese vergelykings.

Table of contents

List of abbreviations and acronyms

Abbreviation or acronym	Description
AC	Alternative coal
ACCAR	Allis-Chalmers Controlled Atmospheric Reduction
ACE	Associated Chemical Enterprises
a.d.b	Air dried basis
AFP	Acos Finos Piratini
AFT	Ash fusion temperature
Afrox	African oxygen
ANOVA	Analysis of variance
ASAP	Accelerated surface area and porosimetry
Aspen	Advanced System for Process Engineering
ASTM	American Society of Testing and Materials
BET	Brunauer-Emmert-Teller
BC	Benchmark coal
BSIL	Buhar Sponge Iron Limited
CI	Confidence interval
CODIR	Coal Ore Direct Iron reduction
CSA	Carbon micropore surface area
csv.	comma separated values
d.a.f	Dry ash free
d.b	Dry basis
d.m.m.f.b	Dry, mineral-matter-free basis
D-R	Dubin-Radushkevich
DRC	Direct Reduction Corporation
DRI	Direct reduced iron
df	Degrees of freedom
EHSV	EVRAZ Highveld Steel and Vanadium
FC	Feed coal
FT	Fluid temperature
H-K	Horvath-Kawazoe
HT	Hemispherical temperature
ICM	Integrated core model

ISCOR	Iron and Steel Corporation
ISO	International Standards Organization
IT	Initial deformation temperature
LC	Lower seam C
LH	Langmuir Hinselworth
LOI	Loss of ignition
LRS	Laser raman spectroscope
LSA	Langmuir surface area
MATLAB	Matrix Laboratory
MFC	Mass flow controllers
m.m.f.b	Mineral-matter-free basis
MVM	Modified volumetric model
NDF	Normal distribution function
NWU	North-West University
NZS	New Zealand Steel
Ox.	Oxidising
PDTF	Pressurised drop tube furnace
PEFR	Pressurised entrained-flow reactor
PRN	Pore resistance number
Red.	Reducing
RPM	Random pore model
SCM	Shrinking core model
SE	Standard error
SL/RN	Stelco-Lurgi/ Republic Steel-National
SPSS	Statistical Package for the Social Sciences
ST	Softening temperature
SUCM	Shrinking unreacted core model
TGA	Thermo gravimetric analyser
V/I	Vitrinite/Inertinite
VIF	Variance inflation factor
VM	Volumetric model
vol.%	Volume percentage
wt. %	Weight percentage
XRD	X-ray diffraction
XRF	X-ray fluorescence

List of figures

List of tables

List of symbols

Symbol	Description	Unit
A	Pre-exponential factor	1/h/Pa
A_c	Cross sectional area	m^2
a_c	External surface area of catalyst per volume of catalytic bed	m^2/m^3
Bi	Biot number	-
C	Sutherland's constant	-
C_A	Concentration of reagent A	mol/m^3
C_1	One-term approximate coefficient	-
CI	Confidence interval	
$c_{p,coal}$	Specific heat of coal particle	J/kg·K
$c_{p,gas}$	Specific heat of reagent gas mixture	J/kg·K
D_{AB}	Molecular diffusion coefficient	m^2/s
D_{eff}	Effective diffusion coefficient	m^2/s
D_{kn}	Knudsen diffusion coefficient	m^2/s
d_{coal}	Coal particle diameter	m or mm
d_i	Difference between ranks for Spearman's correlation coefficient	-
d_{pore}	Pore diameter	Å
E_a	Activation energy	kJ/mol
$Err.$	Experimental error	%
Fo	Fourier number	-
ΔH_0	Enthalpy	MJ/kmol or kJ/mol
ΔH_r	Heat of reaction	kJ/mol
HV	Heating value (a.d.b.)	MJ/kg
HVF	Heating value factor	-
h	Convection coefficient	$W/m^2 \cdot K$
h_m	Mass transfer coefficients	m/s
I	Inertinite (m.m.f.b)	vol.%
Inr	Non-reactive inertinite content (m.m.f.b)	vol.%
j_h	Colburn j-factor for heat transfer	-
j_m	Colburn j-factor for mass transfer	-

k	Reaction rate constant of Wen model	g/g/h
k_{coal}	Thermal conductivity of coal	W/m·K
k_{gas}	Thermal conductivity of reagent gas mixture	W/m·K
k_1, k_{-1}, k_2, k_{-2}	Rate constants	1/h
L	Liptinite content (m.m.f.b)	vol. %
M	Molecular weight	g/mol
M_w	Weisz-Prater criterion	-
MI	Maceral index	-
m	Mass or Wen solid reaction order	g or (-)
N	Number of runs	-
Nu_D	Nusselt number	-
n	Reaction order	-
P	Total pressure	kPa or atm
$P_{CO_2,s}$	Partial pressure at particle surface	kPa or atm
$P_{CO_2,\infty}$	Partial pressure in ambient atmosphere	kPa or atm
Pr	Prandtl number	-
q_{CO_2}	Flux of CO_2 depletion	g/cm^2/h
R	Gas constant (8.314)	J/mol K
R^2	Coefficient of determination	-
Re	Reynolds number	-
RF	Reactivity factor	-
RMI	Reactive maceral index	-
RoV	Vitrinite reflectance	-
$R_{s,0}$	Initial specific reaction rate	g/g/h
R_s	Specific reaction rate	g/g/h
r_A'''	Measured reaction rate	m^3/mol/s
r_{coal}	Coal particle radius	m or mm
r_s	Spearman's correlation coefficient	-
Sc	Schmidt number	-
SE	Standard error	varies
Sh	Sherwood number	-
St	Stanton number	-
St_m	Stanton number for mass transfer	-
T	Temperature	°C or K

T_i	Initial temperature	°C or K
T_∞	Infinite temperature	°C or K
t	Time/t-distribution	seconds or minutes or hours or (-)
V	Volume/ vitrinite content (m.m.f.b)	m^3 or cm^3 or vol. %
$\dot{v}$	velocity	m/s
x	Fractional conversion	-
$\bar{x}$	Average	varies

Greek symbols

α	Thermal diffusivity	m^2/s
ε	Porosity	-
ε_v	Void fraction/ bed porosity	-
η_{ex}	External mass transfer effectiveness factor	-
θ^*	Midplane temperature	-
μ	Dynamic viscosity/ mean values	$N{\cdot}s/m^2$ or varies
μ_s	Dynamic viscosity at surface	$N{\cdot}s/m^2$
ν	Kinematic viscosity	m^2/s
ξ_1	One-term approximate coefficient	rad
π	Pi	-
ρ	significance values	-
ρ_b	Bulk density	kg/m^3 or g/cm^3
ρ_{coal}	Density of coal	kg/m^3 or g/cm^3
ρ_{gas}	Density of gas	kg/m^3 or g/cm^3
σ	Standard deviation	varies
σ_{AB}	Collision diameter	m
$\emptyset$	Scaling factor	-
τ	tortuosity	-
Ω_D	Collision integral	-

CHAPTER 1: Introduction

1.1 Overview

A detailed background and motivation is provided in Section 1.2. Next the problem statement (Section 1.3), aim and objectives (Section 1.4) and project scope (Section 1.5) are given in this chapter. The chapter concludes with an outline in Section 1.6.

1.2 Background and Motivation

Iron is utilised mainly for the production of steel, which plays a vital role in the automotive and construction industry, as well as production of certain electronic components. In 2015 the global steel usage was ± 1 544 Mt and is expected to increase with 1.4% in 2016 (Worldsteel association, 2015). The blast furnace process has been the conventional method of iron production for many years (Feinman, 1999). In the blast furnace operation, coke, iron ore and fluxes are fed to the top of a refractory lined shaft furnace. Hot air (1000 to 1300 °C) is blown from the bottom and heats the materials. The iron and slag continue to move downward into the hearth of the furnace from where it is tapped and further processed (Bugayev *et al.,* 2001). The operating temperature in the furnace is generally greater than 1427 °C for the iron and slag to be tapped from the furnace in the molten state (Peacy & Davenport, 1979). During this process, the blast furnace utilises coke as fuel to reduce iron oxide to iron, due to it being the only solid fuel that can withstand the conditions inside the furnace without pulverising (Bugayev *et al.,* 2001). Due to the limited availability of coking coals, alternative methods of reducing iron ore have been developed such as the direct reduction process.

The direct reduction of iron ore, which utilises an electric arc furnace instead of a blast furnace, has become the favoured method for iron production due to the lower capital and operational costs. During this process iron ore is directly reduced, without melting the ore (Mashhadi *et al.,* 2008). Depending on the type of reductant used, the production of direct reduced iron (DRI) can be divided into two types of processes namely, gas-based DRI and coal-based (solid-based) DRI (Prasad & Ray, 2009; Ünal *et al.,* 2012). Gas-based direct reduction utilises natural gas as a reducing agent. The natural gas is fed to a shaft furnace or stationary-bed reactor, depending on the type of gas-based process utilised (Atsushi *et al.,* 2010; Sibakin, 1980). The iron ore is reduced and sent to the electric arc furnace for further processing. Gas-based direct reduction processes are preferred due to a better and more consistent quality of DRI and lower energy consumption. Gas-based direct reduction is, however, more expensive in comparison to coal-based DRI and also limits plant locations due to the availability of natural gas resources (Feinman, 1999; Michishita & Tanaka, 2010; Prasad & Ray, 2009).

Coal-based direct reduction processes were developed as a result of the high cost of natural gas, as well as the considerable amount of non-coking coal wasted when mining coking coals for blast furnace operations (Mashhadi *et al.,* 2008). Coal-based DRI plants are more flexible since coal deposits are widely distributed and also easily transported (Michishita & Tanaka, 2010). The direct reduction is generally carried out in a rotary kiln; a reactor that has some advantages compared to shaft furnaces utilised for the blast furnace process. The reactor serves as both a coal gasifier and ore reducer, which eliminates the need for external production of reduction gases from coal, which is expensive. Furthermore certain iron ores such as titaniferous magnetite ore can only be reduced in rotary kilns due to the reduction conditions experienced within a blast furnace. The high reduction temperatures cause titanium oxide to form titanium carbide which cokes up the hearth of the furnace (Manamela & Pistorius, 2005; Sutherland, 2000). The rotary kiln, when compared to the blast furnace, is also less energy intensive due to the lower operation temperatures. The disadvantage of the coal-based direct reduction process is the variation in iron quality, lower productivity in comparison to gas-based shaft furnace operations and difficult process control (Prasad & Ray, 2009). In 2013, 21% of the world DRI was produced through coal-based direct reduction. In Figure 1.1 the growth production of coal-based DRI from 1994 to 2013 is shown.

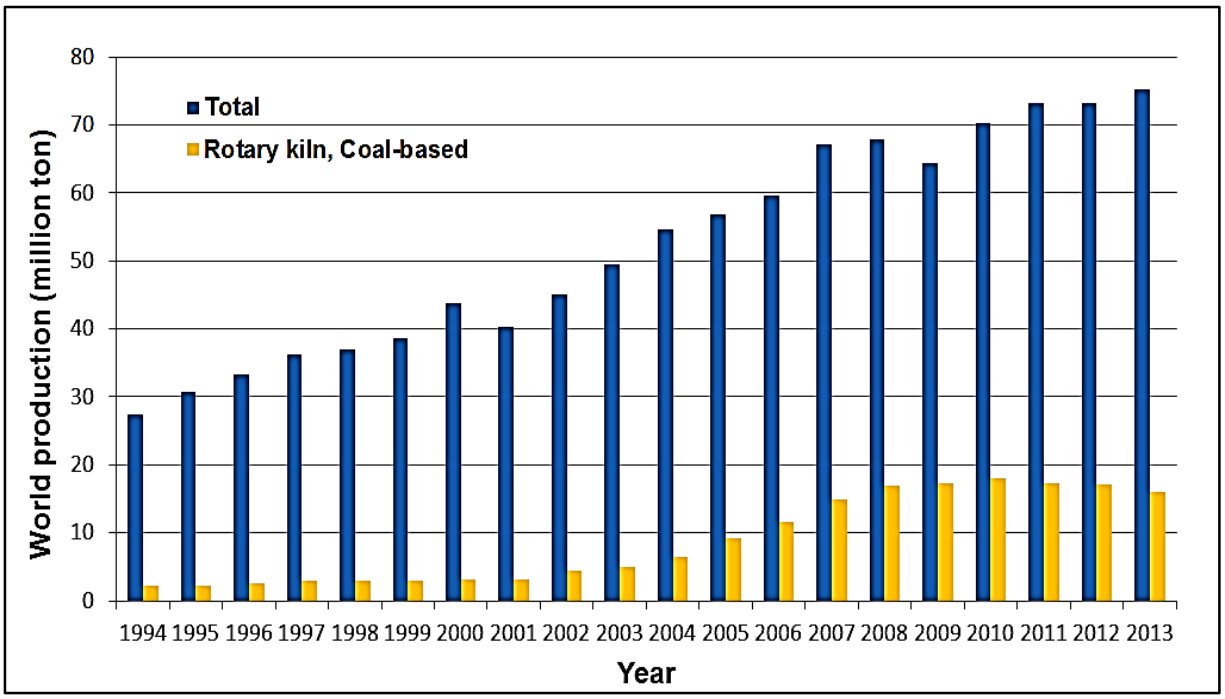

Figure 1.1: World production of DRI from 1994 to 2013 (adapted from MIDREX, 2013)

During pre-reduction, coal firstly devolatilises to produce various gases including carbon monoxide and hydrogen, while the remaining char reacts with carbon dioxide to produce more carbon monoxide. The gases produced during devolatilisation assist to a certain extent with the initial pre-reduction of the ore. The reaction between the coal/char and carbon dioxide to

form carbon monoxide is, however, the crucial reaction for pre-reduction and is given in Equation 1.1 (Higman & Van der Burgt, 2008; Mashhadi *et al.,* 2008):

$$CO_{2(g)} + C_{(s)} \rightarrow 2CO_{(g)} \qquad \Delta H_0 = 172\ MJ/kmol \tag{1.1}$$

This heterogeneous endothermic reaction is known as the Boudouard reaction and is the rate controlling reaction for reduction in the rotary kiln. The CO_2 reactivity, therefore, plays an important role in the process (Cunningham & Stephenson, 1980; Sutherland, 2000). The reactivity also influences the operations of the downstream processes such as the electric arc furnace. A high CO_2 reactivity is normally desired, since a higher pre-reduction will be obtained, reducing the costs of the more energy intensive electric arc furnace. The operation reactivity should, however, not be too high as this could lead to insufficient carbon carry over, alteration of the feed ratio to the kiln and increased consumption of coal, which is also economically disadvantageous (Cunningham & Stephenson, 1980; Sutherland, 2000).

In addition to a suitable CO_2 reactivity, it is preferred that the coal also has other properties such as a low ash yield, low swelling and caking index, low volatile content and a moderate fixed carbon content (Chatterjee, 2010; Sarangi & Sarangi, 2011). These properties are both directly related to the CO_2 reactivity and to the operations of the rotary kiln itself (*e.g.* high ash values promotes the formation of accretions on the kiln wall). It is thus recommended that coals selected for pre-reduction are screened in terms of their coal characteristics and CO_2 reactivity at the rotary kiln operating conditions. Selecting coals suitable for this process can be challenging due to the depletion of South African coal reserves (Hartnady, 2010). When selecting a coal source, factors such as life of the mine and the proximity to the metallurgic plant should also be considered. It is important that the selected coal can be utilised for many years and that the costs of transporting the coal to the plant are kept low.

1.3 Problem statement

EVRAZ Highveld Steel & Vanadium (EHSV) utilises pre-reduction rotary kilns to reduce titaniferous magnetite ore. Pilot plant tests and research have shown that BC-5-53 (see Section 3.2 for explanation of coding) was the best suited coal for the pre-reduction process, achieving optimum pre-reduction values (Hall, 1980; Sutherland, 2000). This coal was utilised for many years; however, owing to the depletion of the mine reserves in 1996 alternative coals had to be identified and utilised (Sutherland, 2000). W. Teessen (personal communication, January 9, 2014a) stated that the use of alternative coals generally decreased the pre-reduction values achieved in the kiln.

Relating CO_2 reactivity to coal/char properties will assist in proposing suitable coals/blends for pre-reduction of titaniferous magnetite ore, with reference to the benchmark coal. This can

serve as an additional guideline for selecting coals/blends for future usage. In addition the influence of particle size on CO_2 reactivity is also investigated, by performing standard CO_2 reactivity tests with pulverised chars and relating it to the results of the coarse particles. This will provide a better understanding of the influence of large particles on CO_2 reactivity as this subject is relatively unexplored. The intrinsic kinetic parameters will also be determined from the pulverised char gasification.

1.4 Aim and objectives

The primary aim of this study is the following:

- To identify and evaluate suitable substitute coals or blends, with a desired CO_2 reactivity for rotary kiln operations, with reference to BC-5-53's (benchmark coal) characteristics and CO_2 reactivity.

The following objectives are formulated:

- Identification of six coals that could be well suited for the pre-reduction process, based on coal characteristics, availability and distance from EHSV.

- Determination of coal and char characteristics for the selected coals, BC-5-53 and the two coals that are currently implemented for pre-reduction at EHSV. The characterisation will include the chemical, mineral, physical, petrographic and thermal analysis and will be compared to preferred pre-reduction values from literature.

- Determination of the various coals CO_2 reactivity with respect to different operating temperatures and particle sizes utilising a laboratory scale, large particle thermo gravimetric analyser (TGA).

- Statistically relating the different coal and char properties to the CO_2 reactivity and deriving empirical equations from which the CO_2 reactivity can be determined as a function of coal/char properties.

- Describing reaction kinetics through the use of reaction rate modelling.

- Evaluate and compare the different characteristics and reactivity of the coals in order to determine the coal/blend best suited for the process.

1.5 Project scope

The project scope was developed to guide the research process and to ensure that the objectives are met. Firstly six coals from different coalfields will be identified and characterised, along with the benchmark coal and the two coals currently used at EHSV. Nine different coals will therefore be evaluated for this study. The CO_2 reactivity of the coals will be measured utilising an in-house constructed large particle TGA. The reactivity experiments will be divided into two phases. The first phase is a screening process, where the reactivity of all nine coals will be determined and compared in order to select two coals for phase two. The influence of different coal/char characteristics on CO_2 reactivity will also be statistically investigated in this phase and empirical equations will be derived to determine the initial specific reaction rate from coal/char characteristics. During the experiments two different temperatures will be investigated, while the pressure and particle size remain constant.

The second phase is a kinetic study, where the influence of particle size and temperature is investigated. The reactivity of the two coals, selected from the phase one results, and the benchmark will be determined. The selection of the coals will be based on coal and char characteristics, CO_2 reactivity and the coal consumption ratio. The experiments will be conducted at four different temperatures and two different particle sizes. Lastly, the coal or blend which would serve as a suitable replacement for BC-5-53 based on coal characterises, reactivity and kinetics will be suggested.

1.6 Project outline

In Chapter 1, a background and motivation, as well as the problem statement will be provided. The aim, objectives and scope will also be given along with a project outline. In Chapter 2 an in-depth literature study on coal-based pre-reduction and important coal properties that influence the efficiency of pre-reduction in the rotary kiln will be presented. A description of CO_2 gasification kinetics and modelling as well as the effect of coal properties and external parameters on the reactivity of coal/char will be given. In Chapter 3, the results of the various coal/char characterisation analyses will be discussed. In Chapter 4, a description of the experimental equipment, set-up and procedures will be given. In Chapter 5, the results and discussion of the phase one experiments will be presented, while the results and discussions for the phase two experiments will be discussed in Chapter 6. The last chapter, Chapter 7, will contain the conclusions made from the accumulated experimental results followed by recommendations for future projects in this field.

CHAPTER 2: Literature study

2.1 Introduction

In Chapter 2, a theoretical background on both coal-based direct reduction and CO_2 gasification is provided. The data and acquired information discussed in Chapter 2 will provide insight into coal reactions and behaviours that are observed during the coal reactivity studies.

In the first sections (2.2 – 2.5) information is provided on aspects that relate to coal-based direct reduction such as background information, process description, different industrial processes and preferred coal characteristics for coal-based direct reduction. In the remaining sections (2.6 – 2.9) aspects of coal gasification such as reactions, reaction mechanism, factors that influence gasification reactivity and kinetics of gasification are discussed.

2.2 Coal-based direct reduction

Direct reduction of iron ore is the process in which the ore is directly converted into reduced ore without melting the ore, typically at temperatures below 1200 °C (Feinman, 1999; Guseman, 1980; Mashhadi *et al.,* 2008). The reduction is achieved through the interaction of the reducing agent (carbon monoxide and hydrogen) with the iron oxide, which reduces the iron oxide from one state to another. The reduction leads to the formation of minute pores which allows for the movement of carbon monoxide deep into the particle. Carbon dioxide is formed and is transported counter-currently which provides the reduced iron with its typical honeycomb structure. For this reason, the reduced iron is also referred to as sponge iron (Mohanty *et al.,* 2009). Depending on the type of reductant used, the production of DRI can be divided into two types of processes, namely gas-based DRI and coal-based (solid-based) DRI (Markotic *et al.,* 2002; Prasad & Ray, 2009; Ünal *et al.,* 2012).

For coal-based direct reduction a non-coking coal is used as the reduction agent. This process usually occurs directly inside a rotary kiln or to a lesser extent in a shaft furnace or hearth (Feinnman, 1999). The coal undergoes CO_2 gasification and produces gases required for the reduction of iron oxides. The coal can either be gasified in an external gasifier, with the gases being fed to the kiln or directly added to the iron ore so that gasification and reduction occurs simultaneously. In addition, the coal can also be utilised as a fuel source for the kiln burner (Guseman, 1980).

2.3 Pre-reduction rotary kiln

Numerous rotary kiln processes have been developed due to the diversity of raw materials and fuels implemented throughout the world. Many of these processes were, however, only

operated experimentally due to the processes being economically unviable or technically insufficient. A few have nonetheless been implemented commercially or even combined to form improved processes. The most conventional processes include the Stelco-Lurgi/Republic Steel-National (SL/RN), Krupp-Coal Ore Direct Iron Reduction (CODIR) and Kawasaki processes (Cunningham & Stephenson, 1980). In Figure 2.1 the basic scheme of the rotary kiln process is illustrated.

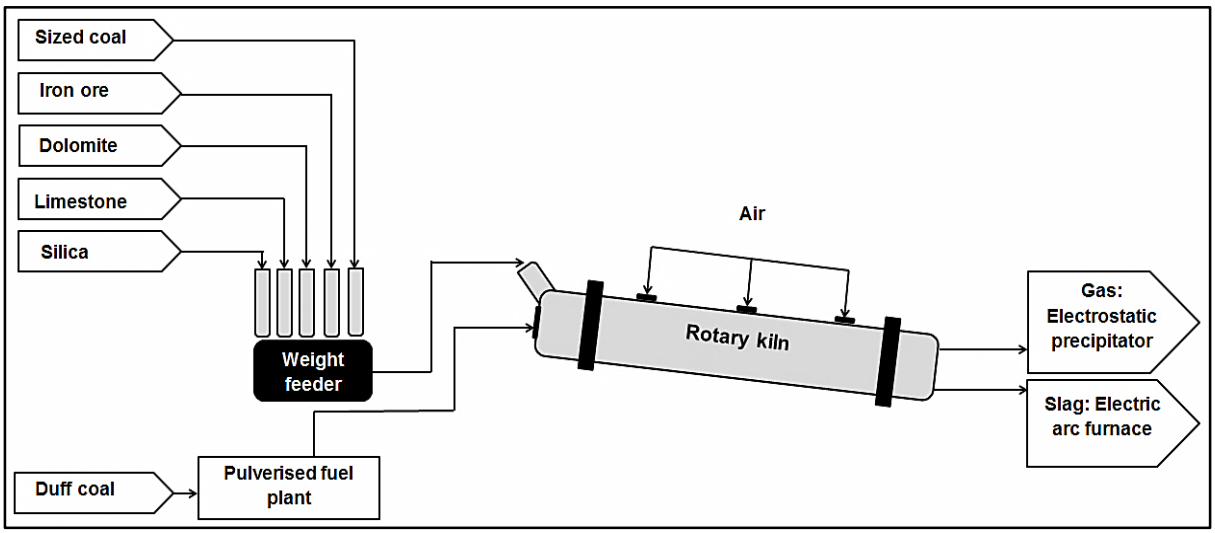

Figure 2.1: Co-current rotary kiln process at EHSV (adapted from Teessen, 2014b)

Although many industrial reduction processes have been designed and implemented, the kiln itself is similar for all processes, with only minor differences with regards to the rotational speed, burner location and kiln dimensions. The rotary kiln is a refractory lined cylinder that is inclined at a slight angle (3 to 4°) from the horizontal towards the discharge end of the kiln. The kiln rotates on its axis at a certain speed to provide a moving bed for the transport of the iron ore, coal and fluxes. The rotating kiln also ensures effective mixing of the interacting solids and acts as a pyrometallurgical reactor in which the reduction of iron, as well as the combustion of the carbonaceous material and volatile matter from the coal occurs (Feinman, 1999; Mohanty *et al.,* 2009; Sutherland, 2000). The residence time in the kiln is dependent of the inclination, rotation speed and granulometry of the raw materials (Chatterjea, 1973).

In order to control the temperature within the kiln, air is injected along the length of the kiln through air pipes and injector rings that are connected to air fans, which in turn are mounted to the outside of the kiln shell (Hall, 1980; Guseman, 1980; Steinberg, 2008; Sutherland, 2000). In Table 2.1 the kiln dimension, configuration type, rotational speed and residence time for different industrial processes are summarised.

Table 2.1 Summary of the operational parameters for various solid-based direct reduction processes (Chatterjea, 1973; Chatterjee, 1993; Chatterjee, 2012; Cunningham & Stephenson, 1980; Erwee & Pistorius, 2012; Feinman, 1999; Sutherland, 2000).

Process	Configuration	Diameter (m)	Length (m)	Rotational speed (rpm)	Residence time (hours)
SL/RN	Counter-current	4 - 6	60 - 125	0.6	12
Krupp-CODIR	Counter-current	4	73	N/A	N/A
DRC*	Counter-current	3.5	45	1	N/A
ACCAR**	Counter-current	5	80	0.25 - 0.75	12
EHSV	Co-current	4	60	0.25 - 0.5	4 - 5

*DRC – Direct Reduction Corporation

**ACCAR - Allis-Chalmers Controlled Atmospheric Reduction

2.4 Reduction process

Two distinctive zones within the kiln are normally observed namely, the pre-heating and reduction zone (Ray *et al.,* 1992; Sutherland, 2000). In Figure 2.2 the two temperature zones experienced within a co-current kiln are presented.

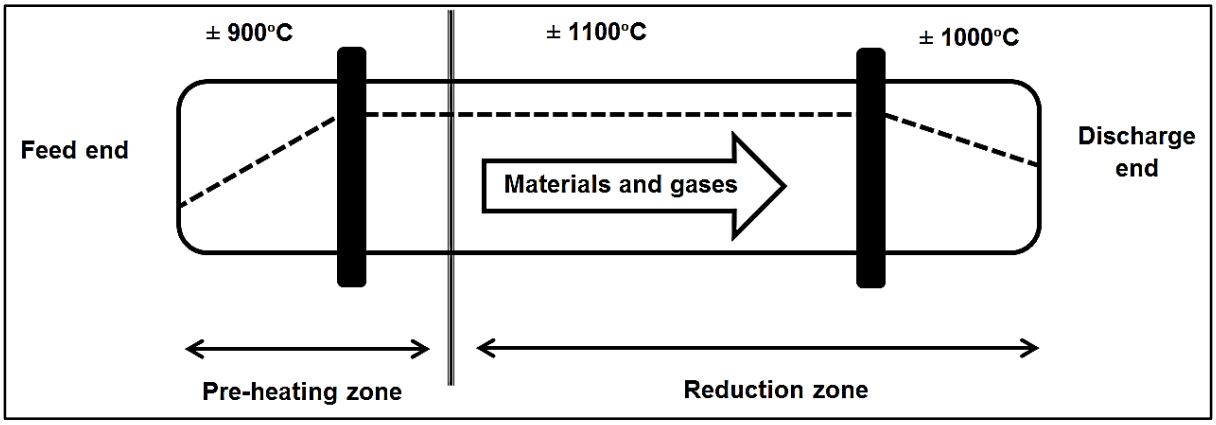

Figure 2.2: Temperature profile of pre-reduction of a co-current kiln (adapted from Sutherland, 2000)

In the pre-heating zone the feed mix is heated to the reduction temperature. The feedstock is comprised of three components namely iron ore, sized coal (6 – 50 mm) and fluxes. The iron ore mainly consists of iron oxides such as Fe_2O_3 (hematite) and Fe_3O_4 (magnetite), sulphides (FeS_2), carbonates ($FeCO_3$), silicates and other minerals (Ross, 1980). The fluxes are a mixture of dolomite, silica and limestone. The function of the fluxes is to control the pH of the slag produced for the downstream arc furnace operations, to capture sulphur and to dilute the titania and reduce the titanium reduction propensity (Chuang *et al.,* 2009; Feinman, 1999; Steinberg, 2008; Steinberg *et al.,* 2011).

The pre-heating zone is usually located in the first 40 to 50% of the kiln length. The feedstock is firstly mixed and enters the kiln, where it is rapidly heated to ± 900 °C (Cunningham & Stephenson, 1980). As the charge moves further along it is heated to about 1100 °C, which is the temperature of the reduction zone. Pulverised coal (duff coal) and natural gas are usually fed as a fuel source to the kiln burner. The sized coal's moisture is driven off and the coal devolatilises producing gases such a carbon monoxide and hydrogen, which are responsible for initial pre-reduction. The fluxes are calcined and the iron oxides are reduced to ferrous oxides as a result of the presence of hydrogen and carbon monoxide. The reduction reactions are given in the Equations 2.1 – 2.4 (Chukwuleke *et al.,* 2009; Cunningham & Stephenson, 1980; Feinman, 1999; Ray *et al.,* 1992; Sutherland, 2000):

Hematite to magnetite:

$$3Fe_2O_{3(s)} + CO_{(g)} \rightarrow 2Fe_3O_{4(s)} + CO_{2(g)} \quad (2.1)$$

$$3Fe_2O_{3(s)} + H_{2\,(g)} \rightarrow 2Fe_3O_{4(s)} + H_2O_{(g)} \quad (2.2)$$

Magnetite to wustite:

$$Fe_3O_{4(s)} + CO_{(g)} \rightarrow 3FeO_{(s)} + CO_{2(g)} \quad (2.3)$$

$$Fe_3O_{4(s)} + H_{2\,(g)} \rightarrow 3FeO_{(s)} + H_2O_{(g)} \quad (2.4)$$

In the reduction zone (metallisation zone), the kiln charge has a temperature of ± 1100 °C, where it remains moderately constant. The final reduction of ferrous oxide occurs to form metallic iron, as illustrated in Equation 2.5 (Chukwuleke *et al.,* 2009; Cunningham & Stephenson, 1980):

Wustite to iron:

$$FeO_{(s)} + CO_{(g)} \rightarrow Fe_{(s)} + CO_{2(g)} \quad (2.5)$$

The reduction of iron oxide occurs for the most part under isothermal conditions (Mashhadi *et al.,* 2008). The reduction is dependent of the temperature, filling degree, rotational speed and reactivity of the coal (Chatterjee, 2010, Sutherland, 2000). In addition to reduction of the iron, the coal char undergoes CO_2 gasification, shown in Equation 2.6 (Cunningham & Stephenson, 1980):

$$CO_{2(g)} + C_{(s)} \rightarrow 2CO_{(g)} \quad (2.6)$$

This reaction is known as the Boudouard reaction and occurs independently and simultaneously with the gaseous reduction of iron oxide. The produced carbon monoxide

further reduces the iron ore to increase pre-reduction achieved within the kiln. This heterogeneous endothermic reaction is required for maintaining reducing conditions within the kiln. The rate of this reaction is reliant on the reactivity of the carbon and kiln temperature and it is therefore important to increase the reaction rate in order to increase pre-reduction achieved in the kiln. Although a high CO_2 reactivity is favoured, care must be taken to ensure that the reactivity is not too high as this will lead to an insufficient carbon carry over to the electric arc furnace, alteration of the feed ratio to the kiln and increased coal consumption (Chatterjee, 2010; Cunningham & Stephenson, 1980; Sutherland, 2000).

After reduction the slag is discharged into a hopper from where it is transported to the electric arc furnace for further reduction. The rotary kiln gases (mainly consisting of carbon dioxide, nitrogen, carbon monoxide and steam) are cooled by water sprays and sent through electrostatic precipitators to remove entrained particles, before being released into the atmosphere (Chatterjea, 1973; Hall, 1980).

2.5 Coal requirements for solid-based pre-reduction

It is preferred that coals utilised for pre-reduction possess certain characteristics to achieve optimum efficiency within the kiln. The chemical, mineral and thermal properties are discussed in Sections 2.5.1 and 2.5.2 respectively.

2.5.1 Chemical & mineral properties

2.5.1.1 Volatile matter

Volatile matter influences the initial pre-reduction, as it provides the preliminary reductant gases for pre-reduction, while the charge is heated to the desired reduction temperature (Donskoi & McElwain, 2003; Mashhadi *et al.,* 2008). In a study by Mashhadi *et al.* (2008) the effect of different coal properties on pre-reduction was investigated. From the results they concluded that a high volatile content will increase the degree of pre-reduction in the initial stages, but it will not be able to sustain pre-reduction throughout the rotary kiln. Coetsee *et al.* (2002) studied both high volatile coals and anthracite, with the results indicating that the high volatile coals resulted in marginally faster reduction. Although several authors have found that the volatile matter influences pre-reduction, others concluded that the volatile matter has little or no effect on the pre-reduction (Reddy *et al.,* 1991; Wang *et al.,* 1998).

A moderate to low amount of volatiles is usually preferred for a pre-reduction coal owing to numerous reasons such as excess gas production, temperature profiles across the kiln and additional fuel source requirements (Chatterjee, 2010; Sarangi & Sarangi, 2011).

2.5.1.2 Fixed carbon

The fixed carbon content of coal contributes to the pre-reduction by acting as the carbon source for the Boudouard reaction (Cunningham & Stephenson, 1980; Donskoi & McElwain, 2003; Sarangi & Sarangi, 2011; Sutherland, 2000). In a study by Mashhadi *et al.* (2008) the results indicated that maximum pre-reduction values were achieved for coals with fixed carbon values above 48 wt.%. The company Stelco also conducted a study to determine which coal properties are best suited for pre-reduction and concluded that even though lignite coals were more reactive, higher rank coals were more suitable due to their higher carbon contents (Guseman, 1980).

Moderate to high values of fixed carbon are preferred in order to ensure a suitable amount of carbon for pre-reduction in the kiln and downstream electric arc furnace, as well as lowered coal consumption (Mohanty *et al.,* 2009). The fixed carbon to total iron ratio (coal consumption ratio) is utilised to determine the coal feed requirement. For Indian conditions, this ratio is typically between 0.42 and 0.54, with a ratio of 0.5 achieving a degree of metallisation above 90%. If the fixed carbon content is low, the coal consumption will have to increase to prevent carbon deficiency in the reduction zone and a decrease in the degree of pre-reduction (Rudramuniyappa *et al.,* 2000; Sarangi & Sarangi, 2011).

2.5.1.3 Ash value and composition

It is preferred that pre-reduction coals have a low ash value for reasons such as slag volume, coal and energy consumption, productivity and the formation of accretions on the kiln wall, which leads to obstructions (Cunningham & Stephenson, 1980; Industrial technical consultant, 2003, Sarangi & Sarangi 2011).

The composition of the ash also influences kiln operations. Elements such as sodium and iron can catalytically increase the CO_2 gasification rate in turn increasing pre-reduction, while aluminium species positively affect direct reduction by influencing the ash fusion temperature (AFT). Silica has opposing effects on pre-reduction. Firstly it increases the viscosity of the slag which lowers the sticking tendency and increases the AFT (Sarangi & Sarangi, 2011). On the other hand silica reacts with ferrous oxide to form ferrous silicate, which has a low melting point and interferes with the reduction of metallic iron (Cunningham & Stephenson, 1980).

2.5.1.4 Sulphur content

In the pre-heating zone of the kiln inorganic sulphur such as pyrite and calcium sulphate transform to COS and H_2S at 600 °C. Organic sulphur is, however, not affected by charring up to temperatures of 1000 °C and is thus accountable for the majority of sulphur pick-up by

sponge iron. For this reason a low total sulphur value (> 1 wt.%) is preferred for pre-reduction coals (Chatterjee, 2010; Sarangi & Sarangi, 2011).

2.5.2 Thermal properties

2.5.2.1 Ash fusion temperature

In order to prevent the formation of accretions on the kiln wall it is preferred that the coals selected for pre-reduction have a high AFT. The initial deformation temperature (IT) specifically should be at least 100 °C higher than the maximum kiln temperatures under reducing conditions, as the IT tends to decrease 50 to 80 °C under these conditions (Chatterjee, 2010). In general it is recommended that the AFT of the coal typically be 50 to 100 °C higher than the kiln discharge temperature, which is normally 1000 °C (Guseman, 1980; Wang & Massoudi, 2013).

2.5.2.2 Caking & Swelling index

A low swelling index is required to prevent agglomeration, which leads to carbon depletion and low metallisation. A high caking index causes sintering, reduces CO_2 char reactivity and promotes the formation of accretions on the kiln wall; therefore the caking index of the coal should preferably be low (Industrial technical consultant, 2003; Sarangi & Sarangi, 2011).

The desired chemical and thermal property values are summarised in Table 2.2.

Table 2.2 Desired coal properties for a pre-reduction coal

Property	Unit	Value (a.d.b)	Reference
Chemical			
Inherent moisture	wt.%	< 4	2,8
Ash yield	wt.%	5 - 25	1,2,8
Volatile matter	wt.%	25 - 30	1,2,4,6,8
Fixed carbon	wt.%	45 - 60	1,5,8,9
Total sulphur	wt.%	< 1	2,3,4,8
Calorific value	MJ/kg	20 – 30	2,3,8,
Thermal			
IT	°C	> 1300	4,5,9
Swelling index	-	< 3	2,3,4,8
Caking index	-	< 3	2,7,8

1 – Carpenter (2004); 2 – Chatterjee (2010); 3 – Feinman (1999); 4 – Guseman (1980); 5 – Industrial technical consultant (2003); 6 – Mashhadi *et al.* (2008); 7 - Mohapatra & Partra (2009); 8 – Sarangi & Sarangi (2011); 9 – Sutherland (2000)

2.5.3 Coal rank

Coal ranks typically favoured for pre-reduction range from sub-bituminous to bituminous coals, but it is dependent on the process conditions. When consulting the values provided in Table 2.2 for moisture content, ash value, volatile matter and fixed carbon, it is seen that most of the properties fall in the range of bituminous and sub-bituminous coals (Speight, 2005).

In 1977 Stelco conducted an investigation to determine which coals would be best suited for their process. The use of lignite resulted in lowered throughputs and higher coal consumption and for this reason sub-bituminous coal was concluded to the best suited for pre-reduction. Additionally the densities of the bituminous coal chars were lower than that of the sub-bituminous coal chars, which resulted in caking and agglomeration within the kiln (Guseman, 1980).

Sutherland (2000) found that medium rank C coals (ortho-bituminous) were best suited for the rotary kiln operations at EHSV. When referring to Table 2.3 it can be seen that the coal rank utilised by the different commercial processes varies from lignite to bituminous.

Table 2.3: Summary of properties (a.d.b.) of the coals utilised for the industrial processes (Chatterjee, 1993; Chatterjee, 2010).

Process		**DRC**	**AFP**		**NZS**	**BSIL**	**ISCOR**
Parameter	**Unit**						
Coal rank		Varies	Lignite	Bituminous	Lignite	Sub-bituminous	Sub-bituminous
Chemical property							
Inherent moisture	wt.%	2 - 25	17	9	18	10	6
Ash yield	wt.%	5 - 20	3	32	7	23	13
Volatile content	wt.%	6 - 33	43	23	34	23	26
Fixed carbon	wt.%	38 - 84	37	36	41	44	55
Total sulphur	**wt.%**	0.4 - 2	0.3	0.4	0.3	0.6	0.7
Swelling index	**-**	0 - 6	N/A	N/A	N/A	N/A	N/A

The sub-bituminous and bituminous coals utilised by Buhar Sponge Iron Limited (BSIL), Iron and Steel Corporation (ISCOR) and Acos Finos Piratini (AFP) correlate well with the preferred properties (Table 2.2) as well as the coals utilised by the DRC to a certain extent. However, the lignite coals utilised for AFP and New Zealand Steel (NZS) differ from these values.

2.6 Coal gasification

Coal gasification is defined as a process where coal or char reacts with an oxidiser at elevated temperatures to produce fuel-rich products. Coal is gasified in the presence of gasifying agents such as air, oxygen, steam, carbon dioxide or mixtures of these agents. The predominant products formed during gasification are combustible gases such as carbon monoxide, hydrogen and methane (Kabe *et al.,* 2004).

The initial step of coal gasification is pyrolysis or devolatilisation, which involves the thermal decomposition of the coal structure to produce volatiles and chars. Pyrolysis occurs rapidly in comparison to char gasification and is illustrated in Equation 2.7 (Kabe *et al.,* 2004; Kenarsari & Zeng, 2014):

$$Coal \rightarrow Char(carbon) + Volatiles \tag{2.7}$$

The volatiles consist of tars, oils, phenols, naphtha, methane, H_2S, carbon monoxide and hydrogen (Kabe *et al.,* 2004; Molina & Mondragón, 1998).

The next step of coal gasification is char gasification, where mostly the carbon in the remaining char reacts with a gasification agent. Equation 2.8 – 2.16 give the most important char gasification reactions, including both homogeneous and heterogeneous reactions (Higman & Van der Burgt, 2008; Kabe *et al.,* 2004; Molina & Mondragón, 1998; Tsai, 1982):

Combustion reactions to form CO and CO_2:

$$C_{(s)} + \frac{1}{2}O_{2(g)} \rightarrow CO_{(g)} \qquad \Delta H_0 = -111\ MJ/kmol \tag{2.8}$$

$$CO_{(g)} + \frac{1}{2}\ O_{2(g)} \rightarrow CO_{2(g)} \qquad \Delta H_0 = -283\ MJ/kmol \tag{2.9}$$

$$C_{(s)} + \ O_{2(g)} \rightarrow CO_{2(g)} \qquad \Delta H_0 = -394\ MJ/kmol \tag{2.10}$$

Oxidation of hydrogen in the volatile matter:

$$H_{2(g)} + \frac{1}{2}O_{2(g)} \rightarrow H_2O_{(g)} \qquad \Delta H_0 = -242\ MJ/kmol \tag{2.11}$$

Boudouard reaction:

$$C_{(s)} + CO_{2(g)} \rightleftarrows 2CO_{(g)} \qquad \Delta H_0 = 172\ MJ/kmol \tag{2.12}$$

Water gas reaction:

$$C_{(s)} + \ H_2O_{\ (g)} \rightleftarrows CO_{(g)} + \ H_{2(g)} \qquad \Delta H_0 = 131\ MJ/kmol \tag{2.13}$$

Water gas shift reaction:

$$H_2O_{(g)} + CO_{(g)} \rightleftarrows H_{2(g)} + CO_{2(g)} \qquad \Delta H_0 = -41\ MJ/kmol \tag{2.14}$$

Methanation reaction:

$$C_{(s)} + 2H_{2(g)} \rightleftarrows CH_{4(g)} \qquad \Delta H_0 = -75\ MJ/kmol \tag{2.15}$$

Steam methane reforming reaction:

$$CH_{4(g)} + H_2O_{(g)} \rightleftarrows CO_{(g)} + 3H_{2(g)} \qquad \Delta H_0 = 206\ MJ/kmol \tag{2.16}$$

The combustion reactions and hydrogen oxidation reactions (2.8 – 2.11) are all exothermic reactions that proceed rapidly and produce the heat necessary to drive the endothermic reactions. Reactions 2.12 – 2.13 are endothermic heterogeneous carbon gasification reactions that utilise the heat released during the combustion reactions, with steam gasification occurring faster than the CO_2 gasification (Higman & Van der Burgt, 2008). The remaining reactions describe the methane-forming and steam methane reforming reactions as well as the water gas shift reaction (Higman & Van der Burgt, 2008; Tsai, 1982).

2.6.1 Char-CO_2 gasification mechanism

Numerous authors have developed different models to describe the Boudouard reaction, with the most widely used model being the two step process described by Ergun (Higman & Van der Burgt, 2008; Laurendeau, 1978). The first step is the reduction of carbon dioxide to carbon monoxide. The dissociation occurs at the carbon active site (C_f), with the remaining oxygen atom forming an oxidised surface complex with the active site. This reaction can occur at temperatures as low as 600 °C and is given in Equation 2.17 (Ergun, 1956; Higman & Van der Burgt, 2008).

Step 1:

$$C_{f(s)} + CO_{2(g)} \underset{k_{-1}}{\overset{k_1}{\rightleftarrows}} C(O) + CO_{(g)} \tag{2.17}$$

Step 1 describes dissociative adsorption, where k_1 and k_{-1} are temperature dependent rate constants. The second step is where the carbon-oxygen complex produces a carbon monoxide molecule and a new free active site (Higman & Van der Burgt, 2008).

Step 2:

$$C(O) \underset{k_{-2}}{\overset{k_2}{\rightleftarrows}} CO_{(g)} + C_{f(s)} \tag{2.18}$$

Step 2 depicts the transfer of carbon from the solid to the gas phase. The forward rate constant (k_2) is dependent on temperature only. This reaction is the rate-limiting reaction and describes the desorption of the carbon-oxygen complex (Ergun, 1956; Higman & Van der Burgt, 2008). Equation 2.18 is often regarded as irreversible; however, others such as Gadsby *et al.* (1948) regards it as reversible to account for the inhibitory effect of carbon monoxide on the Boudouard reaction rate.

2.7 Kinetics of gasification

2.7.1 Specific reaction rate

The specific reaction rate of the char/coal is utilised to describe the gasification rate as a function of carbon conversion and is given in Equation 2.19 (Hodge *et al.,* 2010; Roberts & Harris, 2007):

$$R_s = -\frac{dm_t}{dt}\left(\frac{1}{m_t}\right) \tag{2.19}$$

where m_t is the instantaneous mass of the carbon (dry, ash-free basis) at time *t.* With this method, the reaction rate relative to the instantaneous mass of the carbon in the char is determined, while for the conventional method the rate of conversion is determined relative to the initial carbon mass of the char, as shown in Equation 2.20:

$$x = \frac{m_0 - m_t}{m_0 - m_{final}} \tag{2.20}$$

Where m_0 and m_{final} are the initial and final mass of the char respectively. By utilising the specific reaction rate, the relation between reactivity and char properties can be directly illustrated (Guizani *et al.,* 2013; Jayraman *et al.,* 2015; Roberts & Harris, 2007; Tay & Li, 2010). Liu *et al.* (2011), for example, related the specific surface area and pore volume to initial specific reaction rate.

2.7.2 Structural model

The most commonly used structural models for gasification include, the volumetric model (VM), the random pore model (RPM) and the shrinking core model (SCM) (Wu *et al.,* 2009). Also semi-empirical models, such as the modified volumetric model (MVM) and the Wen model (integrated core model (ICM)), which are able to predict a wider variety of carbon

conversion shapes, are used. The Wen model was developed by Wen (1968) as an improvement of the SCM model, with the general form given in Equation 2.21:

$$\frac{dx}{dt} = k(1-x)^m \tag{2.21}$$

Where *k* represents the reaction rate constant and *m* represents the solid reaction order, which makes the Wen model very versatile. If *m* = 2/3 the Wen model reduces to the chemically controlled shrinking core model and for *m* = 1 the model represents the VM.

2.8 Factors affecting coal gasification reactivity

Coal gasification is influenced by numerous factors, which include both coal characteristics and external conditions such as operating temperature, particle size and fragmentation. In Section 2.8.1 the influence of coal properties is discussed, which include chemical, mineral, petrographic and structural characteristics. The influence of operating temperature, particle size and fragmentation is discussed in Section 2.8.2.

2.8.1 Coal properties affecting gasification

2.8.1.1 Volatile matter and fixed carbon

Volatile matter is mostly associated with pyrolysis and indirectly influences char gasification reactivity by affecting char formation and active site concentration during devolatilisation and the initial stages of char gasification. On the other hand the fixed carbon content which remains in the char after devolatilisation affects gasification reactivity more directly (Dutta *et al.,* 1977).

Haykiri-Acma *et al*. (2012) studied the effect of volatile matter and fixed carbon on the reactivity, in which the volatile matter of the coal was removed and carbon content enriched. The results of the study illustrated the removal of the volatiles and the enhancement of the fixed carbon led to the decrease of reactivity. Miura *et al.* (1989) reviewed various studies on factors affecting CO_2 reactivity and found that some of the studies observed a noteworthy correlation between the CO_2 reactivity of the char and the volatile matter. One of the studies attributed this to the development of the pore structure and increase in active site concentration in the coal matrix caused by stripping the remaining volatiles from the char during the initial stages of gasification. Similar results were also observed by Kim *et al.* (2011) and Zhang *et al.* (2006a). In Figure 2.3 the correlation between the CO_2 reactivity and volatile matter at 1050 °C, for the study of Kim *et al.* (2011) is shown.

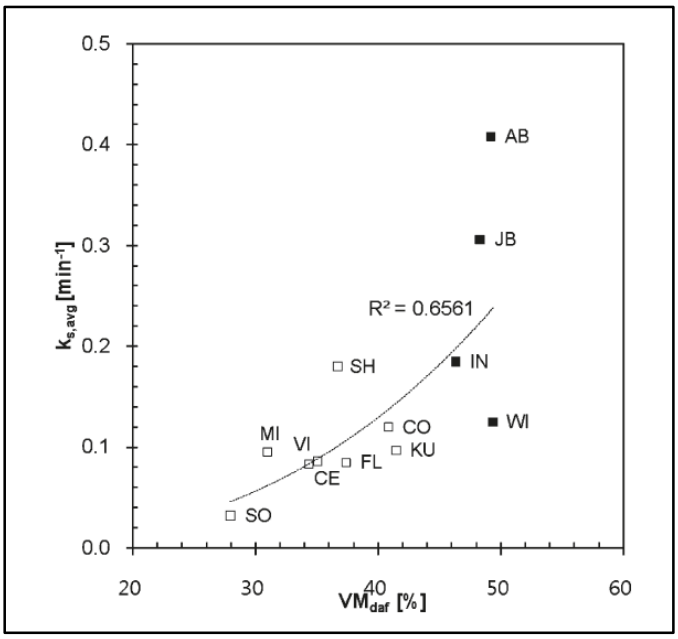

Figure 2.3: Influence of volatile matter on coal CO_2 gasification reactivity (Taken from Kim *et al.,* 2011)

Volatile matter can also lead to the fragmentation of particles which affects coal reactivity (Senneca *et al.,* 2013; Stubington & Linjewile, 1989).

The fixed carbon content, which is directly related to the coal rank, decreases char gasification reactivity due to the decrease in oxygen containing functional groups that acts as active sites. This is verified in studies reviewed by both Irfan *et al.* (2011) and Miura *et al.* (1989), which showed that the gasification reactivity of the char decreased when the carbon content was greater than 80%. Ng *et al*. (1987) also investigated the influence of different coal properties and found that reactivity decreases exponentially when the carbon content in the parent coal was increased. The fuel ratio, which is the ratio of fixed carbon to volatile matter, combines the influence of both factors on combustion/gasification reactivity. Coals with a low fuel ratio usually have a high reactivity and a faster carbon burnout rate (Haykiri-Acma *et al*., 2012; Miura *et al.,* 1989).

2.8.1.2 Mineral matter

The catalytic effect of coal mineral matter is assumed to be due to the presence of the exchangeable metal cations on the coal surface that exchange with a fraction of the hydrogen cations to combine with the carboxylic acid groups in the organic structure. This in turn contributes to the gasification reactivity (Skodras & Sakellaropoulos, 2002; Tsai, 1982). The carboxylic acid groups, however, decrease with increasing rank and for this reason the catalytic effect of the minerals is more predominant in low rank coals (Sha, 2009). The catalytic activity of the mineral matter is dependent on concentration, chemical form in the coal matrix and the dispersion of the mineral matter (Skodras & Sakellaropoulos, 2002; Van Heek & Mühlen, 1985).

Numerous studies have been conducted on the catalytic effect of different elemental components, specifically the alkali and alkaline earth metals such as sodium, magnesium, calcium and potassium species (Kabe *et al.,* 2004; Quyn *et al.,* 2005; Shenqi *et al.,* 2011; Skodras & Sakellaropoulos, 2002; Van Heek & Mühlen, 1985). Walker *et al.* (1979) arranged the different cations in order of reactivity for CO_2 gasification:

$$Na > K \sim Ca > Raw\ coal > Fe > Demineralized\ coal > Mg$$

From the above order it is seen that sodium has the most significant catalytic influence on CO_2 reactivity, which is corroborated by studies done by Kyotani *et al.* (1986), Skodras & Sakellaropoulus (2002) and Ye *et al.* (1998). Skodras & Sakellaropoulus (2002) additionally stated that the concentration of sodium cations in the coal ash needs to be significant for the catalytic effect to be observed. Potassium, specifically K_2CO_3, is a well-established gasification catalyst (Liu *et al.,* 2003). Most of the studies done on the catalytic effect of potassium have revealed that it increases coal gasification reactivity; however, the catalytic effect of small concentrations of potassium is negligible (Irfan *et al.,* 2011; Shenqi *et al.,* 2011; Skodras & Sakellaropoulus, 2002; Walker *et al.,* 1979).

Calcium has also been found to have a substantial catalytic effect on the gasification rate, increasing the reactivity of the char for both CO_2 and steam gasification (Kuznetsov *et al.,* 2013; Liu *et al.,* 2003; Skodras & Sakellaropoulus, 2002; Walker *et al*., 1979). Additionally calcium (and magnesium) is retained within the char after devolatilisation at high temperatures (> 1000 °C) and is therefore able to catalyse gasification at high temperatures (Quyn *et al.,* 2005). Iron catalyses reactivity by contributing to the number of active sites (Asami *et al.,* 1996; Irfan *et al.,* 2011). This catalytic mineral is more effective at high temperatures, but it is important that a reductive atmosphere be maintained or the catalyst will deactivate (Çakal *et al.*, 2007; Skodras & Sakellaropoulus, 2002).

Acidic ash constitutes such as aluminium and silica compounds are inherently non-catalytic but can have opposing effects on reactivity. Firstly the elements can increase reactivity by increasing the AFT which reduces ash fusion, in turn minimising the rate of internal mass transfer and surface area shrinkage (Kim *et al.,* 2009; Van Dyk, 2006). Secondly at high operating temperatures these elements form melts such as amorphous aluminosilicates, which obstructs pores and cover the active surface area. This increases the rate of internal pore diffusion and hinders reagent gases from contacting carbon active sites (Bai *et al*., 2009; Sekine *et al*., 2006). Additionally, the transformation of minerals containing these elements can also hinder reactivity by altering surface area and ash transformation. The transformation of kaolinite to meta-kaolinite via de-hydroxylation has been shown to promote the shrinkage

of surface area and sintering, both factors that decreases reactivity (Argyle & Bartholomew, 2015; Selvakumaran & Bakthavatsalam, 2015; Venturelli & Paganelli, 2007).

In addition to investigating the catalytic effect of each individual inorganic component, researchers have also studied the collective catalytic influence of the coal ash components, as quantified by the alkali index. The alkali index is defined as the ratio of the total basic compounds to the total acidic compounds, multiplied by the ash values (Sakawa *et al.,* 1982). Numerous investigators, including Hattingh *et al.* (2011), Sakawa *et al.* (1982), Skodras & Sakellaropoulus (2002) and Ye *et al.* (1998) found that the gasification reactivity, specifically CO_2 gasification, increases with the alkali index.

2.8.1.3 Coal rank

Lower rank coals such as lignite, sub-bituminous and bituminous coals typically have a higher reactivity, due to the increased concentration of the functional groups (Crelling *et al.,* 1988; De Korte, 2001; Miura *et al.,* 1989). Tomaszewicz *et al.* (2013) and Ye *et al.* (1998) stated that lower-rank coals have a higher gasification rate, owing to the high portion of transitional and macropores, high dispersion of catalytic minerals and the high concentration of oxygen containing functional groups.

2.8.1.4 Petrography

Coal macerals are typically divided into two groups namely reactive (liptinite and vitrinite) and non-reactive (inertinite) macerals. Liptinite and vitrinite are characterised by high to moderate amounts of volatile matter, high hydrogen and oxygen content respectively and low aromaticity, while inertinite is characterised by a low volatile content, high carbon content and high aromaticity (Borrego *et al.,* 1997; Falcon & Ham, 1988; Tsai, 1982). Liptinite is regarded as the most reactive maceral, containing twice the amount of volatile matter in comparison to vitrinite and is typically associated with short combustion times and stable flames. It therefore only influences the pyrolysis stage of gasification, having no significant effect on the char gasification (Borrego *et al.,* 1997; Cloke & Lester, 1994).

Different authors have investigated the effect of inertinite and vitrinite content on char reactivity, with most agreeing that increased vitrinite content increases reactivity (Borrego *et al.,* 1997; Kim *et al.,* 1988; Méndez *et al.,* 2003; Sun *et al.,* 2004). During pyrolysis, low rank vitrinite decomposes to form tenui-network chars, which have a high surface area and char wall porosity, thereby increasing the reactivity (Cloke & Lester, 1994; Tang *et al.,* 2005). The formation of these chars are, however, rank and temperature dependent. Higher temperatures result in more thin-walled chars, while rank increases aromaticity which in turn results in tenui-

network chars being replaced by cenospheric chars (Bend *et al.,* 1991; Cloke & Lester, 1994; Jones *et al.,* 1985).

Although most authors have found that vitrinite-rich coals are more reactive than inertinite-rich coals, Sakawa *et al.* (1982) found that reactivity increased with inertinite content. Even though inertinite is regarded as being an unreactive maceral, certain constituents of inertinite are reactive, such as reactive semi-fusinite (Borrego *et al.,* 1997; Cloke & Lester, 1994; Sanyal, 1997). The effect of inertinite on reactivity is also rank dependant, as the reflectance of this maceral changes with rank. For low rank coals inertinite tends to reduce the reactivity of the chars, as inertinite increases the amount of anisotropic materials. However, for high rank coals the inertinite reduces this material, in turn increasing the reactivity (Alonso *et al.,* 2001; Cloke & Lester, 1994). The influence that inertinite has on reactivity is also dependent on the melting ability of the maceral, which is to a certain extent also rank dependent. Alonso *et al.* (2001) illustrated that the lower the plastic properties of the coal, the greater the reactive effect of inertinite on the char reactivity.

In addition to the influence of the individual macerals, petrographic indices have also been developed which combines the effect of the different macerals on combustion and reactivity behaviour. The maceral and reactive maceral indices are semi-empirical expressions, which were developed by Su *et al.* (2001) and Helle *et al.* (2003) respectively. These semi-empirical expressions are typically utilised to predict the burnout results of coals and coal blends, however, Hattingh (2009) investigated the influence of these indices on the CO_2 gasification reactivity of three different coals at different temperatures and pressures and found that the reactivity tends to increase with the maceral and reactive maceral indices. See Appendix A.5 for the formulas. The petrofactor combines the rank and reactive maceral composition of the coal and relates it to the reactivity. Reactivity typically decreases with the petrofactor (Kizgut & Yilmaz, 2003). In Figure 2.4 the influence of petrofactor on char reactivity is shown.

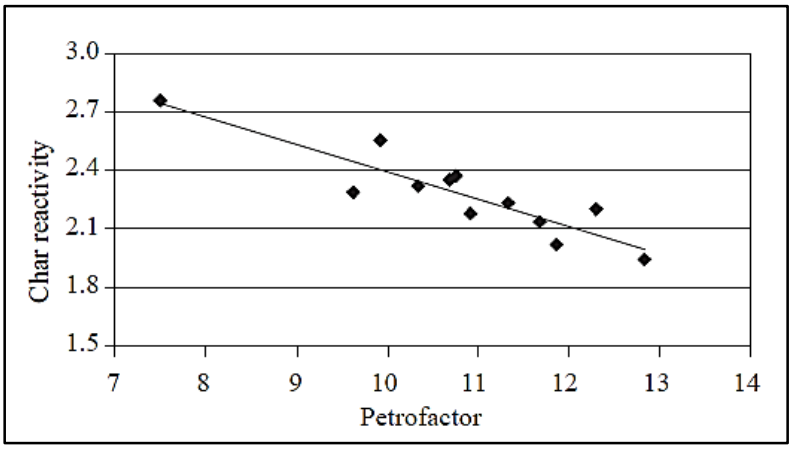

Figure 2.4: Influence of petrofactor on char combustion reactivity (Taken from Kizgut *et al.*, 2003)

2.8.1.5 Pore structure

The surface area and porosity influences heterogeneous gasification reactions as the reaction gas penetrates the particle, reacts with the carbon atoms and afterwards the products diffuse out of the solid structure (Çakal *et al.,* 2007; Feng & Bhaita, 2003). The meso- (20 to 500 Å) and macropores (> 500 Å) act as the passages that transport the reactant gases to the micropores (< 20 Å) where most active sites are located and also transport the product gases out of the solid (Laurendeau, 1978, Jayaraman & Gokalp, 2015). Studies by Ochoa *et al.* (2001), Saha *et al.* (2013), Sliberman *et al.* (2013) and Sinag *et al.* (2003) illustrated that a greater surface area and micropore porosity increases the CO_2 gasification reactivity of the coals/chars.

Pore structure is greatly affected by gasification and pyrolysis conditions. Sinag *et al.* (2003) studied the effect of coking temperature on the surface area and found that the surface area increased with increased temperature. They concluded that the larger surface area was the result of swelling of the pulverised chars, which causes the specific surface area to increase and the volatiles to release more rapidly. Both Jayaraman *et al.* (2015) and Wu *et al.* (2008) studied the influence of pyrolysis heating rate and temperatures on char reactivity and concluded that rapid heating rates increased the pore surface area and also led to a more disordered structure and poorer crystallinity of the carbonaceous material, which facilitates reactivity. This is mainly due to the rapid release of volatiles, which increase porosity and prevents the ash from agglomerating on the external surface. However, in contradiction to Sinag *et al.* (2003); Jayaraman *et al.* (2015) also concluded that as the pyrolysis temperature continues to increase, the reactivity decreases due to a reduction in the surface area.

Pyrolysis temperatures can have opposing effects on the surface area and porosity of chars, either increasing or decreasing these surface characteristics (Çakal *et al.,* 2007; Jayaraman & Gokalp, 2015). The first influence at high temperature is the removal of volatiles and tars, which opens blocked pores and leads to the generation of new pores thereby increasing the surface area and porosity of the chars. The opposing effect is thermal annealing and restructuring of the carbon matrix at further higher temperatures, which leads to pore coalescence and closing of the pore mouths. This in turn decreases the surface area, porosity and active site concentration negatively impacting reactivity (Çakal *et al.,* 2007; Roberts *et al.,* 2015a; Saha *et al.,* 2013).

2.8.1.6 Active surface area

During gasification the entire surface area of the coal particles does not participate in the reaction. Only certain sites are favoured for the reactions, which are known as the active sites and are defined as the imperfections in the crystallite edges of the carbon (Khan, 1989).

Carbon active sites influence the intrinsic reaction kinetics, such as activation energy, pre-exponential factor and dependence on reactant gas. These sites generally increase reactivity, but the accessibility of the active sites for reacting gases is also a determining factor (Laurendeau, 1978; Walker *et al.,* 1959).

Laine *et al.* (1963) investigated the importance of active sites in carbon-oxygen reactions. In the study they differentiated between edge carbon atoms and basal plane carbon atoms, with the edge carbon atoms forming bonds more readily with the chemisorbed oxygen. Additionally it was also concluded that the reactivity of the oxygen is dependent on two factors, namely the geometrics and impurities.

2.8.2 External parameters affecting gasification

2.8.2.1 Operating temperature

High operating temperatures are typically favoured for gasification due to an increase in gasification reaction rates, but the degree of temperature increase is limited owing to factors such as coal properties and reaction regimes. In general, chemical reactions are classified to occur in three regimes: the chemical controlled, internal diffusion controlled and external diffusion controlled regime. In the chemically controlled regime (regime I), which favours low temperatures, the concentration of the gaseous reactants are uniform throughout the porous solid and equal to the concentration of the bulk gas stream. For this regime the activation energy and other kinetic parameters determined are the true values (Higman & Van der Burgt, 2008; Szekely *et al.,* 1976). As the operating temperature increases both pore diffusion and intrinsic chemical reactions influence the overall reaction rate. In this regime (regime ll) the measured reaction parameters do not represent the intrinsic values and the apparent (observed) activation energy is usually half of the true activation energy (Higman & Van der Burgt, 2008; Kabe *et al.,* 2004; Szekely *et al.,* 1976). Regime III is controlled by the external mass transfer of the reactant gas, which occurs on the external surface of the pellet. This regime occurs at high operating temperatures and the apparent activation energy is very small (Higman & Van der Burgt, 2008; Szekely *et al.,* 1976).

Sun *et al.* (2004) studied the effect of temperature on CO_2 gasification reactivity by varying the temperature from 850 to 900 °C. The results illustrated that as the temperature increases, the gasification mechanism changes and that the gasification rate increases. At a temperature of 850 °C the gasification was controlled by the intrinsic reactivity, while for higher temperatures (950 °C) gasification was controlled by both diffusion and intrinsic reactivity. Most studies on small particle (< 1 mm) CO_2 gasification have found that at temperatures greater than 1000 °C internal mass transfer limitations start to influence the rate of gasification, while for larger particles internal mass transfer starts to influence reactivity at temperatures greater than 850

°C (Jayaraman & Gokalp 2015; Kim *et al.,* 2011; Ochoa *et al.,* 2001; Veca & Adrover, 2014). The influence of operating temperature is quantitatively investigated by determining the activation energy using the Arrhenius equation (Fogler, 2006):

$$k = Ae^{\frac{-Ea}{RT}} \tag{2.22}$$

2.8.2.2 Particle size

Numerous authors have investigated the effect of particle size on gasification reactivity, with most concluding that the reactivity increases with a decrease in particle size (Irfan *et al*., 2011; Kok *et al.,* 1998; Zhu *et al.,* 2008). Van Heek & Muhlen (1985) explained that this is due to the dispersion of mineral matter in the coal particle as a smaller particle size leads to more minerals being liberated and therefore increased reactivity. Another reason is that for smaller particles the volatile matter is released more rapidly due to a shorter distance travelled (Griffin *et al.,* 1993).

Particle size greatly influences devolatilisation, particle heating rate and temperature gradient as well as, char formation and reactivity (Stubington & Sasongko, 1998). Zhu *et al.* (2008) investigated the influence of coal particle size on both pyrolysis and char reactivity. The results illustrated that large particle sizes will increase the char yield, but the reactivity of the coal char will decrease with increased particle size. The influence of particle size on the reactivity is given in Figure 2.5.

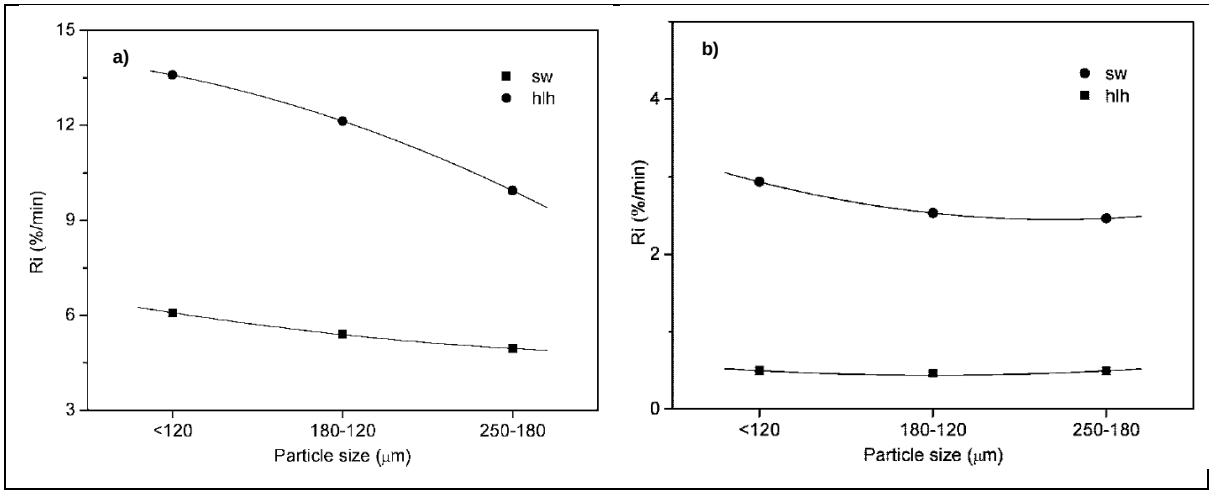

Figure 2.5: Influence of particle size on CO_2 gasification reactivity a) raw coals b) demineralised (Taken from Zhu *et al.,* 2008) [1]

It was concluded that the influence of particle size on gasification is due to the secondary reactions of volatile matter and mineral matter dispersion. The secondary reactions include

[1] sw: Shangwan bituminous coal; hlh: Huolinhe lignite

caking, condensation and polymerisation, which occur inside the coal particle and influence the formation of char.

2.8.2.3 Particle fragmentation

Larger particles have the propensity to undergo fragmentation caused by thermal stresses and internal pressure build-up caused by the rapid release of volatile matter (Hanson *et al.,* 2002). Thermal fragmentation can be divided into two types, namely primary and secondary fragmentation. Primary fragmentation occurs during devolatilisation, while secondary fragmentation arises during combustion and gasification of chars when the internal pore structure further develops and pores are enlarged. When the pore size increases the connecting carbon bridges are weakened, with some of the bridges fragmenting. A third type of fragmentation, known as attrition fragmentation, also occurs due to mechanical interaction with inert materials and the development of small particles that are elutriated, but not burnt (Basu, 2006; Oka, 2004).

The possibility of particle fragmentation is influenced by various factors, which include both coal characteristics and external aspects such as particle heating rate, particle size and temperature. The way in which coal characteristics can be related to the possibility of primary fragmentation is done by estimating the pore resistance number (PRN), which is defined as the ratio of volatile matter to inherent moisture (Dakic *et al.,* 1989). A high PRN implies a greater resistance to volatile release, therefore promoting pressure build-up within the particle. Coals with a PRN of 15 - 17 tend to experience intensive fragmentation, while coals with smaller PRNs possess a suitable amount of pores to allow for easy passage of the volatiles (Oka, 2004).

Another characteristic that influences fragmentation is the swelling index. Authors such as Dakic *et al.* (1989) stated that the swelling index of the coal reduces the probability of fragmentation due to the plastic behaviour of the coal, which causes the particle to deform rather than break. In contradiction to the study done by Dakic *et al.* (1989), authors such as Boëlle *et al.* (2002) and Senneca *et al.* (2011) stated that swelling of coal particles can facilitate particle breakage, owing to the fact that swollen chars have thin and weak walls which easily break under additional stress. A high heating rate will facilitate particle fragmentation due to a high pressure build-up within the particle, caused by the rapid release of volatiles. A high heating rate can also lead to thermal shock of the particle, which leads to exfoliation breakage (Cai *et al.,* 1996; Senneca *et al.,* 2011).

Fragmentation influences gasification reactivity by altering the coal structure. Certain authors have found that fragmentation decreases the devolatilisation time and thus enhances the

devolatilisation rate. This is due to a reduction in coal depth to which the heat must be transferred (Stubington & Linjewile, 1989). Fragmentation of coal particles also leads to large openings in the coal structure that enhances gasification rates (Matzakos & Zygourakis, 1990).

2.9 Small and large particle kinetics

Numerous studies have been executed to determine the kinetics of different coals/chars under varying conditions such as temperature, gasification reagent, pressure, particle size *etc.* and to model the gasification behaviour of these different chars and conditions. For the purpose of this section the reviewed studies are divided into small and large particle studies with large particles referring to particle sizes above 1 mm, while small particles or pulverised fuels are defined as 1 mm and below.

2.9.1 Small particles studies

Wu *et al.* (2008) studied CO_2 gasification of chars prepared at varying pyrolysis temperatures and heating rates for entrained flow gasifier operations. The rapidly heated chars had a higher reactivity, while the results of the various gasification temperatures indicated that reactivity increases with the temperature till above 1100 °C where ash fusion starts increasing the intraparticle diffusion rate. The reaction for 950 – 1150 °C was chemically controlled, while for 1150 – 1400 °C the reaction rate was gas diffusion controlled. Liu *et al.* (2008) and Ochoa *et al.* (2001) also investigated high temperature CO_2 gasification of Chinese and Argentinean chars (sub-bituminous & high volatile bituminous) and found that at temperatures above 1150 and 1060 °C correspondingly, the regime shifted from chemically controlled to diffusion controlled mainly due to ash fusion. Studies done by both Ahn *et al.* (2009) and Roberts *et al.* (2010) also agreed with these findings, but stated that the shift to the diffusion regime is attributed to the shrinkage of the micropore surface area in addition to ash fusion. Liu *et al.* (2008) and Ochoa *et al.* (2001) modelled the gasification behaviour though the RPM, while Wu *et al.* (2008) utilised the MVM.

Jayaraman *et al.* (2015) investigated the effect of particle size on reactivity for high ash Indian chars prepared at different pyrolysis heating rates and gasified under varying conditions (temperature and reagent). The results indicated that reactivity increases with decreased particle size and that a trade-off existed between the chemical controlled and diffusion controlled regime as the temperature increased. The increased reaction rate with smaller particles is attributed to the larger surface area. The VM, SCM and RPM were utilised to model the gasification behaviour, with all three models fitting the data smoothly for CO_2 gasification.

Huo *et al.* (2014) studied the influence of both temperature and particle size on CO_2 gasification for different Chinese coals and cokes. The conclusions that were drawn are firstly that increased particle size decreases reactivity and that pore diffusion resistance influences the reaction rate more strongly with increased particle size and temperature. Furthermore the influence of particle size on reactivity is dependent on the coal properties, with the particle size of high reactivity coals having a more significant effect on reactivity and a stronger pore diffusion resistance. For temperatures below 1000 °C most of the particle sizes and coals were in the chemically controlled regime, while for temperatures above 1000 °C the effectiveness factor for the 100, 250 and 500 µm particles decreased below one and the rate of pore diffusion was no longer negligible.

Kim *et al.* (2011) investigated 12 different bituminous coals to determine the influence of coal type and particles size on CO_2 gasification reactivity. At temperatures below 1150 °C the reactions were chemically controlled, but as the temperature continued to increase diffusional resistance influenced the reaction rates. The results indicated positive correlations between the reactivity, volatile matter, alkali index, alkali ratio, specific surface area and meso pore-volume, while a negative relationship was observed for the ash values. The volatile matter and alkali ratio were shown to have the strongest association with reactivity; however, as temperature increased the meso-pore volume correlated better with reactivity in comparison to the alkali ratio. With regards to particle size, the reactivity decreased with an increase in size and the effect became more pronounced as temperature continued to increase. Additionally, activation energies also decreased with particle size. Lastly the SCM model was better suited in describing the kinetics of the larger particles, while the VM was more applicable to the smaller particles. The results of the modelling are presented in Figure 2.6.

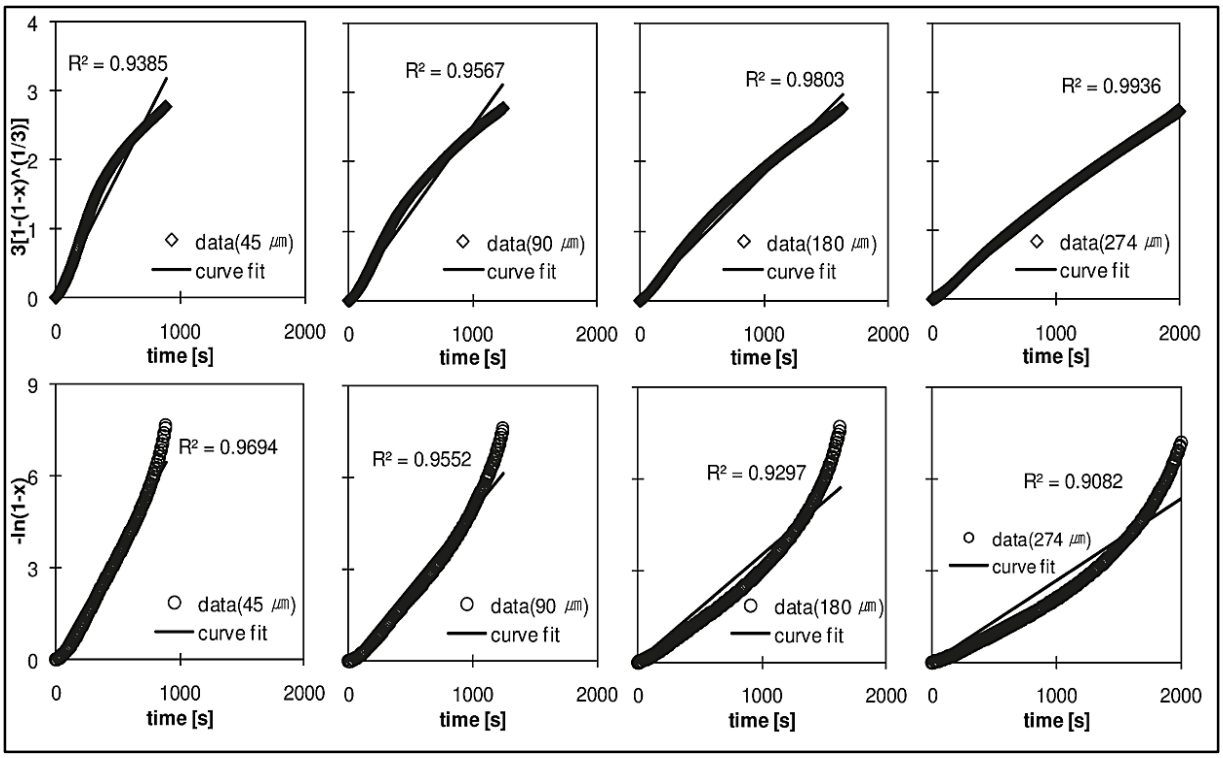

Figure 2.6: Kinetic modelling result for CO2 gasification of South African chars at 1050 °C: SCM (top) and VM (bottom) (Taken from Kim *et al.,* 2011).

Gomez & Mahinpey (2015) investigated the influence of different coal properties on reactivity in an attempt to develop a model which predicts CO_2 gasification rate constants based on the properties of the parent coals. The reaction conditions were chosen to ensure that reaction occurred in the chemically controlled regime. The results indicated that the carbon based micropore surface area and alkaline content of the coal had the greatest positive influence on the gasification rate, with these two parameters consequently utilised for the mathematical model. The model was a semi-empirical model based on the Arrhenius equation, which presented with a good fit for a wide range of ash yields.

The studies done by Wang *et al.* (2015), Silbermann *et al.* (2013) and Tomaszewicz *et al.* (2013) compared different models for describing the gasification behaviour. Wang *et al.* (2015) utilised the RPM, shrinking unreacted core model (SUCM) and VM model for the kinetic analysis for both isothermal and non-isothermal CO_2 gasification of anthracite. The RPM showed the highest correlation coefficient for both the isothermal and non-isothermal reactivity and was able to reflect the changing trend of the conversion rate. This is due to the RPM accounting for changes in the reaction surface.

Silbermann *et al.* (2013) investigated five different models to describe the CO_2 gasification of seven different Canadian coal samples. The aim of the study was to evaluate a newly developed method where the CO_2 is present throughout the entire experiment, without switching from N_2 to CO_2 after isothermal conditions are reached. This was done to more

accurately determine gasification reactivity at conditions experienced within industrial gasifiers. It was concluded that the ICM and normal distribution function (NDF) provided the best matches. The RPM model was not able to accurately describe the gasification behaviour, which was attributed to the different experimental method used to measure reactivity. The VM and SCM were able to describe the high reactivity coals accurately, but were not applicable to the low reactivity coals. Lastly Tomaszewicz *et al.* (2013) concluded that the SCM, RPM and MVM were suitable models to describe the CO_2 gasification of three different coals (lignite and sub-bituminous). The RPM and MVM described the gasification behaviour most accurately, due to incorporation of additional parameters in the kinetic expressions. The VM was not able to fit the data accurately. All the experiments were carried out in the chemically controlled regime. A summary of the relevant studies on small particle CO_2 gasification is given in Table 2.4.

Table 2.4: Previous studies on small particle gasification

Reference	Analysis technique	Particle size	Gasification reagent	Temperature (°C)	Pressure (MPa)	Models	Activation energy (kJ/mol)
Ahn *et al.* (2001)	PDTF*	45 – 64 µm	CO_2	900 - 1400	0.5 – 1.5	SUCM	72
Everson *et al.* (2006)	TGA	Pulverised chars	CO_2 & Steam	800 - 950	Ambient	SUCM – LH*	109 – 137 / 93 – 96
Everson *et al.* (2008b)	TGA	1 mm	CO_2	850 - 900	Ambient & 0.288	RPM	192 – 247
Everson *et al.* (2013)	TGA	1 mm	CO_2	900 – 950	Ambient	RPM	163 – 236 (CO_2)
Gomez & Mahinpey (2015)	TGA	< 90 µm	CO_2	800- 900	Ambient	ICM	117 - 233
Huang *et al.* (2010)	TGA	< 200 µm	CO_2/Steam	850- 950	Ambient	LH*, VM	74 – 216
Huo *et al.* (2014)	TGA	< 40 - 500 µm	CO_2	850- 1300	Ambient	Effectiveness factor	133 - 176
Jayaraman *et al.* (2015)	TGA	60 - 900 µm	CO_2 & Steam	900- 1000	Ambient	RPM, SCM, VM	130 – 214 (CO_2)
Kim *et al.* (2011)	Horizontal fixed bed reactor	45 – 274 µm	CO_2	1050 - 1400	Ambient	SCM, VM	23 – 137 (pore diff.) 125 – 207 (chemical)
Liu *et al.* (2008)	TGA	0.175 - 0.355 mm	CO_2	1000- 1300	Ambient	RPM	160 & 180
Ochoa *et al.* (2001)	TGA	< 45 µm	CO_2	900- 1160	Ambient	RPM	151 – 184
Roberts *et al.* (2010)	PEFR*	45 – 180 µm	CO_2	1000 - 1400	1 – 2	LH*	41 – 282
Sliberman *et al.* (2013)	TGA	< 90 µm	CO_2	800 - 900	Ambient	VM,SCM,ICM,RPM,NDF	117 - 233
Tomaszewicz *et al.* (2013)	TGA	< 200 µm	CO_2	900- 1000	Ambient	RPM,MVM,VM,SCM	180 & 240
Wang *et al.* (2015)	TGA	0.074 mm	CO_2	900 -1000	Ambient	RPM, SUCM, VM	213
Wu *et al*. (2008)	TGA	< 73 µm	CO_2	950- 1400	Ambient	MVM	14 – 205
Zhang *et al.* (2006a)	TGA	< 0.1 mm	CO_2 & Steam	920 - 1050	0.02 – 0.1	VM, SCM	146 – 201 (CO_2) 214 – 250 (H_2O)

* LH – Langmuir Hinshelwood *PDTF – Pressurised drop tube furnace * PEFR – Pressurised entrained-flow reactor

2.9.2 Large particle studies

Large particle gasification has not been as extensively studied as small particle or pulverised coal gasification. Most of the large particle kinetic studies were done for steam gasification or a mixture of CO_2 and steam.

Jayaraman & Gokalp, (2015) studied CO_2, steam and CO_2/steam gasification for high ash Turkish coals with particle sizes between 0.8 and 3 mm. The purpose of the study was to investigate the influence that pyrolysis heating rates have on the reactivity of the chars. From the results they firstly concluded that the chars that underwent rapidly heated pyrolysis had a higher reactivity, which agrees with the results of both Wu *et al.* (2008) and Jayaraman *et al.* (2015). The CO_2 reactivity results indicated that for larger particle gasification, diffusion restrictions and heat transfer limitations cannot be neglected as the reactivity was slower than that of the small particles. The reaction rate vs. conversion graph, given in Figure 2.7, indicated that the initial CO_2 reactivity increases rapidly until a conversion of 20 to 40% after which the reactivity starts to decrease.

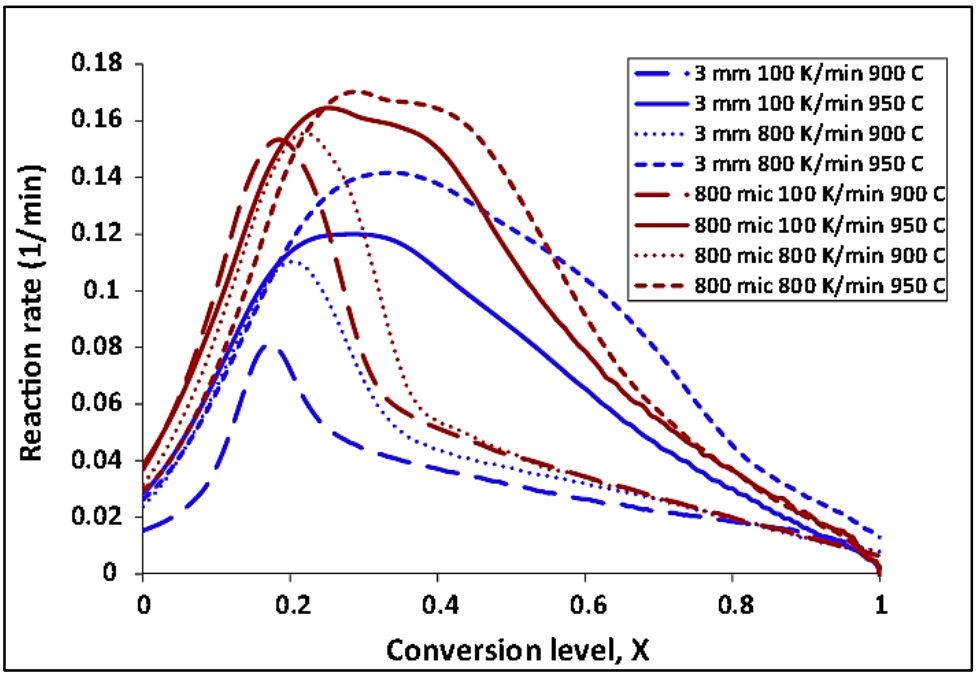

Figure 2.7: Reaction rate vs. time graph for large particle CO_2 gasification (Taken from Jayaraman & Gokalp, 2015).

This is due to the growth of the pore structure in the initial stages of gasification followed by the gradual collapse of the structure as gasification proceeds and CO inhibition affects reactivity. Three kinetic models namely, VM, SCM & RPM were utilised so determine the kinetic parameters, with all three models being able to closely predict the activation energy of the experimental conditions.

Ye *et al.* (1998) conducted a study similar to Jayaramen & Gokalp (2015). For this study the CO_2 and steam gasification reactivity of Australian coals with particle sizes between 0.8 and 3 mm were investigated. From the results they concluded that for both steam and CO_2 gasification the reaction occurred uniformly within the particles at a gasification temperature of 765 °C and therefore particle size did not influence the reactivity. The VM and SCM was utilised for the kinetic modelling with both models fitting the data satisfactory. Although both models fitted the data well, Ye *et al.* (1998), concluded that the VM was best suited to fit the data as this model is independent of particle size in contrast to the SCM.

Coetzee *et al.* (2013) studied the large particle steam gasification of raw and K_2CO_3 impregnated coals at 800 to 875 °C. Similar to the results of Ye *et al.* (1998) it was concluded that the reactivity was independent of particles size and that reaction was chemically controlled. The VM was also utilised to evaluate the gasification behaviour and was able to accurately predict the data up to a conversion of 70%.

Isothermal CO_2 gasification kinetics of two sub-bituminous coals were investigated by Veca & Adrover (2014). The particle size varied from 0.125 to 1.4 mm and the gasification temperature from 800 to 1100 °C. The results indicated that at 800 and 850 °C the influence of particle size was negligible, but as the temperature increased above 850 °C, mass transfer limitations influenced the large particles and decreased reactivity. Three gasification models were applied to the experimental data, namely the VM and the SCM for the reaction controlled regime and the SCM for the diffusional controlled regime. The VM was not able to accurately fit the data. For the small (0.125 – 0.15 mm) to medium sized particles (0.15 – 0.25 mm) the SCM with diffusion resistance was able to accurately predict the experimental data, but appeared to over predict for the large particle (1 – 1.4 mm) gasification, which they concluded was due to the non-uniform distribution of solid reagents within the particle. For this reason they derived a formula for the SCM that accounts for the non-uniform distribution of the solid reagent and were able to predict the gasification behaviour for the large particles, with a non-uniform distribution of solid reagents.

Wu *et al.* (2006) studied steam gasification of 3 – 6 mm Chinese chars. From the results it was found that gasification temperatures had greater influence on reactivity when compared to the pyrolysis temperatures, increasing reactivity with temperature. Chars prepared at higher pyrolysis temperatures have a lowered reactivity, but as the gasification temperature increases the lowering effect of the pyrolysis temperature on reactivity decreases. The gasification reactivity was modelled utilising both the VM and SUCM. The VM was not able to accurately fit the experimental data for char steam gasification as a result of gas diffusion limitations. Both the SUCM for reaction controlled regime and diffusion controlled regime was

implemented, with the latter being more accurate in modelling the data. The modelling results indicated that diffusion limitations increased with increasing temperature, but that the effect was limited and that as a whole the reactions could still be observed as being chemically controlled.

Guizani *et al.* (2015) examined the influence of temperature and particle size for CO_2 and steam gasification of biomass. The results for CO_2 gasification indicated that as the particle size increases at temperatures above 900 °C diffusional limitations decreased reactivity. For the modelling of the gasification the effectiveness factor approach was utilised to quantify the extent of internal diffusion limitations, with both CO_2 and steam has similar effectiveness factors.

A summary of some of the studies done on large particle gasification is given in Table 2.5.

Table 2.5: Previous studies in large particle gasification

Reference	Analysis technique	Particle size	Gasification reagent	Temperature (°C)	Pressure (MPa)	Model	Activation energy (kJ/mol)
Coetzee *et al.* (2013)	TGA	5 & 10 mm	Steam	800 - 875	Ambient	VM	191
Guizani *et al.* (2015)	TGA	0.04 – 13 mm	CO_2/Steam/mixture	800 - 1100	Ambient	Effectiveness factor approach	202 – 208
Hanson *et al.* (2002)	TGA	0.5 - 2.8 mm	Steam, CO_2	900	2	-	-
Huang & Watkinson (1996)	Stirred bed reactor	0.85 - 3 mm	Steam	750 - 900	Ambient	Semi-empirical kinetic expression	57 – 132
Jayaraman & Gokalp (2015)	TGA	0.8 & 3 mm	CO_2/Steam /mixture	850 - 950	Ambient	RPM, SCM, VM	116 – 139 (CO_2)
Kasaoka *et al.* (1985)	Quart tube reactor	0.5 – 2 mm	CO_2 & Steam	800 - 1400	Ambient	MVM	197 – 310 (CO_2)
Koba & Ida (1980)	TGA	3 - 6 mm	CO_2/ Steam/mixture	1200	Ambient	-	-
Veca & Adrover (2014)	TGA	0.125 – 1.4 mm	CO_2	800 - 1100	Ambient	SCM, VM	176 – 188
Wu *et al.* (2006)	Fixed-bed reactor	3 – 6 mm	Steam	900 - 1200	Ambient	SUCM, VM	127 – 197
Ye *et al.* (1998)	Quartz tube reactor	0.8 - 3 mm	CO_2 & Steam	714 - 892	Ambient	SCM, VM	91

2.10 Summary

Coals utilised for solid-based pre-reduction should preferably possess desired characteristics to ensure that optimum pre-reduction values are achieved within the kiln. A suitable CO_2 reactivity is a preferred characteristic, as this property directly influences the degree of pre-reduction achieved within the rotary kiln. CO_2 gasification reactivity is closely related to coal properties, with certain properties promoting gasification reactivity, while others inhibit reactivity. Numerous authors have investigated the influence of these various properties on reactivity for different operating conditions. In addition to coal properties, external conditions such as operating temperature, particle size and fragmentation influence the CO_2 reactivity and furthermore also the effect of the coal properties on CO_2 reactivity.

Small particle CO_2 gasification has been extensively studied for numerous coals at different operating conditions. The RPM was mostly utilised to describe the gasification behaviour and kinetics of the small particles. Large particle gasification has not been as extensively investigated as small particles. Authors have generally found that reactivity tends to decrease with particle size; however, some did not observe an influence. Most studies utilised the SCM for the diffusional controlled regime to model the gasification behaviour of large particles.

CHAPTER 3: Coal preparation and characterisation

3.1 Introduction

In this chapter a detailed discussion on the characteristics of the coals and chars utilised for the reactivity experiments is given. The method for coal selection and the manner in which the different samples were prepared is detailed (Section 3.2 – 3.3) followed by a description of the analyses, methods and procedures (Section 3.4). The results of the various coal and char analyses which include chemical, mineralogical, thermal, petrographic and physical characterisation are discussed in Section 3.5. This includes a comparison of the different samples as well as a comparison with the preferred values as reported in Table 2.2. The chapter concludes with a summary in Section 3.6.

3.2 Sample origin and selection

Nine different washed coals, originating from the South African Highveld, Witbank and Ermelo coalfields were investigated. The samples are named according to the description, seam number and vitrinite content (vol.%) on an air dried basis (a.d.b) *e.g.* AC-5-72 is the alternative coal, originates from seam five and has a vitrinite content of 72 vol.%. As a benchmark, BC-5-53 is used[2]; BC-5-53 was utilised in the past by EHSV as a pre-reduction coal, but due to the depletion of the mine this coal could no longer be used. BC-5-53 was obtained from an archived sample at the North-West University (NWU). The archived sample was obtained in 2009 and stored in large plastic containers inside the coal stores. Two of the samples namely FC-2-13 and FC-2-21 are currently used as a blend by EHSV for pre-reduction.

The remaining six coals were identified as suitable pre-reduction coals. The criteria for selecting the coals were the following:

- The coals had to originate from a mine that was in close proximity to EHSV (< 200 km).
- The mine that sourced the coals has to have a life-of-mine that exceeds ten years, to ensure availability of the coal.

The coal selection was done in consultation with EHSV and the Bulletin 114 (Pretorius *et al.,* 2002). In Table 3.1, the nine selected coals are listed.

[2] Coding was used for intellectual property (IP) reason

Table 3.1 Selected coals

Coal	Seam	Coalfield	Distance from EHSV (km)	Description
BC-5-53	5	Witbank	22	Benchmark coal
FC-2-13	2	Witbank	125	Currently used
FC-2-21	2	Witbank	160	Currently used
AC-5-72	5	Highveld	81	Alternative feedstock
AC-5-50	5	Witbank	60	Alternative feedstock
AC-4-56	4	Witbank	91	Alternative feedstock
AC-4-41	4	Witbank	41	Alternative feedstock
AC-4-22	4	Witbank	76	Alternative feedstock
AC-LC-41	Lower C	Ermelo	50	Alternative feedstock

3.3 Sample preparation

The sample preparation methods are illustrated in Figure 3.1.

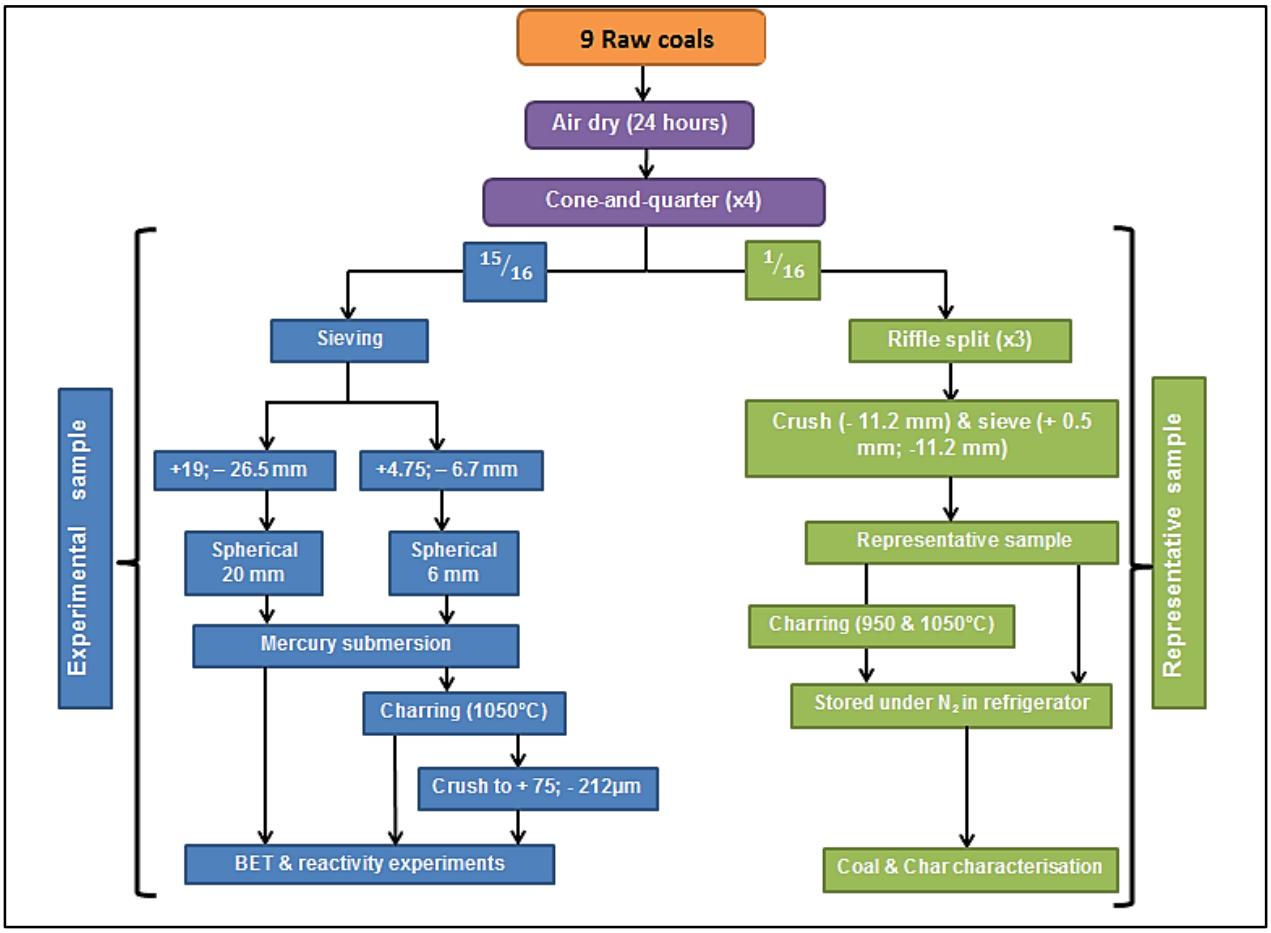

Figure 3.1: Sample preparation method

The first step of the preparation was to air dry the samples for a period of 24 hours. Two types of samples were prepared namely an experimental and a representative one. The experimental sample was utilised for the structural characterisation of coals and chars as well

as the reactivity experiments, while the representative sample was used for the chemical, mineral, petrographic and thermal characterisation.

3.3.1 Representative sample

The representative sample was obtained by firstly cone-and-quartering the bulk sample. The bulk sample (typically > 100 kg) was placed on a flat clean tarp and the cone-and-quarter method was applied four times to obtain one sixteenth of a sample (Allen & Khan, 1970). The sample was then sent through a riffle splitter three times to obtain representative samples for the various laboratories. Afterwards the sample was crushed to - 11.2 mm and the fines were sieved out. The majority (80%) of the representative sample was between 4.75 and 11.2 mm. For the archived BC-5-53 sample, the representative sample was prepared by sieving the cone-and-quartered sample to only include + 13.2 mm particles. Due to the age of the sample, only large particles were selected in order not to use particles that were severely oxidised. The results of the proximate and ultimate were compared to that of the former study and no significant differences were observed, therefore the sample is still suitable for usage. The particles were then crushed and fines were removed. The coal representative samples were stored in two Ziploc bags under a nitrogen atmosphere in the refrigerator. All the sieves, the tarp and riffle splitter were cleaned with compressed air prior to usage.

The char representative samples were further prepared at 950 and 1050 °C respectively in a TMH16/75/610 horizontal tube furnace (supplied by Elite Thermal systems Ltd.) with a nitrogen flow of 6 Nl/min. The furnace was first heated to the desired temperature, once the temperature stabilised the sample was loaded into the heating zone and kept in the zone for 30 minutes. Afterwards the sample was moved to a cooler zone within the furnace for an additional 30 minutes. After charring the samples were weighed and the mass loss was compared to the proximate results of the coal (Table 3.5) to ensure that all the volatiles were removed. Lastly the samples were placed in two Ziploc bags under a nitrogen atmosphere in the refrigerator.

All samples were then further prepared according to the ISO 13909-4: 2001 standard, upon the arrival at the respective laboratories. For the X-ray diffraction analysis (XRD) 50 g of each representative coal and char sample was crushed to - 75 µm, while the ash samples were prepared during the CO_2 gasification experiments.

3.3.2 Experimental samples

The experimental samples were prepared by firstly sieving the bulk sample into two size fractions: +19; -26.5 mm and +4.75; -6.7 mm.

From the first size fraction (+19; -26.5 mm) particles that are referred to as 20 mm particles, with dimensions close to 20 mm were selected. A grid was used to measure the particles on a three dimensional basis, namely length, width and height. If the particles were slightly outside the grid range or had sharp edges, pliers were used to reduce the particle size and remove sharp edges. Afterwards the selected particles were also sandpapered to remove remaining sharp edges and to ensure that the particles were more uniform in size and near spherical. In Figure 3.2 an example of a typical 20 mm particle is shown.

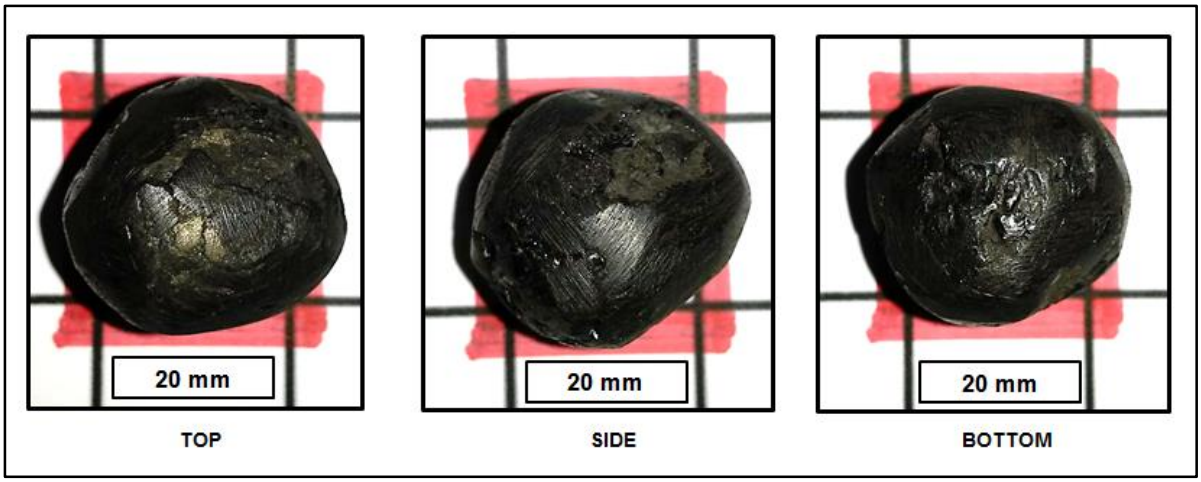

Figure 3.2 Example of a 20 mm particle utilised for CO_2 reactivity analysis

The acceptable dimensions of the particles were taken as 20 ± 3 mm. From the second size fraction (+4.75; -6.7 mm) particles referred to as the 6 mm particle were selected. A sized grid was used to measure the sample on a three dimensional basis, with the acceptable particle dimensions being taken as 6 ± 0.5 mm. If the particles were slightly larger or had sharp edges, pliers were used to modify the particles. In Figure 3.3 an example of a typical 6 mm particle is shown.

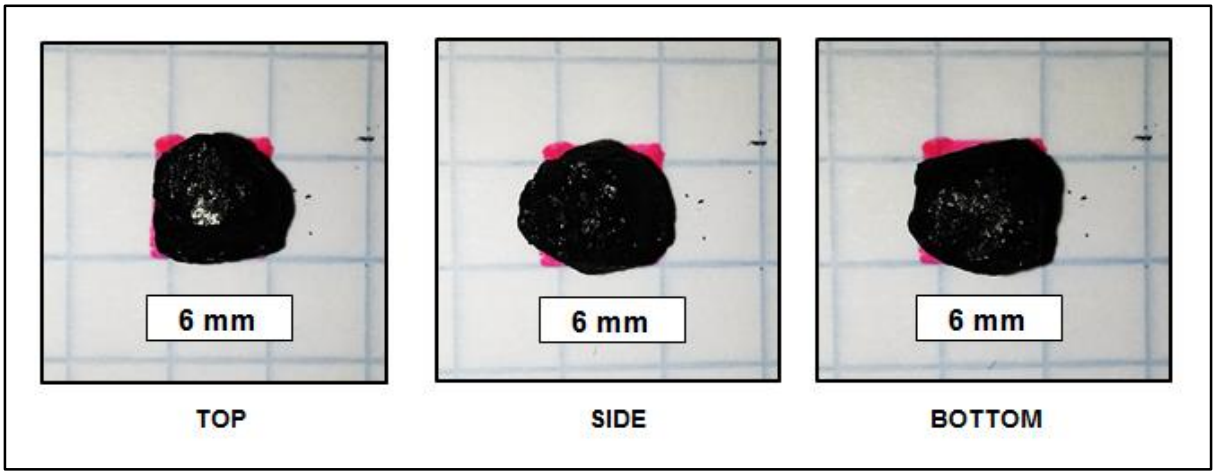

Figure 3.3 Example of a 6 mm particle utilised for CO_2 reactivity analysis

After selection and density preparation (Section 3.3.3) the 6 mm particles were charred at 1050 °C in a TMH16/75/610 horizontal tube furnace with a nitrogen flow of 6 Nl/min to reduce

the impact of pyrolysis conditions on the kinetic characteristics of the chars (see Appendix B for temperature profile and flow calibration curve). Once charring was completed the samples were weighed and compared to the proximate results of the coal, after which a fraction of the chars were re-screened and stored under nitrogen atmosphere in the refrigerator. The remaining fraction was crushed into smaller particles referred to as 212 µm particles (+ 75; 212 µm) and stored in the same manner.

3.3.3 Density preparation

Mercury submersion was conducted to determine particle density of either a single 20 mm particle or an average density of multiple 6 mm particles. The density range of each coal sample was determined, after which particles within the most frequently appearing density range were selected and used for the reactivity experiments and CO_2 adsorption analysis. The experimental equipment and procedure for mercury submersion is given Section 3.3.3.1 to 3.3.3.3.

3.3.3.1 Experimental set-up

The experimental equipment used for mercury submersion consisted of a laboratory balance, double distilled mercury supplied by Associated Chemical Enterprises (ACE) chemicals (13534 kg/m^3; Purity >99.5%) and a particle plunger. The experimental set-up is given in Figure 3.4.

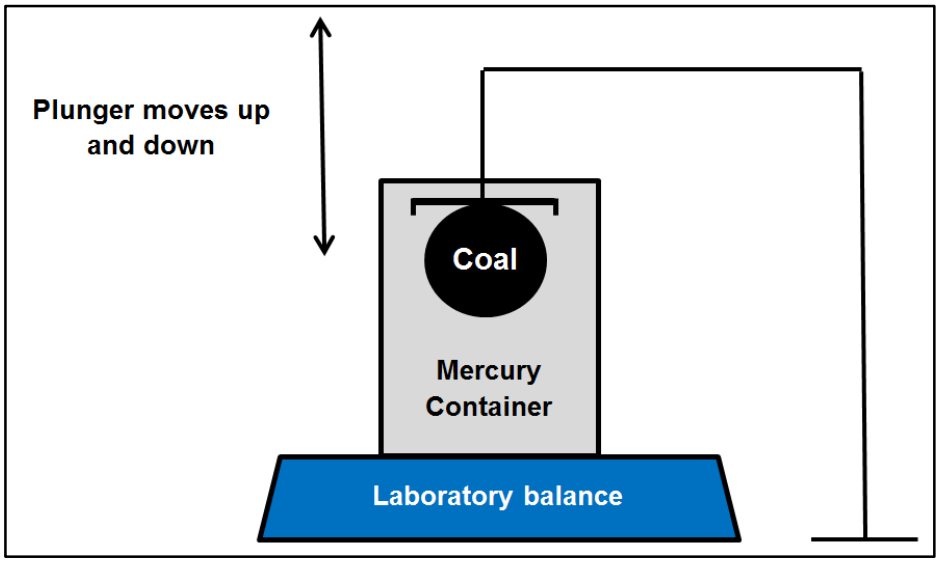

Figure 3.4: Experimental set-up of mercury submersion analysis

A laboratory balance (Sartorius ED 4202S) with a capacity of 4200 g and an accuracy of 0.01 g was used. The entire experimental set-up was located in a ventilation chamber. The mercury filled container was placed on the scale, with the basket plunger located above both the scale and container. The accuracy of the mercury submersion set-up was tested using a 28.5 mm stainless steel ball, with a density of 7833 kg/m^3. This analysis was performed on

ten separate occasions during the mercury submersion runs, with an average difference of 1.5%.

3.3.3.2 Experimental procedure

For the 20 mm density determination, single coal particles were used, while for the 6 mm density determination ten particles were submerged from which the average density of the particles was measured. The first step was to determine the mass (m_{coal}) of the coal particle. Secondly the mass of the submerged plunger ($m_{plunger}$) was determined, followed by the mass of both the submerged particle and plunger ($m_{coal+plunger}$). The particle density was then calculated by utilising Archimedes' principle as given in Equation 3.1 (Walker *et al.,* 2008):

$$\rho_{coal} = \left(\frac{m_{coal}}{m_{coal+plunger} - m_{plunger}}\right) \times \rho_{mercury} \tag{3.1}$$

The experimental procedure was repeated three times in order to determine repeatability and error of the density results. A confidence level interval of 95% was selected when determining the error, with the largest error obtained being 7%.

3.3.3.3 Selected densities

The density ranges selected for the various coal samples are presented in Table 3.2.

Table 3.2: Selected density cuts and average densities for the 20 and 6 mm coal particles.

Coal	Density range (kg/m^3)	Average density (kg/m^3)
BC-5-53	1300 – 1400	1337
AC-5-72	1200 – 1300	1288
AC-5-50	1300 – 1400	1337
AC-4-56	1300 – 1400	1342
AC-4-41	1300 – 1400	1342
AC-4-22	1400 – 1500	1451
FC-2-13	1300 – 1400	1346
FC-2-21	1300 – 1400	1367
AC-LC-41	1300 – 1400	1346

As can be seen almost all of the density ranges are between 1300 and 1400 kg/m^3, which correlates with a bituminous coal, as this coal typically has a density of between 1280 and 1350 kg/m^3 (Speight, 2005). AC-5-72 has a lower density range of 1200 to 1300 kg/m^3, the reason being that this coal has a low ash value and high vitrinite content. AC-4-22 has a higher density range of between 1400 and 1500 kg/m^3, which is due to the coal's high ash

value (Tsai, 1982). See Appendix A.1 for the density distribution curve of each coal sample, as well as for the results of the 6 mm chars of phase two.

3.3.4 CO_2 BET sample preparation

The sample preparation for the CO_2 Brunauer-Emmert-Teller (BET) analysis is divided into two sections, as this analysis was conducted on both coal and char particles. For the coal analysis 6 and 20 mm particles were crushed to -212 µm and stored in the refrigerator under nitrogen until the analysis was performed.

20 mm char samples were prepared in the TGA (Section 4.3). The density selected 20 mm char particles were prepared at 950 and 1050 °C respectively. The vertical tube furnace was heated to the desired temperature at a nitrogen flow of 8 Nl/min and allowed to stabilise. Once the temperature stabilised, three 20 mm particles were directly inserted into the heating zone for a holding time of 30 minutes, after which the furnace was raised and the particles were held in a cooler zone for another 30 minutes. Six 20 mm char particles were prepared per temperature per coal sample. For the 6 mm a fraction of the crushed chars (-212 µm) prepared for the reactivity experiments was utilised for the analysis.

3.4 Coal and char characterisation analyses and standards

Once the representative samples were prepared the samples were sent to different laboratories for coal and char characterisation analyses. In Table 3.3 the characterisation analyses and the respective laboratories where they were performed, is summarised.

Table 3.3 Coal and char characterisation analyses

Property	Analysis	Sample	Laboratory responsible
Chemical & Mineralogy	Proximate	Coal & Char	Bureau Veritas Testing and Inspection
	Ultimate	Coal & Char	Bureau Veritas Testing and Inspection
	Calorific value	Coal & Char	Bureau Veritas Testing and Inspection
	Total sulphur	Coal & Char	Bureau Veritas Testing and Inspection
	Forms of sulphur	Coal	UIS analytical services
	Mineral (XRD)	Coal, Char & Ash	North-West University
	Ash (XRF)	Coal	Sci-ba laboratories
Thermal	Ash fusion temperature	Coal	Bureau Veritas Testing and Inspection
	Free swelling index	Coal	Bureau Veritas Testing and Inspection
Petrographic	Maceral composition	Coal	Bureau Veritas Testing and Inspection
	Vitrinite reflectance	Coal	Bureau Veritas Testing and Inspection
Structural	CO_2 adsorption	Coal & Char	North-West University

3.4.1 Chemical, mineral and thermal analyses

All sample analyses were conducted according to standard methods. In Table 3.4 the standards followed for the chemical, mineral and thermal analyses are given.

Table 3.4 Standard methods followed for the chemical, mineral and thermal coal analyses

Analysis	Standard
Chemical and Mineral	
Proximate	
• Inherent moisture	ISO 11722:1999
• Ash yield	ISO 1171:2010
• Volatile matter	ISO 562: 2010
• Fixed carbon	By difference
Ultimate (C, H, N and O by difference)	ISO 29541: 2010
Total sulphur	ISO 19579: 2006
Calorific value	ISO 1982: 2009
XRF	In-house developed method, calibrated with international matrix Certified Reference Materials
Thermal	
Free swelling index	ISO 1982: 2009
Ash fusion temperature	ISO 540: 2008

3.4.2 Petrographic analysis

The coal petrographic analyses were carried out according to ISO 7404: 1994 Part 1 to 5, more specifically maceral analysis was done in accordance with ISO 7404 part 3, which is the 500 point count technique. The vitrinite reflectance was done in accordance with ISO 7404 part 5. Both the maceral composition and vitrinite reflectance analysis were conducted using a Zeiss Axio Imager M2m and magnification of x50 under oil immersion. The rank was determined according to ISO 11760 – Classification of coals.

3.4.3 Structural analysis

The CO_2 adsorption analysis was done using a Micromeritics Accelerated Surface Area and Porosimerty System (ASAP) 2020, which allows the determination of pore sizes 3.5 to 5000 Å (Micrometrics, 2015). Prior to degassing, the samples were dried in an oven at 105 °C for 24 hours. 200 mg coal samples were then degassed at 75 °C and 4 µm Hg for another 24 hours, while the char samples were degassed at 380 °C and 4 µm Hg for 24 hours. After degassing, CO_2 was used as the absorbent at 273.15 K to determine the micropore structure. The temperature of the sample was controlled through the use of an ice bath. The short coal

method was used for analysis, which includes the following measuring techniques; BET, Langmuir, Dubin-Radushkevich (D-R), Horvath-Kawazoe (H-K). The micropore surface area and monolayer capacity were determined through the D-R equation, while the H-K method was used to determine the micropore volume and median pore width (Micrometrics, 2006). The carbon micropore surface area is the ratio of the surface area to carbon content as determined by the ultimate analysis (Silberman *et al.,* 2013). The BET and Langmuir surface area were determined from isotherm data. The micropore porosity was determined using the following formula (Gregg & Sing, 1982):

$$\varepsilon = \rho_b \int \left(\frac{dV}{dD_{pore}}\right) \cdot dD_{pore} \tag{3.2}$$

3.4.4 XRD analysis

PANalytic Inc. XRD along with Rietveld-based X'Pert Highscore Plus Software was used for the mineralogical analysis, with copper utilised as the X-ray source (Speakman, 2012).

3.5 Results and Discussion

3.5.1 Chemical analyses

3.5.1.1 Proximate analysis

In Table 3.5 the proximate and calorific results of the nine coal samples are given. Firstly when comparing the overall results to previous studies it is seen that the results are comparable with the values of typical South African coals (Coetzee *et al.,* 2013; Everson *et al*., 2013; Hattingh *et al.,* 2013; Pretorius *et al.,* 2002).

The ash values of the coals are low, which is due to the coals being washed (Speight, 2005). The ash yield ranges from a minimum value of 10.1 wt.% for AC-5-72 to a maximum value of 25.8 wt.% for AC-4-22. The desired ash yield of coals utilised for pre-reduction is 5 to 25 wt.% and therefore eight coals are well suited for pre-reduction in terms of the ash yield (Carpenter, 2004; Chatterjee, 2010; Sarangi & Sarangi, 2011).

The volatile values range from 22 to 34 wt.%. According to Carpenter (2004) and Mashhandi *et al.* (2008) the desired volatile content for pre-reduction coals is between 25 and 30 wt.%. The only coals that fall within this range are AC-4-41, FC-2-21 and AC-LC-41. The seam five coals, as well as AC-4-56 have slightly higher volatile values, while AC-4-22 and FC-2-13 have values marginally below this range. The fixed carbon values of all nine coals are within the desired range, which is 45 to 60 wt.% (Carpenter, 2004; Chatterjee, 2010; Sarangi & Sarangi, 2011).

The fuel ratio (fixed carbon/volatile matter) was estimated with the values of all nine coals falling within the range of a bituminous coal (Van Krevelen, 1981). The gross calorific values were determined, with AC-5-72 having the highest value which correlates with it having the lowest fuel ratio. AC-4-22 has the lowest calorific value, due to its high ash value.

Table 3.5 The proximate and calorific value results for coal samples (a.d.b.)

		BC-5-53	AC-5-72	AC-5-50	AC-4-56	AC-4-41	AC-4-22	FC-2-13	FC-2-21	AC-LC-41
Parameter	**Unit**									
Proximate										
Inherent moisture	wt.%	4.6	7.1	4.2	3.8	2.8	3.6	2.5	2.8	2.3
Ash yield	wt.%	12.9	10.1	14.2	13.6	16.3	25.8	16.4	19.6	18.9
Volatile matter	wt.%	32.0	34.3	31.7	33.5	28.4	23.9	22.4	25.1	29.3
Fixed carbon	wt.%	50.5	48.5	49.9	49.1	52.5	46.7	58.7	52.5	49.5
Total	**wt.%**	**100.0**	**100.0**	**100.0**	**100.0**	**100.0**	**100.0**	**100.0**	**100.0**	**100.0**
Fuel ratio (FC/VM)	**-**	**1.6**	**1.4**	**1.6**	**1.5**	**1.9**	**1.9**	**2.6**	**2.1**	**1.7**
Gross calorific value	**MJ/kg**	**26.8**	**26.9**	**26.7**	**26.5**	**25.9**	**21.7**	**26.7**	**25.4**	**25.4**

The proximate results for the chars prepared at 950 and 1050 °C respectively are given in Table 3.6. Firstly when comparing the results of the coals and chars, it is seen that small amounts of moisture and volatile matter remain after charring, while the ash yield and fixed carbon increases. This is due to an increase in aromatic carbon, which is caused by the release of aliphatic carbon, hydrogen and oxygen during devolatilisation (Gale *et al.,* 1996). Similar results were obtained by Everson *et al.* (2008a), Everson *et al.* (2013) and Roberts *et al.* (2015a) for South African chars prepared at various temperatures. In general AC-4-22 has the highest ash yield at both temperatures, which correlates with this sample having the highest coal ash yield. Additionally AC-4-22 has the highest remaining volatile content for each temperature, while BC-5-53 has the highest fixed carbon values.

By comparing the results of the 950 °C chars to the 1050 °C chars it is observed that the moisture and volatile matter is lower for the chars prepared at 1050 °C, which is due to the higher charring temperature that promotes the release of these two constitutes. Particles prepared at 1050 °C also fragment more severely, further increasing the release of volatiles and moisture. The fuel ratio of the chars increased compared to the coal values, due to the removal of volatile matter and increase in fixed carbon. The gross calorific value decreased slightly with charring temperature.

Proximate analysis was also done on the 6 mm chars utilised for phase two, refer to Table A.2 for the results.

Table 3.6: The proximate and calorific value results for char samples (a.d.b.)

		BC-5-53		AC-5-72		AC-5-50		AC-4-56		AC-4-41		AC-4-22		FC-2-13		FC-2-21		AC-LC-41	
Charring temperature (°C)		**950**	**1050**	**950**	**1050**	**950**	**1050**	**950**	**1050**	**950**	**1050**	**950**	**1050**	**950**	**1050**	**950**	**1050**	**950**	**1050**
Parameter	**Unit**																		
Proximate																			
Inherent moisture	wt.%	1.0	0.4	0.9	0.6	0.9	0.3	1.0	0.3	0.7	0.2	0.3	0.0	0.5	0.2	0.6	0.2	0.7	0.3
Ash yield	wt.%	19.3	17.9	22.7	19.4	21.5	21.9	20.8	23.7	22.0	22.4	33.9	34.7	22.8	23.0	22.1	23.0	28.9	29.8
Volatile matter	wt.%	1.2	0.6	1.1	0.8	1.0	0.7	1.2	0.8	1.5	1.0	1.7	1.2	1.2	0.4	1.0	0.6	1.5	0.7
Fixed carbon	wt.%	78.5	81.1	75.3	79.2	76.6	77.1	77.0	75.2	75.8	76.4	64.1	64.1	75.5	76.4	76.3	76.2	68.9	69.2
Total	**wt.%**	**100.0**	**100.0**	**100.0**	**100.0**	**100.0**	**100.0**	**100.0**	**100.0**	**100.0**	**100.0**	**100.0**	**100.0**	**100.0**	**100.0**	**100.0**	**100.0**	**100.0**	**100.0**
Fuel ratio (FC/VM)	**-**	**65.4**	**141.1**	**66.3**	**104.8**	**77.0**	**107.8**	**66.9**	**90.1**	**51.4**	**78.8**	**38.4**	**53.0**	**65.4**	**184.0**	**80.4**	**133.7**	**47.2**	**95.5**
Gross calorific value	**MJ/kg**	**25.2**	**24.6**	**24.5**	**25.8**	**24.9**	**23.1**	**25.6**	**24.9**	**26.3**	**25.0**	**21.3**	**20.4**	**23.2**	**21.4**	**22.4**	**21.1**	**21.6**	**20.6**

The fixed carbon and gross calorific values were used to rank the coals and chars according to the American Society of Testing and Materials (ASTM) system. The ranks are given in Table 3.7. Most of the coals are ranked as high-volatile B bituminous, with the exception of FC-2-13 and FC-2-21 which are ranked as medium-volatile bituminous due to their fixed carbon value being greater than 69 wt.%. The rank of all the chars increased to meta-anthracite due to the increased fixed carbon values (> 98wt% d.m.m.f.b) (Speight, 2005).

Table 3.7 Rank of coals according to the ASTM system

Sample	Coal	Char – 950 °C	Char – 1050 °C
BC-5-53	High-volatile B bituminous	Meta-anthracite	Meta-anthracite
AC-5-72	High-volatile B bituminous	Meta-anthracite	Meta-anthracite
AC-5-50	High-volatile B bituminous	Meta-anthracite	Meta-anthracite
AC-4-56	High-volatile B bituminous	Meta-anthracite	Meta-anthracite
AC-4-41	High-volatile B bituminous	Meta-anthracite	Meta-anthracite
AC-4-22	High-volatile B bituminous	Meta-anthracite	Meta-anthracite
FC-2-13	Medium-volatile bituminous	Meta-anthracite	Meta-anthracite
FC-2-21	Medium-volatile bituminous	Meta-anthracite	Meta-anthracite
AC-LC-41	High-volatile B bituminous	Meta-anthracite	Meta-anthracite

3.5.1.2 Ultimate analysis

The elemental composition of the coal was determined through the ultimate analysis, with the results presented in Table 3.8. The findings indicate that the elemental composition of the coals do not differ significantly. FC-2-13 has the highest carbon value, while AC-4-22 has the lowest, similar to the fixed carbon values reported in Table 3.5. The total sulphur values for AC-5-50, AC-4-41 and AC-LC-41 are high in comparison with the other samples. Typically a total sulphur value of below 1.0 wt.% is desired to reduce the amount of sulphur pick-up in the sponge iron, which is mainly organic sulphur (Chatterjee, 2010; Sarangi & Sarangi, 2011).

The results of the ultimate analysis for the chars are presented in Table 3.9. It is observed that the hydrogen and oxygen content decreased with charring, with the hydrogen content being insignificant for many of the 1050 °C chars. The carbon content in turn increases with charring temperature. The nitrogen and sulphur content remained constant, which illustrates that these species are incorporated into the carbon structure and therefore only partially devolatilised. AC-4-41 once more contains the highest total sulphur concentration along with BC-5-53. In general similar results were obtained by both Everson *et al.* (2008a) and Roberts *et al.* (2015a).

Table 3.8: Ultimate analysis results of coals (d.a.f)

		BC-5-53	AC-5-72	AC-5-50	AC-4-56	AC-4-41	AC-4-22	FC-2-13	FC-2-21	AC-LC-41
Parameter	**Unit**									
Carbon	wt.%	81.1	80.2	81.6	80.5	81.5	78.5	84.7	82.7	81.0
Hydrogen	wt.%	5.4	5.7	5.5	5.5	4.9	4.7	4.4	4.8	5.3
Nitrogen	wt.%	2.3	2.4	2.0	2.1	2.1	1.9	2.1	2.1	2.1
Oxygen	wt.%	10.4	11.1	9.9	11.0	10.2	14.3	8.4	9.9	10.3
Total sulphur	wt.%	0.8	0.6	1.0	0.9	1.3	0.6	0.4	0.5	1.3
Atomic H/C ratio	-	**0.80**	**0.85**	**0.81**	**0.81**	**0.71**	**0.71**	**0.62**	**0.70**	**0.78**
Atomic O/C ratio	-	**0.10**	**0.10**	**0.09**	**0.10**	**0.09**	**0.14**	**0.07**	**0.09**	**0.10**

Table 3.9: Ultimate analysis results of chars (d.a.f)

		BC-5-53		AC-5-72		AC-5-50		AC-4-56		AC-4-41		AC-4-22		FC-2-13		FC-2-21		AC-LC-41	
Charring temperature (°C)		**950**	**1050**	**950**	**1050**	**950**	**1050**	**950**	**1050**	**950**	**1050**	**950**	**1050**	**950**	**1050**	**950**	**1050**	**950**	**1050**
Parameter	**Unit**																		
Carbon	wt.%	95.0	96.5	94.8	96.9	96.1	96.6	97.0	96.7	96.7	97.3	95.3	96.4	96.4	97.6	95.8	97.3	95.4	97.4
Hydrogen	wt.%	0.1	0.0	0.1	0.0	0.0	0.0	0.0	0.0	0.1	0.0	0.2	0.1	0.1	0.0	0.1	0.0	0.1	0.0
Nitrogen	wt.%	1.9	1.6	2.0	1.6	1.9	1.4	2.1	1.7	1.8	1.3	1.8	1.5	1.4	1.2	1.4	1.2	1.7	1.4
Oxygen	wt.%	1.2	0.8	2.4	0.9	1.4	1.4	0.0	0.0	0.0	0.0	2.1	1.5	1.8	0.9	2.0	0.8	1.8	0.3
Total sulphur	wt.%	1.8	1.1	0.7	0.6	0.6	0.6	0.9	1.6	1.4	1.4	0.6	0.5	0.3	0.3	0.7	0.7	1.0	0.9

The atomic H/C and O/C ratios of the coals were also determined. AC-5-72 has the highest atomic H/C ratio, which correlates with this coal also having the highest volatile content (Tsai, 1982). The atomic H/C and O/C ratios of the coals are presented on a Van Krevelen diagram, which gives an indication of the degree of coalification (Van Krevelen, 1981). The results are illustrated in Figure 3.5.

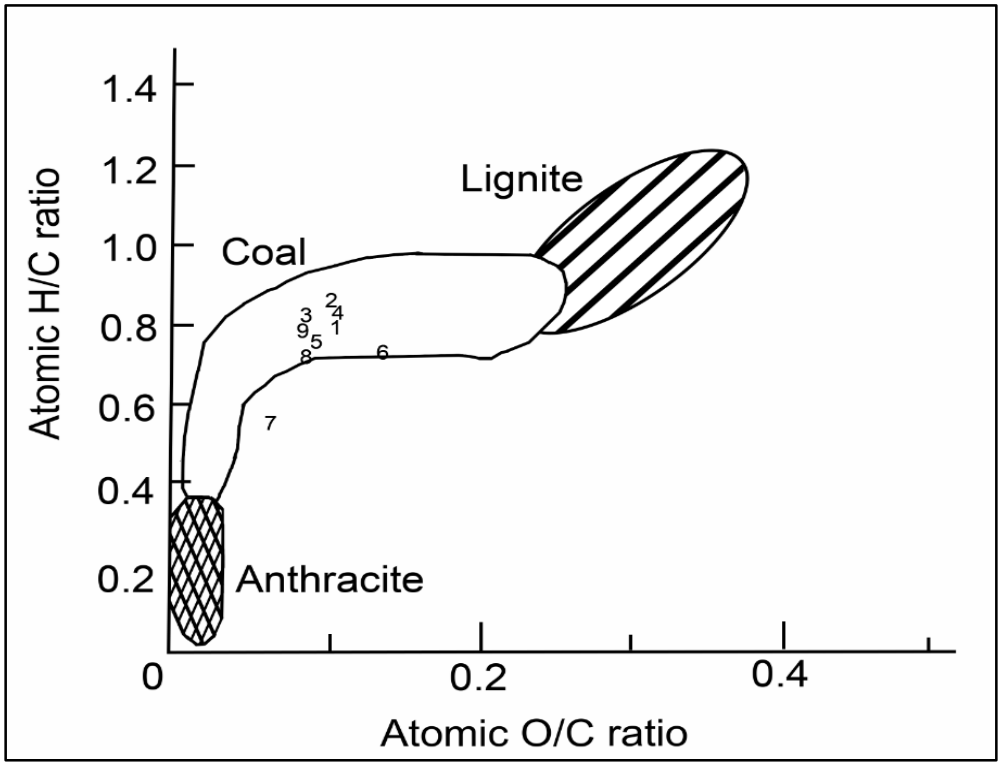

Figure 3.5: Atomic H/C vs. O/C coal ratio on the Van Krevelan diagram (1: BC-5-53; **2:** AC-5-72**; 3:** AC-5-50**; 4:** AC-4-56**; 5:** AC-4-41**; 6:** AC-4-22**; 7:** FC-2-13; **8:** FC-2-21; **9:** AC-LC-41 **- adapted from Clingan, 2013).**

Firstly it is observed that all nine coals fall within the normal range of coal. All the samples are grouped together, except for number six and seven. AC-4-22 is located to the right of the diagram, which associates with this coal having the lowest carbon content, while FC-2-13 is located to the left of diagram correlating with this coal having the highest carbon value and highest rank (see Table 3.8).

Lastly the ultimate analysis of the 6 mm chars utilised for the phase two experiments was also done, see Table A.3 for the results.

3.5.1.3 Forms of sulphur analysis

The forms of sulphur analysis was conducted in order to determine which constitutes of sulphur contribute the most to the total sulphur of the coal. The results are given in Table 3.10.

Table 3.10 Normalised forms of sulphur results (a.d.b)

Coal	Pyrite (wt. %)	Sulphates (wt. %)	Organic (wt.%)
BC-5-53	15.4	2.6	82.0
AC-5-72	19.6	2.0	78.4
AC-5-50	10.8	2.7	86.5
AC-4-56	60.0	1.1	38.9
AC-4-41	14.5	1.8	83.7
AC-4-22	8.8	2.9	88.3
FC-2-13	6.0	2.0	92.0
FC-2-21	14.6	2.4	83.0
AC-LC-41	27.3	1.8	70.9

From the results it is evident that organic sulphur and pyrite are the two main contributors to the total sulphur content of the coal, which is typical for coal as the sulphate levels are usually low (Calkins, 1993; Kostova *et al*., 2005; Speight, 2005). For most of the coals the organic sulphur values range between 71 and 92 wt.%, with the exception of AC-4-56 which has a low organic sulphur value of 38.9 wt.%. AC-4-56, however, contains a substantial amount of pyrite, which causes this coal to have the highest inorganic sulphur content.

As mentioned in Section 3.5.1.2 the chars of AC-4-41 and BC-5-53 all have higher total sulphur values; however, when comparing the results to the organic sulphur values, these samples have moderate amounts of organic sulphur. This suggests that the high total sulphur values could be due to mineral matter transformation during pyrolysis and gasification.

3.5.2 Mineral matter analysis

3.5.2.1 Mineral analysis

XRD analysis was done to determine the mineral composition of the coal, char and ash. In Table 3.11 the results of the coal mineral analysis are given. Firstly it is seen that the mineral matter mainly consists of kaolinite, quartz and microcline, with minor concentrations of dolomite, illite and muscovite. In general the results in Table 3.11 compare well with the mineral composition for South African coals from the Highveld and Witbank coalfields (Hattingh *et al.,* 2011; Matjie *et al.,* 2011; Pinetown *et al.,* 2007). The pyrite concentrations for many of the samples are low due to the minerals not being properly liberated during pulverisation, as the pyrite is predominantly mixed with organic matter in the coal. When referring to Table 3.10 it is seen that the coals do contain pyrite. Most of the coals also contain anatase, while only AC-4-41 contains a small concentration of fluoroapatite.

The mineral results for the chars prepared at 950 °C are given in Table 3.12. Firstly it is observed that for the nine samples quartz, microcline, graphite 2H and gypsum have the highest concentrations. Quartz and microcline are inert minerals that do not react at 950 °C and increase in concentration due to the removal of other minerals. Kaolonite is transformed into meta-kaolonite, that when further heated transforms to form mullite (Deng *et al.,* 2015; Van Dyk *et al.,* 2006). Gypsum is not present in coal minerals and was formed due to the interaction of organic sulphur and lime, which originated as a result of the reaction between calcite and dolomite (Deng *et al.,* 2015; Van Dyk *et al.,* 2006). Small concentrations of minerals such as anhydrite, hematite and cristobalite also formed during pyrolysis. Anhydrite developed as a result of the gypsum losing its water, while hematite originated from pyrite. Cristobalite is the result of the amorphous decomposition product of clay minerals, illite and kaolinite, while periclase is the other product formed during the transformation of dolomite and calcite (Matjie *et al.,* 2008; Matjie *et al.,* 2011; Van Dyk *et al.,* 2006). With regards to the high total sulphur values of BC-5-53 and AC-4-41 chars (Table 3.9), it is seen that these samples contain moderate amounts of pyrrhotite, gypsum and anhydrite which could contribute to the increased sulphur concentrations for the ultimate analysis.

Lastly the mineral analysis of the coal ash derived from CO_2 gasification at 950 and 1050 °C respectively is given in Table 3.13. Quartz, anorthite and mullite are the most abundant minerals present in the ash, with minor concentrations of anhydrite, lime, cristobalite and periclase also being present for most of the samples. Quartz and anorthite decreases with temperature, while mullite increases with the exception of AC-4-22. Mullite and anorthite is produced either by solid-state reaction or crystallisation from molten silicate material. Calcite, dolomite, kaolinite and quartz agglomerate to form a melt from which the anorthite and mullite crystallises (Matjie *et al*., 2011). For this reason a decrease in the concentrations of both calcite and quartz is observed with an increase in temperature. Both Van Dyk *et al.* (2006) and Wu *et al.* (2010) stated that as the temperature increases to above 1000 °C, the concentration of anorthite decreases due to the melting of the phase, which is also observed for the results in Table 3.13. Both mullite and cristobalite are shown to increase with ashing temperature, which could be due to these species only reacting with the melt at 1400 °C for calcium-poor ashes. Additionally the increased mullite could also be due to initial transformation of meta-kaolinite (Matjie *et al.,* 2008; Mayoral *et al.,* 2001; Van Dyk *et al.,* 2006). Bai *et al.* (2009) and Gupta *et al.* (2007) also found that the mullite and cristobalite concentrations increased with rising temperatures. The amorphous content of BC-5-53's coal, char and ash was also determined and is presented in Appendix A.6. In general the concentrations of the species decreased in comparison to the results in Table 3.11, 3.12 and 3.13. The amorphous content also seemed to decrease for char and ash.

Table 3.11: XRD results for minerals present in the coal samples.

		BC-5-53	AC-5-72	AC-5-50	AC-4-56	AC-4-41	AC-4-22	FC-2-13	FC-2-21	AC-LC-41
Parameter	**Unit**									
Quartz	wt.%	24.2	17.7	23.3	8.7	8.7	-	12.9	4.9	14.2
Kaolinite	wt.%	47.9	49.0	41.5	54.0	37.7	60.4	37.3	54.4	62.8
Illite	wt.%	4.7	9.3	8.1	9.6	0.7	0.6	0.3	4.5	1.1
Microcline	wt.%	12.2	17.7	18.9	20.2	13.8	9.0	9.2	34.7	12.9
Calcite	wt.%	-	-	0.2	-	4.6	14.4	-	-	1.3
Goyazite	wt.%	-	-	-	-	0.2	-	-	0.1	0.1
Pyrite	wt.%	0.8	-	-	0.4	0.6	-	-	0.5	0.4
Dolomite	wt.%	0.2	-	-	5.4	2.7	11.5	-	0.1	2.5
Anatase	wt.%	0.9	0.9	-	0.7	0.9	1.0	0.7	0.1	1.0
Graphite 2H	wt.%	7.5	-	6.5	0.8	28.7	0.2	39.3	0.1	0.5
Graphite 3R	wt.%	-	-	-	-	-	0.2	-	-	2.8
Muscovite	wt.%	1.6	5.4	1.5	0.2	1.1	2.7	0.3	0.6	0.4
Fluoroapatite	wt.%	-	-	-	-	0.3	-	-	-	-
Total	**wt.%**	**100.0**	**100.0**	**100.0**	**100.0**	**100.0**	**100.0**	**100.0**	**100.0**	**100.0**

Table 3.12: XRD results for minerals present in the char samples prepared at 950 °C.

		BC-5-53	AC-5-72	AC-5-50	AC-4-56	AC-4-41	AC-4-22	FC-2-13	FC-2-21	AC-LC-41
Parameter	**Unit**									
Quartz	wt.%	19.1	22.2	7.2	43.8	12.4	0.1	18.7	5.7	18.1
Microcline	wt.%	39.1	25.2	36.7	31.2	27.5	27.9	45.9	39.2	39.6
Pyrrhotite	wt.%	0.3	0.2	0.5	0.2	0.5	0.7	-	0.1	-
Anatase	wt.%	0.8	1.0	1.0	1.5	1.2	1.1	1.2	0.6	1.1
Graphite 2H	wt.%	21.0	20.4	25.9	15.5	21.3	18.1	21.6	31.2	21.6
Muscovite	wt.%	-	-	1.8	-	5.2	11.8	-	-	-
Gypsum	wt.%	17.3	24.0	19.6	1.9	21.0	22.0	2.0	14.6	12.8
Anhydrite	wt.%	1.1	1.3	4.0	1.6	2.3	6.7	1.3	6.2	4.8
Lime	wt.%	-	-	0.3	-	0.4	6.1	-	-	0.5
Hematite	wt.%	0.1	0.1	0.2	0.5	0.3	0.3	0.4	0.4	0.3
Anorthite	wt.%	-	4.2	0.9	0.9	5.3	0.8	7.9	1.0	-
Cristobalite	wt.%	1.0	0.9	0.9	0.9	1.1	1.1	0.8	0.7	0.9
Mullite	wt.%	-	-	-	2.0	0.2	-	-	-	-
Periclase	wt.%	0.2	0.5	0.8	-	1.0	1.6	0.2	0.3	0.3
Portlandite	wt.%	-	-	0.2	-	0.3	1.7	-	-	-
Total	**wt.%**	**100.0**	**100.0**	**100.0**	**100.0**	**100.0**	**100.0**	**100.0**	**100.0**	**100.0**

Table 3.13: XRD results for minerals present in the CO_2 gasified ash prepared at 950 & 1050 °C.

		BC-5-53		AC-5-72		AC-5-50		AC-4-56		AC-4-41		AC-4-22		FC-2-13		FC-2-21		AC-LC-41	
Gasification temperature (°C)		**950**	**1050**	**950**	**1050**	**950**	**1050**	**950**	**1050**	**950**	**1050**	**950**	**1050**	**950**	**1050**	**950**	**1050**	**950**	**1050**
Parameter	**Unit**																		
Quartz	wt.%	62.9	55.9	41.3	33.7	61.8	58.6	32.6	11.6	39.1	27.5	0.4	4.9	49.0	47.6	13.3	16.3	50.2	28.2
Calcite	wt.%	0.1	-	-	-	0.1	-	1.0	1.5	2.7	0.2	9.0	2.1	1.4	0.1	-	-	3.5	0.9
Pyrrhotite	wt.%	-	-	-	-	0.1	-	0.3	0.2	0.4	0.1	0.3	0.4	-	-	-	0.1	0.6	0.2
Rutile	wt.%	-	0.2	-	-	-	0.1	-	0.1	0.3	0.5	1.6	0.9	0.4	0.6	0.9	0.9	-	-
Anhydrite	wt.%	0.5	0.2	0.4	0.2	0.6	0.3	0.9	1.0	1.9	0.2	4.8	0.4	1.1	0.4	0.6	0.3	10.0	1.0
Wustite	wt.%	0.1	0.1	-	-	-	0.1	-	-	0.4	-	-	-	-	-	-	-	-	-
Lime	wt.%	0.2	0.2	0.1	0.1	0.4	0.1	0.8	0.7	0.5	0.3	0.9	0.5	0.6	0.3	0.4	0.3	0.7	0.6
Magnetite	wt.%	-	-	0.3	0.5	0.1	0.1	-	0.3	-	-	-	-	-	-	0.1	-	-	-
Maghemite	wt.%	-	-	-	-	-	-	-	0.4	-	-	-	0.3	-	-	-	-	-	-
Hematite	wt.%	-	-	0.4	0.6	0.1	-	0.9	0.6	-	0.4	0.2	0.6	-	-	0.2	0.3	0.6	0.3
Anorthite	wt.%	8.5	6.6	24.8	18.8	8.5	6.2	16.8	17.3	9.4	8.4	12.7	7.7	8.9	6.0	19.9	6.3	1.6	15.3
Cristobalite	wt.%	0.4	0.7	0.4	0.8	0.5	0.6	1.0	0.8	0.4	2.7	-	0.1	0.8	1.3	14.0	14.4	0.6	1.8
Mullite	wt.%	27.0	36.0	31.3	44.9	24.9	33.5	42.0	48.7	28.9	40.1	43.8	36.4	35.9	43.7	49.6	61.1	22.0	42.9
Sillimanite	wt.%	-	-	-	-	2.0	-	0.3	1.3	0.2	-	-	0.5	0.6	-	-	-	0.2	1.8
Periclase	wt.%	0.2	0.1	0.2	0.3	0.2	0.2	2.3	2.0	5.2	2.1	5.2	3.7	0.3	-	-	-	8.3	4.6
Portlandite	wt.%	0.1	-	0.3	0.1	0.2	0.2	1.1	13.5	10.6	17.5	21.1	41.5	1.0	-	0.6	-	1.7	2.4
Diopside	wt.%	-	-	0.5	-	0.5	-	-	-	-	-	-	-	-	-	0.4	-	-	-
Total	**wt.%**	**100.0**	**100.0**	**100.0**	**100.0**	**100.0**	**100.0**	**100.0**	**100.0**	**100.0**	**100.0**	**100.0**	**100.0**	**100.0**	**100.0**	**100.0**	**100.0**	**100.0**	**100.0**

3.5.2.2 Ash analysis

Major elemental X-ray fluorescence (XRF) was done in order to determine the elemental composition of the coal ash. The results are presented on a loss of ignition (LOI) – free basis in Table 3.14. In general the XRF composition is comparable to the values reported in the Bulletin 114 for different South African coals and also to the results reported by Hattingh *et al.* (2011) and Coetzee *et al.* (2013). Firstly it is observed that the ash has an acidic nature due to the abundant presence of silica and aluminium species, which corresponds with the concentration of kaolinite and quartz in the coal mineral matter as well as the high concentration of quartz in the ash (Table 3.11 & 3.13). The seam five coals have the highest concentrations of silica species and the highest concentrations of quartz in the coal minerals.

With regards to the iron content, both BC-5-53 and AC-4-41 have high iron values in comparison to the other coals. Firstly the increased iron values can be due to the presence of illite in the coal minerals. These two coals also had the highest pyrite concentration in comparison to the other samples (see Table 3.11). Secondly the formation of wustite (BC-5-53) and pyrrhotite (AC-4-41) in the ash could also contribute to the iron content (see Table 3.13). Even though the iron values are high in comparison with the other coals, the values are still within the limits for bituminous coals (Speight, 2005; Tsai, 1982). AC-4-56, AC-4-41, AC-4-22 and AC-LC-41 all present with high calcium values. When referring to Table 3.11 it is seen that these four samples contained the highest concentrations of calcite and dolomite. Additionally when referring to the ash XRD results it is observed that these samples also contain the highest amounts of calcite and portlandite. The phosphate concentration of AC-4-41 is also significant in comparison to the other coals, due to the presence of fluoroapatite and goyazite in the coal minerals.

Lastly the sulphur values of AC-5-50, AC-4-56, AC-4-41, AC-4-22 and AC-LC-41 are considerably higher when compared to the other samples. The ash of these five samples additionally had the greatest concentrations of pyrrhotite and anhydrite, which contributed to the increased sulphur values. Even though the sulphur contents of AC-5-50, AC-4-22 and AC-LC-41 are high, these values still fall within the expected limits of bituminous coal ash composition. AC-4-56's and AC-4-41's values are above the expected limits (Tsai, 1982). The alkali index was estimated as follow (Sakawa *et al.,* 1982):

$$Alkali\ index = ash\ \% \times \left(\frac{CaO\ +\ K_2O + MgO +\ Na_2O +\ Fe_2O_3}{Al_2O_3 + SiO_2}\right) \tag{3.3}$$

AC-4-41 has the highest alkali index of 13.0, which is due to its high calcium and iron values, while FC-2-13 and FC-2-21 have the lowest alkali index values owing to their high concentration of aluminium and silica species.

Table 3.14 Major elemental XRF results (LOI-free basis)

		BC-5-53	AC-5-72	AC-5-50	AC-4-56	AC-4-41	AC-4-22	FC-2-13	FC-2-21	AC-LC-41
Parameter	**Unit**									
SiO_2	wt.%	63.0	63.1	63.9	35.4	22.9	42.3	56.6	55.4	47.2
TiO_2	wt.%	1.1	1.6	0.7	0.9	1.6	1.8	2.0	2.1	1.4
Al_2O_3	wt.%	23.7	22.8	18.1	28.9	19.6	35.9	35.9	38.5	30.4
Fe_2O_3	wt.%	7.6	3.3	1.9	2.3	12.6	<0.0	0.7	1.4	<0.1
MnO	wt.%	<0.1	<0.1	<0.1	0.1	0.1	0.1	<0.1	<0.1	0.1
MgO	wt.%	<1.2	2.0	0.8	3.2	1.5	1.4	0.4	0.5	1.9
CaO	wt.%	1.4	4.9	2.9	12.9	19.7	10.5	2.4	0.8	8.7
Na_2O	wt.%	<0.1	0.3	0.1	0.8	0.2	0.2	0.1	0.2	0.2
K_2O	wt.%	1.4	1.2	1.8	<0.1	0.1	1.8	0.4	0.6	0.1
P_2O_5	wt.%	<0.1	<0.1	0.2	0.4	3.7	0.6	1.2	0.2	0.3
Cr_2O_3	wt.%	<0.1	<0.1	<0.1	0.1	<0.1	0.0	0.1	<0.1	0.1
SO_3	wt.%	0.2	0.5	9.4	14.9	17.9	5.4	0.1	<0.1	9.5
Total	**wt.%**	**100.0**	**100.0**	**100.0**	**100.0**	**100.0**	**100.0**	**100.0**	**100.0**	**100.0**
Alkali index	-	**1.73**	**1.37**	**1.30**	**4.08**	**13.0**	**4.58**	**0.72**	**0.73**	**2.64**

3.5.3 Thermal analyses

3.5.3.1 Swelling index

The results of the swelling index characterisation are presented in Table 3.15. Most of the coals have a value of 0.0 and 0.5, which indicates that the coals are non-caking. AC-LC-41 has a swelling index value of 1.0 and is classified as a weakly caking coal (Speight, 2005). The typical desired swelling value for pre-reduction coals is below three and thus all coals are within the desired range (Chatterjee, 2010; Sarangi & Sarangi, 2011).

Table 3.15 Free swelling index results

Coal	Crucible swelling index
BC-5-53	0.0
AC-5-72	0.5
AC-5-50	0.0
AC-4-56	0.5
AC-4-41	0.5
AC-4-22	0.0
FC-2-13	0.0
FC-2-21	0.0
AC-LC-41	1.0

3.5.3.2 Ash fusion temperatures

In Table 3.16 the AFT of the nine coals for both a reducing and an oxidising atmosphere is given. Chatterjee (2010) stated that the initial deformation temperature (IT) should be at least 100 °C higher than the maximum kiln temperature under reducing conditions. The IT for the samples, under a reducing atmosphere, range from 1326 to above 1550 °C (1550 °C is the temperature limitation of the used equipment). Therefore all the temperatures are above 100 °C of the maximum kiln temperature, which ranges from 1100 to 1130 °C (Sutherland, 2000). Other studies have stated that the AFT in general should be a minimum of between 1300 and 1400 °C (Industrial technical consultant, 2003; Sutherland, 2000). The lowest AFT value is 1320 °C (oxidising atmosphere) for AC-4-41.

FC-2-13 and FC-2-21 have the highest AFT for both an oxidising and a reducing atmosphere, which is due to their high amounts of aluminium and silica species and low concentrations of basic compounds. The XRD ash results of these two samples also indicated high concentrations of mullite, which increases AFT (Deng *et al.,* 2015). In contrast AC-4-41 has the lowest AFT owing to its high values of iron and calcium.

Table 3.16 AFT results for both an oxidising and reducing atmosphere

		BC-5-53		AC-5-72		AC-5-50		AC-4-56		AC-4-41		AC-4-22		FC-2-13		FC-2-21		AC-LC-41	
		Red.	Ox.	Red.	Ox.	Red.	Ox.	Red.	Ox.	Red.	Ox.	Red.	Ox.	Red.	Ox.	Red.	Ox.	Red.	Ox.
Parameter	**Unit**																		
IT	°C	1514	>1550	1409	1440	1434	1477	1326	1369	1329	1320	1445	1489	>1550	>1550	>1550	>1550	1369	1500
ST	°C	1547	>1550	1444	1515	1494	1545	1368	1395	1342	1340	1463	1504	>1550	>1550	>1550	>1550	1475	1515
HT	°C	>1550	>1550	1476	1538	1526	>1550	1412	1414	1356	1360	1484	1528	>1550	>1550	>1550	>1550	1508	1533
FT	°C	>1550	>1550	>1550	>1550	1548	>1550	1456	1468	1413	1382	1544	1541	>1550	>1550	>1550	>1550	1548	1550

IT – Initial deformation temperature

ST – Softening temperature

HT – Hemispherical temperature

FT – Fluid temperature

3.5.4 Petrographic analysis

3.5.4.1 Maceral composition

The maceral composition results are given in Table 3.17. From the results it can be seen that AC-5-72, AC-4-56, BC-5-53 and AC-5-50 are all vitrinite-rich coals, with AC-5-72 having the highest vitrinite content of 77 vol.% on a mineral matter-free basis (m.m.f.b.). The high vitrinite value of AC-5-72 explains why this sample has a swelling index value of 0.5, as the vitrinite is the maceral responsible for the caking/coking properties of the coal (England *et al.,* 2002). The high vitrinite value of AC-5-72 also accounts for the coal's high atomic H/C ratio, since vitrinite has a higher atomic H/C ratio in comparison to inertinite (Tsai, 1982).

AC-4-22, FC-2-13 and FC-2-21 are all inertinite rich coals, which is typical for southern hemisphere coals (Falcon & Ham, 1988). The remaining coals which are AC-4-41 and AC-LC-41 have evenly distributed vitrinite and inertinite contents. The total inertinite content of the coal is calculated as the sum of different inertinite constitutes given in Table 3.17. The reactive semi-fusinite and inert semi-fusinite contribute the most to the total inertinite. The fusinite and secretinite values are low and the micrinite value is zero for many of the coals.

The liptinite content of all the coals is low, which is also distinctive for southern hemisphere coals (Falcon & Ham, 1988). AC-4-22 has the highest liptinite value of 10.4 vol.%. The total reactives is determined by adding the vitrinite, liptinite and reactive semi-fusinite. AC-5-72 has the highest total reactives due to its high vitrinite content, followed by BC-5-53. Even though AC-4-22, FC-2-13 and FC-2-21 have low vitrinite values, the moderate amounts of reactive semi-fusinite and in AC-4-22's case, liptinite, assisted in increasing their total reactives. FC-2-13 has the lowest total reactives and consequently the highest total inerts.

Table 3.17: Maceral composition results (m.m.f.b.)

		BC-5-53	AC-5-72	AC-5-50	AC-4-56	AC-4-41	AC-4-22	FC-2-13	FC-2-21	AC-LC-41
Parameter	**Unit**									
Vitrinite	vol.%	56.9	76.6	54.1	62.9	45.3	25.9	14.5	23.5	45.7
Liptinite	vol.%	7.4	7.4	8.7	6.8	7.6	10.4	3.6	4.9	9.2
Total Inertinite	vol.%	35.8	16.0	37.2	30.3	47.1	63.7	81.8	71.6	45.1
Reactive Semi-fusinite	vol.%	19.6	5.6	19.6	13.0	26.5	31.0	27.5	34.4	23.1
Inert Semi-fusinite	vol.%	15.0	9.1	14.0	11.7	16.5	30.4	52.5	36.0	14.4
Fusinite + Secretinite	vol.%	1.2	1.2	2.8	3.6	2.4	1.9	1.8	1.2	6.8
Micrinite	vol.%	0.0	0.0	0.8	2.0	1.7	0.4	0.0	0.0	0.8
Total Reactives	**vol.%**	**83.8**	**89.7**	**82.4**	**82.7**	**79.4**	**67.3**	**45.7**	**62.8**	**77.9**
Total Inerts	**vol.%**	**16.2**	**10.3**	**17.6**	**17.3**	**20.6**	**32.7**	**54.3**	**37.2**	**22.1**

* % Total Inertinite: % Reactive Semi-fusinite + % Inert Semi-fusinite + % Fusinite + Secretinite + % Micrinite

** % Total Reactives: %Vitrinite + %Liptinite + %Reactive Semi-fusinite

3.5.4.2. Vitrinite reflectance

The vitrinite reflectance analysis was done in order to determine the rank of the coals. In Table 3.18 a summary of the results are given as well as the estimated standard deviation and random reflectance. The reflectance histograms are provided in Appendix A.3.

Table 3.18 Vitrinite reflectance results

Coal	RoV (random) (%)	Standard deviation (%)	Rank
BC-5-53	0.56	0.06	Bituminous Medium rank D
AC-5-72	0.51	0.04	Bituminous Medium rank D
AC-5-50	0.62	0.05	Bituminous Medium Rank C
AC-4-56	0.59	0.05	Bituminous Medium Rank D
AC-4-41	0.68	0.06	Bituminous Medium Rank C
AC-4-22	0.68	0.05	Bituminous Medium Rank C
FC-2-13	0.74	0.13	Bituminous Medium Rank C
FC-2-21	0.65	0.08	Bituminous Medium Rank C
AC-LC-41	0.67	0.05	Bituminous Medium Rank C

Typically for single seam non-blended coals the standard deviation is less than 0.1% (Economic Commission for Europe, 1988; Pearson, 2008). All of the coals, with the exception of FC-2-13, have a standard deviation of 0.04 to 0.08%. FC-2-13 has a standard deviation of 0.13%. Pearson (2008) stated that higher rank coals tend to have a higher standard deviation, due to the spread of the reflectance being greater.

BC-5-53, AC-5-72 and AC-4-56 are bituminous medium rank D coals, while the remaining six coals are all bituminous medium rank C coals. This corresponds with the typically desired rank of pre-reduction coals (Section 2.5.3).

3.5.4.3. Petrographic indices

The maceral index and reactive maceral index values as well as the petrofactor for the nine different samples are presented in Table 3.19.

Table 3.19: Petrofactor, maceral and reactive maceral index results (m.m.f.b.)

Coal	Maceral index	Reactive maceral index	Petrofactor
BC-5-53	1.6	5.8	0.7
AC-5-72	7.2	16.3	0.6
AC-5-50	1.2	4.2	0.8
AC-4-56	1.9	5.3	0.7
AC-4-41	0.6	2.4	0.9
AC-4-22	0.2	0.8	1.0
FC-2-13	0.1	0.2	1.6
FC-2-21	0.2	0.7	1.0
AC-LC-41	0.6	2.3	0.9

From the results in Table 3.19 it is observed that AC-5-72 has both the highest maceral and reactive maceral index values due to its high vitrinite content. In contrast FC-2-13 has the lowest values, which correlates with this coal having highest total inertinite content.

3.5.5 CO_2 adsorption

CO_2 adsorption analysis was used to determine the micropore surface area and structure of both the coals and chars (950 & 1050 °C). The results of the coal and char analysis are given in Table 3.20 and 3.21 respectively. The micropore surface areas of the coal is comparable to the results obtained by Everson *et al*. (2013), Okolo *et al.* (2015) and Roberts *et al.* (2015a) for South African coals, while the monolayer capacity, micropore volume, median pore width and calculated micropore porosity also agreed with the results of Okolo *et al.* (2015) and Roberts *et al.* (2015a). The micropore surface area does not vary greatly for the different coals ranging from 135 to 152 m^2/g. The micropore porosity for the coals also did not vary greatly, ranging from 2.5 to 3.0%.

When comparing the micropore surface area of the coals and chars prepared at 950 °C it is observed that the micropore surface areas, BET and Langmuir surface area and micropore volume increases. Cakal *et al.* (2007), Everson *et al.* (2013), and Saha *et al.* (2013) also observed increased micropore surface areas for chars prepared at 875 and 900 °C respectively. The increased surface area is due to the development of the pore structure, which generates new pores, enlarges pre-existing pores and opens blocked pores by removing volatiles and tars. By comparing the increased surface areas for the different samples it can be seen that coals with higher vitrinite contents showed a more significant increase in micropore surface area, with AC-5-72 having the greatest surface area increase. Tang *et al.* (2005) stated that during pyrolysis vitrinite-rich coals form tenui-network chars

which have a high surface area, while inertinite-rich coals tend to form more dense chars with lower surface areas. In addition to char formation, vitrinite-rich coals also have a higher swelling tendency which also attributes to an increased surface area. Roberts *et al.* (2015a) compared the physical and structural characteristics of inertinite - and vitrinite-rich South African coals, with the results indicating that the vitrinite-rich chars had a higher surface area in comparison to the inertinite-rich chars. In addition to a high vitrinite content, volatile matter also increases the surface area as the removal of volatiles during pyrolysis facilitates the formation of a porous char by forming new pores and opening blocked pores (Jayaraman *et al.,* 2015; Wu *et al.,* 2008). A high volatile content also increases the propensity of fragmentation, which increases surface area (Dakic *et al.,* 1989). AC-5-72 and AC-4-56 have the highest and second highest volatile matter and correspondingly the largest and third largest micropore surface areas.

For the chars prepared at 1050 °C the micropore surface areas, BET and Langmuir surface area and micropore volume decrease in comparison to the coal and char (950 °C) results. Similar results were observed by Cakal *et al.* (2007), Roberts *et al.* (2015a) and Saha *et al.* (2013) for the micropore surface area of chars prepared at 1000 °C. The higher the charring temperatures the more ordered the carbon structure becomes (smooth and flattened), which in turn decreases the surface area (Gale *et al*., 1996). The ratio with which the surface area decreased in comparison to the coal ranges from 0.3 to 0.6.

The results of the CO_2 adsorption analysis of the 6 mm chars for phase two is given in Table A.4.

Table 3.20: CO_2 adsorption results for coal derived from 20 mm coal particles

		BC-5-53	AC-5-72	AC-5-50	AC-4-56	AC-4-41	AC-4-22	FC-2-13	FC-2-21	AC-LC-41
Parameter	**Unit**									
Coal micropore surface area (D-R)	m^2/g	144	150	143	139	152	148	147	152	135
Carbon micropore surface area (D-R)	m^2/g	205	210	206	201	224	257	209	230	207
Monolayer capacity (D-R)	cm^3/g	31.5	32.8	31.3	30.4	33.4	32.3	32.2	33.2	29.6
BET surface area	m^2/g	94	98	93	91	100	97	91	95	88
Langmuir surface area	m^2/g	103	107	100	98	107	103	99	109	94
Micropore volume x 10^{-2} (H-K)	cm^3/g	3.2	3.3	3.3	3.1	3.5	3.5	3.1	3.0	3.0
Median pore width (H-K)	Å	3.96	3.98	3.95	3.99	3.94	3.88	3.91	3.96	3.98
Micropore porosity	%	2.7	2.8	2.7	2.7	2.9	3.0	2.6	2.5	2.7

Table 3.21: CO_2 adsorption results for chars derived from 20 mm particles

		BC-5-53		AC-5-72		AC-5-50		AC-4-56		AC-4-41		AC-4-22		FC-2-13		FC-2-21		AC-LC-41	
Charring temperature	**(°C)**	**950**	**1050**	**950**	**1050**	**950**	**1050**	**950**	**1050**	**950**	**1050**	**950**	**1050**	**950**	**1050**	**950**	**1050**	**950**	**1050**
Parameter	**Unit**																		
Char micropore surface area (D-R)	m^2/g	280	58	334	84	212	74	278	56	213	56	217	41	172	39	175	48	202	40
Carbon micropore surface area (D-R)	m^2/g	366	73	456	107	282	98	363	75	282	73	346	65	231	52	234	64	299	59
Monolayer capacity (D-R)	cm^3/g	61.4	12.7	73.1	18.3	46.4	16.2	60.9	12.3	46.7	12.2	47.6	9.0	37.6	8.6	38.2	10.5	44.3	8.8
BET surface area	m^2/g	175	45	203	58	139	51	176	43	134	42	141	34	110	96	114	39	127	33
Langmuir surface area	m^2/g	184	50	214	62	149	55	185	46	143	45	148	36	117	123	122	43	135	35
Micropore volume x 10^{-2} (H-K)	cm^3/g	6.5	1.2	7.4	1.8	5.0	1.7	6.6	1.4	4.9	1.3	5.3	1.0	4.0	0.7	4.1	1.0	4.7	1.0
Median pore width (H-K)	Å	3.69	4.32	3.70	4.14	3.80	4.12	3.65	4.18	3.81	4.24	3.66	4.30	3.81	4.47	3.81	4.35	3.78	4.30

3.6 Summary

The characterisation results are summarised in the accompanying A3 insert. In terms of ash yield and fixed carbon content all nine coals are well suited for pre-reduction. The volatile matter of the coals varied from being slightly above to below the desired values; however, these differences were minimal and were not considered as having a negative impact on pre-reduction. The charring process decreased the moisture and volatile content of the coals and in turn increased the ash yield and fixed carbon content. Most of the coals were ranked as high volatile B bituminous coals, while only the seam two coals (FC-2-21 and FC-2-13) were ranked as medium-volatile bituminous coals. Charring increased the rank of all of the chars to meta-anthracite.

The carbon content for the coal varied between 79 and 85 wt.% (d.a.f). Charring increased the carbon content to above 90 wt.% (d.a.f), while decreasing the hydrogen and oxygen contents. The nitrogen and sulphur content remained constant. The forms of sulphur results showed that organic sulphur and pyrite contribute the most to the total sulphur of the coals. AC-4-56 contained the greatest amount of pyrite, while FC-2-13 had the highest organic sulphur content.

The XRD results showed that kaolinite and microcline were the main contributors to the coal minerals. For the char results it was seen that quartz and microcline had the highest concentrations, while for the ash analysis quartz, anorthite and mullite were the most abundant. The majority of coal ashes could be described as being acidic in nature due to the high amounts of silica and aluminium species; however, AC-4-41 was more basic in nature due to large amounts of calcium and iron. This in turn caused the AFT of AC-4-41 to be lower in comparison with the other nine coals.

With regards to the petrographic analyses, AC-5-72 has the highest vitrinite value, while FC-2-13 has the highest inertinite value. Vitrinite reflectance analysis was also done to determine the rank of the coals. BC-5-53, AC-5-72 and AC-4-56 are classified as medium rank D bituminous coals, while the remaining six coals are all classified as medium rank C bituminous coals.

Lastly CO_2 adsorption analysis was done to determine the structural and physical parameters of the coal and char samples. Charring the sample at 950 °C increased the surface area and volumes, with the greatest increases being observed for the vitrinite-rich coals. Charring the samples at 1050 °C decreased the micropore surface areas, BET and Langmuir surface areas as well as the micropore volume.

CHAPTER 4: Experimental

4.1 Introduction

In this chapter the experimental set-up and methods used for the measurement of the coal/char CO_2 gasification reactivity are given. Firstly the materials and equipment are discussed in Section 4.2, followed by a detailed description of the experimental rig in Section 4.3. In Section 4.4 the experimental program is provided followed by a description of the method (Section 4.5). The experimental errors and data processing procedures are provided in Section 4.6 and 4.7 respectively. In Sections 4.8 and 4.9 the experimental regimes and the statistical analysis of phase one are discussed. Lastly a brief summary is given in Section 4.10.

4.2 Materials and equipment

4.2.1 Materials

The materials used for the reactivity experiments consisted of coal/char particles and reactant gases. Nine different coals/chars (20 mm, 6 mm and 212 µm) originating from the Ermelo, Highveld and Witbank South African coalfields were used. All the coal particles were selected according to a specific size, mass and density with the characteristics of these coals/chars provided in Chapter 3. The reactant gases utilised were CO_2, N_2 and compressed air. The specifications of CO_2 and N_2 are given in Table 4.1.

Table 4.1: Reagent gas specifications

Gas	Grade	Purity
CO_2	Technical	> 99.0%
N_2	High purity	> 99.999%

The CO_2 and N_2 cylinders were provided by African oxygen (Afrox), while the compressed air was supplied directly from a line, running from an air compressor to the experimental set-up.

4.2.2 Experimental rig

The equipment that formed part of the experimental rig is given in Table 4.2, along with the model, range and accuracy.

Table 4.2: Equipment specifications

Equipment	Model	Range	Accuracy
Mass balance	Radwag PS 750/c/2	0 – 750 g	0.001 g
Mass flow controller: N_2	Sierra Smart Trak 50 Series: N_2	0 – 15 Nl/min	± 0.1%
Mass flow controller: CO_2	Sierra Smart Trak 50 Series: He	0 – 2 Nl/min	± 0.1%
Vertical furnace	Elite Thermal Systems Ltd: TSV15/50/180	0 – 1100 °C cont.	± 5 °C

The CO_2 and N_2 mass flow controllers (MFC) were calibrated continuously throughout the study to ensure that a gas mixture with known concentrations was fed to the vertical tube furnace. The calibrations were done by utilising a bubble flow meter and the calibration curves are presented in Appendix B.1. The accuracy of the mass balance was tested using calibration weights. The results of this assessment can be seen in Appendix B.3. Lastly the temperature profile of the vertical tube furnace was measured to ensure that the sample was in the thermal stable zone and that the temperature in the furnace was the same as the desired set point temperature (see Appendix B.2).

4.3 Experimental set-up

The experimental set-up of the large particle TGA is given in Figure 4.1.

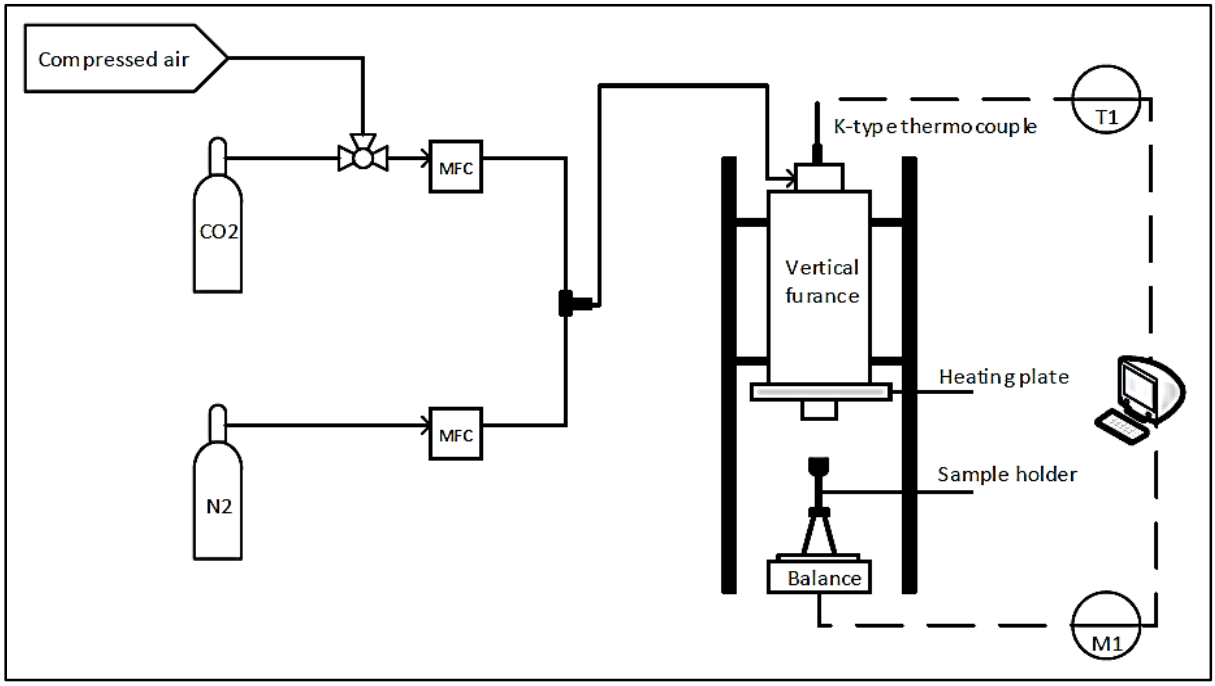

Figure 4.1: Large particle TGA experimental set-up

CO_2 and N_2 gas cylinders were connected to a MFC, which controlled the flow of gases. A three-way valve was connected to the CO_2 line so that the flow to the MFC could alternate between CO_2 and compressed air. The gases were mixed and entered at the top of a 50 mm ID Kanthal pipe, through a 0.25 inch line. The pipe was fitted inside the vertical furnace. A K-type thermocouple was also located at the top of the furnace in order to monitor the temperature of the sample inside the reaction zone. A heating plate was located at the bottom of the tube furnace to ensure that the volatile gases did not condense to form tars. The sample holder was placed directly beneath the tube furnace on a balance, which measured the mass loss continuously. The sample holder was a quartz bucket with openings at the bottom to allow the reactant and product gases to flow through, therefore preventing a stagnant reagent gas layer (see Appendix B.4 for schematic of sample holder). Quartz wool was placed inside the bucket to prevent the ash from falling through the openings, while still allowing the reactant gas to flow through. For the 212 µm experiments an additional sandstone sieve was placed inside the sample holder, with a thin layer of quartz wool on top and then the pulverised chars. The data was logged using Advantech VisiDAQ Runtime software. The data was saved as a comma separated values (csv.) file and exported to Matrix laboratory (MATLAB) V 7.10 R2010a and Microsoft Excel 2010 for further analysis.

4.4 Experimental program

The reactivity experiments were divided into two phases namely phase one and two. This was done in order to accommodate the large number of variables investigated. The first phase served as the screening process. The reactivity of all nine coals were measured and compared at two different temperatures, 950 and 1050 °C. The pressure was atmospheric (87.5 kPa) and only the 20 mm particles were used. These conditions were selected to simulate the operating conditions in the kiln. The first temperature, 1050 °C, was according to the high initial temperature at the feed end of the kiln where the burner is located. The second temperature was selected in order to represent the reactivity of the coals near the discharge of the kiln, where the charge temperature is lower. From the results produced in phase one, two coals were selected to investigate in phase two along with the benchmark coal. The selection was based on the coal and char characteristics, CO_2 reactivity and the coal consumption ratio.

The second phase was an in-depth study of the kinetics of the two selected coals and the benchmark coal. For this phase, four different temperatures were investigated in order to determine the influence of the temperature on reactivity and the activation energies. The temperatures were 900, 950, 1000 and 1050 °C. The pressure was kept atmospheric and the particle sizes were 6 mm and 212 µm. Smaller particles were utilised for phase two, owing to

the fragmentation of some 20 mm particles, which was caused by the rapid heating of the particles (see Section 5.2).

4.5 Experimental method

4.5.1 Experimental conditions

In Table 4.3 the experimental conditions selected are summarised.

Table 4.3: Experimental conditions

Phase one	
Coal feedstock:	Nine different coal samples (Table 3.1)
Coal particle size:	20 mm
Coal sample mass:	± 9.0 g (One particle)
Gas feedstock:	CO_2, N_2 (Compressed air to obtain ash yield)
Gas concentration and feed rate:	• 25 vol.% CO_2 – 1.0 Nl/min • 75 vol.% N_2 – 3.0 Nl/min
Total gas flow rate:	• CO_2/N_2 – 4.0 Nl/min
Pressure:	87.5 kPa (Atmospheric)
Temperature:	950 & 1050 °C
Phase two	
Coal feedstock:	BC-5-53, AC-5-72 & FC-2-21 chars
Char particle size:	6 mm / 212 µm
Char sample mass:	3 g / 1 g
Gas feedstock:	CO_2, N_2 (Compressed air to obtain ash yield)
Gas concentration and feed rate:	• 25 vol.% CO_2 – 1.0 Nl/min / 0.5 Nl/min • 75 vol.% N_2 – 3.0 Nl/min / 1.5 Nl/min
Total gas flow rate:	• CO_2/N_2 – 4.0 Nl/min / 2.0 Nl/min
Pressure:	87.5 kPa (Atmospheric)
Temperature:	900, 950, 1000 & 1050 °C

Both 20 and 6 mm particles were selected, due to the fact that these sizes occur within the coal feedstock of the kiln, with 6 mm being the smallest acceptable size. The reactivity of pulverised chars (212 µm) was also investigated to determine the extent of diffusion on 6 mm particles and to determine the intrinsic kinetic parameters. The pressure and temperatures were selected in order to replicate conditions experienced within the kiln. The CO_2 concentration value was arbitrarily chosen, by referencing the outlet gas composition of the kiln.

4.5.1.1 Influence of sample mass

For the 212 µm the influence of sample mass was investigated to determine if bed diffusion influenced reactivity. 1.0, 1.5 and 2.0 g char samples were loaded and gasified at 1050 °C, with 25 vol.% CO_2 and 75 vol.% N_2. The conversion was determined and the results are given in Figure 4.2.

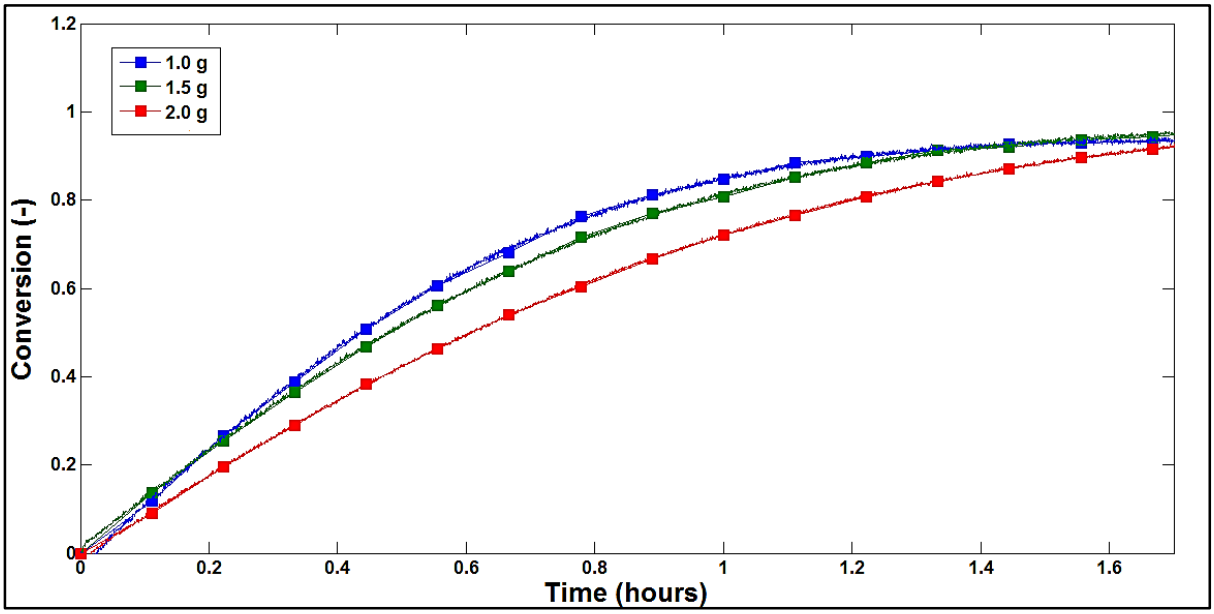

Figure 4.2: Influence of sample mass of AC-4-56 at 1050°C

From Figure 4.2 it can be seen that the conversions of 1.0 and 1.5 g sample masses are similar. For a sample mass of 2.0 g the rate of conversion decreased indicating possible bed diffusion effects. The use of smaller samples sizes (< 1.0 g) resulted in significant noise for the mass loss data and required additional filtering of the data. A sample size of 1.0 g was therefore selected for the 212 µm experiments.

4.5.1.2 Influence of gas flow

The influence of the gas flow rate on the pulverised char particles was investigated to experimentally determine the influence of external mass transfer on reactivity. Pulverised chars were selected as they have the highest reaction rate. The gas flow rates were 1.5, 1.75, 2.0 and 4.0 Nl/min, with the results presented in Figure 4.3.

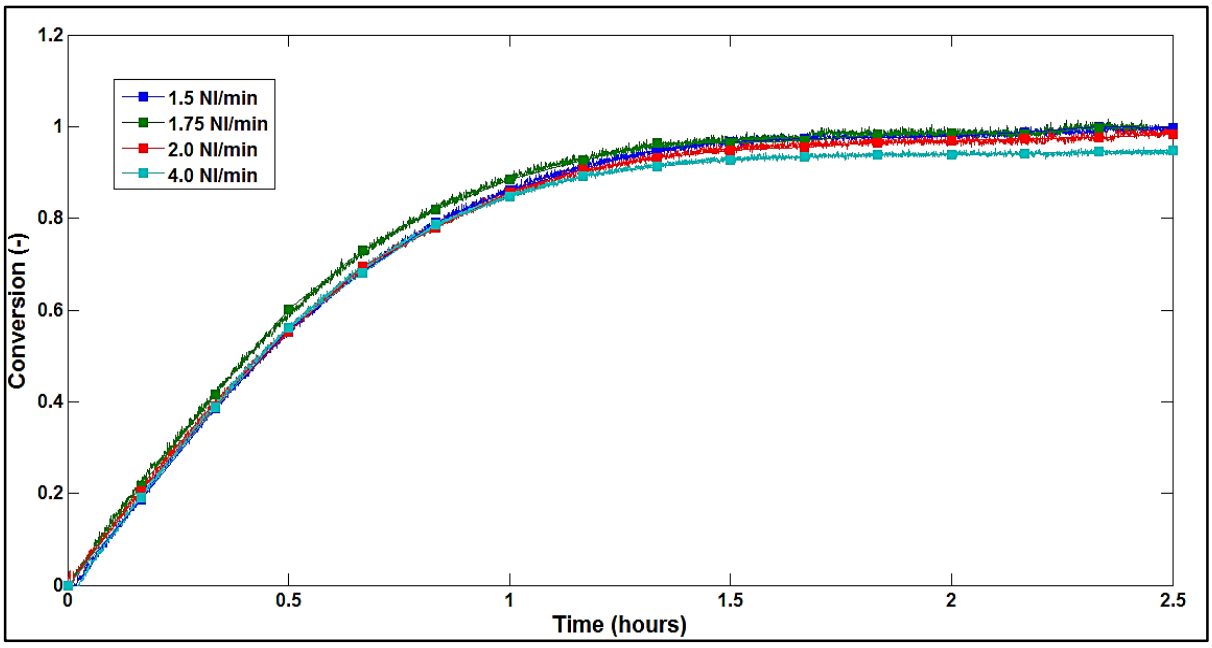

Figure 4.3: Influence of gas flow rate on 212 µm for AC-4-56 at 1050°C

As shown in Figure 4.3 the gas flow rate does not have a significant effect on the gasification reactivity. The measured ash yields of the experimental runs indicated that for a flow rate of 1.5, 1.75 and 2.0 Nl/min no ash mass was lost; however, for a flow rate of 4.0 Nl/min the measured ash yield was lower in comparison to the other flow rates and proximate results, which indicates that the flow rate was too high. The repeatability of the runs was similar and a flow rate of 2.0 Nl/min was chosen.

For the larger particles (6 and 20 mm) a flow rate of 4.0 Nl/min was selected as the external efficiency factor increased and no ash mass loss was observed, compared to lower flow rates.

4.5.1.3 Influence of particle size

The rate of internal diffusion for the pulverised char (212 µm) was experimentally investigated by gasifying - 75 µm char particles (samples selected for phase two) at the lowest (900 °C) and highest (1050 °C) temperatures for phase two. The results are shown in Figure 4.4.

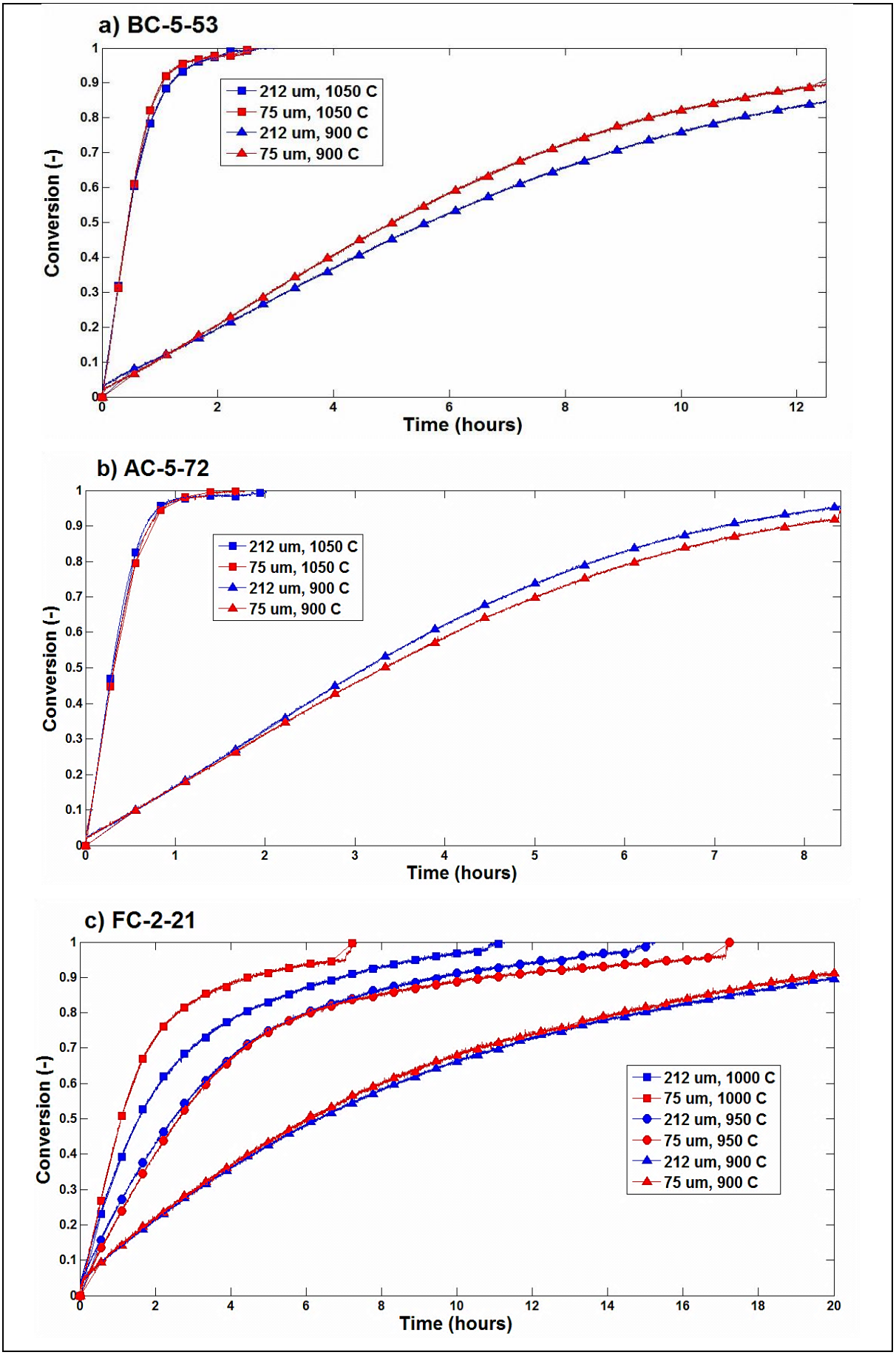

Figure 4.4: Influence of particle size at 900 and 1050 °C

In Figure 4.4 it is seen that for both BC-5-53 and AC-5-72 the rate of conversion for 75 and 212 µm runs at 900 and 1050 °C are similar, leading to the conclusion that for these two samples the rate of internal diffusion is negligible and therefore all the phase two experiments for these two samples are carried out in the chemically controlled regime. Even though there is a marginal difference between the conversions at 900 °C it is assumed to be due to accumulated experimental errors. The other two temperatures (950 and 1000 °C) were also investigated but no difference between the conversions rates of the two sizes was observed, confirming that the rate of internal pore diffusion is negligible.

The conversions for FC-2-21, at 1050 °C, were initially compared and a significant difference between the reactivity of the two sizes was obtained. For this reason 950 and 1000 °C were also investigated to establish at which temperature the rate of internal mass transfer becomes negligible, as shown in Figure 4.4 for FC-2-21. From the results it is seen that for 1000 °C the rate of conversion for the two particle sizes differ, while for 900 and 950 °C they are similar. It is therefore concluded that for 1000 and 1050 °C the experiments were done in the chemical and diffusion controlled regime (regime ll), while for 900 and 950 °C the experiments were carried out in the chemically controlled regime (regime l).

Both BC-5-53 and AC-5-72 are vitrinite-rich coals, which produce more porous chars with greater surface areas (Table A.4). For this reason reagent gases are able to diffuse more easily into the interior of the particles (Fogler, 2006). FC-2-21 is an inertinite-rich coal producing dense chars with smaller surface areas (Table A.4). This in turn decreases the diffusion rate of the reagent gases into the interior of the particle. As the reaction temperature and the chemical reaction rate increases it becomes the rate controlling step, limiting the rate of reaction (Fogler, 2006).

4.5.2 Experimental procedure

4.5.2.1 Phase one

The experimental method for the phase one experiments commenced with heating the vertical tube furnace to either 950 or 1050 °C. Once the desired temperature was reached and the furnace temperature stabilised, the reactant gas mixture was introduced. The furnace was flushed with this mixture for five minutes. In order to eliminate weight fluctuations caused by gas flow, the empty sample holder was placed on the balance and the furnace was lowered to the desired height, after which the balance was zeroed. Next, the sample holder was loaded with a single 20 mm particle. The data logger was started and the furnace was lowered over the sample holder to the predetermined height, within the heating zone. The heating rate of the coal particle was therefore rapid due to the oven being heated prior to the introduction of

the coal particle. This was done in order to mimic the action of the coals moving directly through the kiln burner upon entering the rotary kiln.

Once the mass stabilised or 24 hours passed, the CO_2 and N_2 flow were turned off and compressed air (1.3 Nl/min) was introduced to combust the remaining carbon. After the mass stabilised, the CO_2/N_2 was once more introduced, to return to the original conditions when the balance was zeroed, and this mass was taken as the final mass of the ash. The 1050 °C experiments were repeated four to ten times, depending on the swelling and fragmentation of the particles, while the 950 °C were repeated four to six times, due to the long duration of the runs.

As the experiment proceeded, the temperature and mass were logged at two second intervals. For both the 950 and 1050 °C runs, the experiment proceeded until no significant change in mass loss was observed and the ash yield was generally found to be lower than the value obtained from the proximate analysis. This could possibly be ascribed to the experimental method, where some of the ash was lost from the bucket due to ash segregation and entrainment in the gas flow.

4.5.2.2 Phase two

For the second phase experiments, the procedure was similar to that of phase one, namely the oven was pre-heated to the respective temperatures, the same gas mixture was used and the char particles were rapidly heated. Multiple (3.0 g) 6 mm char particles were packed inside the sample holder in a single layer. These particles were allowed to react for a maximum of 72 hours, after which the run was ended by introducing compressed air. For the pulverised char experiments 1.0 g of sample was weighed and spread in a uniform layer inside the sample holder. The maximum reaction time for the pulverised chars was 36 hours.

4.6 Repeatability

The experimental error was estimated up to a conversion of 60% using a 95% confidence level interval (see Appendix B.5 for description). For phase one the experimental error ranged from 3 to 19% with an average of 9%. The largest errors were observed for AC-4-22 (19%) which could be a result of the heterogeneous nature of this sample due to its high ash value. The smallest error was observed for AC-LC-4. Refer to Table B.2 for a summary of the errors.

The experimental errors for phase two ranged from 2 to 28% for 6 mm and 3 to 12% for 212 µm. The experimental errors for the 6 mm chars (average: 11%) were larger in comparison to 212 µm (average: 6%), due to larger particles being more heterogeneous in nature. The experimental errors for the three difference particle sizes, at 950 and 1050 °C are compared in Table 4.4.

Table 4.4: Comparison of experimental error (%) for different particle sizes

	BC-5-53	AC-5-72	FC-2-21	Average
950 °C				
212 µm	3	5	4	4
6 mm	7	5	19	10
20 mm	5	7	2	5
1050 °C				
212 µm	7	5	5	6
6 mm	11	14	7	11
20 mm	9	6	9	8

As shown in Table 4.4, the average experimental error for the 6 mm particle is the largest in comparison to the other two particle sizes. Typically it is expected that the larger particles have a greater error due to the heterogeneous nature of these particles. For the density preparation individual 20 mm particles were tested, while for the 6 mm particles an average density of ten particles was obtained. The mixture of the various densities for the 6 mm particles could have caused the experimental error to increase. The 212 µm chars had the smallest experimental error, since smaller particles are more homogeneous in nature.

4.7 Data processing

4.7.1 Phase one

An example of a mass loss curve generated during the reactivity experiments is shown in Figure 4.5.

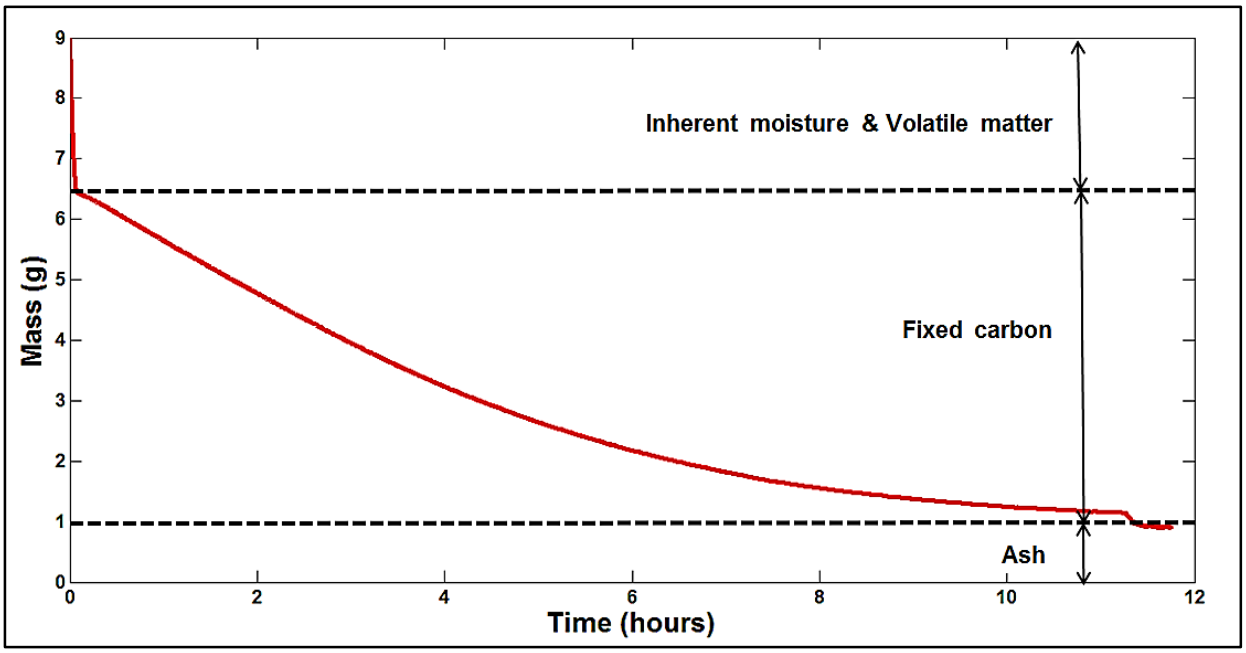

Figure 4.5: Mass loss curve of AC-4-41 at 1050 °C

From the curve it is seen that for the first 8 to 15 minutes the mass loss is rapid due to the release of the volatiles and inherent moisture. After devolatilisation the rate of mass loss decreases as the fixed carbon reacts with CO_2 and the rate continues to decrease with time. The mass loss rate once again increases at the end of the curve owing to the introduction of compressed air that combusts the residual carbon.

The measured volatile + inherent moisture values for both the 950 and 1050 °C were higher in comparison to the proximate measured values, as seen in Table 4.5.

Table 4.5: Comparison between TGA measured volatile + inherent moisture and proximate results.

Coal	Proximate wt.%)	TGA (wt.%) – 950 °C	TGA (wt.%) – 1050 °C
BC-5-53	36.6	39.0 ± 1.4	38.8 ± 1.2
AC-5-72	41.1	44.4 ± 0.6	45.4 ± 1.6
AC-5-50	35.9	39.7 ± 2.5	40.3 ± 3.0
AC-4-56	37.3	40.8 ± 2.7	41.1 ± 1.6
AC-4-41	31.2	36.9 ± 2.2	35.7 ± 2.2
AC-4-22	27.4	32.8 ± 3.4	32.8 ± 4.7
FC-2-13	24.9	26.1 ± 4.7	24.9 ± 0.9
FC-2-21	27.9	28.6 ± 2.9	32.7 ± 1.8
AC-LC-41	31.6	35.6 ± 2.2	38.3 ± 1.0

The difference can be attributed to the rapid particle heating rate and high temperatures, which causes particle fragmentation and promotes the release of volatiles (Senneca *et al.,* 2011). The method of devolatilisation during gasification differs from the proximate method, which could also influence the volatile content. The standard for determining the volatile content is to heat a pulverised sample to 950 °C in a covered crucible to ensure that no air is admitted (Speight, 2005). The experimental runs were done at both 950 and 1050 °C for 20 mm particles under a reactive atmosphere (CO_2/N_2) which could have increased the release of volatiles. When comparing the results of 950 °C to that of 1050 °C it is seen that the values are comparable for the two temperatures. The measured ash yields (based on CO_2/N_2 flow) were lower in comparison to proximate results as shown in Table 4.6.

Table 4.6: Comparison between TGA measured ash values and proximate results

Coal	Proximate wt.%)	TGA (wt.%) – 950 °C	TGA (wt.%) – 1050 °C
BC-5-53	12.9	11.1 ± 1.7	11.1 ± 3.3
AC-5-72	10.1	9.1 ± 3.0	7.8 ± 2.1
AC-5-50	14.2	14.7 ± 0.4	9.2 ± 1.1
AC-4-56	13.6	15.4 ± 4.1	14.3 ± 1.1
AC-4-41	16.3	14.8 ± 6.5	13.3 ± 6.4
AC-4-22	25.8	12.3 ± 0.8	13.4 ± 3.6
FC-2-13	16.4	13.9 ± 2.9	11.1 ± 1.8
FC-2-21	19.6	8.9 ± 3.1	11.9 ± 2.3
AC-LC-41	18.9	17.2 ± 0.7	18.6 ± 4.3

The lower ash yield can be ascribed to a number of reasons including difference in measurement technique between the proximate and TGA experiments and thermal shock owing to the rapid particle heating rate. Another possible reason could be due to a change in the momentum of the gas flow rate over the sample holder. During the last stages of the experimental run, the gas is switched from a CO_2/N_2 mixture to compressed air which alters the momentum of the gas flow over the sample holder leading to the loss of ash. Even though the measured ash yields are lower than the proximate determined values, the values are still similar to each other for the two different temperatures.

From the generated mass loss curve the specific reaction rate of the coal was determined on a dry-ash free basis (d.a.f), using the experimentally determined ash values. The normalised average mass loss curve was first fitted with a spline function, after which the function is differentiated and the specific reaction rate is calculated (Roberts & Harris, 2007):

$$R_s = -\frac{dm_t}{dt}\left(\frac{1}{m_t}\right) \tag{4.1}$$

Afterwards the specific reaction rate was displayed against carbon conversion, which was calculated as follow:

$$x = \frac{m_0 - m_t}{m_0 - m_{final}} \tag{4.2}$$

The conversion vs. time graphs were also drawn, see Section 5.3 for the results of phase one and Section 6.2 for the results of phase two.

4.7.2 Phase two

The generated mass loss curves of phase two are similar to those of Figure 4.5, with the exception of the initial rapid mass loss due to devolatilisation, as chars and not coal are gasified. The data processing for phase two is also similar to that of phase one. The measured ash yields (based on the CO_2/N_2 flow) for phase two are compared to the proximate determined values in Table 4.7.

Table 4.7: Comparison between TGA measured ash values and proximate results

	BC-5-53		AC-5-72		FC-2-21	
	212 µm	**6 mm**	**212 µm**	**6 mm**	**212 µm**	**6 mm**
Proximate (wt.%)	13.5	13.5	12.3	12.3	23.7	23.7
TGA (wt.%) – 900 °C	7.8 ± 2.2	14.9 ± 3.8	10.3 ± 1.2	15.8 ± 1.4	23.9 ± 1.0	19.0 ±2.4
TGA (wt.%) – 950 °C	8.8 ± 1.3	12.8 ± 2.0	4.9 ± 0.8	16.3 ± 6.7	21.7 ± 1.5	24.7 ± 5.1
TGA (wt.%) – 1000 °C	9.0 ± 1.1	13.5 ± 2.0	5.8 ± 3.4	12.6 ± 1.9	25.9 ± 2.0	22.2 ± 3.4
TGA (wt.%) – 1050 °C	6.2 ± 1.0	17.0 ± 2.4	8.8 ± 1.5	11.1 ± 3.8	23.2 ± 1.1	21.7 ± 3.5

From the results it is seen that the ash yields of the 6 mm chars compared well with the proximate values for all four temperatures. For the 212 µm chars the determined ash values are lower, but still comparable to one another for the four temperatures. The lowered ash values could be due to difference in measurement technique and also the change in gas flow momentum when switching from a CO_2/N_2 mixture to compressed air.

4.8 Experimental regime

4.8.1 Isothermal conditions

Isothermal reaction conditions were determined by utilising criteria of Anderson, (1963) (Appendix C). The results of the calculations illustrated that all experiments were done under isothermal conditions. Additionally the time to reach isothermal conditions was also estimated, utilising the approximate solution for transient conduction. The approximate time to reach isothermal conditions at 1050 °C for the phase one experiments is between 3 and 13% of the total reaction time, while for the phase two experiments the time to reach these conditions was between 0.4 and 1.1% for the 6 mm char bed and between 0.008 and 0.015% for the 212 µm char bed (Table C.3 & C.4). From the results it can be assumed that the experiments were carried out under isothermal conditions.

4.8.2 Internal mass transfer

The influence of pore diffusion rate on reactivity was determined both experimentally and numerically. The Weisz-Prater criterion was estimated to determine the extent of internal

mass transfer resistance (Section C.2.1). The determined values were all below one, indicating that the rate of pore diffusion is negligible. Experimentally the influence of mass transfer resistance was determined by comparing the 75 and 212 µm char particles. For the vitrinite-rich coals (BC-5-53 and AC-5-72) no differences were observed between the conversion rates of the two particles sizes for both the lowest (900 °C) and highest (1050 °C) temperatures. From both the experimental and numerical results the conclusion was made that the rate of pore diffusion in negligible for the two samples. A difference was observed between the conversion rate of FC-2-21 for 1000 and 1050 °C, while the conversion rates for 900 and 950 °C were similar. For this reason it was concluded that the 1000 and 1050 °C experiments were carried out in regime ll, even though the numerical results showed otherwise. For 900 and 950 °C the experiments were conducted in the chemically controlled regime, corresponding to the numerical results.

4.8.3 External mass transfer

In order to determine whether external mass transfer limitations existed, the influence of gas flow rate was investigated. From Figure 4.3 it can be seen that the gas flow had little effect on the initial slope of the conversion vs. time graph. Additionally the external effectiveness factor was also estimated for the phase one and two runs, with the values ranging from 0.9 to 1.0 (Section C.2.2). From the results in Section 4.5.1.2 and estimated external effectiveness factors the rate of external mass transfer is assumed to be negligible.

4.9 Statistical analysis

After the reactivity of phase one was determined, the initial specific reaction rate of each sample was statistically related to the coal and char properties given in Chapter 3 as well as additional derived properties given in Appendix A.4. This analysis was performed for both 950 and 1050 °C using Statistical Package for the Social Sciences (SPSS) version 22. The purpose of the analysis was to statistically determine the influence of coal and char properties on CO_2 reactivity at rotary kiln conditions. From the analysis conclusions can be made about which properties have the greatest influence on reactivity and empirical equations can be derived that would assist with the selection of future coals.

For both the coal and char properties Spearman's correlation coefficient (Spearman's ρ) was used to estimate the linear correlations between the properties and initial reactivity. Spearman's correlation coefficient is a non-parametric statistic and therefore can be utilised if the data violates certain parametric assumptions (Field, 2009). Before Spearman's correlation coefficient was estimated, a two-way analysis of variance (ANOVA) was done to compare the mean difference between the two groups and to understand the interaction between the independent variables (temperature and coal) with the dependent variables (coal & char

properties). The results of the ANOVA analysis showed that the data violated the null hypothesis for equal variance, but was still normally distributed. It was concluded that the data is non-parametric in nature and for this reason Spearman's correlation coefficient was selected to estimate the linear correlation coefficients, refer to Appendix D for the analysis. The initial reaction rate was selected due to properties changing during the gasification process and the measured values representing the properties of the samples at the initial stages of gasification.

Spearman's correlation coefficient is also referred to as rank-order and commenced with the data (coal/char properties & initial specific reaction rate) being ranked according to values. Scores were assigned to the rank, with 1 being the highest and 10 the lowest (McDonald, 2014). Next the differences between the ranks were estimated, after which the correlation coefficient was derived using the Equation 4.3 (Laerd Statistics, 2013a):

$$r_s = 1 - \frac{6\sum d_i^2}{N(N^2 - 1)} \tag{4.3}$$

With d_i representing the difference between rank and N the number of data points. A total of 105 coal properties (80 raw - and 25 derived) and 36 char properties (32 – raw; 4 – derived) were evaluated. All properties were on an a.d.b. It was found that 67 coal properties and 19 char properties had a statistically significant linear relationship with the initial reaction rate. For a property to have a significant relationship with the initial reactivity, the significance value of the coefficient should be less than .05 indicating that there is a 95% confidence interval (Devore & Farnum, 2005; Field, 2009).

4.10 Summary

All experiments were done in an in-house constructed large particle TGA, with all equipment tested and calibrated prior to usage. The reagent gas concentrations and pressures were constant, while the particle size and coal/char samples varied. Tests and numerical calculations were performed in order to determine the experimental regimes. From the results it was concluded that no external mass transfer limitations were present and that the experiments were done under isothermal conditions. Further it was concluded that the rate of internal mass transfer resistance was negligible for BC-5-53 and AC-5-72; however, for FC-2-21 the rate of pore diffusion was only negligible for 900 and 950 °C.

The experimental error for phase one ranged from 3 to 19%, while for phase two the errors ranged from 2 to 28% for 6 mm and 3 to 12% for 212 µm. The experimentally determined volatile and inherent moisture values for phase one were higher in comparison to the proximate results. The ash values for phase one and phase two (212 µm) were lower than the proximate results, while that of the phase two (6 mm) compared well.

Lastly a statistical analysis was performed to determine the influence of coal and char properties on the initial reaction rate of the phase one experiments. A total of 67 coal properties and 19 char properties had a statistically significant relationship with the initial reaction rate.

CHAPTER 5: Results and discussion – Phase one

5.1 Introduction

The results of the phase one experiments are presented and discussed. Firstly thermal fragmentation behaviour is reviewed in Section 5.2. The CO_2 reactivity at 950 and 1050 °C is presented qualitatively and quantitatively in Sections 5.3.1 and 5.3.2 followed by a comparison in Section 5.3.3. The statistical influence of coal and char properties on CO_2 reactivity is discussed in Sections 5.4 and 5.5 respectively. In Section 5.6 empirical equations which relate initial reaction rate to coal/char properties are formulated and lastly the selection of samples for phase two is provided in Section 5.7.

5.2 Thermal fragmentation

The three types of transformations and fragmentation are shown in Figure 5.1 (a-c).

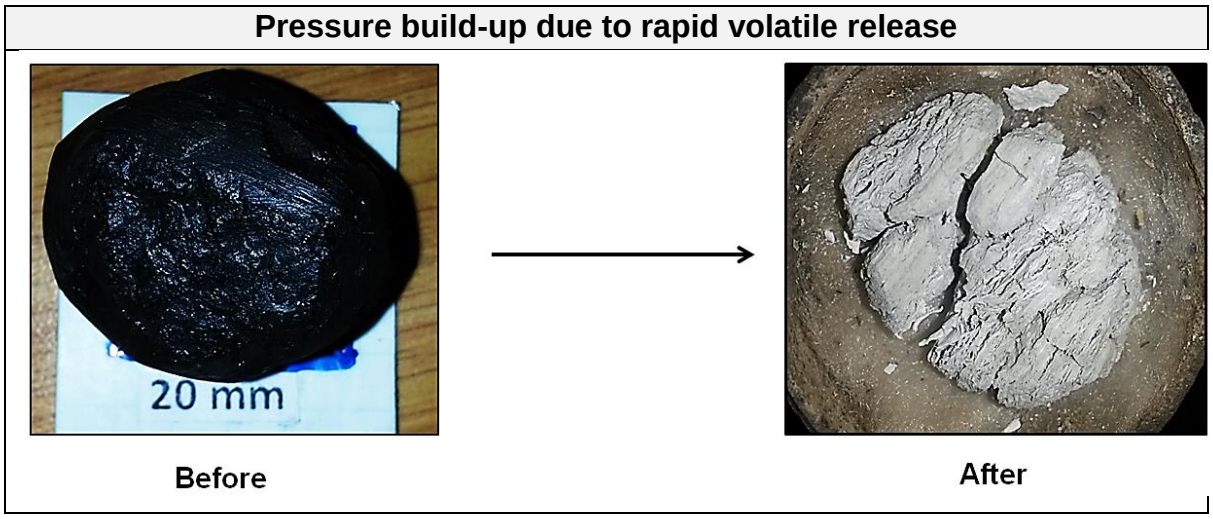

Figure 5.1 a: Example of pressure build-up due to rapid volatile release, AC-4-41 at 1050 °C

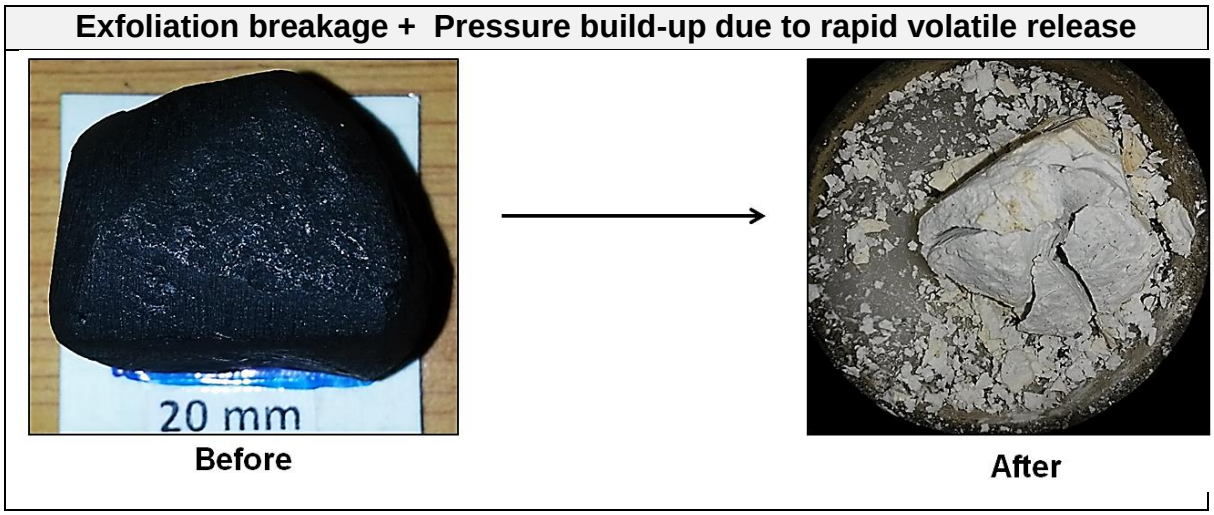

Figure 5.1 b: Example of exfoliation breakage for FC-2-21 at 950 °C

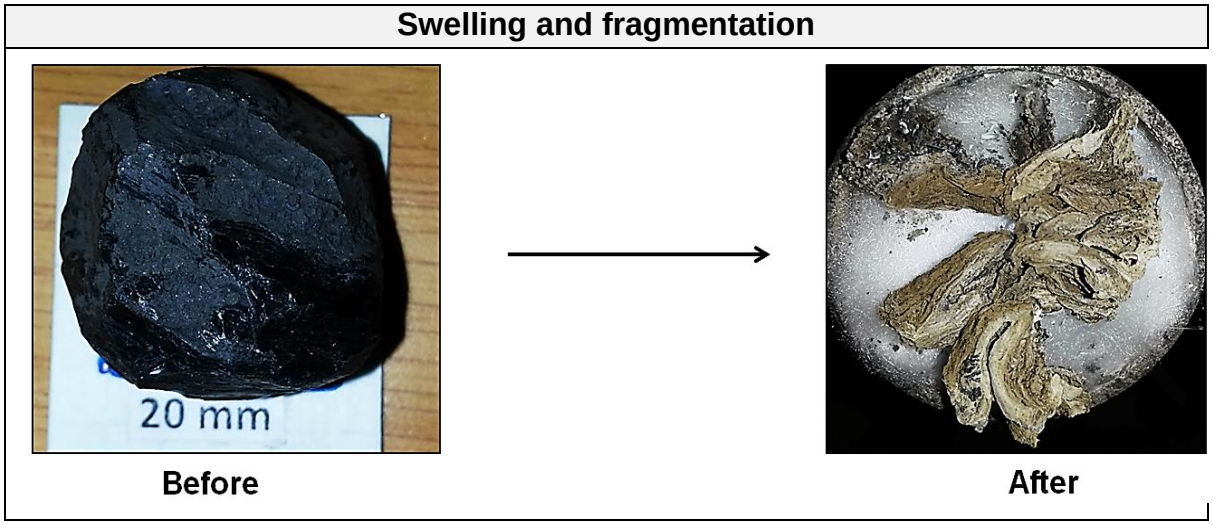

Figure 5.1 c: Example of swelling and fragmentation for AC-5-72 at 1050 °C

Particle fragmentation occurs due to high operating temperatures and rapid particle heating rates. By observing the remaining ash after gasification, conclusions can be made about the different modes of fragmentation. From the ash it is seen that most of the fragmentation and transformation occurred during devolatilisation and that primary thermal fragmentation, possibly due to an internal pressure build-up of volatiles, is the cause of breakage for most of the particles. Volatiles remain trapped within the particle, during devolatilisation, leading to an internal pressure build-up causing the particle to rupture. Primary thermal fragmentation due to rapid release of volatiles is typically characterised by the particle breaking into several smaller pieces which are still comparable in size to the original parent coal (Basu, 2006; Paprika *et al.,* 2013). The direction and evolution of both the primary crack and secondary fissures are dependent on factors such as pre-existing crevices and volatile release paths, which can be characterised by further tomographic experimentation.

The second type of fragmentation observed was exfoliation breakage due to a thermal shock. This type of fragmentation is characterised by the fine ash fragments scattered around the parent particle (Senneca *et al.,* 2013). The exfoliation breakage is possibly due to thermal shock, which is also a mechanism of primary thermal fragmentation initiated by large temperature gradients in the outer core of the particle when the particle is rapidly heated (Paprika *et al.,* 2013; Senneca *et al.,* 2013). Exfoliation breakage is most likely the cause of mass loss, described in Section 4.7.1, as pieces of the particles could have travelled outside the sample holder and furnace.

The third type of transformation observed during gasification is swelling and fragmentation. In the study done by Dakic *et al.* (1989) it was stated that swelling of the particle will relieve the internal pressure build-up thereby preventing fragmentation; however, for these experimental runs it appeared as if swelling of the particles assisted in fragmentation. This supports the

statements made by both Boëlle *et al*. (2002) and Senneca *et al.* (2011) that swelling of particles facilitate breakage due to thinning and weakening of the pore walls. In contrast to fragmentation, the structure of some coals remained fairly intact during gasification. In Figure 5.2 an example of a non-fragmenting particle is given.

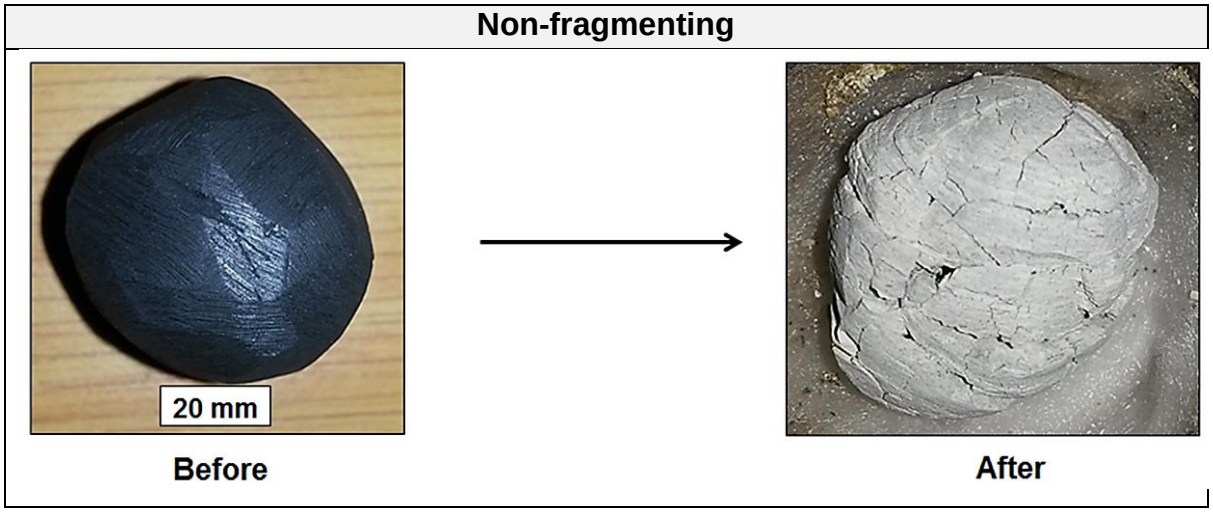

Figure 5.2: Example of non-fragmenting particle during CO_2 gasification, FC-2-13 at 1050 °C

Overall no significant difference was observed for the fragmentation behaviour at 950 and 1050 °C. This is possibly due to most of the volatiles already being released at 950 °C (Cakal *et al.,* 2007; Speight, 2005). The fragmentation behaviour for each sample at both 950 and 1050 °C is given in Table 5.1, with the highlighted cells indicating the most frequent mode of transformation.

Table 5.1: Fragmentation behaviour of coal at both 950 and 1050 °C

	Fragmenting			**Non-fragmenting**
	Volatile release	**Exfoliation**	**Swelling**	
BC-5-53	**X**	X	X	
AC-5-72			**X**	
AC-5-50	**X**		X	
AC-4-56	**X**	X	X	
AC-4-41	**X**	X		
AC-4-22	**X**	X		X
FC-2-13	**X**	X		X
FC-2-21	**X**	X		
AC-LC-41	**X**	X		X

From Table 5.1 it can be seen that the main cause of fragmentation is pressure build-up due to rapid volatile release. It is also observed that for vitrinite-rich coals such as BC-5-53, AC-

5-72, AC-5-50 and AC-4-56 swelling occurred which promoted fragmentation. Even though these coals had low swelling index values (Table 3.15), swelling still occurred for the larger particles. Coetzee *et al.* (2014) concluded that the swelling behaviour of large particles differs from that of the pulverised sample and that the free swelling index cannot generally be used to predict the swelling behaviour of large coal particles. Conversely inertinite-rich coals such as AC-4-22 and FC-2-13 as well as the intermediate coal AC-LC-41 did not undergo fragmentation with each experimental run.

Lastly, secondary fragmentation occurs during gasification when the connecting carbon bridges fracture due to pore development (Basu, 2006). Although this type of fragmentation occurred it was not observed; further tomography experimentation is required to identify this type of fragmentation.

5.3 CO_2 reactivity

In Section 5.3.1 and 5.3.2 the CO_2 reactivity is discussed for 950 and 1050 °C respectively, with results of the two temperatures compared in Section 5.3.3. Traditionally reactivity is qualitatively compared using conversion curves, which are given in Appendix G. For Section 5.3.1 and 5.3.2 the specific reaction rate curves are utilised to qualitatively compare the reactivity.

5.3.1 950 °C

The CO_2 reactivity results at 950 °C are presented in Figure 5.3.

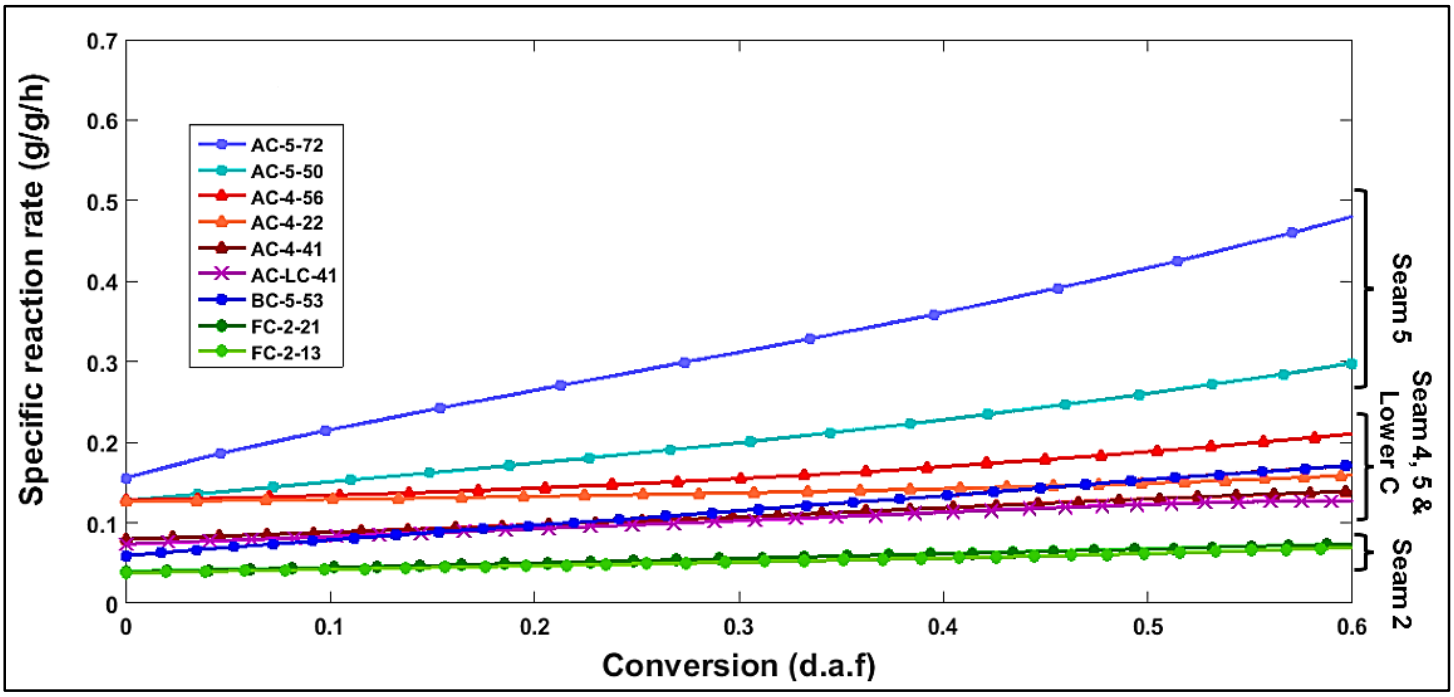

Figure 5.3: Specific reaction rate at 950 °C

It is firstly observed that the reaction rate increases with conversion owing to the development of the pore structure, which expands the pore network and increases the surface area and active site concentration (Jayaraman & Gokalp, 2015; Kajitani *et al.,* 2002; Roberts & Harris, 2000). The seam five coals (indicted by the blue lines) AC-5-72 and AC-5-50 have the highest specific reaction rate, followed by the seam four coals (red lines), the benchmark coal and AC-LC-41, which has similar properties as the seam four coals. The seam two coals (green lines) have the lowest reactivity and appear to remain constant with conversion, relative to the other samples. AC-LC-41 and AC-4-41 have similar reaction rates to BC-5-53, until a carbon conversion of 20%, after which the specific reaction rate of BC-5-53 increases and becomes comparable to AC-4-22.

The reactivity at 950 °C is quantified by presenting the initial specific reaction rate in Table 5.2 ($R_s(x = 0)$). The order of reactivity does not change significantly with conversion and therefore the initial specific reaction rate was selected for discussion. The samples are arranged from most reactive to least reactive and the benchmark coal is highlighted.

Table 5.2: Initial specific reaction rate for 950 °C

Coal	Initial specific reaction rate (g/g/h)
AC-5-72	0.156
AC-4-56	0.128
AC-5-50	0.127
AC-4-22	0.127
AC-4-41	0.080
AC-LC-41	0.074
BC-5-53	0.059
FC-2-21	0.039
FC-2-13	0.038

As shown in Table 5.2, AC-5-72 showed the highest reactivity followed by AC-4-56, AC-5-50 and the remaining two seam four coals. A possible cause is the high vitrinite content of AC-5-72 as well as the swelling behaviour of this coal, which directly influences the internal surface area and reactivity. Both AC-4-56 and AC-5-50 also underwent fragmentation and swelling. It is observed that AC-5-50 has a similar initial specific reaction rate to both AC-4-56 and AC-4-22, however, when observing Figure 5.3 it is seen that the specific reaction rate of AC-5-50 surpasses the reaction rate of the other two samples at higher conversions. This is due to greater pore and structure development during gasification, making AC-5-50 the more reactive coal.

It is seen that the benchmark coal has a low initial specific reaction rate even though this coal is vitrinite-rich and also underwent fragmentation during gasification. A possible reason could be delayed pore and structure development due to closure of pores during heat treatment (devolatilisation) or blockage of pores during the initial stages of gasification (Feng & Bhaita, 2003; Jayaraman & Gokalp, 2015). It is seen from Figure 5.3 that even though BC-5-53 has a low initial reactivity, the specific reaction rate increases to above that of AC-4-22 at a carbon conversion of 60%. FC-2-21 and FC-2-13 have the lowest initial specific reaction rates, which could be due to these coals being inertinite-rich, having the smallest micropore surface area (Table 3.21) and FC-2-13 not fragmenting for each run (Borrego *et al*., 1997; Ochoa *et al*., 2001; Sun *et al*., 2004).

5.3.2 1050 °C

The CO_2 reactivity results at 1050 °C are presented in Figure 5.4.

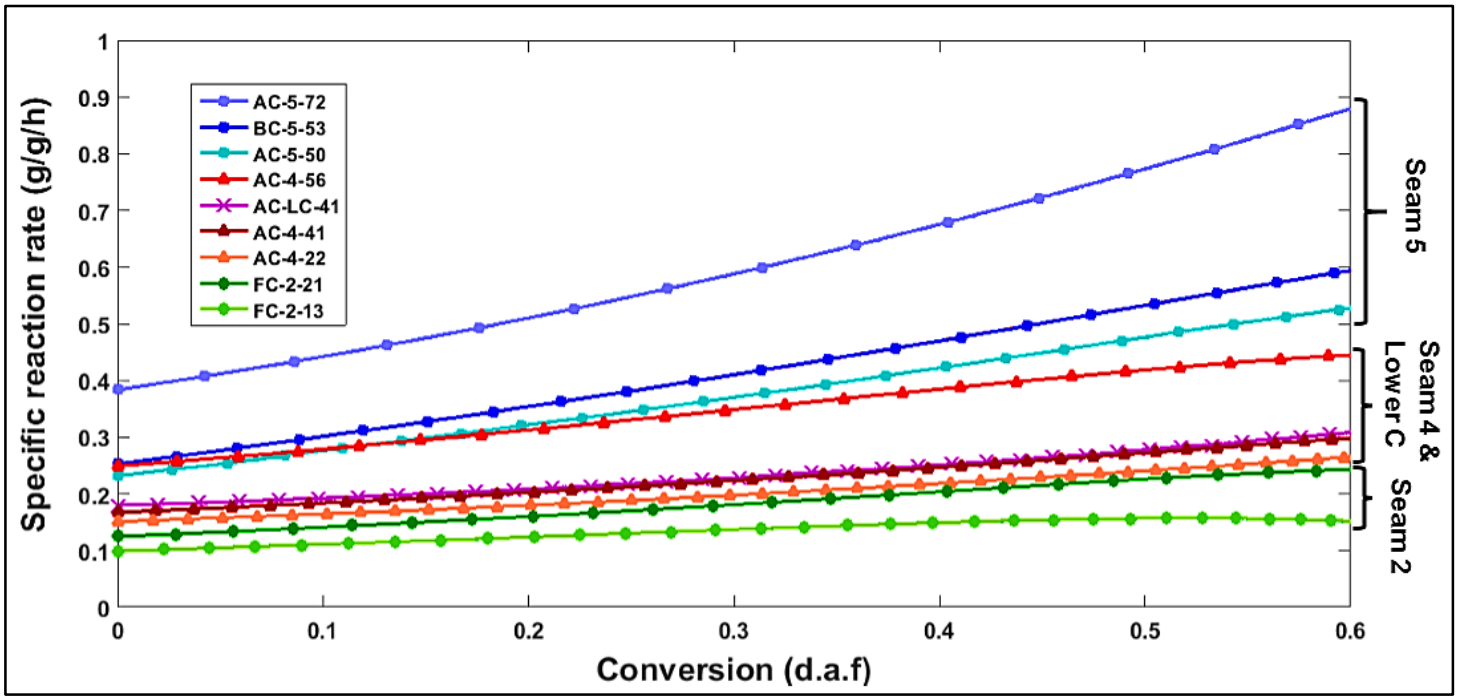

Figure 5.4: Specific reaction rate at 1050 °C

It is again seen that the specific reaction rate increases with conversion, due to the pore structure development and an increase in surface area and active site concentration (Kajitani *et al.,* 2002; Roberts & Harris, 2000). From Figure 5.4 it is also seen that the specific reaction rates of the coals are grouped together according to seams. The seam five coals (blue lines) are the most reactive followed by the seam four coals (red) and AC-LC-41 and then the seam two coals (green).

Similarities between Figure 5.3 and 5.4 include AC-5-72 having the highest reactivity and, FC-2-13 and FC-2-21 having the lowest and second lowest reactivity respectively. Additionally the specific reaction rates of these two coals also appear to remain relatively constant for carbon conversion. The reactivity for 1050 °C is also quantified by presenting the initial specific reaction rate in Table 5.3, in order of reactivity most reactivate to least reactive. The benchmark coal is once more highlighted.

Table 5.3: Initial specific reaction rate for 1050 °C

Coal	Initial specific reaction rate (g/g/h)
AC-5-72	0.384
BC-5-53	0.252
AC-4-56	0.249
AC-5-50	0.232
AC-LC-41	0.180
AC-4-41	0.168
AC-4-22	0.151
FC-2-21	0.125
FC-2-13	0.099

By observing Table 5.3 it is seen that the reactivity of the coals is ordered with vitrinite-rich coals having the highest reactivity, followed by the intermediate coals (equal amounts of vitrinite and inertinite) and then the inertinite-rich coals. AC-5-72 once more has the highest initial specific reaction rate, which is attributed to the same reasons mentioned in Section 5.3.1. From Table 5.3 it is also seen that reactivity of BC-5-53 increased and is now comparable with the other seam five coals.

From the reactivity data it is observed that AC-4-56 has the closest initial specific reaction rate to the benchmark sample; however, when observing Figure 5.4 it is seen that AC-5-50 is more comparable to BC-5-53. The initial reaction rates of FC-2-13 and FC-2-21 seem to deviate more from each other for 1050 °C as seen from both Figure 5.4 and Table 5.3, which could be due to the greater difference in micropore surface area for 1050 °C (Table 3.21).

5.3.3 950 vs. 1050 °C

The reactivity of 950 and 1050 °C is quantitatively compared by estimating the ratio of the initial specific reaction rate of 1050 to 950 °C. The results are presented in Table 5.4.

Table 5.4: Comparison between the reactivity of 950 and 1050 °C

Coal	$R_{s,0\ -\ 1050\ °C} / R_{s,0\ -\ 950\ °C}$
BC-5-53	4.3
AC-5-72	2.5
AC-5-50	1.8
AC-4-56	1.9
AC-4-41	2.1
AC-4-22	1.2
FC-2-13	2.6
FC-2-21	3.2
AC-LC-41	2.4

From the findings it is seen that increasing the reaction temperature with 100 °C, increases the initial specific reaction rate with a factor of 1.2 to 4.3. The results indicate that BC-5-53 is the most affected by the change in temperature. A possible reason could be due to the iron content of the sample ash. When referring to Table 3.14 (Section 3.5.2.2) it is seen that BC-5-53 ash contains a high amount of iron, a compound which is known to catalyse gasification at high temperatures; therefore substantially increasing the reactivity of BC-5-53 at 1050 °C (Çakal *et al.*, 2007; Skodras & Sakellaropoulus, 2002). Refer to Section 5.4.2 for further explanation. AC-4-41 also contained a significant amount of iron compounds, but did not increase with temperature as substantially as BC-5-53, due to its moderate amount of vitrinite.

Possible explanations for AC-4-22 being the least affected by the temperature change are the high ash yield and change in micropore surface area. The ash yield hinders reactivity at higher temperatures due to loss of catalytic activity, reduction of surface area and an increase in the rate of pore diffusion (Higman & Van der Burgt, 2008; Kim *et al.,* 2011; Liu *et al.,* 2008). The negative influence of ash is further investigated in Section 5.4.1. Secondly when estimating and comparing the ratio of the char micropore surface area at 950 °C to that of 1050 °C it is observed that AC-4-22 has the highest ratio, therefore its micropore surface area decreased the most with charring temperature. For this reason the specific reaction rate did not increase significantly with gasification temperature, due to the shrinkage in surface area (Saha *et al.,* 2013; Sinag *et al.,* 2013).

5.4 Influence of coal characteristics

The influence of coal properties on CO_2 gasification reactivity was statistically investigated by determining linear correlations between the initial reactivity, at both 950 and 1050 °C, and the coal properties. The results for the chemical, mineral, thermal, petrographic and physical

properties are presented in Section 5.4.1 - 5.4.5. The properties with a correlation coefficient value greater than .70 are reported, while the remaining statistical significant correlations are given in Appendix E.

5.4.1 Chemical properties

In Table 5.5 Spearman's correlation coefficients (two-tailed) and the significant values for the chemical coal properties at both 950 and 1050 °C are given.

Table 5.5: Statistical parameters for chemical coal properties with CO_2 reactivity

Property	**950°C**		**1050°C**	
	r_s **(two – tailed)**	ρ	r_s **(two – tailed)**	ρ
Raw				
Fixed carbon	-.75	7.4×10^{-6}	-	-
Volatile matter	-	-	.93	4.2×10^{-12}
Hydrogen content	-	-	.88	9.8×10^{-10}
Inherent moisture	-	-	.79	9.7×10^{-7}
Ash value	-	-	-.81	4.2×10^{-7}
Derived				
Atomic H/C ratio	.71	3.0×10^{-5}	.93	1.2×10^{-12}
Fuel ratio	-.71	3.0×10^{-5}	-.93	1.2×10^{-12}
Mineral matter	-	-	-.76	4.5×10^{-6}

From the results in Table 5.5 is can be seen that at 950 °C there is only a statistical significant negative relationship between fixed carbon and reactivity. Studies reviewed by both Irfan *et al.* (2011) and Miura *et al.* (1998), as well as a study by Ng *et al.* (1987) found a similar relationship between fixed carbon and reactivity, which is due to the decrease in functional groups as carbon content (and rank) increases.

For 1050 °C, significant linear relationships are found between the ash value, inherent moisture content, volatile and hydrogen content, with volatile matter having the strongest relationship with reactivity. Kim *et al.* (2011) and Zhang *et al.* (2006a) also observed positive correlations between reactivity and volatile matter. They stated that lower rank coals contain a higher volatile content and that the release of the volatiles facilitates the formation of new pores and opening of blocked pores, which in turn increases access to and utilisation of the active sites in the micropores, as well as the dispersion of the catalytic minerals. Other studies have found that volatile matter increases fragmentation of large particles, which in turn also increases the external area and enhances reactivity (Stubington & Linjewile, 1989). The

statistical analysis revealed a significant correlation between hydrogen content and volatile matter (r_s = .97, ρ = 2.6 x 10^{-16}), which is due to volatiles containing moderate amounts of hydrogen (Tsai, 1982). For this reason, the hydrogen content is also shown to increase reactivity.

With regards to the negative relationship between the ash value and reactivity, a similar trend was observed by Kim *et al.* (2011) who stated that at higher operating temperatures part of the ash melts and loses its catalytic activity. The melted ash covers the pores and surface area, causing internal diffusion limitations and preventing the reagent gases from accessing the active sites (Lui *et al.,* 2008; Ochoa *et al.,* 2001; Wu *et al*., 2008).

The inherent moisture content of the coal is also shown to positively influence the reactivity. This could be due to inherent moisture's relationship with surface area and coal rank. The statistical analysis revealed that there are positive statistically significant relationships between micropore volume (r_s = .45, ρ = .018), BET surface area (r_s = .43, ρ = .026), micropore porosity (r_s = .41, ρ = .034) and inherent moisture. Dakic *et al.* (1988) showed that porosity and equilibrium moisture are directly related and that porosity (and surface area) increases with the moisture content. Thomas & Damberger (1976) also showed a positive correlation between the moisture of the coal and the internal surface area. A greater surface area is known to increase reactivity and therefore inherent moisture can also be indirectly related to reactivity due to an increased surface area.

A statistically significant relationship (r_s = -.82, ρ = 1.7 x 10^{-7}) between vitrinite reflectance and inherent moisture was also obtained, which indicates that moisture decreases with increased coal rank similar to the results observed by Thomas & Damberger (1976). It is known that reactivity decreases with coal rank therefore inherent moisture can once more indirectly influence reactivity due to coal rank (see Section 5.4.4).

The results for the derived properties show that for both temperatures, the fuel ratio and atomic H/C ratio have the most significant influence on the reactivity, with the relationship for 1050 °C being greater than that of 950 °C. The fuel ratio relates to the fixed carbon and volatile matter, while the atomic H/C ratio is related to the hydrogen content. The negative impact of the fuel ratio on reactivity is confirmed in the review by Miura *et al.* (1989) and also by the results of Haykiri-Acma *et al.* (2012). The mineral matter is a function of both ash yield and total sulphur content and has a negative influence on reactivity due to the opposing impact of the ash value.

5.4.2 Mineral properties

For the mineral properties statistical relationships were determined for the XRD analysis of the coal and ash, as well as the XRF analysis of the coal ash. In Table 5.6 the results of the mineral properties are given at 1050 °C, as no correlation coefficients greater than .70 were derived for 950 °C.

Table 5.6: Statistical parameters for mineral properties with CO_2 reactivity at 1050 °C

Property	**r_s (two – tailed)**	**ρ**
Coal properties		
Illite	.70	4.8×10^{-5}
Ash properties		
Magnetite	.75	8.3×10^{-6}
Rutile	-.70	4.5×10^{-5}
Mullite	-.76	5.3×10^{-6}

The findings in Table 5.6 show that for the coal properties only illite has a significant relationship with reactivity at 1050 °C. Illite contains potassium, magnesium and iron, which have a catalytic effect on gasification reactivity (Çakal *et al.*, 2007; Huffman & Huggins, 2009; Skodras & Sakellaropoulos, 2002). As shown in Table E.3 iron increases reactivity at 1050 °C, while magnesium is shown to increase reactivity at 950 °C.

Firstly for the ash properties it is seen that magnetite has a positive influence on reactivity, due to the catalytic influence of iron. In Table E.2 it is shown that hematite (950 °C), which is an iron bearing mineral, also has a positive statistically significant relationships with reactivity. Different studies have shown that magnetite and the addition thereof increases reactivity due to the catalytic effect of iron on gasification (Kim *et al.,* 2009; Ma *et al.,* 2014; Straka, 2011). The formation of magnetite is related to illite and for this reason magnetite could also be seen as having a positive relationship with reactivity. The analysis indicated a statistically significant correlation of .78 ($\rho = 1.4 \times 10^{-6}$) between the illite concentration in the coal and the magnetite concentration in the ash at 1050 °C.

Secondly rutile is shown to have a negative influence on the initial specific reaction rate at 1050 °C. A possible reason for the negative influence is that the mineral inhibits the reactivity of vitrinite. In a study done by Matjie *et al.* (2007) it is shown that there are significant proportions of titanium in the vitrinite of coal, which could interfere with the combustion/gasification reactivity of the coal/char. When referring to the results of the statistical analysis it is seen that there is a statistically significant correlation of -.71 ($\rho = 3.2$ x

10^{-5}) between rutile and vitrinite and a correlation of -.77 ($\rho = 3.1 \times 10^{-6}$) between the titanium and vitrinite at 1050 °C.

Lastly mullite is shown to have a negative influence on the initial reaction rate. Typically mullite is expected to increase reactivity as the presence of this mineral increases the AFT, which in turn decreases the propensity of the ash melting and the internal pore diffusion rate (Deng *et al.,* 2015; Kim *et al.,* 2009). The negative influence of mullite can be indirectly related to sintering of the ash. Kaolinite is transformed to meta-kaolinite and water through de-hydroxylation, which later leads to the formation of crystallised mullite and cristobalite which also decrease reactivity, see Table E.2 (Mayoral *et al.,* 2001). Studies by Selvakumaran & Bakthavatsalam (2015) and Venturelli & Paganelli (2007) showed that structural transformation of the clay with final de-hydroxylation leads to sintering and shrinkage of the surface area. The analysis showed that there are statistically significant correlations between the mullite in the ash and the micropore surface area (r_s = -.80, $\rho = 5.5 \times 10^{-7}$) of the char at 950 °C, supporting the statement that the transformation of kaolinite could cause surface area shrinkage. Shrinkage of the surface area is known to reduce reactivity, while sintering reduces the catalytic activity of the minerals which also decreases reactivity (Argyle & Bartholomew, 2015; Eley, 1994; Ochoa *et al*., 2001).

For the XRF ash properties a strong correlation coefficient is only found for the initial reactivity at 1050 °C. The findings are given in Table 5.7.

Table 5.7: Statistical parameters for coal ash composition with CO_2 reactivity at 1050 °C

Property	**r_s (two – tailed)**	**ρ**
Ti_2O	-.76	5.3×10^{-6}
Al_2O_3	-.79	1.1×10^{-6}

The results in Table 5.7 indicate that titanium and aluminium species negatively influence the reactivity of the coal. Additionally silica species also have a negative correlation with reactivity, when referring to Table E.3. Firstly the negative influence of titanium species is related to the opposing influence of rutile in the ash, which inhibits the reactivity of vitrinite. The influence of aluminium and silica species can be associated with the negative effect of mullite (Table 5.6) and cristobalite in the coal ash (see Table E.2). Acidic coal ash constitutes are typically non-catalytic in nature, however, these elements are still able to inhibit the reactivity by forming melts at high temperatures, which cover the carbon surface area, thereby prohibiting access of the reactant gas. A study done by Sekine *et al.* (2006) showed that aluminium and silica species reduced reactivity by means of covering the carbon surface area. Laser Raman Spectroscope (LRS) mapping of the carbonaceous structure, after steam gasification at 1000

°C, showed that the locations of aluminium and silica species were in accordance with the non-graphite carbon locations indicating that reagent gas could not reach the carbon. Bai *et al*. (2009) observed the formation of molten amorphous aluminosilicates at high temperatures, which covers the surface area and obstructs pores, thereby hindering gasification reactivity.

In general when observing the results it is seen that for 950 °C more elements are observed to have an influence on the reactivity (Appendix E.3), which is expected as most alkali and alkaline earth metals devolatilise at temperatures above 1000 °C (Li, 2007; Quyn *et al.,* 2005). Similar results were also observed by Kim *et al.* (2011) for temperatures above 1050 °C and Ochoa *et al.* (2001) for temperatures above 1060 °C. When referring to Table E.3 for 950 °C, it is seen that calcium and magnesium species have a positive relationship with initial reactivity, as these species are retained within the chars after devolatilisation at high temperatures. Additionally, the catalytic effect of the calcium and magnesium is also observed due to the substantial concentration of these species in the coal ash in comparison to other elements (Kyotani *et al.,* 1986; Quyn *et al.,* 2005; Skodras & Sakellaropoulus, 2002; Walker *et al.* 1979). No statistically significant relationship is observed for the inherent catalytic effect of sodium and potassium species separately, which is due to low concentration of these species. For gasification at 1050 °C, only iron has a positive influence on reactivity, which corresponds with the results of Cakal *et al.* (2007) who stated the catalytic influence of iron is more effective at higher operating temperatures.

For the derived mineral properties no statistically significant relationship, with a value greater than .70, was obtained. The alkali index, base/acid ratio, fouling index, iron + calcium and the silica/aluminium ratio all positively influence reactivity (refer to Table E.3). Numerous studies have confirmed that gasification reactivity increases with alkali index (Hattingh *et al.,* 2011; Sakawa *et al.,* 1982; Skodras & Sakellaropoulus, 2002). The results of Kim *et al.* (2011) indicated a positive relationship between reactivity and both the alkali index and base/acid ratio (alkali ratio), with the alkali ratio having a stronger correlation, corresponding to the results of this study. It is concluded that this is mainly due to the negative influence of the ash value which reduces the positive catalytic influence of the alkali index as well.

5.4.3 Thermal properties

For the thermal properties statistically significant correlation coefficients were only obtained for an initial reaction rate at 950 °C and are shown in Table 5.8.

Table 5.8: Statistical parameters for thermal properties with CO_2 reactivity at 950 °C

Property	r_s (two – tailed)	ρ
Raw		
IT - oxidising	-.72	2.0×10^{-5}
Derived		
Slagging index - oxidising	-.72	2.0×10^{-5}

As shown in Table 5.8 the IT for an oxidising atmosphere reduces reactivity, which is due to the loss of catalytic activity and increase in pore diffusion resistance as ash melts (Kim *et al*., 2011, Wu *et al*., 2008). The slagging index is determined as a function of the IT and HT, both properties which negatively influence gasification reactivity (Table E.4). The slagging index will, therefore, also have an opposing effect on reactivity.

5.4.4 Petrographic properties

The statistical results for the petrographic coal properties are presented in Table 5.9.

Table 5.9: Statistical parameters for petrographic properties with CO_2 reactivity

Property	950°C		1050°C	
	r_s (two – tailed)	ρ	r_s (two – tailed)	ρ
Raw				
Inert semi-fusinite	-.74	1.3×10^{-5}	-	-
Vitrinite	-	-	.93	1.7×10^{-12}
Reactive semi-fusinite	-	-	-.88	1.7×10^{-9}
Inert semi-fusinite			-.89	5.5×10^{-10}
Vitrinite reflectance	-	-	-.86	7.7×10^{-9}
Derived				
V/I ratio	-	-	.94	2.8×10^{-13}
Total reactives	-	-	.93	2.3×10^{-12}
Maceral index	-	-	.93	4.2×10^{-12}
Reactive maceral index	-	-	.93	2.3×10^{-12}
Petrofactor	-	-	-.92	2.3×10^{-11}
Total inertinite	-	-	-.94	2.8×10^{-13}

From the results presented in Table 5.9 it is seen that there are stronger statistically significant relationships between the petrographic properties and the initial reactivity at 1050 °C in comparison to the initial reactivity at 950 °C. For an initial reactivity at 950 °C only the inert semi-fusinite has a correlation coefficient value greater than .70, which indicates a negative

relationship with reactivity. The correlation coefficients for 1050 °C also indicate a negative relationship for the inert semi-fusinite as well as the reactive semi-fusinite. Many authors have stated that reactivity of lower rank coals decrease with inertinite due to the dense chars formed by this maceral during pyrolysis (Alonso *et al.,* 2001; Cloke & Lester, 1994; Tang *et al.,* 2005).

Vitrinite in turn increases the reactivity by forming tenui-network chars during pyrolysis which increases the surface area (Bend *et al.,* 1991; Cloke & Lester, 1994; Jones *et al.,* 1985). When referring to Table 3.21 it can be seen that the micropore surface areas of the vitrinite-rich coals are larger, in comparison to the inertinite-rich coals. Additionally vitrinite and volatile content are also related, having a statistically significant correlation of .98 (ρ = 5.0 x 10^{-20}). Vitrinite typically contains a moderate amount of volatile content (18 to 40%) and therefore vitrinite-rich coals will contain higher amounts of volatile content, which is shown to also increase reactivity, see Table 5.2 (Falcon & Ham, 1988; Tsai, 1982). Lastly a negative linear correlation is observed between the vitrinite reflectance and reactivity. Similar results were found by Crelling *et al.* (1988), Tomaszewicz *et al.* (2013) and Ye *et al.* (1998), who attributed the lowered reactivity with increased rank to the chemical, physical and mineral properties of high ranked coals.

Even though statistically significant relationships are observed between the derived petrographic properties and the initial reaction rate at 950 °C, no correlation coefficients greater than .70 are obtained. The results given in Table 5.9 indicate that for all the derived petrographic properties a strong significant relationship is observed for reactivity at 1050 °C. The total inertinite content decreases the reactivity, while the total reactives and vitrinite/ inertinite ratio (V/I) ratio increase reactivity. These properties relate to the semi-fusinite and vitrinite content respectively. Both the maceral and reactive maceral index have correlation coefficients of .93. These two indices combine the influence of maceral composition, rank and calorific value to predict the carbon burnout for combustion operations; however, results from the study done by Hattingh (2009) showed that the CO_2 reactivity increases with both maceral and reactive maceral index. Since no strong relationship is identified between the reactivity and the calorific values it can be assumed that the influence of the maceral and reactive maceral index is mainly due to the coal rank and maceral composition. Lastly the influence of both the coal rank and reactive maceral content is reflected by the petrofactor. Studies by Choudhury *et al.* (2007) and Kizgut *et al.* (2003) showed a decrease in reactivity with petrofactor, corresponding with the result in Table 5.9.

5.4.5 Physical properties

The particle density is the only raw physical property that has a strong statistically significant relationship with reactivity at 1050 °C.

Table 5.10: Statistical parameters for raw physical properties with CO_2 reactivity at 1050 °C

Property	r_s (two – tailed)	ρ
Density	-.77	2.2×10^{-6}

From Table 5.10 it can be seen that particle density negatively influences reactivity, with similar results observed by Gale *et al.* (1996). The decrease in reactivity with density is most likely due to the increase in the ash yield of the coal. The analysis indicated that there is a statistically significant relationship of .86 ($\rho = 3.7 \times 10^{-17}$) between the ash yield and particle density. The ash yield is shown to have a negative impact on reactivity and for this reason the gasification rate will also decrease with density. The relationship between density and inertinite content could also cause the density to negatively influence reactivity. A correlation coefficient of .76 ($\rho = 3.9 \times 10^{-6}$) was obtained between the particle density and total inertinite content. Inertinite is known to have the highest density in comparison to vitrinite and liptinite (Tsai, 1982). For the derived physical properties only micropore porosity has a statistically significant relationship with reactivity at 950 °C.

Table 5.11: Statistical parameters for derived physical properties with CO_2 reactivity at 950°C

Property	r_s (two – tailed)	ρ
Micropore porosity	.73	1.3×10^{-5}

Table 5.11 indicates that reactivity increases with micropore porosity, which is due to the increased surface area and access to active sites (Silberman *et al.,* 2013; Sinag *et al.,* 2003).

From the results presented in Table 5.5 to 5.11 it can be concluded that chemical and petrographic properties have the largest influence on CO_2 reactivity. For reactivity at 1050 °C the raw chemical and petrographic properties that have the greatest influence, are the volatile and vitrinite content. For 950 °C the fixed carbon and inertinite content, have the greatest influence. In general stronger relationships were estimated for reactivity at 1050 °C than at 950 °C. This is mostly likely owing to the fact that at 1050 °C most of the catalytic minerals have devolatilised and that there are fewer properties that influence reactivity.

5.5 Influence of char characteristics

The influence of char characteristics is statistically determined in the same manner as described for the coal properties, with the results given in Section 5.5.1 - 5.5.3.

5.5.1 Chemical properties

In Table 5.12 the statistical results for the raw chemical properties are shown. Only reactivity at 1050 °C has a statistically significant relationship greater than .70.

Table 5.12: Statistical parameters for chemical char properties with CO_2 reactivity at 1050 °C

Property	r_s (two – tailed)	ρ
Nitrogen content	.85	1.9×10^{-8}
Inherent moisture	.81	3.4×10^{-7}

As shown in Table 5.12 both nitrogen and inherent moisture have a positive linear relationship with reactivity at 1050 °C. Most of the moisture is driven off during pyrolysis and thus the influence of inherent moisture is most likely a result of re-adsorption of moisture after pyrolysis, which is related to the surface area of the char. A larger surface area facilitates the adsorption of moisture and therefore inherent moisture is shown to increase reactivity (De Korte & Mangena, 2004; Hand, 2000). When referring to the statistical analysis it can be seen that there exists strong positive statistically significant relationships between micropore surface area (r_s = .88, $\rho = 1.2 \times 10^{-18}$), monolayer capacity ($r_s$ = .88, $\rho = 1.2 \times 10^{-18}$), micropore volume ($r_s$ = .86, $\rho = 1.2 \times 10^{-16}$) and inherent moisture. For this reason the increased reactivity with moisture is most likely indirectly due to the increased surface area and porosity, similar to the coal properties.

Nitrogen is also shown to have a positive influence on reactivity. Kabe *et al.* (2004) reviewed a study done by Ismail (1987), which stated that nitrogen sites influence char and coal reactivity by encouraging ring attacks due to the concentration of electrons. Another explanation for the influence of nitrogen on reactivity is the relationship between nitrogen and vitrinite. Hindmarsh *et al.* (1994), Matjie *et al.* (2007) and Walker & Mastalerz (2004), found that vitrinite had the highest nitrogen content when compared to the other macerals. The statistical results revealed a correlation of .93 ($\rho = 1.3 \times 10^{-12}$) between the coal vitrinite and char nitrogen content. Nitrogen also has statistically significant relationships with physical characteristics such as micropore surface area and volume, but this could once again be due to the vitrinite which increases surface area.

No strong statistically significant relationships were determined for the derived chemical properties.

5.5.2 Mineral properties

For the char mineral properties XRD analysis was done only for chars prepared at 950 °C. Overall no strong statistically significant coefficients were obtained. Refer to Table E.8 for the char minerals that have a statistically significant relationship with the initial reaction rate.

5.5.3 Physical properties

The statistical results for the physical char properties are given in Table 5.13.

Table 5.13: Statistical parameters for structural char properties with CO_2 reactivity

Property	950°C		1050°C	
	r_s (two – tailed)	ρ	r_s (two – tailed)	ρ
Raw				
Micropore volume (H-K)	.73	1.7×10^{-5}	.81	3.8×10^{-7}
BET surface area	.73	1.7×10^{-5}	-	-
Langmuir surface area	.73	1.5×10^{-5}	-	-
Micropore surface area (D-R)	-	-	.84	3.3×10^{-8}
Monolayer capacity (D-R)	-	-	.84	3.3×10^{-8}
Limiting micropore volume (D-R)	-	-	.84	3.3×10^{-8}
Derived				
Carbon micropore surface area (D-R)	-	-	.86	9.0×10^{-9}

In comparison to the coal results (Table 5.10 & 5.11), it can be seen that for the char reactivity the physical characteristics have a much larger influence. This is due to the structural development during pyrolysis, which in turn increases the surface area of the coal and access to the active sites thereby increasing reactivity (Laurendeau, 1978; Sinag *et al.,* 2003; Walker *et al.,* 1959). Another possible reason is that there is a greater variance in the data for the char properties than for the coal properties, which could lead to better correlations. The results indicate that reactivity increases with increased micropore surface area and volume, which is due to improved access of the reagent gas to the catalytic minerals and the carbon active sites. Studies by Ochoa *et al.* (2001); Saha *et al.* (2013), Silbermann *et al.* (2013) and Sinag *et al.* (2003) also found that a larger surface area increases reactivity.

The influence of the surface areas can also be related to the vitrinite content of the parent coal, as vitrinite-rich coals produce chars with a greater surface area, see Section 3.5.5 (Roberts *et al.,* 2015a; Tang *et al.,* 2005). The statistical analysis revealed a correlation of .87 ($\rho = 5.1 \times 10^{-9}$) between the micropore surface area, monolayer capacity and limiting micropore volume of the chars and the vitrinite content of the parent coal for both 950 and 1050 °C. Furthermore a r_s of .90 ($\rho = 1.7 \times 10^{-10}$) was estimated for micropore volume and BET surface area at 950 °C and a r_s of .95 ($\rho = 3.8 \times 10^{-14}$) for the Langmuir surface area at 950 °C.

For the derived properties only the carbon based micropore surface area at 1050 °C was shown to have a statistically strong influence on reactivity. In the study done by Gomez & Mahinpey (2015) the carbon based micropore surface area was also shown to have a strong

positive influence on reactivity, however, it was based on the parent coal characteristics and not characteristics of the chars.

From the results in Table 5.12 and 5.13, as well as Table E.7 it can be seen that for both 950 and 1050 °C the nitrogen content is the chemical property that has the greatest influence on reactivity. In terms of physical and structural characteristics, micropore surface area, monolayer capacity and limiting micropore volume have the greatest influence for reactivity at 1050 °C, while the micropore volume, BET and Langmuir surface area have the greatest influence for a reactivity at 950 °C. Similar to the coal properties, the correlations coefficients for 1050 °C are greater than for 950 °C.

5.6 Empirical equations

Utilising the results from Section 5.4 and 5.5, empirical equations were determined from which the initial specific reaction rates for both 950 and 1050 °C can be estimated as a function of coal/char properties. Multiple linear regression analyses were done in MATLAB V 7.10 R2010a to determine the empirical equations. The independent coal/char properties that had statistical correlation coefficients with values greater than .70 were selected for regression. Care was taken to ensure that the selected properties did not correlate with one another as multicollinearity may not be present when utilising multiple linear regression. If the equation contained two properties that were related, the property containing the highest correlation with the initial reaction rate was selected. If the resulting equation had a small coefficient of determination or did not meet the necessary statistical requirements (significance values > .05), the property with the smallest correlation coefficient value was eliminated and the regression analysis was repeated. This procedure is known as the backward elimination process and was followed until an equation with a suitable coefficient of determination and acceptable significance values was derived (Field, 2009). If the above mentioned procedure was not successful other combinations of variables were evaluated. The empirical equations with the highest coefficient of determination (R^2) are given in Section 5.6.1 and 5.6.2. Multiple linear regression analysis was also done using SPSS v22, to verify the results, which were comparable for each equation. Additional empirical equations are given in Appendix F.

5.6.1 Coal properties

The following equation was derived to determine the initial specific reaction rate at 950 °C as a function of coal properties:

$$R_{s,0-950^{\circ}C} = 0.11\, Micropore\ porosity - \ 0.0014\, Total\ inertinite - 0.15 \qquad (5.1)$$

From Equation 5.1 it can be seen that micropore porosity increases reactivity while total inertinite decreases reactivity, which corresponds with the trend of the estimated correlation

coefficients (Table 5.11 & Table E.6). In Figure 5.5 the experimental data is compared to the results of Equation 5.1.

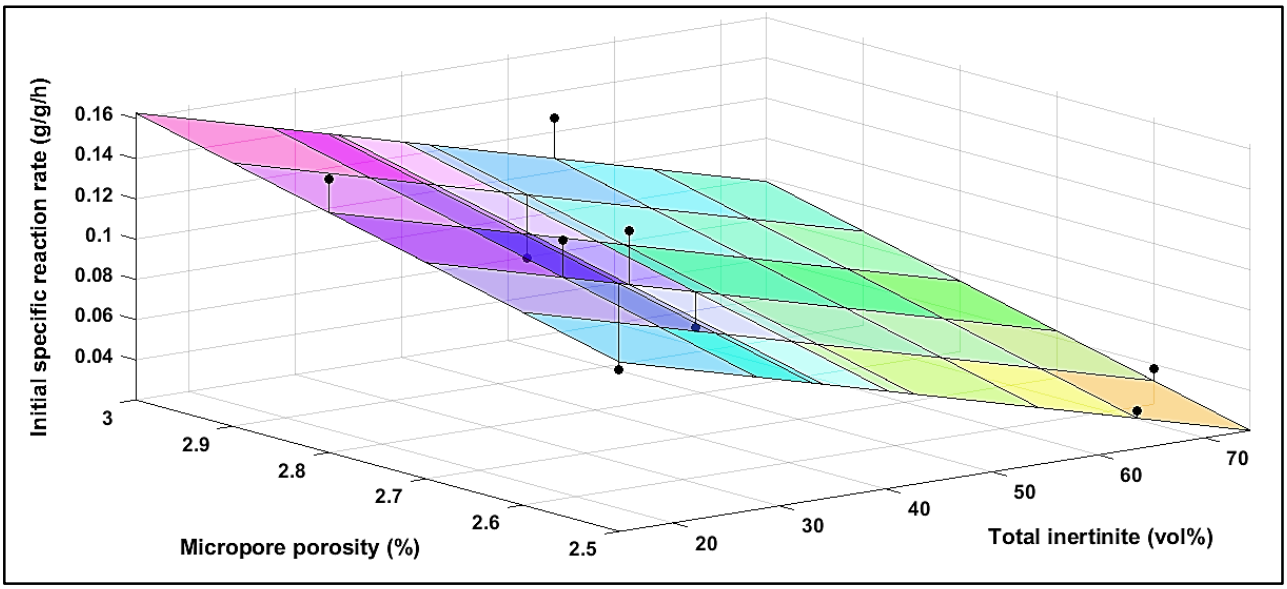

Figure 5.5: Comparison between Equation 5.1 and experimental data for 950 °C (● Experimental results)

From Figure 5.5 it is seen that the differences between the estimated and experimental results are significant and that the data is scattered. For an initial specific reaction rate at 1050 °C the following equation was derived:

$$R_{s,0-1050℃} = 0.013\ RMI - 0.076\ Fuel\ ratio + 0.29 \quad (5.2)$$

With RMI referring to the reactive maceral index. The experimental and determined results are compared in Figure 5.6.

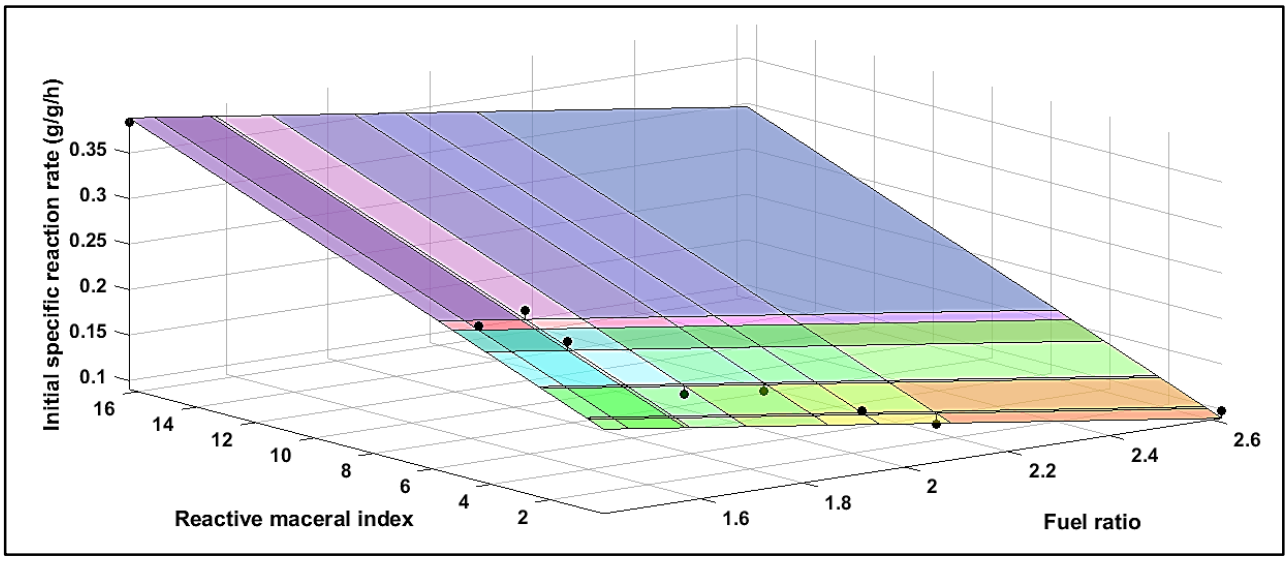

Figure 5.6: Comparison between Equation 5.2 and experimental data for 1050 °C (● Experimental results)

As shown in Figure 5.6 the estimated results compare well with experimental results, which is evident from the minimal differences between the experimental data and Equation 5.2. In comparison to Figure 5.6 it is seen that Equation 5.2 is more accurate in predicting the initial reaction rate at 1050 °C, which is due to the linear correlations coefficients of 1050 °C being greater than those of 950 °C. The coefficient of determination, F-values, significance values and average difference between the experimental and estimated values are given in Table 5.14.

Table 5.14: Statistical parameters for coal equations

Equation	R^2	F-value	ρ	Average difference (%)
5.1 (950 °C)	0.55	14	0.04	21.8
5.2 (1050 °C)	0.90	112	1.3×10^{-6}	4.7

From the results in Table 5.14 it is firstly noticed that the coefficient of determination for 1050 °C is significantly greater than for 950 °C. The F-values, which provides the systematic variation to the unsystematic variation, indicate that the above equations have an influence on initial reactions rate with Equation 5.2 having the greatest influence. The significance values for both equations are below .05; therefore, the equations have a statistically significant relationship with the initial reaction rate at the respective temperatures. Lastly the average difference between the experimental and estimated results shows that Equation 5.1 is the least effective in predicting the initial reaction rate at 950 °C. In Figure 5.7 the experimental and estimated results for the two equations are compared.

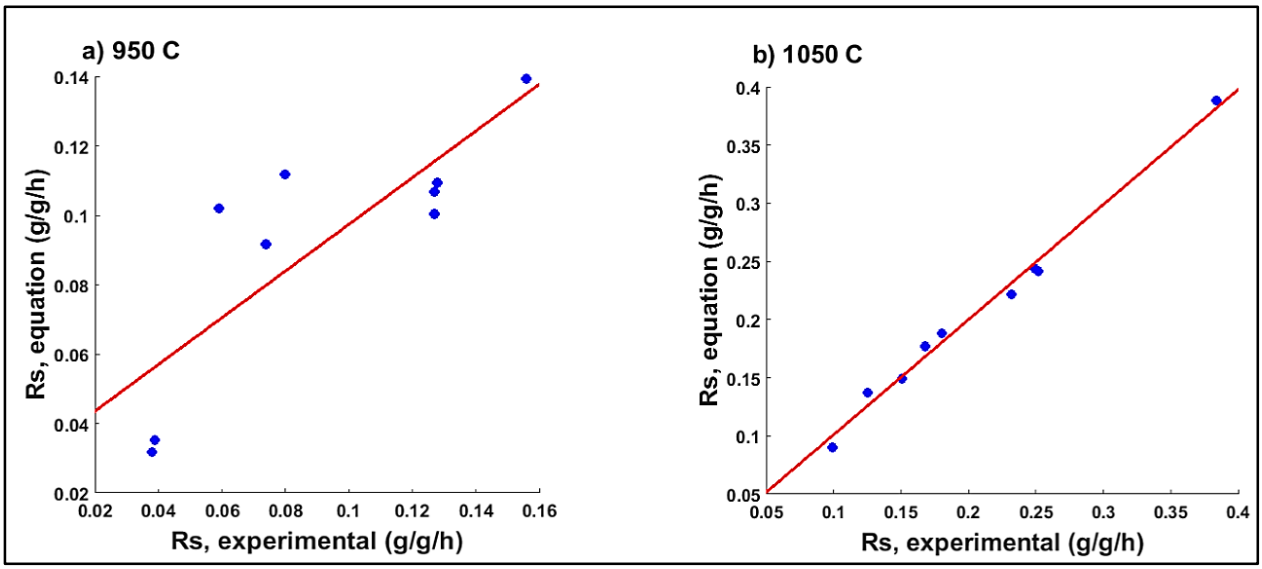

Figure 5.7: Comparison between experimental and estimated results (• Equations ;- Fit)

As shown in Figure 5.7 the data is scattered for 950 °C. The results for 1050 °C indicate that the estimated values are in good correlation with the experimental results. In comparison to

950 °C, the data is much more concentrated around the linear fit, which is attributed to the stronger correlations coefficients estimated for 1050 °C.

5.6.2 Char properties

With regards to the char properties, Equation 5.3 is derived to determine the initial reaction rate at 950 °C:

$$R_{s,0-950℃} = 0.00092\, LSA - 0.051 \quad (5.3)$$

It can be seen that only Langmuir surface area (LSA) of the chars has a positive influence on the initial reaction rate. Equation 5.3 only contains one variable, which is due to this equation giving the highest correlation coefficient in comparison to the other equations evaluated. The comparisons between the experimental and estimated results are given in Figure 5.8.

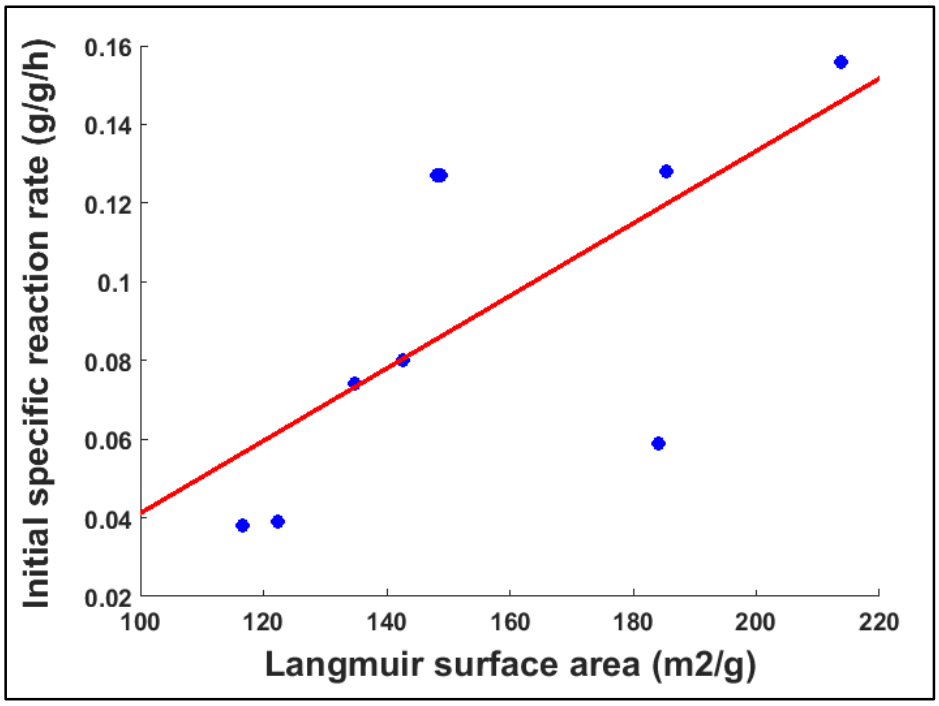

Figure 5.8: Comparison between Equation 5.3 and experimental data for 950°C (● Experimental; - Equation)

As shown in Figure 5.8, the experimental results do not correlate very well with Equation 5.3, which was already indicated by the smaller correlation coefficients between the reactivity and coal char properties at 950 °C.

Equation 5.4 was derived to determine the initial specific reaction rate at 1050 °C as a function of char nitrogen content and carbon micropore surface area:

$$R_{s,0-1050℃} = 0.30\, Nitrogen + 0.0027\, CSA - 0.31 \quad (5.4)$$

As shown in Equation 5.4 the initial reaction rate at 1050°C will increase with nitrogen content and carbon micropore surface area (CSA), which corresponds with the results in Table 5.12 and 5.13. The experimental and estimated results are compared in Figure 5.9.

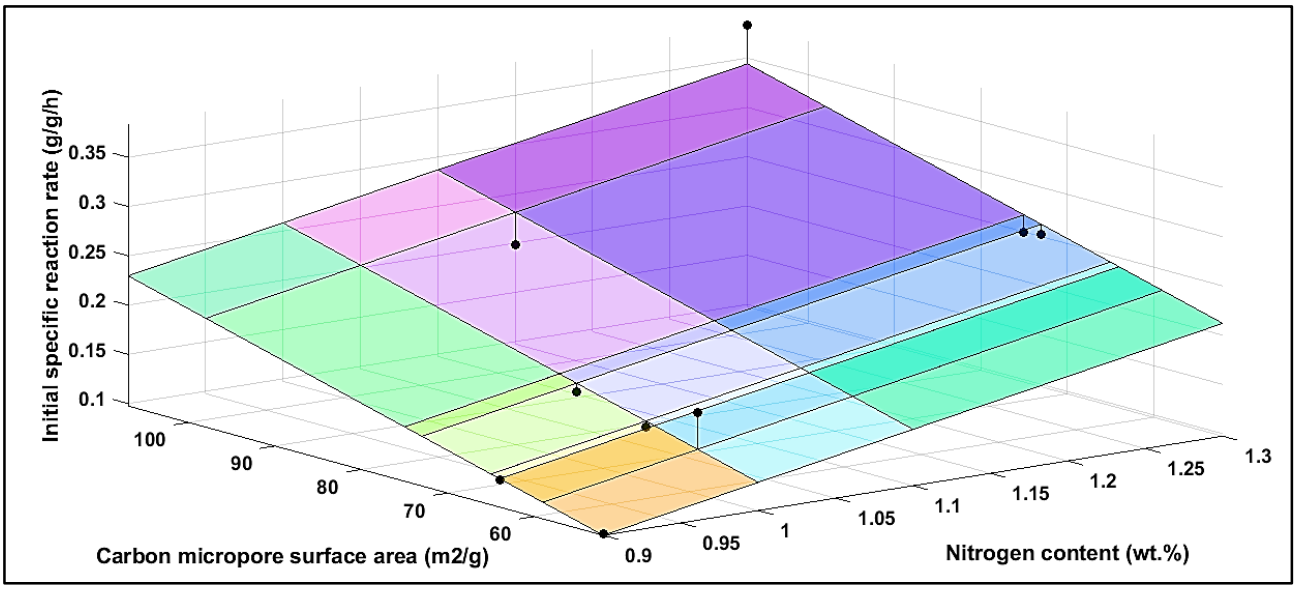

Figure 5.9: Comparison between Equation 5.4 and experimental data for 1050 °C (● Experimental results)

From Figure 5.9 it is observed that the difference between the experimental and estimated results is similar to the results of Figure 5.6. This indicates that Equation 5.4 is able to accurately predict the initial specific reaction rate at 1050 °C. The statistical parameters are given in Table 5.15.

Table 5.15: Statistical parameters for char equations

Equation	R^2	F-value	ρ	Average diff. (%)
5.3 (950 °C)	0.39	16	0.04	32.0
5.4 (1050 °C)	0.84	62	4.7×10^{-4}	7.6

As seen from Table 5.15 the coefficient of determination is close to one for Equation 5.4, indicating a strong correlation. Equation 5.3 has a coefficient of determination of 0.39, indicating that only 39% of the variance in the data was predicted by the equation. The significance values are less than .05, which illustrates that the equation has a statistically significant influence on the initial specific reaction rate. The average difference between the experimental and estimated results show that Equation 5.4 is able to accurately predict the initial reaction rate at 1050 °C. The predicted and experimental results are compared in Figure 5.10.

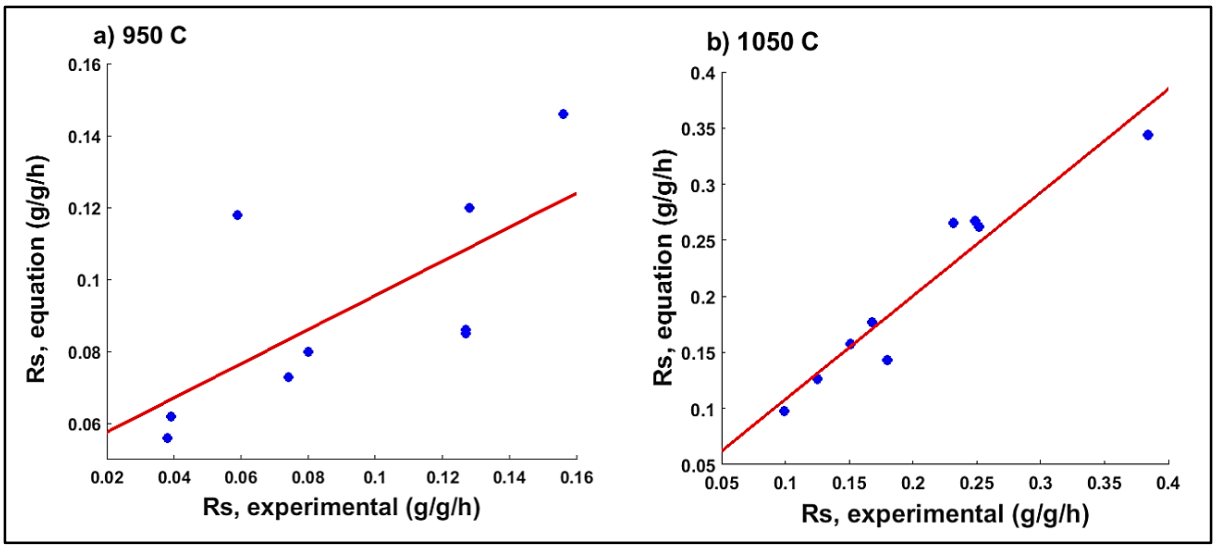

Figure 5.10: Comparison between experimental and estimated results (• Equations; - Fit)

The results in Figure 5.10 show that for 950 °C the data is scattered and that the correlation coefficient is small. There is a strong correlation between the experimental and estimated results for Equation 5.4, which is in accordance with the results in Table 5.15.

5.7 Selection of coals for phase two

For the phase two experiments two coals are selected along with the benchmark coal. The coals selected for phase two are AC-5-72 and FC-2-21. Firstly AC-5-72 is the most reactive coal as seen from the results and the use of this coal will possibly increase pre-reduction values (Chatterjee, 2010; Cunningham & Stephenson, 1980; Sutherland, 2000).

Secondly, as part of the selection process the coal consumption ratio (Fixed carbon/Total iron of feedstock ore) was estimated relative to the coal consumption of BC-5-53, with the results given in Table 5.16. From the findings it is apparent that most of the coals have coal consumption ratios similar to the benchmark coal. AC-5-72 has a higher ratio indicating that this coal has the propensity of burning out too quickly, which increases the coal consumption.

FC-2-21 in turn has a lower coal consumption ratio, indicating that the use of this coal would decrease the coal feed rate, in comparison to the use of the benchmark coal. Even though FC-2-13 has the lowest coal consumption ratio it is also the slowest reacting coal for both 950 and 1050 °C and is thus not recommended for pre-reduction. FC-2-21 has the second lowest coal consumption ratio and is also more reactive in comparison to FC-2-13. FC-2-21 is therefore selected along with AC-5-72. FC-2-21 is less reactive than AC-5-72 which will prevent carbon depletion near the discharge end of the kiln once the fast reacting AC-5-72 has burned out. Lastly both AC-5-72 and FC-2-21 have been investigated by EHSV

separately with the results indicating an increase in pre-reduction and consequently a decrease in energy use.

Table 5.16: Relative coal consumption ratios

Coal	Relative coal consumption ratio
BC-5-53	1.0
AC-5-72	1.1
AC-5-50	1.0
AC-4-56	1.0
AC-4-41	1.0
AC-4-22	1.1
FC-2-13	0.8
FC-2-21	0.9
AC-LC-41	1.0

5.8 Summary

Thermal fragmentation due to rapid particle heating rates and high operating temperatures occurred for some of the coals. From the remaining ash it was observed that primary fragmentation due to internal pressure build-up of volatiles was the main cause of fragmentation for most of the particles. For the vitrinite-rich coals swelling was also observed, which promoted the fragmentation of the particles due to the thinning and weakening pore walls. This in turn increased the reactivity of the coals. For a temperature of 950 °C, the reactivity of the benchmark coal was low, being more comparable to the specific reaction rate of the seam four coals. At an operating temperature of 1050 °C, the specific reaction rates of the coals grouped together according to seam, with the seam five coals having the highest reactivity and the seam two coals having the lowest reactivity. The reactivity of the coals was quantified by comparing the initial specific reaction rates for both 950 and 1050 °C. The results indicated that an increased operating temperature, increases the reactivity with factors of 1.2 to 4.3. From the statistical results it could be seen that chemical and petrographic properties had the greatest influence on reactivity for both 950 and 1050 °C. For 950 °C, inertinite and fixed carbon content had the strongest influence, decreasing reactivity as these values increased. At 1050 °C the vitrinite and volatile content had the greatest influence, increasing reactivity. For the char properties nitrogen and physical properties such as micropore surface area and volume had the greatest influence. Empirical equations were derived to predict initial reaction rate as a function of coal and char properties. The equations derived for reaction rates at 1050°C were able to predict the reaction rate more accurately than the equations for 950 °C. Lastly for phase two AC-5-72 and FC-2-21 will be investigated along with BC-5-53.

CHAPTER 6: Results and discussion – Phase two

6.1 Introduction

In Chapter 6 the results and discussions of phase two are given. Firstly the CO_2 reactivity of both the 212 µm and 6 mm chars is discussed in Section 6.2, followed by the influence of particle size (Section 6.3) and temperature (Section 6.4). In Section 6.5 the kinetic modelling is provided. The chapter concludes with a summary (Section 6.6).

6.2 CO_2 gasification reactivity

6.2.1 212 µm

The conversion vs. time results are presented in Figure 6.1.

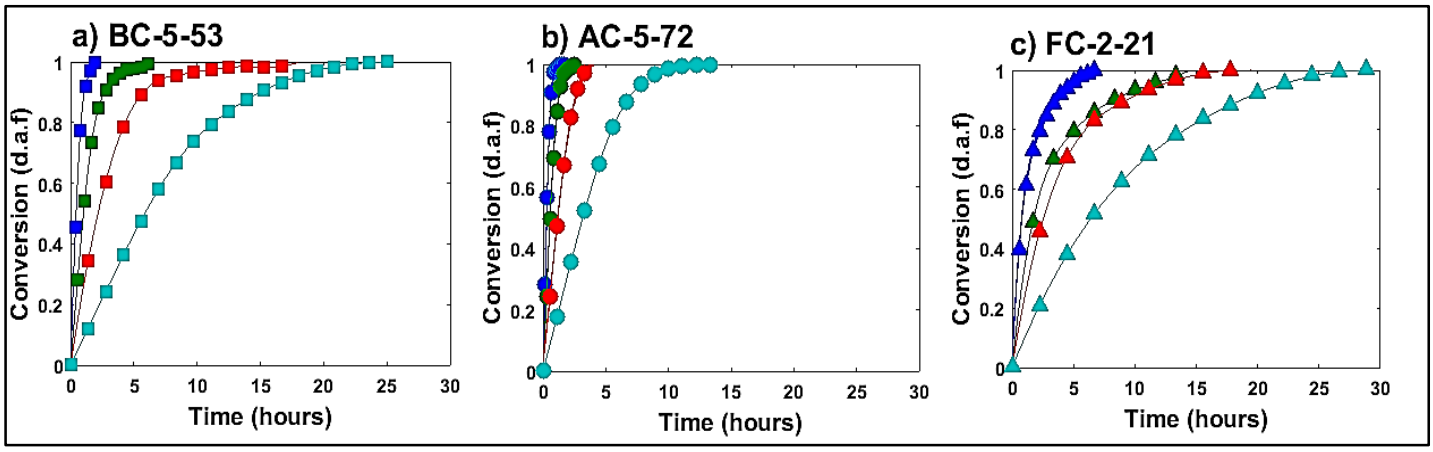

Figure 6.1: Conversion vs. time for 212 µm chars T = 900 – 1050 °C (■ 1050 °C; ■ 1000 °C; ■ 950 °C; ■ 900 °C)

From Figure 6.1 it is seen that temperature increases reactivity. This type of temperature dependence compares well with numerous studies done including, Coetzee *et al.* (2013), Liu *et al.* (2008), Ochoa *et al*. (2001), Sun *et al.* (2004) and Wu *et al.* (2008). The associated specific reaction rates for the 212 µm chars are given in Figure 6.2.

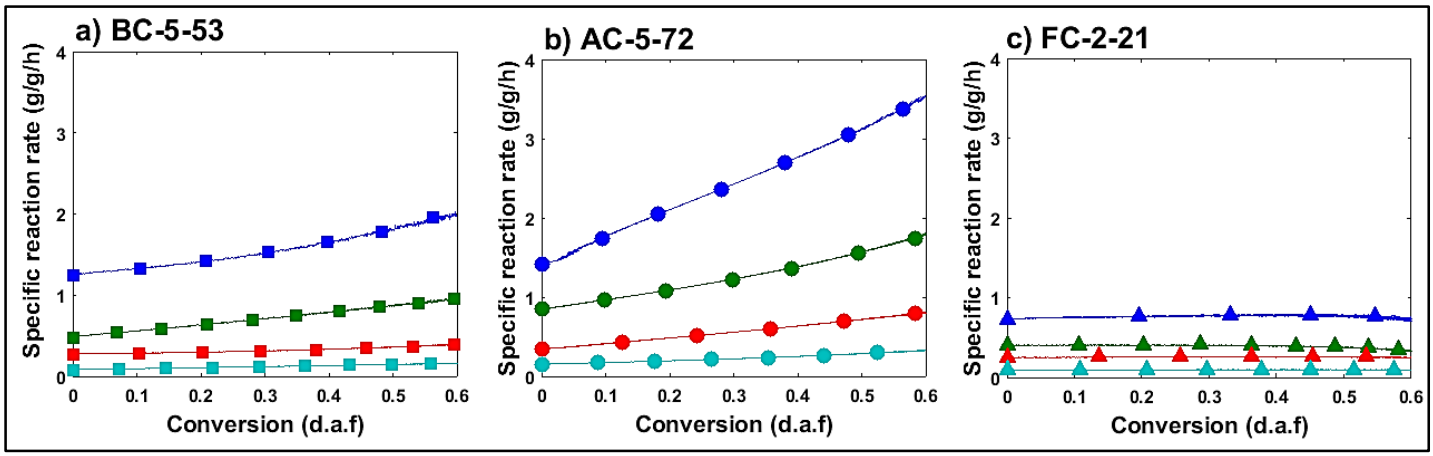

Figure 6.2: Specific reaction rate for 212 µm chars T = 900 – 1050 °C (■ 1050 °C; ■ 1000 °C; ■ 950 °C; ■ 900 °C)

Firstly, when comparing Figure 6.1 and 6.2 it is seen that both figures show a similar temperature dependence. The results in Figure 6.2 illustrate that the specific reaction rates for BC-5-53 and AC-5-72 increase with conversion, with the higher temperature runs increasing more rapidly. These findings are similar to those of phase one (Figure 5.3 & 5.4), with the increase in reaction rate attributed to pore structure development and an increase in the surface area and active site concentration (Jayaraman & Gokalp, 2015; Kajitani *et al.,* 2002). For FC-2-21 it is seen that the specific reaction rates for 1000 and 1050 °C decrease at a conversion of 50%, while the specific reaction rates for 950 and 900 °C appear to remain constant. Jayaraman & Gokalp (2015) and Roberts & Harris (2000) observed similar trends which they attributed to the growth of the pore structure during the initial stage of gasification followed by the gradual collapse of the pore structure due to the coalescence of neighbouring pores. According to Wu *et al.* (2006) the decrease in reaction rate is most likely due to a decrease in active site concentration. The reactivity is quantified, by reporting the initial specific reaction rates as a function of operating temperature in Table 6.1.

Table 6.1: Initial specific reaction rates for 212 µm chars as a function of temperature

Sample	**Initial specific reaction rate (g/g/h)**			
	900 °C	**950 °C**	**1000 °C**	**1050 °C**
BC-5-53	0.08	0.27	0.48	1.25
AC-5-72	0.15	0.35	0.85	1.41
FC-2-21	0.09	0.24	0.39	0.73

As shown in Table 6.1 the reactivity increases with temperatures, which is comparable to the results of both Figure 6.1 and 6.2. The results also indicate that AC-5-72 and BC-5-53 have the highest and second highest reactivity for each temperature respectively, except for 900 °C where the reactivity of FC-2-21 is higher than that of BC-5-53. This is attributable to these coals having high vitrinite contents, which gives the chars a more porous structure (Table A.4). Similar results were also observed for phase one, with AC-5-72 having the highest reactivity, BC-5-53 having the intermediate reactivity and FC-2-21 having the lowest reactivity (Table 5.2 & 5.3). FC-2-21 is an inertinite-rich coal which produces a dense char with smaller surface area, and therefore the reactivity of the char is lower (Tang *et al.,* 2005). Additionally, when referring to Table 3.14, it is seen that AC-5-72 and BC-5-53 have higher alkali index values in comparison to FC-2-21. The catalytic effect of the minerals also increases reactivity.

6.2.2 6 mm

The conversion vs. time graphs are given in Figure 6.3.

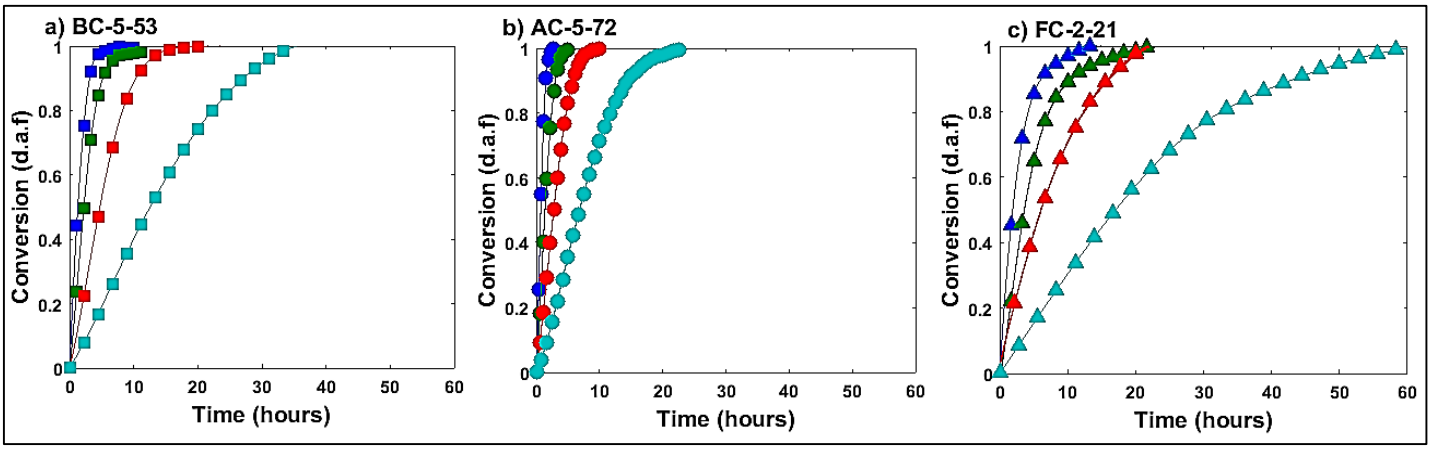

Figure 6.3: Conversion vs. time for 6 mm chars T = 900 – 1050 °C (■ 1050 °C; ■ 1000 °C; ■ 950 °C; ■ 900 °C)

The results in Figure 6.3 are similar to that of Figure 6.1, with the reactivity increasing with an increase in operating temperature. The associated specific reaction rates as a function of conversion for the 6 mm chars are presented in Figure 6.4.

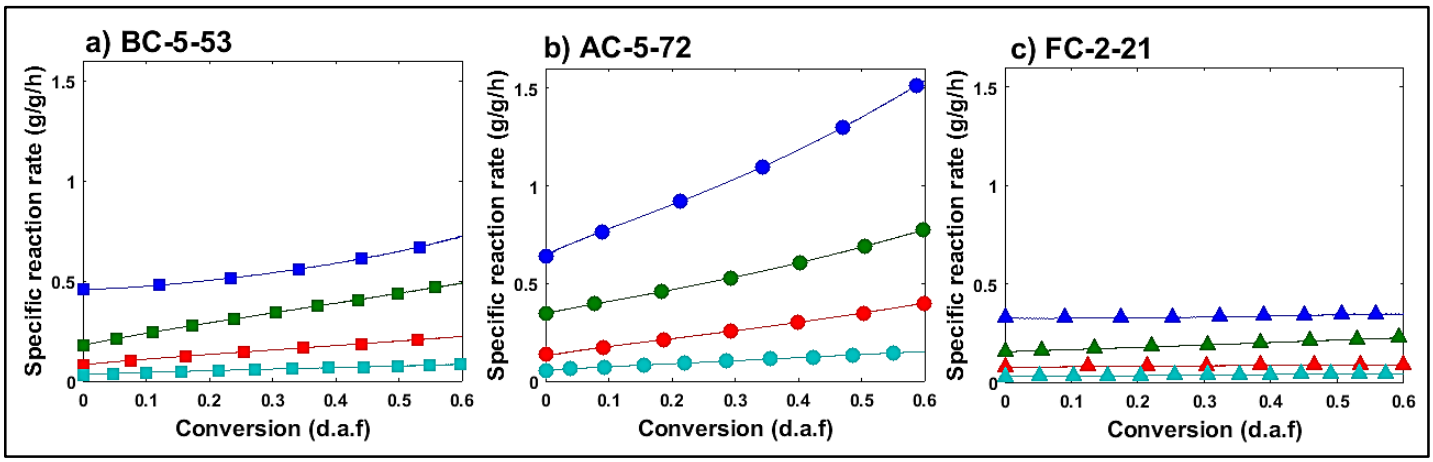

Figure 6.4: Specific reaction rate for 6 mm chars T = 900 – 1050 °C (■ 1050 °C; ■ 1000 °C; ■ 950 °C; ■ 900 °C)

Firstly from Figure 6.4 it is observed that the specific reaction rates increase with conversion for BC-5-53 and AC-5-72, similar to Figure 6.2. It is also seen that reaction rates for the higher temperatures are greater in comparison to the lower operating temperatures. The specific reaction rates of FC-2-21 seem to remain constant, with the exception of 1000 °C which increases with conversion. The reaction rate for 950 °C also decreases slightly at a conversion of 50%, which corresponds to the results for the 212 µm chars. The initial specific reaction rates are reported in Table 6.2.

Table 6.2: Initial specific reaction rates for 6 mm chars as a function of temperature

Sample	Initial specific reaction rate (g/g/h)			
	900 °C	950 °C	1000 °C	1050 °C
BC-5-53	0.03	0.08	0.18	0.46
AC-5-72	0.05	0.14	0.34	0.64
FC-2-21	0.03	0.08	0.16	0.33

From Table 6.2 it is seen that the initial specific reaction rates increases with temperature and that the reactivity behaviour of the chars are similar to the findings of the 212 µm particles. Further when comparing the results of Table 6.1 and 6.2 it is seen that the reactivity decreases with an increase in particle size. Similar findings have been reported in literature; see Section 6.3 for the influence of particle size (Huo *et al.,* 2014; Jayaraman *et al.,* 2015; Kim *et al.,* 2011; Veca & Adrover, 2014).

6.3 Influence of particle size

The influence of particle size on reactivity is quantitatively investigated by comparing the initial specific reaction rates at 1050 °C, given in Table 6.3. Only the reaction rates at 1050 °C for all three particle sizes are compared due to samples being charred at the same temperature.

Table 6.3: Initial specific reaction rate at 1050 °C as a function of particle size and ratio

Sample	Initial specific reaction rate (g/g/h)			Ratio		
	212 µm	6 mm	20 mm	$R_{s,0-6\,mm}/R_{s,0-20\,mm}$	$R_{s,0-212\,\mu m}/R_{s,0-20\,mm}$	$R_{s,0-212\,\mu m}/R_{s,0-6\,mm}$
BC-5-53	1.25	0.46	0.25	1.8	5.0	2.7
AC-5-72	1.41	0.64	0.38	1.7	3.7	2.2
FC-2-21	0.73	0.33	0.13	2.5	5.6	2.2

The results in Table 6.3 show that the specific reaction rate is sensitive to particle size, increasing with a decrease in size which corresponds with results found in literature (Huo *et al.,* 2014; Jayaraman *et al.,* 2015; Kim *et al.,* 2011; Veca & Adrover, 2014). This is due to an increase in the influence of internal diffusion, mineral matter dispersion, greater surface area and secondary reactions of volatiles inside the particle. Van Heek & Muhlen (1985) stated that for smaller particles the minerals are liberated more easily, leading to enhanced reactivity. Zhu *et al.* (2008) additionally stated that the reactivity decreases with particle size due to mineral matter dispersion and secondary reactions of volatiles such as caking and condensation inside the particle, which influences char formation. When comparing the effect of particle size, it is seen that FC-2-21 is the most affected by the change in particle size

(except for the ratio of 212 µm to 6 mm), which is expected as this sample is the most affected by the internal diffusion rate (See Section 4.5.1.3). AC-5-72 is the least influenced, which is due to the porous nature of the char that increases the internal diffusion rate, thereby reducing its effect on the chemical reaction rate. For a ratio of 212 µm to 6 mm, it is seen that BC-5-53 was the most affected by the change in particle size. In Figure 6.5, the initial specific reaction rates, relative to 212 µm, of the three samples at 1050 °C is presented as a function of particle size.

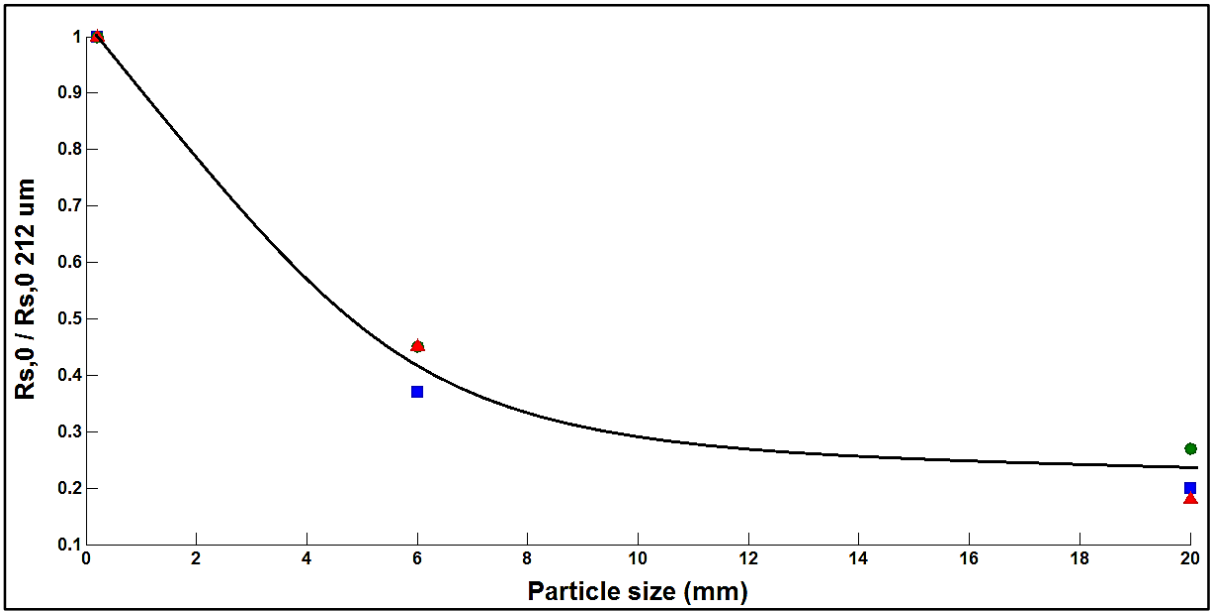

Figure 6.5: Relative initial specific reaction rate as a function of particle size (■ BC-5-53; ● AC-5-72; ▲FC-2-21; - Fit)

From Figure 6.5 it follows that reactivity decreases with particle size, similar to the results of Table 6.3. Furthermore, it can also be seen that even though the reactivity decreases with particle size, the CO_2 reactivity of the large particles can still be related to the standard CO_2 reactivity, which is determined with pulverised chars. This is illustrated by the general size dependent trend shown in Figure 6.5.

6.4 Influence of temperature

The influence of operating temperature was firstly examined by determining the ratio with which the reactivity increased relative to 900 °C. In Table 6.4 the ratios of the initial specific reaction rates of 950, 1000 and 1050 °C relative to the initial reaction rate of 900 °C for both 212 µm and 6 mm chars are presented.

Table 6.4: Reactivity increase relative to 900 °C for 212 µm and 6 mm chars

Sample	$R_{s,0-1050\,°C}/R_{s,0-900\,°C}$	$R_{s,0-1000\,°C}/R_{s,0-900\,°C}$	$R_{s,0-950\,°C}/R_{s,0-900\,°C}$
212 µm			
BC-5-53	15.5	5.9	3.4
AC-5-72	9.4	5.7	2.3
FC-2-21	8.0	4.3	2.7
6 mm			
BC-5-53	13.9	5.4	2.4
AC-5-72	11.8	6.3	2.5
FC-2-21	11.9	5.6	2.7

From Table 6.4 it can be seen that for 212 µm chars, BC-5-53 is the most affected by the increase in operating temperature, which is similar to the results for phase one (see Section 5.3.3). FC-2-21 is the least affected by the temperature increase, with the exception of 950 °C. This could be due to the rate of internal diffusion not limiting the chemical reaction rate at 950 °C for FC-2-21 (Section 4.5.1.3). For the 6 mm chars the samples most affected by temperature varied for the different temperatures. The high vitrinite chars are most affected at the higher temperatures, which is attributable to the porous nature of the char that decreases the rate of internal diffusion. FC-2-21 is most affected at 950 °C, similar to the results of 212 µm (Fogler, 2006; Higman & Van der Burgt, 2008). When comparing the ratio increase of temperature to that of particle size (Table 6.3), it is seen that operating temperature (1000 & 1050 °C) has the greatest influence on CO_2 reactivity, of the two parameters. For 950 °C, the ratios are similar.

The apparent activation energies are estimated utilising the linear form of the Arrhenius equation and are given in Table 6.5 (see Appendix H for Arrhenius plots).

Table 6.5: Estimated apparent activation energies

Sample	Apparent activation energies (kJ/mol)	
	212 µm	**6 mm**
BC-5-53	227 ± 21	223 ± 52
AC-5-72	197 ± 11	216 ± 95
FC-2-21	174 ± 14	211 ± 27

From the results in Table 6.5 it is firstly seen that BC-5-53 has the highest activation energies for both particle sizes followed by AC-5-72 and then FC-2-21. A possible reason could firstly

be the rank of the coals. In a study by Nugroho *et al.* (2000) it was found that the activation energy for combustion decreased with coal rank. When referring to Table 3.7, (Section 3.5.1.1) and Table 3.18 (Section 3.5.4.2) it is observed that FC-2-21 has a higher rank in comparison to AC-5-72 and BC-5-53 and therefore has a lower activation energy. Another explanation could be the ash yield of the parent coals. Although not stated directly it is observed from the results of studies by both Kasaoka *et al.* (1985) and Silbermann *et al.* (2013) that the activation energies tend to increase with a decrease in ash yield. In Table A.2, it is seen that both BC-5-53 and AC-5-72 have lower ash values and for this reason the activation energies are also higher. A higher ash yield could relate to a higher concentration of catalytic minerals that reduces the activation energy.

Initially, when comparing the activation energies for the different particle sizes it is seen that the activation energy increases with particle size, with the exception of BC-5-53 which remains constant. Different studies have observed similar relationships between activation energy and particles sizes, which they attributed to variation in reaction temperature, gas penetration through particle and reaction mechanisms (Jayaraman & Gökalp, 2014; Jayaramsn & Gokalp, 2015; Kim *et al.,* 2011; Veca & Adrover, 2014). This is, however, contradictory to the traditional chemical reaction theory that activation energy decreases with particle size because of the shift to regime II (Higman & Van der Burgt, 2008; Kabe *et al.,* 2004; Szekely *et al.,* 1976). When examining the errors for the activation energies it is firstly seen that the errors of 6 mm are greater in comparison to that of 212 µm, similar to the experimental errors determined for the mass loss curves (see Section 4.6). The conclusion made from the obtained uncertainties, is that it cannot be statistically proven that the activation energy increases with particle size.

When comparing the values in Table 6.5 to reported literature values, it is observed that the activation energies of the 212 µm particles correspond well with the literature reported values (Table 2.3). Both studies by Everson *et al.* (2008b) and Everson *et al.* (2013) obtained activation energies of 192 – 247 kJ/mol and 163 – 236 kJ/mol respectively for small particle CO_2 gasification of South African inertinite-rich coals. Roberts *et al.* (2015b) estimated the activation energies of South African inertinite – and vitrinite-rich pulverised chars, for CO_2 gasification. The results indicated an activation energy of 191 ± 25 kJ/mol for the vitrinite-rich samples and 210 ± 8 kJ/mol for the inertinite samples. The values in general are comparable to results in Table 6.5; however, for this study it was found that the vitrinite-rich samples had a higher activation energy in comparison to the inertinite-rich chars. Lastly Gomez & Mahinpey (2015) found activation energies between 117 – 233 kJ/mol for CO_2 gasification for a wide range of Canadian coals with various ranks.

The 6 mm char particles also corresponded well with literature values. Veca & Adrover (2014) observed activation energies of 176 – 188 kJ/mol for CO_2 gasification of sub-bituminous Sulcis and South African chars. Kasoaka *et al.* (1985) determined the activation energies of 23 different chars of varying rank and found that the values for CO_2 gasification ranged from 197 – 310 kJ/mol. Jayaraman & Gokalp (2015) determined the activation energies of high ash low rank Turkish coals, with the values ranging from 116 to139 kJ/mol for CO_2 gasification. These values are low in comparison to the results of Table 6.5, which is a result of the high ash values of the Turkish coals.

6.5 Kinetic modelling

Different models were investigated to describe the gasification behaviour of the coals, which include the MVN, Wen model and SCM. It was found that the semi-empirical Wen model, developed by Wen (1968), described the gasification rate for both the 6 mm and 212 µm chars, the most accurate. The general form of the model is given in Equation 6.1:

$$\frac{dx}{dt} = k(1-x)^m \tag{6.1}$$

With the constant *m* and *k* regressed using the sum of least squares method. In order to determine the constants, Equation 6.1 is rewritten in terms of R_s:

$$R_s = k(1-x)^{m-1} \tag{6.2}$$

With the linear form:

$$\ln(R_s) = (m-1)\ln(1-x) + \ln(k) \tag{6.3}$$

Modelling was done up to a conversion of 60% for BC-5-53 and AC-5-72 and up to a conversion of 40% for certain FC-2-21 samples, due to the data only following Equation 6.3 up to a conversion of 40%. An example of a linear fit is shown in Figure 6.6:

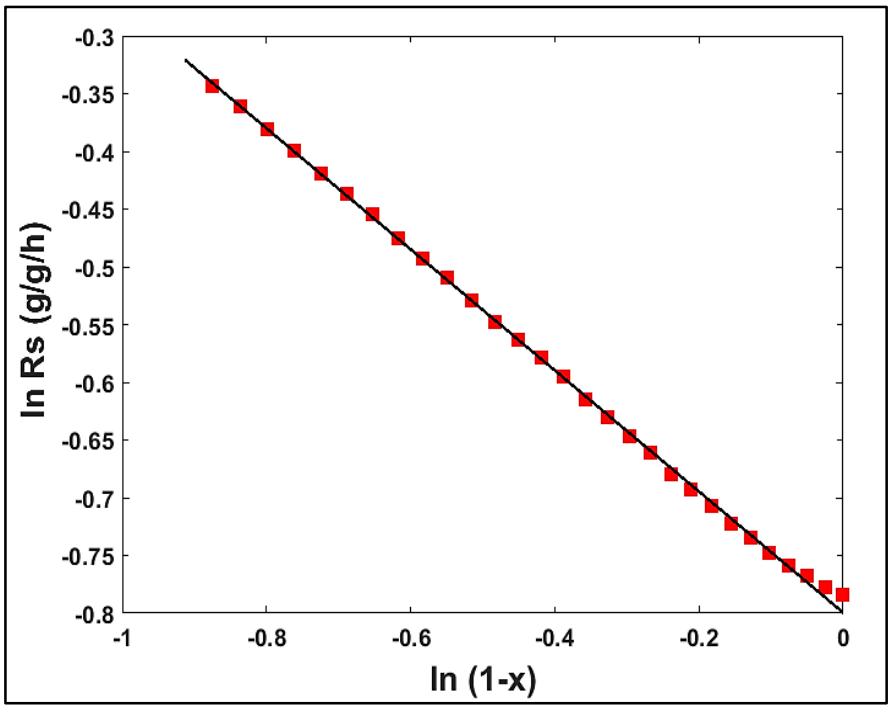

Figure 6.6: Linear fit of the Wen model for BC-5-53, 6 mm char at 1050 °C (■ Data; - Fit)

The determined constants are listed in Table 6.6 and 6.7.

Table 6.6: Determined *m* and *k* (g/g/h) values for 212 µm

	900 °C		950 °C		1000 °C		1050 °C	
	m	***k***	***m***	***k***	***m***	***k***	***m***	***k***
BC-5-53	0.29	0.09	0.61	0.27	0.28	0.53	0.48	1.26
AC-5-72	0.17	0.16	0.11	0.40	0.17	0.90	0.04	1.65
FC-2-21	0.98	0.10	1.00	0.25	1.18	0.42	1.06	0.78

Table 6.7: Determined *m* and *k* (g/g/h) values for 6 mm

	900 °C		950 °C		1000 °C		1050 °C	
	m	***k***	***m***	***k***	***m***	***k***	***m***	***k***
BC-5-53	0.07	0.04	0.00	0.10	0.00	0.22	0.48	0.45
AC-5-72	0.00	0.07	0.00	0.16	0.09	0.37	0.02	0.69
FC-2-21	0.48	0.03	0.74	0.08	0.55	0.16	0.91	0.32

For both the 212 µm and 6 mm particles it is observed that the rate constant (*k*) increases with temperature and that the values for the 212 µm are larger in comparison to the 6 mm. No general trend is observed for the solid reaction order (*m*). The rate constant values also compare well with the initial specific reaction rates, given in Table 6.1 and 6.2. For FC-2-21 the values for 212 µm are close to one, indicating that FC-2-21 follows the homogenous model

for this particle size. The obtained reaction order for some 6 mm samples is zero indicating that the rate is independent of the reactant conversion. The average *m* values are listed in Table 6.8.

Table 6.8: Estimated average *m* values for 6 mm and 212 µm Wen models

Sample	212 µm	6 mm
BC-5-53	0.41	0.14
AC-5-72	0.12	0.03
FC-2-21	1.00	0.67

As shown in Table 6.8 the average reaction order for AC-5-72 is the smallest, while FC-2-21 has the largest reaction order. Also the reaction order decreases with particle size. These average values were used to model the gasification behaviour for particles sizes as shown in Figure 6.7 and 6.8.

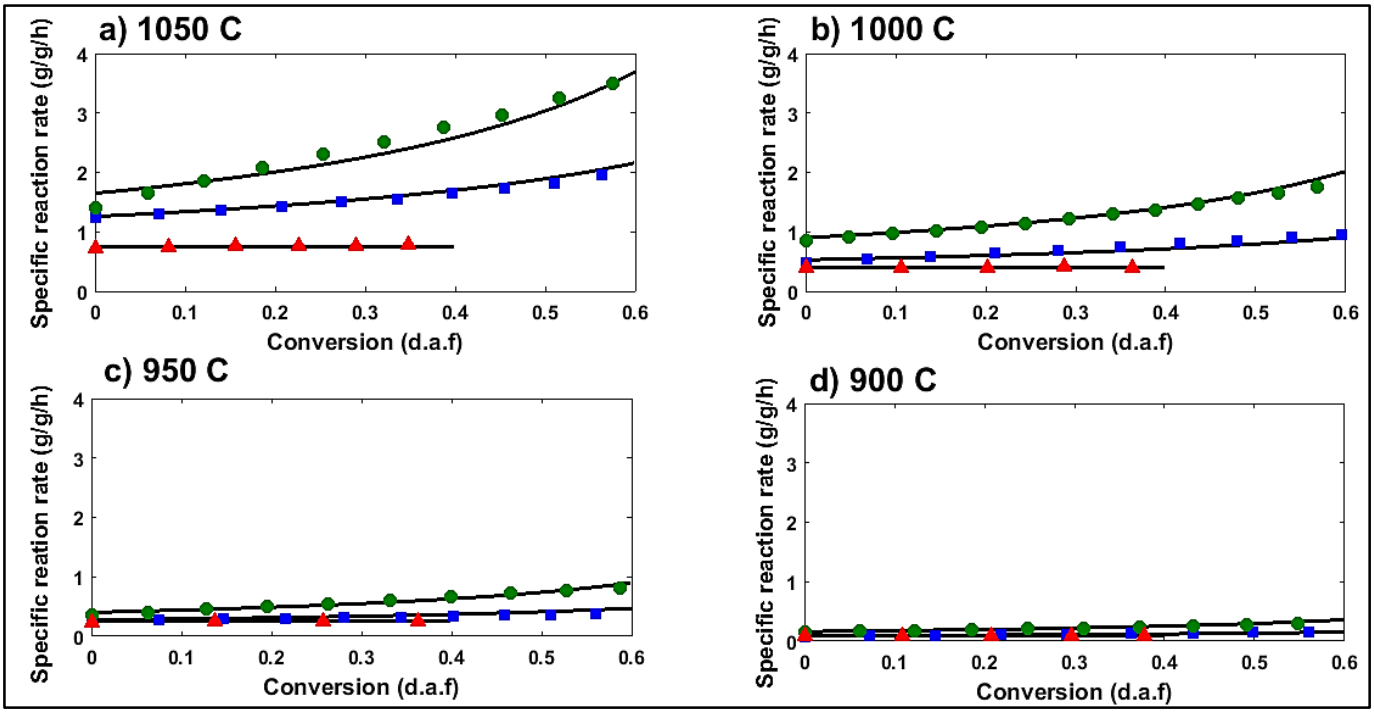

Figure 6.7: Comparison between modelled and experimental data for 212 µm at T = 900 – 1050 °C (■ BC-5-53; ● AC-5-72, ▲FC-2-21; - Model)

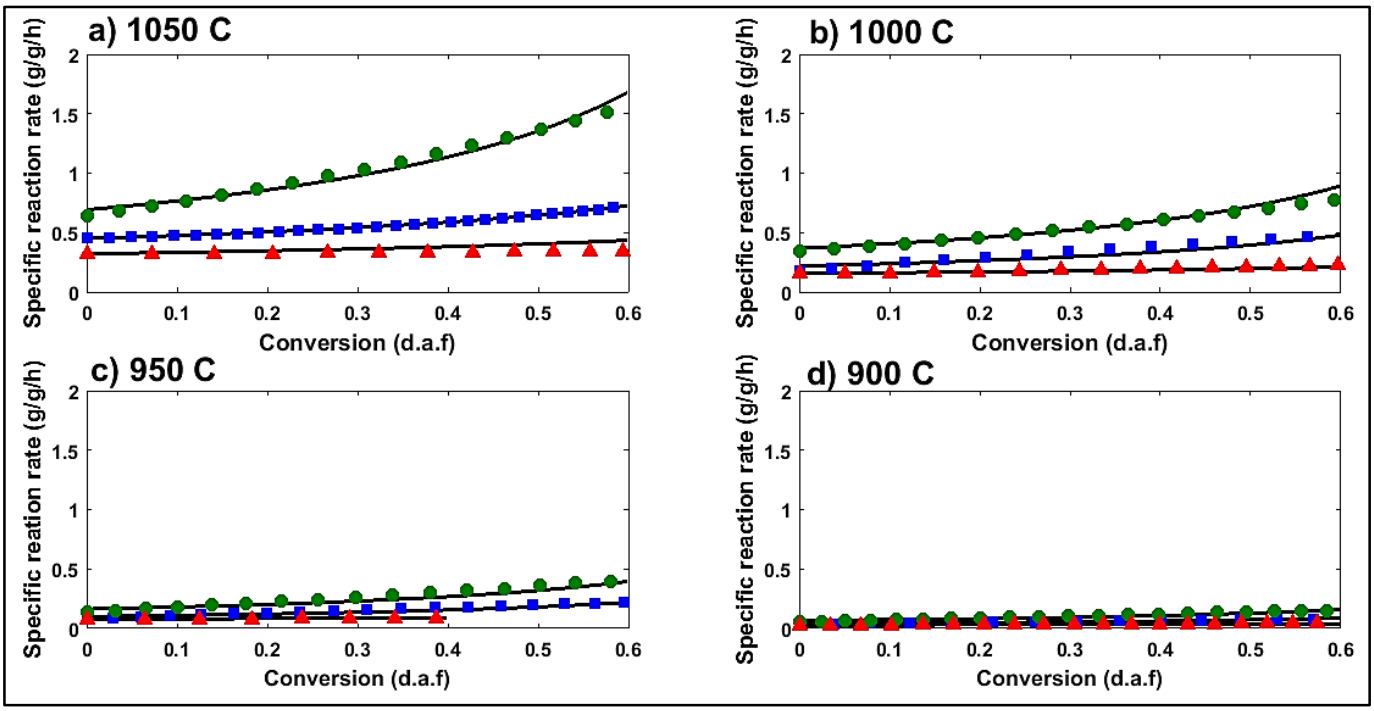

Figure 6.8: Comparison between modelled and experimental data for 6 mm at T = 900 – 1050 °C(■ BC-5-53; ● AC-5-72, ▲ FC-2-21; - Model)

From Figure 6.7 and 6.8 it can be seen that for smaller particles the Wen model is able to fit the data more accurately in comparison to the larger particles. The average quality of fit for the three samples varied between 94 and 98% for 212 µm and between 90 and 94% for the 6 mm particles. The apparent activation energies are also estimated using the modelled values of *k* and compared to the experimental data, and these results are presented in Table 6.9. The experimentally determined activation energies are based on $R_{s,0}$, while the model determined activation energies are based on *k* (see Appendix H for Arrhenius plots).

Table 6.9: Apparent activation energy (kJ/mol) comparison

	212 µm			6 mm		
	Experimental	**Model**	**Diff. (%)**	**Experimental**	**Model**	**Diff. (%)**
BC-5-53	227	222	2	223	208	7
AC-5-72	197	201	2	216	204	6
FC-2-21	174	173	1	211	205	3

In Table 6.9 it is shown that the model determined activation energies for the small particles are similar to the experimentally determined values with the percentage differences being less than 2%. For the 6 mm the differences between the model and experimentally determined values were greater, but still < 7%. The results show, that the Wen model is able to accurately predict the gasification rate of the pulverised and coarse chars.

Previous studies that evaluated the Wen model (ICM) include Silbermann *et al.* (2013), Xu *et al.* (2009) and Zou *et al.* (2007). Xu *et al.* (2009) utilised the Wen model to determine the reaction order for the char, coarse and fine slag CO_2 gasification reactivity, with values ranging between 0.48 and 1.01. For the study by Zou *et al.* (2007) estimated *m* values ranged from 0.54 to 0.88 for CO_2 gasification of petroleum coke. Silbermann *et al.* (2013) investigated numerous models and found that the ICM (Wen model) was best suited to fit the reaction rate vs. conversion curves due to its adaptable parameters (*m* & *k*).

6.6 Summary

The CO_2 reactivity results showed that for both 6 mm and 212 µm chars AC-5-72 had the highest specific reaction rate, while FC-2-21 had the lowest. This is mainly attributed to the physical and petrographic characteristics of the chars, similar to the 20 mm coal and char particles of phase one. The influence of particle size was investigated with the initial specific reaction rate decreasing with particle size also illustrating that internal mass transfer resistance is present. It was also seen that reactivity of coarse particles is lower than that of the standard reactivity estimated with pulverised chars.

The influence of temperature was investigated by determining the ratio increase of reactivity with temperature relative to 900 °C. The results showed that for the pulverised chars, BC-5-53 was the most affected at high temperatures, while FC-2-21 was the most influenced at 950 °C. The Arrhenius curves were also drawn and the apparent activation energies were determined. The estimated apparent activation energies ranged from 211 to 223 kJ/mol for 6 mm and 174 to 227 kJ/mol for 212 µm particles and also agreed with the results of previous studies.

Lastly, for the kinetic evaluation it was found that the semi-empirical Wen model was able to predict the gasification behaviour of both the 212 µm and 6 mm char particles. In general the Wen model described the gasification behaviour of the smaller particles more accurately.

CHAPTER 7: Conclusions and recommendations

7.1 Introduction

In Chapter 7 the main conclusions are given with regards to coal and char characteristics and the results of both phase one and two (Section 7.2). In Section 7.3 the contributions made to the knowledge of coal science and technology are discussed. The recommendations for the selection of pre-reduction coals are given in Section 7.4 and lastly the recommendations for future projects are provided in Section 7.5

7.2 Conclusions

7.2.1 Coal and char characteristics

For the coal characteristics, all nine coal samples fit most of the criteria as defined in literature and it can be concluded that the samples are suitable for pre-reduction. Most of the coals were classified as high-volatile B bituminous coals, while the seam two coals were classified as medium-volatile bituminous coals. Charring at both 950 and 1050 °C increased the rank of the samples to meta-anthracite.

It is also concluded that charring the particles at 950 °C increases the surface area, due to the removal of volatiles and development of the pore structure. If the charring temperature is increased to 1050 °C, the surface area decreases due to ordering of the carbon structure. Further it is concluded that vitrinite-rich coals produce chars with a larger surface area.

7.2.2 Phase one

It was concluded that two modes of primary thermal fragmentation were experienced namely internal pressure build-up due to rapid volatile release and exfoliation breakage due to a thermal shock. It was further concluded that vitrinite-rich coals tend to swell and fragment and that swelling also assisted with the fragmentation of the particles. Fragmentation increased reactivity by reducing particle size, which is advantageous for pre-reduction. The particles should, however, not fragment too severely as this could increase CO_2 reactivity to the extent were the coal consumption ratio would increase.

For the CO_2 reactivity it was concluded that the specific reaction rate increases with conversion, due to pore structure development and an increase in the associated active site concentration. From the statistical analysis, it was concluded that for the coal properties, the chemical and petrographic characteristics had the greatest influence on reactivity. For 950 °C, the fixed carbon and inert semi-fusinite content affected the reaction rate the most

profoundly. Volatile matter and vitrinite were the two parent coal properties that had the greatest influence at 1050 °C, both increasing reactivity.

For the char properties, the nitrogen content was shown to increase reactivity at 1050 °C and to a lesser extent reactivity at 950 °C. The physical properties, such as BET surface area, micropore surface area and micropore volume also had a significant influence at both temperatures. It was further concluded that the developed empirical equations were more accurate in predicting initial reaction rates at 1050 °C compared to 950 °C.

7.2.3 Phase two

The conclusion made for phase two was that the specific reaction rate of the smaller particles and pulverised chars increase with carbon conversion. With regards to the influence of particle size it is seen that reactivity decreases with an increase in particle size and that internal mass transfer resistance was not negligible for the larger particles. It was also concluded that even though the reactivity decreases with particle size, as a general dependent trend was obtained, which relates the standard CO_2 reactivity (pulverised chars) with the CO_2 reactivity of large particles. Next it was concluded that temperature has a greater influence of reactivity, in comparison to particle size and that the estimated apparent activation energies for both 212 µm and 6 mm chars compare well with values previously reported in literature.

With regards to the kinetic evaluation it was concluded that the semi-empirical Wen model was the best suited to describe the behaviour of both the 212 µm and 6 mm particles. Additionally it was seen that the model is able to describe the gasification behaviour of the pulverised chars more accurately.

7.3 Contributions to the knowledge of coal science and technology

The following is regarded as contributions made to coal science:

- Detailed characterisation of nine South African coals and their associated chars, derived from large coal particles, relevant to iron pre-reduction purposes.

- Determination of statistical relations between char reactivity and coal and char properties.

- Derivation of empirical equations that will assist with selection of alternative coals for the iron pre-reduction process.

7.4 Recommendations for pre-reduction medium

After evaluation of the results, the following recommendations are made for the selection of future feed coals. Firstly when screening for new coals a proximate analysis is recommended to determine the volatile and fixed carbon content. The statistical analysis indicated that a strong significant relationship exists between the volatile matter for the reactivity at 1050 °C and the fixed carbon for the reactivity at 950 °C. Additionally, the maceral composition should be determined, as the vitrinite and inert semi-fusinite content strongly influences the reaction rate. CO_2 adsorption analysis is also recommended to determine the micropore porosity for the determination of the initial reaction rate at 950 °C.

Alternatively, a standard TGA analysis (pulverised sample) can be done to determine the CO_2 reactivity of the new coals at kiln conditions, which in turn can be compared to the reactivity of the benchmark coal. Figure 6.5 can then also be used to determine the reactivity of the larger particles, which is used inside the kiln. This method entails only one TGA analysis, instead of three different characterisation analyses.

From the current coals evaluated, AC-5-72 is recommended as the coal best suited for pre-reduction. This selection is made with reference to the coal and char characteristics as well as the results of phase one and two. AC-5-72, in comparison to BC-5-53, is a more reactive coal, which could cause this coal to burnout too quickly inside the kiln. This in turn could lead to an insufficient carbon carry-over and possible increased coal consumption. FC-2-21 on the other hand has a lower reactivity, but also a lower coal consumption ratio. Therefore blending of the two samples is recommended in order to account for both the high coal consumption ratio of AC-5-72 and the low CO_2 reactivity of FC-2-21.

7.5 Recommendations for further study

After consideration of the main results and discussions, as well as the conclusions, the following recommendations are made for improvement of this study as well as further studies.

- The influence of coal characteristics, for the selected coal, on CO_2 gasification reactivity should be further investigated by examining the reactivity of pulverised coals. The small particles size will reduce the effect of internal mass transfer and fragmentation which alters the reaction rate. This results can also be compared to those for the large particles.

- The CO_2 concentration is varying within the kiln and it is recommended that the influence of CO_2 partial pressure on the gasification reactivity be investigated.

- The empirical equations as discussed in this study should be evaluated with other coal samples, which are also suitable for pre-reduction.

- Combustion reactivity of the coals/chars should also be investigated as combustion air is injected continuously along the length of the kiln during pre-reduction.

- The relation between CO_2 reactivity and pre-reduction values obtained from the industrial operations should be investigated.

- Investigate the reactivity of different blends of AC-5-72 and FC-2-21. From the results of phase two the following blends are suggested.

  Table 7.1: Suggested blending ratios for future studies

Blending option	AC-5-72	FC-2-21
6 mm		
1	0.20	0.80
2	0.08	0.92
3	0.12	0.88
4	0.41	0.59
212 µm		
1	0.29	0.71
2	0.19	0.81
3	0.77	0.23

  The suggested blending ratios were estimated from the initial reactivity at the four different temperatures for both the 6 mm and 212 µm particles utilising the linear additive rule (Pan *et al.,* 1991). The ratios are based on initial specific reaction rate of the benchmark coal for phase two. The blending ratios can further be optimised by statistical analysis in combination with reactivity experiments.

- The recommended coals/blends and the benchmark coal should be allowed to react with the ore and fluxes. From the experimental studies two things can be investigated:
  - The effect of the additives on char properties and reactivity.
  - The rate of pre-reduction for the different coals/blends.

References

Allen, T. & Khan, A.A. 1970. Critical evaluation of powder sampling procedures. *The Chemical Engineer,* 238:108-112.

Ahn, D.H., Gibbs, B.M., Ko, K.H. & Kim, J.J. 2001. Gasification kinetics of an Indonesian sub-bituminous coal-char with CO_2 at elevated pressure. *Fuel,* 80(11):1651-1658.

Alonso, M.J.G., Borrego, A.G., Alvarez, D., Parra, J.B. & Menéndez, R. 2001. Influence of pyrolysis temperature on char optical texture and reactivity. *Journal of Analytical and Applied Pyrolysis,* 58-59:887-909.

Anderson, J.B. 1963. A criterion for isothermal behavior of a catalyst pellet. *Chemical Engineering Science,* 18: 147-150.

Argyle, M.D. & Bartholomew, C.H. 2015. Heterogeneous catalyst deactivation and regeneration: a review. *Catalysts,* 5: 145 – 269.

Asami, K., Sears, P., Furimsky, E. & Ohtsuka, Y. 1996. Gasification of brown coal and char with carbon dioxide in the presence of finely dispersed iron catalysts. *Fuel Processing Technology,* 47(2): 139-151.

Atsushi, M., Uemura, H. & Sakaguchi, T. 2010. Midrex Processes. *Kobelco Technology Review*, 29: 50 – 57.

Bai, J., Li, W., Li, C., Bai, Z. & Li, B. 2009. Influences of mineral matter on high temperature gasification of coal char. *Journal of Fuel Chemistry and Technology,* 37(2): 134-138.

Basu, P. 2006. Combustion and Gasification in Fluidized beds. London:Taylor & Francis Group, LLC

Bend, S.L., Edwards, I.A.S. & Marsh, H. 1991. The influence of rank upon char morphology and combustion. *Fuel,* 71(5): 493-501.

Boëlle, A., Qian, M., Jaud, P., Chirone, R., Salatino, P., Winter, F., Lui, X., Olsson, D., Amand, L.& Leckner, B. 2002. Coal Comminution Characterization of Industrial Scale Circulation Fluidized Bed. A research program in the frame of the International Energy Agency (IEA) implementing agreement for co-operation in the field of fluidized bed conversion of fuels applied to clean energy production. Final Joint Report.

Borrego, A.G., Alvarez, D. & Menéndez, R. 1997. Effects of Inertinite Content in Coal on Char Structure and Combustion. *Energy & Fuels,* 11(3): 702-708.

Burgayev, K., Konovalo, Y., Bychkov, Y., Tretyakov, E. & Savin, I.V. 2001. Iron and steel production. Washington D.C.: The Minerva Group, Inc.

Cai, H.Y., Güell, A.J., Chatzakis, I.N., Lim, J.Y., Dugwell, D.R. & Kandiyoti, R. 1996. Combustion reactivity and morphological change in coal chars: effect of pyrolysis, temperature, heating rate and pressure. *Fuel,* 75(1): 15-24.

Çakal, G.O., Yücel., H. & Gürüz, A.G. 2007. Physical and chemical properties of selected Turkish lignites and their pyrolysis and gasification rates determined by thermogravimetric analysis. *Journal of Analytical and Applied Pyrolysis,* 80(1): 262-268.

Calkins, W.H. 1993. The chemical forms of sulphur in coal: a review. *Fuel,* 73(4): 475-484.

Carpenter, A. 2004. Profiles: Use of coal in direct ironmaking processes. http://iea-coal.org/documents/81118/5528/Use-of-coal-in-direct-ironmaking-processes. Date of access: 4 March 2014.

Chatterjea, A.B. 1973. On Some Fundamental aspects of Operational Parameters of Direct Reduction in a Rotary Kiln. Paper presented at the Symposium on science and technology of sponge Iron and its Conversion to Steel, Jamshedpur, 19-21 February. http://eprints.nmlindia.org/4572/1/182-193.PDF. Date of access: 24 March 2014.

Chatterjee, A. 1993. Beyond the Blast Furnace. 1st ed. London: CRC Press.

Chatterjee, A. 2010. Sponge Iron Production By Direct Reduction of Iron Oxide. New Delhi: PHI Learning Pvt. Ltd.

Chatterjee, A. 2012. Sponge iron production by direct reduction of iron oxide. 2nd ed. New Delhi: PHI Learning.

Choudhury, N., Boral, P., Mitra, T., Adak, A.K., Choudhury, A. & Sarkar, P. 2007. Assessment of nature and distribution of inertinite in Indian coals for burning characteristics. *International Journal of Coal Geology,* 72(2): 141 – 152.

Chuang, H., Hwang, W. & Lui, S. 2009. Effects of Basicity and FeO Content on the Softening and Melting Temperatures of the CaO-SiO_2-MgO-Al_2O_3 Slag system. *Materials Transactions,* 50(6):1448 – 1456.

Chukwuleke, O.P., Jiu-ju, C.A.I., Chukwujekwu, S. & Song, X.I.A.O. 2009. Shift From the Coke to Coal Using Direct Reduction Method and Challenges. *Journal of Iron and Steel Research,* 16(32): 1-5.

Clingan, W.R. 2013. Process for production of fuels and chemicals form biomass feedstocks. (Patent: US20130232856).

Cloke, M & Lester, E. 1994. Characterization of coals for combustion using petrographic analysis: a review. *Fuel*, 73(3):315-320.

Coaltech. 2007. Slagging and fouling indices. http://www.coaltech.com.au/LinkedDocuments/Slagging%20&%20Fouling.pdf. Date of access: 15 April 2015.

Coetsee, T., Pistorius, P.C. & De Villiers, E.E. 2002. Rate-determining steps for reduction in magnetite-coal pellets. *Minerals Engineering,* 15(11):919-929.

Coetzee, S., Neomagus, H.W.J.P., Bunt, J.R. & Everson, R.C. 2013. Improved reactivity of large coal particles by K_2CO_3 addition during steam gasification. *Fuel Processing Technology,* 114: 75-80.

Coetzee, S., Neomagus, H.W.J.P., Bunt, J.R., Strydom, C.A. & Schobert, H.H. 2014. The transient swelling behaviour of large (- 20 + 16 mm) South African coal particles during low-temperature devolatilisation. *Fuel,* 136: 79 – 88.

Crelling, J.C., Skorupska, N.M. & Marsh, H. 1988. Reactivity of coal macerals and lithotypes. *Fuel,* 67(6): 781-785.

Cunningham, B.C. & Stephenson, J.G. 1980. Direct Reduction Processes. (*In* Stephenson, R.L., *ed.* Direct Reduced Iron: Technology and Economics of Production and Use. Warrendale: The Iron & Steel Society of AIME. p. 64 – 103).

Dakic, D., Vand der Honing, G. & Valk, M. 1989. Fragmentation and swelling of various coals during devolatilization in a fluidized bed. *Fuel*, 68:911-916.

De Korte, G.J. 2001. Beneficiation of Weathered Coal. Coaltech 2020 Projects 4.6.2. Interim report. Division of Mining Technology, CSIR.

De Korte, G.J. & Mangena, S.J. 2004. Thermal drying of fine and ultra-fine coal. Coaltech 2020, Report number 2004 – 2005.

Deng, C., Zhang, C., Tan., P., Fang, Q. & Chen, G. 2015. The melting and transformation characteristics of minerals during co-combustion of coal with different sludges. *Energy & Fuels* (In press).

Devore, J. & Farnum, N. 2005. Applied Statistics for Engineers and Scientists. 2nd ed. London: Brooks/Cole.

Donskoi, E. & McElwain, D.L.S. 2003. Estimation and Modelling of Parameters for Direct Reduction in Iron Ore/Coal Composites: Part 1. Physical Parameters. *Metallurgical and Materials Transactions B,* 34(1): 93-102.

Du Toit, G.J.D. 2013. The influence of CO2 on steam gasification rate of a typical South African coal. Potchefstroom: NWU (Dissertation – Masters).

Dullien, F.A.L. 1979. Porous Media: Fluid Transport and Pore Structure. New York: Academic Press.

Dutta, S., Wen, C.Y. & Belt, R.J. 1977. Reactivity of Coal and Char. 1. In Carbon Dioxide Atmosphere. *Industrial & Engineering Chemistry Process Design and Development,* 16(1):20-30.

Economic Commission for Europe. 1988. International codification system for medium and high rank coals. New York: United nations publication.

Eghlimi, A., Lu, L., Sahajwalla, V. & Harris, D. 1999. Computational modeling of char combustion based on the structure of char particles. Paper presented at the Second International Conference on CFD in the Minerals and Process Industries CSIRO, Melbourne, Australia, 6-8 December. http://www.cfd.com.au/cfd_conf99/papers/075EGHL.PDF. Date of access: 6 April 2014.

Elley, D.D. 1994. Advances in Catalysis. Amsterdam: Elsevier (Volume 40).

England, T., Hand, P.E., Michael, D.C., Falcon, L.M. & Yell, A.D. 2002. Coal preparation in South Africa. Pietermaritzburg: Natal Witness Commercial Printers.

Ergun, S. 1956. Kinetics of the reaction of carbon dioxide with carbon. *The Journal of Physical Chemistry,* 60(4): 480-485.

Erwee, M.W. & Pistorius, P.C. 2012. Nitrogen in SL/RN Direct Reduced Iron: Origin and Effect on nitrogen control in EAF steelmaking. http://repository.up.ac.za/bitstream/handle/2263/20077/Erwee_Nitrogen%282012%29.pdf?sequence=1. Date of access: 5 November 2014.

Everson, R.C., Neomagus, H.W.J.P., Kasaini, H. & Njapha, D. 2006. Reaction kinetics of pulverised coal-chars from inertinite-rich coal discards: Gasification with carbon dioxide and steam. *Fuel,* 85(7-8): 1076-1082.

Everson, R.C., Neomagus, H.W.J.P. Kaitano, R., Falcon, R., Van Alphen, C. & Du Cann, V.M. 2008a. Properties of high ash char particles derived from inertinite-rich coal: 1 Chemical, structural and petrographic characteristics. *Fuel,* 87(13-14): 3082 – 3090.

Everson, R.C., Neomagus, H.W.J.P., Kaitano, R., Falcon, R. & Du Cann, V.M. 2008b. Properties of high ash coal-char particles derived from inertinite-rich coal: ll. Gasification kinetics with carbon dioxide. *Fuel,* 87(15-16): 3403-3408.

Everson, R.C., Okolo, G.N., Neomagus, H.W.J.P. & Dos Santos, J. 2013. X-ray diffraction parameters and reaction rate modelling for gasification and combustion of chars derived from inertinite-rich coals. *Fuel*, 109: 148-156.

Falcon, R. & Ham, A.J. 1988. The characteristics of Southern African coals. *Journal of South African Institute of Mining and Metallurgy,* 88(5):145-161.

Feinman, J. 1999. Direct Reduction and Smelting Processes. (*In* Wakelin, D., *ed.* The Making, Shaping and Treating of Steel. Pittsburgh: The AISE Steel Foundation. p. 741-780).

Feng, B. & Bhaita, S.K. 2003. Variation of the pore structure of coal chars during gasification. *Carbon*, 41(3):507-523.

Field, A. 2009. Discovering Statitics using SPSS. 3rd ed. London: Sage.

Figueiredo, J.L. & Moulijn, J.A. 1986. Carbon and Coal Gasification: Science and Technology. Dordrecht: Martinus Nijhoff Publishers.

Fogler, H.S. 2006. Elements of Chemical Reaction Engineering. 4th ed. Upper saddle river: Prentice Hall

Gadsby, J., Long, F.J., Sleightholm, P. & Sykes, K.W. 1948. The mechanism of cerabon dioxide-carbon reaction. *Proceedings of the Royal Society of London. Series A, Mathematical and Physical Sciences,* 193(1034):357-376.

Gale, T.K., Bartholomew, C.H. & Fletcher, T.H. 1996. Effect of pyrolysis heating rate on intrinsic reactivities of coal chars. *Energy & Fuels,* 10:766-775.

Gomez, A. & Mahinpey, N. 2015. A new model to estimate CO_2 coal gasification kinetics based only on parent coal characterization properties. *Applied Energy,* 137: 126-133.

Gregg, S.J. & Sing, K.S.W. 1982. Adsorption, surface area and porosity. 2nd ed. London: Academic Press.

Griffin, T.P., Howard, J.B. & Peters, W.A. 1993. An experimental and modelling study of heating rate and particle size effect in Bituminous coal pyrolysis. *Energy & Fuel,* 7(2):297-305.

Guizani, C., Escudero Sanz, F.J. & Salvador, S. 2013. The gasification reactivity of high-heating-rate chars in single and mixed atmosphere of H_2O and CO_2. *Fuel,* 108:812-823.

Guizani, C., Escudero Sanz, F.J. & Salvador, S. 2015. Influence of temperature and particle size on the single and mixed atmosphere gasification of biomass char with H_2O and CO_2. *Fuel Processing Technology,* 134:175-188.

Gulyurtlu, I., Teixeira, P., Lopes, H., Lapa, N., Freire, M., Galhetas, M. & Cabrita, I. 2008. Prediction of slagging and fouling tendency of biomass co-firing in fluidized bed combustion. http://www.processeng.biz/iea-fbc.org/upload/56_15_Gulyurtlu.pdf. Date of access: 11 July 2015. [PowerPoint Presentation].

Gupta, S., Dubikova, M., French, D. & Sahajwalla, V. 2007. Effect of CO2 gasification on the transformations of coke minerals at high temperatures. *Energy & Fuels,* 21(2): 1052 – 1061.

Guseman, J.R. 1980. Fuels and Reductants. (*In* Stephenson, R.L., *ed.* Direct Reduced Iron: Technology and Economics of Production and Use. Warrendale: The Iron & Steel Society of AIME. p. 49 – 63).

Hall, J. 1980. Spotlight on Highveld Steel and Vanadium Corporation Limited. *Journal of the South African Institute on Mining and Metallurgy,* 80(9): 323-326.

Hand, P.E. 2000. Task 4.8.1. Dewatering and drying of fine coal to a saleable product. Coalreach 2020.

Hanson, S., Patrick, J.W. & Walker, A. 2002. The effect of coal particle size on pyrolysis and steam gasification. *Fuel,* 81(5):531-537.

Hartnady, C.J.H. 2010. South Africa's diminishing coal reserves. *South African Journal of Science,* 106(9/10): 1-5.

Hattingh, B.B. 2009. The Determination of the Reaction Mechanism involved in the CO_2 gasification of inertinite-rich, high ash coal. Potchefstroom: NWU (Dissertation – Masters).

Hattingh, B.B., Everson, R.C., Neomagus, H.W.J.P. & Bunt, J.R. 2011. Assessing the catalytic effect of coal ash constituents on the CO_2 gasification rate of high ash, South African coal. *Fuel Processing Technology,* 92(10): 2048-2054.

Hattingh, B.B., Everson., R.C., Neomagus, H.W.J.P., Bunt, J.R., Van Niekerk, D., Jordaan, J.H.L. & Mathews, J.P. 2013. Elucidation of the Structural and Molecular Properties of Typical South African Coals. *Energy & Fuels,* 27(6): 3161 – 3172.

Haykiri-Acma, H., Yaman, S. & Kucukbayral, S. 2012. Effect of pyrolysis temperature on burning reactivity of lignite char. *Energy Education Science and Technology Part A: Energy Science and Research,* 29(2): 1203-1216.

Helle, S., Gordon, A., Alfaro, G., Garcia, X. & Ulloa, C. 2003. Coal blend combustion: link between unburnt carbon in fly ash and maceral composition. *Fuel Processing Technology,* 80(3): 209-223.

Higman, C. & Van der Burgt, M. 2008. Gasification. 2nd ed. Amsterdam: Elsevier.

Hindmarsh, C.J., Wang, W., Thomas, K.M. & Crelling, J.C. 1994. The release of nitrogen during the combustion of macerals, microlithotypes and their chars. *Fuel,* 73(7): 1229 – 1234.

Hodge, E.M., Roberts, D.G., Harris, D.J. & Stubington, J.F. 2010. The significance of char morphology to the analysis of high-temperature char-CO_2 reaction rates. *Energy & Fuels*, 24:100-107.

Huang, J. & Watkinson, A.P. 1996. Coal gasification in a strirred bed reaction. *Fuel,* 75(14): 1617-1624.

Huang, Z., Zhang, J., Zhao, Y., Zhang, H., Yue, G., Suda, T. & Narukawa, M. 2010. Kinetic studies of char gasification by steam and CO2 in the presence of H_2 and CO. *Fuel Processing Technology,* 91(8): 843-847.

Huffman, G.P. & Huggins, F.E. 2009. Reaction and transformations of coal mineral matter at elevated temperatures. *ACS Symposium Series*, 301:100- 113.

Huo, W., Zhou, Z., Wang, F. & Yu, G. 2014. Mechanism analysis and experimental verification of pore diffusion on coke and coal char gasification with CO_2. *Chemical Engineering Journal,* 244: 227-233.

Irfan, M.F., Usman, M.R. & Kusakabe, K. 2011. Coal gasification in CO_2 atmosphere and its kinetics since 1984: A brief review. *Energy,* 36(1):12-40.

Incropera, F.P., DeWitt, D.P., Bergman, T.L. & Lavine, A.S. 2007. Fundamental of heat and mass transfer. 6th ed. Hoboken: John Wiley & Sons.

Industrial Technical Consultant. 2003. Raw material. http://www.spongeitc.com/down/iron_plant.pdf. Date of access: 14 April 2014.

Jayaraman, K. & Gokalp, I. 2014. Thermal characterization, gasification and kinetic studies of different sized Indian coal and char particles. *International Journal of Advances in Engineering Sciences and Applied Mathematics,* 6(1-2):31 – 40.

Jayaraman, K. & Gokalp, I. 2015. Effect of char generation method on steam, CO_2 and blended mixture gasification of high ash Turkish coals. *Fuel*, 153:320-327.

Jayaraman, K. Gokalp, I., Bonifaci, E. & Merlo, N. 2015. Kinetics of steam and CO_2 gasification of high ash coal-char produced under various heating rates. *Fuel*, 154: 370-379.

Johnsson, J.E. & Jensen, A. 2000. Effective diffusion coefficients in coal chars. *Proceedings of the Combustion Institute,* 28: 2353 – 2359.

Jones, R.B., McCourt, C.B., Morley, C. & King, K. 1985. Maceral and rank influences on the morphology of coal char. *Fuel,* 64(10): 1460-1467.

Kabe, T., Ishihara, A., Qian, E.W., Sutrisna, I.P. & Kabe, Y. 2004. Coal and coal-related compounds: Structures, Reactivity and Catalytic reactions. Amsterdam: Elsevier.

Kajintani, S., Hara, S. & Matsuda, H. 2002. Gasification rate analysis of coal char with a pressurised drop tube furnace. *Fuel*, 81(5): 539 – 546.

Kasaoka, S., Sakata, Y. & Tong, C. 1985. Kinetic evaluation of the reactivity of various coal chars for gasification with carbon dioxide in comparison to steam. *International Chemical Engineering,* 25(1): 160 – 175.

Kenarsari, S.D. & Zheng, Y. 2014. CO_2 gasification of coal under concentrated thermal radiation: A numerical study. *Fuel Processing Technology,* 18: 218-227.

Khan, M.R. 1989. Variations in the oxygen chemisorption capacity of mild gasification char at various levels of burnoff. *American Chemical Society, Division of Fuel Chemistry,* 34(1): 192-201.

Kim, B.C., Gupta, S., French, D., Sakurovs, R. & Sahajwalla, V. 2009. Effect of thermal treatment on coke reactivity and catalytic iron mineralogy. *Energy & Fuels,* 23(7): 3694 – 3702.

Kim, R.G., Hwang, C.W. & Jeon, C.H. 2014. Kinetics of coal char gasification with CO_2: Impact internal/external diffusion at high temperature and elevated pressure. *Applied Energy,* 129: 299-307.

Kim, S., Scarconi, A.W. & Fatemi-Babi, M. 1988. Effect of Maceral Composition and Vitrinite Reflectance on the Combustion Behaviour of Six hvA Bituminous Coals. Paper presented as the Coal combustion and soot formation, Los Angeles, CA, USA, 25-30 September. https://web.anl.gov/PCS/acsfuel/preprint%20archive/Files/33_4_LOS%20ANGELES_09-88_0842.pdf. Date of access: 5 April 2014.

Kim, Y.T., Seo, D.K. & Hwang, J. 2011. Study of the effect of coal type and particle size on char-CO_2 gasification via gas analysis. *Energy & Fuels,* 25:5044-5054.

Kizgut, S., Cuhadaroglu, D. & Toroglu, I. 2003. Thermogravimetric Characterization of Turkish Bituminous Coals for Combustion. *Turkish Journal of Chemistry,* 27: 521 – 528.

Koba, K. & Ida, S. 1980. Gasification reactivities of metallurgical cokes with carbon dioxide, steam and their mixtures. *Fuel,* 59(1): 59-63.

Kok, M.V., Özbas, E., Karacan, O. & Hicyilmaz, C. 1998. Effect of particle size on coal pyrolysis. *Journal of Analytical and Applied Pyrolysis,* 45(2):103-110.

Kostova, I., Marinov, S., Stefanova, M., Markova, K. & Stamenova, V. 2005. The distribution of sulpur form in the high-S coals of the Maritza West Basin, Bulgaria. *Bulletin of Geosciences,* 80(1): 23-32.

Kuznetsov, P.N., Kolesnikova, S.M. & Kuznetsova, L.I. 2013. Steam gasification of different brown coals catalysed by the naturally occurring calcium species. *International Journal of Clean Coal and Energy,* 2(1):1-11.

Kyotani, T., Karasawa, S. & Tomita, A. 1986. A TPD study of coal chars in relation to the catalysis of mineral matter. *Fuel,* 65(10): 1466-1469 (abstract).

Laurendeau, N.M. 1978. Heterogeneous kinetics of coal char gasification and combustion. *Progress in Energy and Combustion Science,* 4(4):221-270.

Laerd Statistics. 2013a. Spearman's Rank-Order Correlation. https://statistics.laerd.com/statistical-guides/spearmans-rank-order-correlation-statistical-guide.php. Date of access: 13 November 2015.

Laerd Statistics. 2013b. Two-way ANOVA in SPSS Statistics. https://statistics.laerd.com/spss-tutorials/two-way-anova-using-spss-statistics.php. Date of access: 8 June 2015.

Laerd Statistics. 2013c. Multiple Regression Analysis using SPSS Statistics. https://statistics.laerd.com/spss-tutorials/multiple-regression-using-spss-statistics.php. Date of access: 29 September 2015.

Li, C. 2007. Some recent advances in the understanding of pyrolysis and gasification behaviour of Victorian brown coal. *Fuel,* 86(12 - 13): 1664 – 1683.

Liane, N.R., Vastola, F.J. & walker, P.L. 1963. The importance of active surface area in the carbon-oxygen reaction. *Journal of Physical Chemistry,* 67(10): 2030-2034.

Liu, Q., Hu, H., Zhou, Q., Zhu, S. & Chen, G. 2003. Effect of inorganic matter on reactivity and kinetics of coal pyrolysis. *Fuel Chemistry Division Preprints,* 48(1):368-369.

Liu, T., Fang, Y. & Wang, Y. 2008. An experimental investigation into the gasification reactivity of chars prepared at high temperatures. *Fuel,* 87(4-5): 460-466.

Liu, H., Zhu, H., Yan, L., Huang, Y., Kato, S. & Kojima, T. 2011. Gasification reactivity of char with CO2 at elevated temperatures: the effect of heating rate during pyrolysis. *Asia-pacific journal of chemical engineering,* 6: 905-911.

Ma, Z., Bai, J., Bai, Z., Kong, L., Guo, Z., Yan, J. & Wen, L. 2014. Mineral transformation in char and its effect on coal char gasification reactivity at high temperatures, Part 2: Char gasification. *Energy & Fuels,* 28:1846-1853.

Manamela, M.M. & Pistorius, P.C. 2005. Ore size does affect direct reduction of titaniferous magnetite. *The Journal of The South African Institute of Mining and Metallurgy,* 105:183-186.

Markotic, A., Dolić, N. & Trujić, V. 2002. State of the direct reduction and reduction smelting processes. *Journal of Mining and Metallurgy,* 38(3-4): 123-141.

Mashhadi, H.A., Rastgoo, A.R. & Khaki, J.V. 2008. An Investigation on the Reduction of iron Ore Pellets in Fixed Bed of Domestic Non-Coking Coals. *International Journal of ISSI,* 5(1): 8-14.

Matjie, R.H., French, D., Ward, C.R., Pistorius, P.C. & Zhongsheng, L. 2011. Behaviour of coal mineral matter in sintering and slagging of ash during the gasification process. *Fuel Processing Technology,* 92(8): 1426 – 1433.

Matjie, R.H., Li, Z. & Ward, C.R. 2007. Determination of mineral matter and elemental composition of individual macerals in coals form Highveld mines. Paper presented at the Proceeding of 24th Pittsburgh International Coal Conference, Johannesburg, South Africa, 10 – 14 September.

Matjie, R.H., Zhongsheng, L., Ward, C.R. & French, D. 2008. Chemical composition of glass and crystalline phases in coarse coal gasification ash. *Fuel,* 87(6): 857 – 869.

Matzakos, A. & Zygourakis, K. 1990. Pyrolysis of Plastic coals: Pore structure development and char reactivity. *Reprint , American Chemical Society, Division of Fuel Chemistry,* 35(2): 505-515.

Mayoral, M.C., Izquierdo, M.T., Andres, J.M. & Rubio, B. 2001. Aluminosilicates transformation in combustion followed by DSC. *Thermochimica Acta,* 373 (2): 173 – 180.

McDonald, J.H. 2014. Handbook of Biological Statistics. 3rd ed. Baltimore, Maryland: Sparky House Publishing.

Méndez, L.B., Borrego, A.G., Martinez-Tarazona, M.R. & Menéndez, R. 2003. Influence of petrographic and mineral matter composition of coal particles on their combustion reactivity. *Fuel,* 82(15-17): 1875-1882.

Michisita, H & Tanaka, H. 2010. Prospects for Coal-based Direct Reduction Process. *Kobelco Technology Review,* 29: 69-76.

Micrometrics. 2006. Accelerated surface area and porosimetry system (ASAP 2020). Operator's manual v3.01. Norcoss, Georgia US: Micromeritics Instrument Corporation. P4:15 – 25; C:11-44.

Micrometrics, 2015. ASAP 2020: Accelerated surface area and porosimetry system. http://www.micromeritics.com/Repository/Files/ASAP_2020_Brochure_4.pdf. Date of access: 6 October 2015.

MIDREX. 2013. World Direct Reduction Statistics. . http://www.midrex.com/assets/user/news/MIDREX_World_DRI_Stats.pdf. Date of access: 11 March 2015.

Miura, K., Hashimoto, K. & Silverson, P.L. 1989. Factors affecting the reactivity of coal chars during gasification, and indices representing reactivity. *Fuel,* 68(11): 1461-1475.

Mohanty, D., Chandra, A. & Chakraborti, N. 2009. Genetic algorithms based multi-objective optimization of an iron making rotary kiln. *Computational Materials Science,* 45(1): 181-188.

Mohapatra, B. & Patra, D. 2009. Study of Reduction Behaviour of Iron Ore Lumps. Rourkela: National Institute of Technology (These- Bachelaors).

Molina, A. & Mondragón, F. 1998. Reactivity of coal gasification with steam and CO_2. *Fuel,* 77(15):1831-1839.

Ng, S.H., Fung, D.P.C. & Kim, S.D. 1987. Study of the pore structure and reactivity of Canadian coal-derived chars. *Fuel,* 67(5): 700-706.

Nugroho, Y.S., McIntosh, A.C. & Gibbs, B.M. 2000. Low-temperature oxidation of single and blended coals. *Fuel,* 79(15): 1951 – 1961.

Ochoa, J., Cassanello, M.C., Bonelli, P.R. & Cukierman, A.L. 2001. CO_2 gasification of Argentinean coal chars: a kinetic characterization. *Fuel Processing Technology*, 74(3):161-176.

Oka, S.N. 2004. Fluidized Bed Combustion. New York: Marcel Dekker, Inc.

Okolo, G.N., Everson, R.C., Neomagus, H.W.J.P., Roberts, M.K. & Sakurovs, R. 2015. Comparing the porosity and surface areas of coal as measured by gas adsorption, mercury intrusion and SAXS techniques. *Fuel,* 141: 293 – 304.

Pan, W., Gan, Y. & Serageldin, M.A. 1991. A study of thermal analytical values for coal blends burned in an air atmosphere. *Thermochimica Acta,* 180: 203 – 217.

Paprika, M.J., Komatina, M.S., Dakic, D.V. & Nemoda, S.D. 2013. Prediction of Coal Primary Fragmentation and Char particle Size Distribution in Fluidized Bed. *Energy & Fuels,* 27(9): 5488 – 5494.

Peacy, J.G. & Davenport, W.G. 1979. The iron blast furnace: Theory and Practice. 1st ed. Oxford: Pergamon Press.

Pearson, D.E. 2008. Numerical Modeling of Reflectance of Coking Coals. http://www.coalpetrography.com/library/pdf/ModelingCoals.pdf. Date of access: 10 December 2014.

Perry, R.H., Green, D.W & Maloney, J.O. 1997. Perry's chemical engineers' handbook. 7th ed. New York: McGraw-Hill.

Pinetown, K.L., Ward, C.R. & Van der Westhuizen, W.A. 2007. Quantitative evaluation of minerals in coal deposits in the Witbank and Highveld Coalfields and the potential impact on acid mine drainage. *International Journal of Coal Geology,* 70(1-3): 166 – 183.

Prasad, K.K. & Ray, H.S. 2009. Advances in Rotary Kiln Sponge iron Plant. 1st ed. New-Delhi: New Age International Publishers.

Pretorius, C.C., Boshoff. H.P. & Pinheiro, H.J. 2002. Analyses of coal product samples of South African Collieries. (*In* Bulletin 114. SABS: Pretoria 97p.).

Quyn, D.M., Wu, H. & Li, C., 2005. Volatilisation and catalytic effects of alkali and alkaline earth metallic species during the pyrolysis and gasification of Victorian brown coal. Part I. Volatilisation of Na and Cl from a set of NaCl-loaded samples. *Fuel,* 81(2):143-149.

Ray, A.K., Prasad, K.K. & Sen, P.K. 1992. A model for the isothermal reduction of iron ore with coal char. *Solid State Ionics,* 50(3-4): 217-226.

Reddy, G.V., Sharma, T. & Chakravorty, S. 1991. Kinetic rate equation for direct reduction of iron ore by non-coking coal. *Ironmaking and Steelmaking,* 18(3): 211 – 213.

Roberts, D.G. & Harris, D.J. 2000. Char Gasification with O_2, CO_2 and H_2O: Effects of Pressure and Intrinsic Reaction kinetics. *Energy & Fuels,* 14: 483 – 489.

Roberts, D.G. & Harris, D.J. 2007. Char gasification in mixtures of CO_2 and H_2: Competition and inhibition. *Fuel,* 86(17-18): 2672-2678.

Roberts, D.G., Hodge, E.M., Harris, D.J. & Stubington, J.F. 2010. Kinetics of Char Gasification with CO_2 under Regime II Conditions: Effect of Temperature, Reactant and Total Pressure. *Energy Fuels,* 24(10): 5300-5308.

Roberts, M.J., Everson, R.C., Neomagus, H.W.J.P., Okolo, G.O., Van Niekerk, D. & Mathews, J.P. 2015a. The characteristics of slow-heated inertinite – and vitrinite-rich coals form the South African coalfields. *Fuel,* 158:591-601.

Roberts, M.J., Everson, R.C., Domazetis, G., Noemagus, H.W.J.P., Jones, J.M., Van Sittert, C.G.C.E., Okolo, G.N., Van Niekerk, D. & Mathews, J.P. 2015b. Density functional theory molecular modelling and experimentation particle kinetics for CO_2-char gasification. *Carbon*, 93: 295 – 314.

Ross, H.U. 1980. Physical Chemistry Part 1 - Thermodynamics. (*In* Stephenson, R.L., *ed.* Direct Reduced Iron: Technology and Economics of Production and Use. Warrendale: The Iron & Steel Society of AIME. p. 9 – 34).

Rudramuniyuppa, M.V., Hubballi, P.J. & Patil, M.R. 2000. Studies on composite pre-reduced pellets of iron ore fines of Sandur area, Bellary district, Karnatakam India. *Processing of Fines,* 2:263-268.

Saha, S., Sahu, G., Datta, S., Chavan, P., Sinha, A.K., Sharma, B.K. & Sharma, T. 2013. Studies on CO_2 Gasification reactivity of high ash Indian coal. *International Journal of Emerging Technology and Advanced Engineering,* 3(3):29-33.

Sakawa, M., Sakurai, Y. & Hara, Y. 1982. Influence of coal characteristics on CO_2 gasification. *Fuel*, 16(8): 717-720.

Sanyal, A. 1997. Role of Macerals – An Underappreciated Coal Quality Parameter For Unburned Carbon Characterization and Control. Paper presented at the Third Annual Conference on Unburned Carbon on Utility Fly Ash, Pittsburgh, 13-14 May. http://www.netl.doe.gov/publications/proceedings/97/97ub/sanyal.pdf. Date of access: 24 April 2014.

Sarangi, A. & Sarangi, B. 2011. Sponge Iron Production in Rotary Kiln. 1st ed. New Delhi: Raj Press.

Sha, X. 2009. Coal Gasification. (*In* Encyclopaedia of Life support systems. http://www.eolss.net/sample-chapters/c08/e3-04-03-04.pdf Date of access: 29 April 2014).

Sekine, Y., Ishikawa, K., Kikuchi, E., Matsukata, M. & Akimoto, A. 2006. Reactivity and structural change of coal char during steam gasification. *Fuel,* 85(2): 122-126.

Selvakumaran, P. & Bakthavatsalam, A.K. 2015. Effect of chemical composition of ash on sintering of lignites in circulating fluid bed combustion and successful operation of large CFBC boilers. *Applied Thermal Engineering,* 85: 135 – 147.

Senneca, O., Urciuolo, M. & Chirone, R. 2013. A semidetailed model of primary fragmentation of coal. *Fuel,* 104: 253 – 261.

Senneca, O., Urciuolo, M., Chirone, R. & Cumbo, D. 2011. An experimental study of fragmentation of coals during fast pyrolysis at high temperature and pressure. *Fuel,* 90(9): 2931-2938.

Shenqi, X., Zhijie, Z., Jie, X., Guangsuo, Y. & Fuchen, W. 2011. Effect of alkaline metal on coal gasification at pyrolysis and gasification. *Fuel,* 90(5):1723-1730.

Skodras, G. & Sakellaropoulos, G.P. 2002. Mineral matter effect in lignite gasification. *Fuel Processing Technology,* 77-78:151-158.

Sibakin, J.G. 1980. Development of Direct Reduction in the Iron and Steel Industry. (*In* Stephenson, R.L., *ed.* Direct Reduced Iron: Technology and Economics of Production and Use. Warrendale: The Iron & Steel Society of AIME. p. 3 – 8).

Silbermann, R., Gomez, A., Gates, I. & Mahinpey, N. 2013. Kinetic studies of a novel CO_2 gasification method using coal from deep unmineable seams. *Industrial & Engineering research,* 52: 14787-14797.

Sinag, A., Sinek, K., Tekes, A.T., Misirlioglu, Z., Canel, M. & Wang, L. 2003. Study on CO_2 gasification reactivity of chars obtained from Soma-Isiklar liginite(Turkey) at various coking temperatures. *Chemical Engineering and Processing,* 42(12):1027-1031.

Speakman, S.A. 2012. Introduction to PANalytical X'Pert HighScore Plus v3.0, Ph.D. MIT Center for Materials Science and Engineering. http://prism.mit.edu/xray/oldsite/tutorials.htm. Date of access: 11 November 2015.

Speight, J.G. 2005. Handbook of coal analysis. 1st ed. Hoboken: John Wliey & Sons.

Steinberg, W.S. 2008. Development of a control strategy for the open slag bath furnaces at the Highveld Steel and Vanadium Corporation Ltd. Pretoria: University of Pretoria (Dissertation – Masters).

Steinberg, W.S., Geyser, W. & Neil, J. 2011. The history and development of the pyrometallurgical processes at EVRAZ Highveld Steel & Vanadium. *The Journal of The Southern African Institute of Mining and Metallurgy,* 111:1-6.

Straka, P. 2011. Kinetics of Fe-catalyzed gasification of chars from lignite admixtures. *Acta Geodyn. Geomater.,* 8(1): 79 – 88.

Stubington, J.F. & Linjewile, T.M. 1989. The effect of fragmentation on devolatilization of large coal particles. *Fuel,* 68(2):155-160.

Stubington, J.F. & Sasongko, D. 1998. On the heating rate and volatiles yield for coal particles injected into fluidised bed combustors. *Fuel,* 77(9/10): 1021-1025.

Su, S., Pohl, J.H., Holcombe, D. & Hart, J.A. 2001. A proposed maceral index to predict combustion behaviour of coal. *Fuel,* 80(5):699-706.

Sun, Q., Li, W., Chen, H. & Li, B. 2004. The CO_2-gasification and kinetics of Shenmu maceral chars with and without catalyst. *Fuel,* 83(13): 1787-1793.

Sutherland, K. 2000. Coal utilization at Highveld Steel and Vanadium Corporation. Paper presented at The Southern African Institute of Mining and Metallurgy Colloquium Coal Preparation, Witbank, 7 March. : http://www.saimm.co.za/Conferences/CoalPreparation/005-Sutherland.pdf. Date of access: 16 January 2014.

Szekely, J., Evans, J.W. Sohn, H.Y. 1976. Gas-Solid Reactions. New York: Academic Press.

Tang, L., Gupta, R., Seng, C. & Wall, T. 2005. The char structure characterisation from the coal reflectogram. *Fuel,* 84(10): 1268-1276.

Tay, H. & Li, C. 2010. Changes in char reactivity and structure during the gasification of Victorian brown coal: Comparison between gasification in O_2 and CO_2. *Fuel Processing Technology,* 91(8): 800-804.

Teessen, W. 2014a. Pre-reduction process at EHSV [personal meeting]. 9 January, NWU, Potchefstroom.

Teessen, W. 2014b. The Iron Plant Process. [PowerPoint presentation – unpublished].

Thomas, J. & Damberger, H.H. 1976. Internal surface area, moisture content, and porosity of Illinois Coals: Variations with coal rank. *Illinois State Geological Survey,* Circular 493.

Tomaszewicz, M., Labojko, G., Tomaszewicz, G. & Kotyczka-Moranska, M. 2013. The kinetics of CO2 gasification of coal chars. *Journal of Thermal Analysis and Calorimetry,* 113:1327-1335.

Tsai, S.C. 1982. Coal Science and Technology 2: Fundamentals of coal beneficiation and utilization. Amsterdam: Elsevier Scientific Publishing Company.

Ünal, H.I., Turgut, E., Atapek, S.H. & Alkan, A. 2012. Direct reduction of ferrous oxides to form an iron-rich alternative charge material and its characterization. Paper presented at the International Iron & Steel Symposium, Karabük, Türkiye, 02 -04 April. http://iiss12.karabuk.edu.tr/papers/.pdf. Date of access: 27 Feb. 2014.

Van Dyk, J.C. 2006. Understanding the influence of acidic components (Si, Al and Ti) on ash flow temperature of South African coal sources. *Minerals Engineering,* 19(3): 280-286.

Van Dyk, J.C., Melzer, S. & Sobiecki, A. 2006. Mineral matter transformation during Sasol-Lurgi fixed bed dry bottom gasification – utilization of HT-XRD and FactSage modelling. *Minerals Engineering,* 19(10): 1126 – 1135.

Van Heek, K.H. & Mühlen, H. 1985. Aspects of coal properties and constitution important for gasification. *Fuel,* 64(10): 1405-1414.

Van Krevelen, D.W. 1981. Coal Science and Technology 3: Coal, Typology-Chemistry-Physics-Constitution. 2nd ed. Amsterdam: Elsevier Scientific Publishing Company.

Veca, E. & Adrover, A. 2014. Isothermal kinetics of char-coal gasification with pure CO_2. *Fuel,* 123:151-157.

Venturelli, C. & Paganelli, M. 2007. Sintering behaviour of clays for the production of ceramics. *Process Engineering,* 84(5): E1 – E4.

Walker, J., Haliday, D. & Resnick, R. 2008. Fundamentals of Physics. 8th ed. Hoboken, New Jersey: John Wiley & Sons.

Walker, P.L., Mahajan, O.P. & Komatsu, M. 1979. Catalysis of lignite char gasification by various exchanged cations – dependence of activity on reactive atmosphere. *Preprint Paper – American Society, Division of Fuel Chemistry,* 24: 10 -16.

Walker, R. & Mastalerz. M. 2004. Functional group and individual maceral chemistry of high volatile bituminous coals from southern Indiana: controls on coking. *International Journal of Coal Geology,* 58(3): 181 – 191.

Walker, P.L., Rusinko, F. & Austin, L.G. 1959. Gas Reaction of Crabon. *Reprinted from Advances in Catalysis,* 11:133-221.

Wang, G., Zhang, J., Shao, J., Li, K. & Zuo, H. 2015. Investigation of non-isothermal and isothermal gasification process of coal char using different kinetic model. *International Journal of Mining Science and Technology,* 25(1): 15-21.

Wang, P. & Massoudi, M. 2013. Slag Behaviour in Gasifiers. Part 1: Influence of Coal Properties and Gasification Conditions. *Energies,* 6: 784-806.

Wang, Q., Yang, Z., Tian, J., Li, W. & Sun, J. 1998. Reduction kinetics of iron ore-coal pellet during fast heating. *Ironmaking and Steelmaking,* 25(6): 443-447.

Welty, J.R., Wicks, C.E., Wilson, R.E. & Rorrer, G.L. 2008. Fundamentals of Momentum. Heat, and Mass Transfer. 5th ed. Hoboken, NJ: John Wiley & Sons.

Wen, C.Y. 1968. Noncatalytic heterogeneous solid fluid reaction models. *Industrial engineering,* 60: 34 – 54.

Worldsteel association. 2015. Worldsteel short range outlook 2015 – 2016. https://www.worldsteel.org/media-centre/press-releases/2015/worldsteel-Short-Range-Outlook-2015---2016.html. Date of access: 12 November 2015.

Wu, S., Gu, J., Li, L., Wu, Y. & Gao, J. 2006. The reactivity and kinetics of Yanzhou coal chars from elevated pyrolysis temperatures during gasification in steam at 900-1200°C. *Process Safety and Environmental Protection*, 84(B6): 420-428.

Wu, S., Gu, J., Zhang, X., Wu, Y., Gao, J. 2008. Variation of carbon crystalline structures and CO_2 gasification reactivity of Shenfu coal chars at elevated temperatures. *Energy & Fuels,* 22(1): 199-206.

Wu, X., Zhang, Z., Chen, Y., Zhou, T., Fan, J., Piao, G., Kobayashi, N., Mori, S. & Itaya, Y. 2010. Main mineral melting behaviour and mineral reaction mechanism at molecular level of blended coal ash under gasification condition. *Fuel Processing Technology,*91(11): 1591 – 1600.

Wu, Y., Wu, S. & Gao, J. 2009. A study on the applicability of kinetic models for Shenfu coal char gasification with CO2 at elevated temperatures. *Energies,* 2: 545 – 555.

Xu, S., Zhou, Z., Gao, X., Yu, G. & Gong, X. 2009. The gasification reactivity of unburned carbon present in gasification slag form entrained-flow gasifier. *Fuel Processing Technology,* 90(9): 1062 – 1070.

Ye, D.P., Agnew, J.B. & Zhang, D.K. 1998. Gasification of a South Australian low-rank coal with carbon dioxide and steam: kinetics and reactivity studies. *Fuel,* 77(11):1209-1219.

Zhang, L., Huang, J., Fang, Y. & Wang, Y. 2006a. Gasification reactivity and kinetics of typical Chinese anthracite chars with steam and CO_2. *Energy & Fuels*, 20(3): 1201-1210.

Zhang, W., Thompson, K.E., Reed, A.H. & Beeken, L. 2006b. Relationship between pacing structure and porosity in fixed beds of equilateral cylindrical particles. *Chemical Engineering Science,* 61: 8060 – 8074.

Zhu, W., Song. W. & Lin, W. 2008. Effect of Coal Particle Size on Pyrolysis and Char Reactivity for Two Types of Coal and Demineralized Coal. *Fuels and Energy,* 22(4):2482-2487.

Zou, J.H., Zhou, Z.J., Wang, F.C., Zhang, W., Dai, Z.H., Liu, H.F. & Yu, Z.H. 2007. Modeling reaction kinetics of petroleum coke gasification with CO_2. *Chemical Engineering and Processing,* 46(7): 630-636.

APPENDIX A: Additional characterisation results

A.1 Density distribution curves

A.1.1 Coal

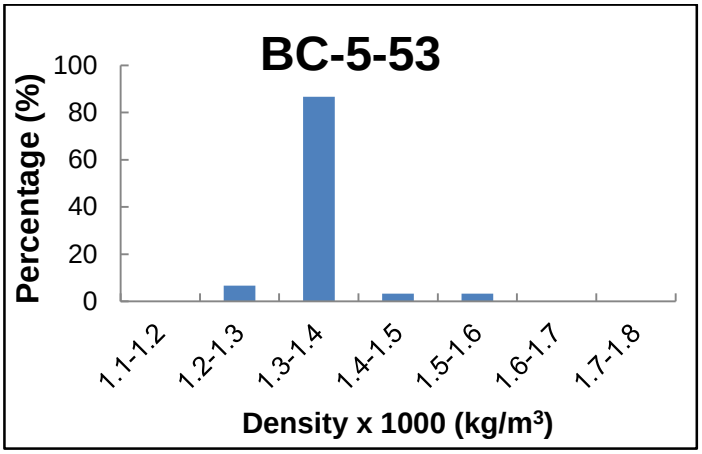

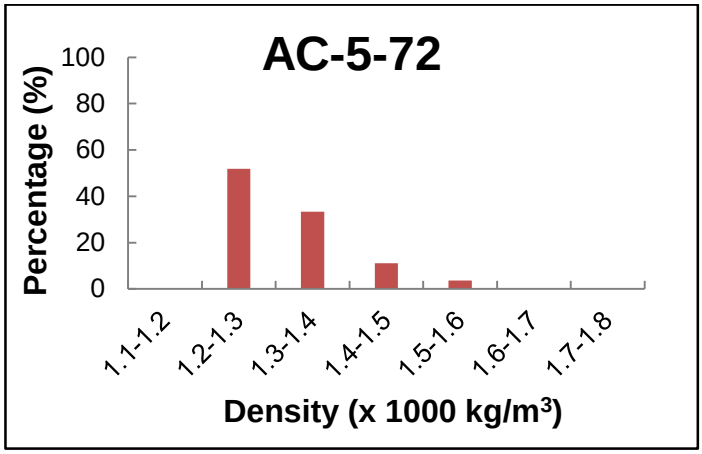

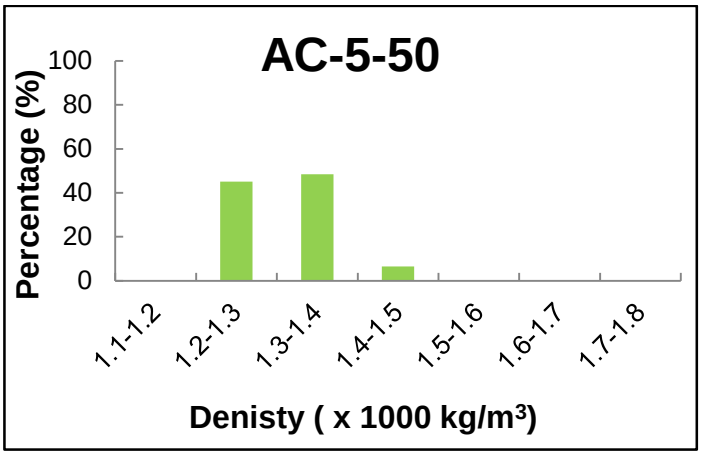

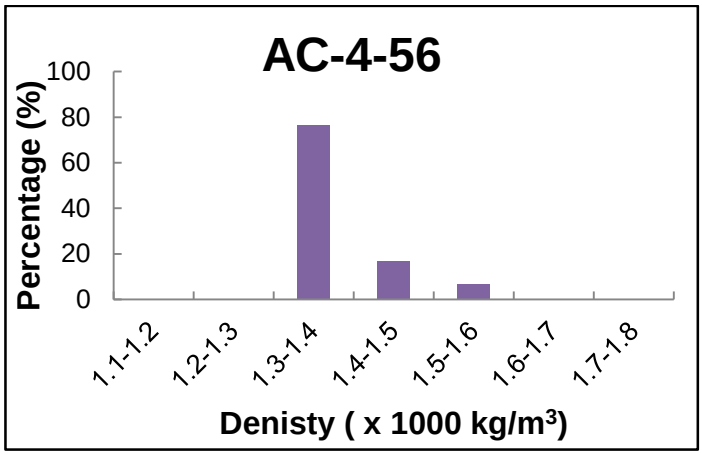

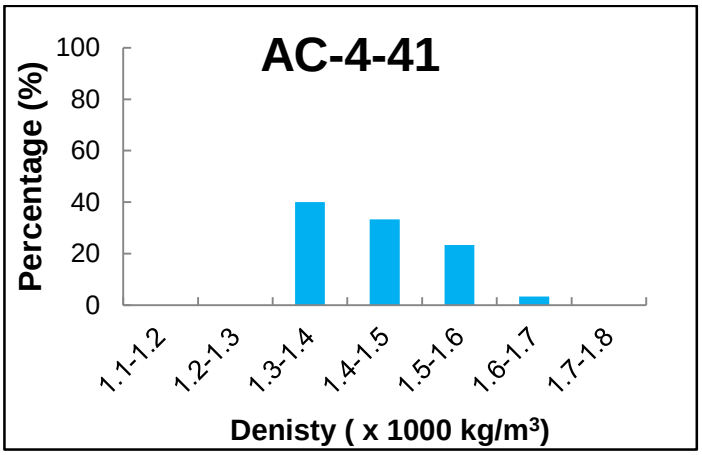

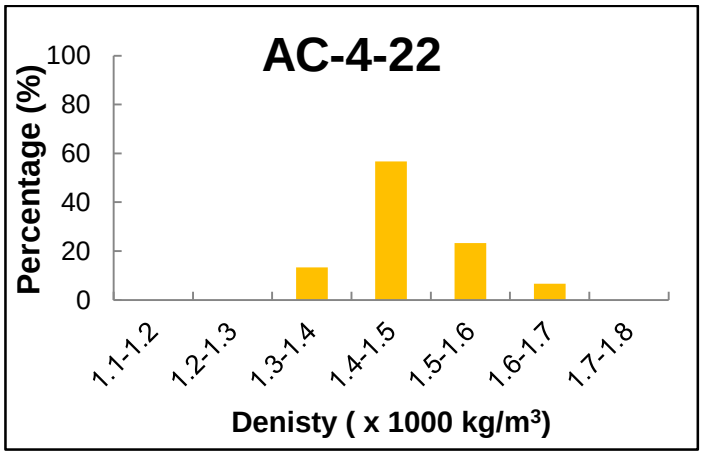

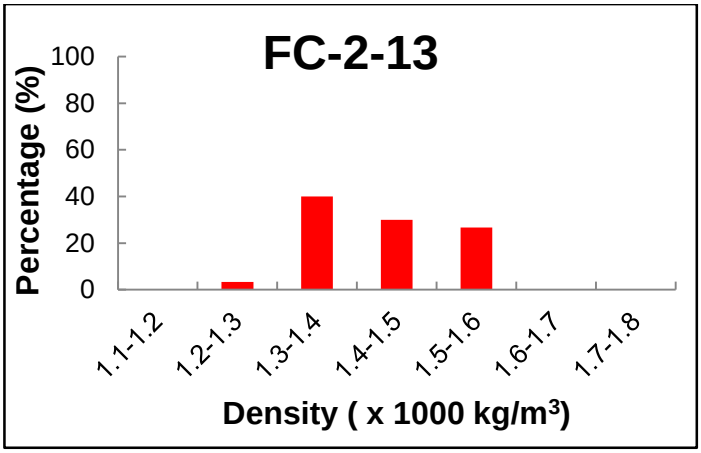

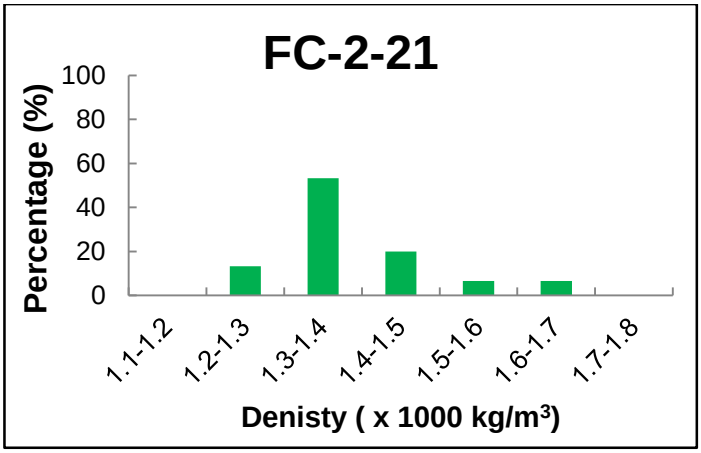

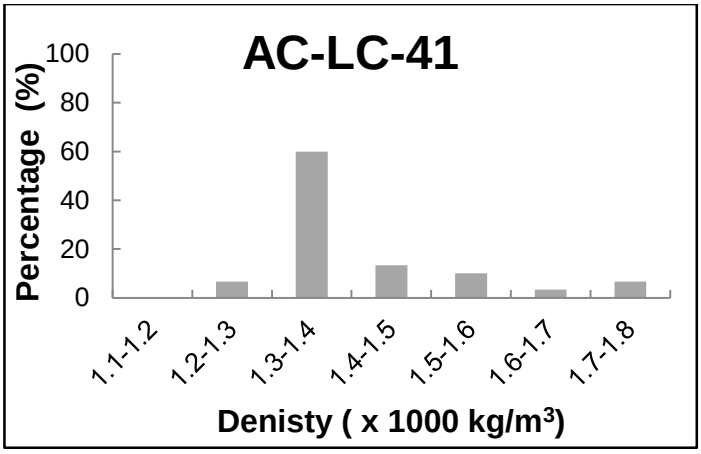

A.1.2 Char

Table A.1 Selected density cuts and average densities for the 6 mm char particles.

Char	Density range (kg/m^3)	Average density (kg/m^3)
BC-5-53	600 - 700	690
AC-5-72	500 - 600	518
FC-2-21	1000 - 1100	1110

From Table A.1 it is seen that density decreases with devolatilisation, with AC-5-72 having the lowest density. FC-2-21 has the highest density due to its high inertinite content, which forms dense chars during pyrolysis (Tang *et al.,* 2005). The density distribution curves are given below.

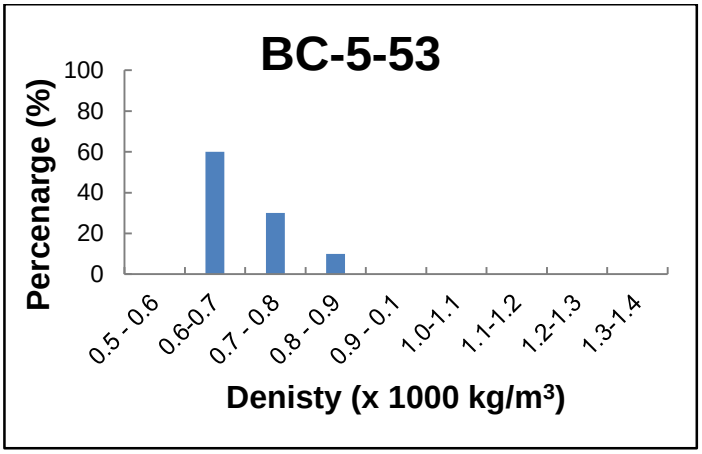

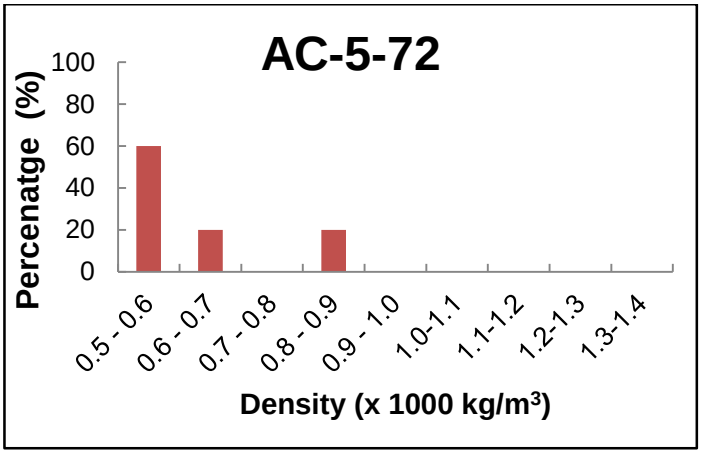

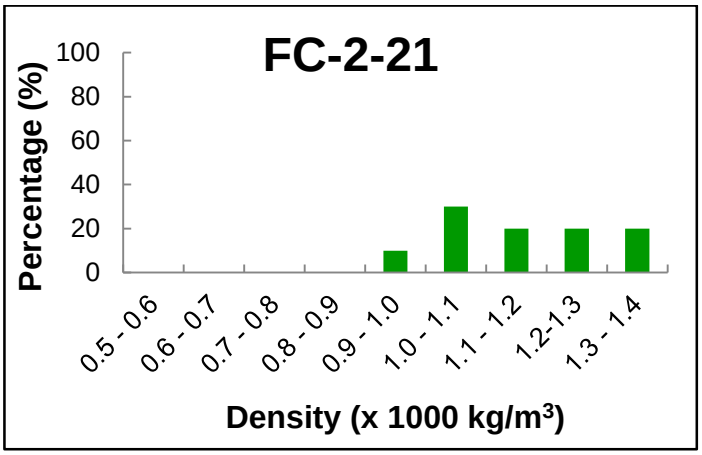

A.2 6 mm char characteristics

Table A.2: Proximate and calorific results for 6 mm char (a.d.b).

		BC-5-53	AC-5-72	FC-2-21
Parameter	**Unit**			
Proximate				
Inherent moisture	wt.%	0.9	1.1	0.3
Ash yield	wt.%	13.5	12.3	23.7
Volatile matter	wt.%	0.9	1.2	0.8
Fixed carbon	wt.%	84.7	85.4	75.2
Total	**wt.%**	**100.0**	**100.0**	**100.0**
Fuel ratio (FC/VM)	**-**	**89.5**	**73.7**	**92.8**
Gross calorific value	**MJ/kg**	**28.1**	**28.5**	**21.3**

Table A.3: Ultimate analysis results for 6 mm chars (d.a.f)

		BC-5-53	AC-5-72	FC-2-21
Parameter	**Unit**			
Carbon	wt.%	96.1	96.0	96.1
Hydrogen	wt.%	0.0	0.0	0.0
Nitrogen	wt.%	1.8	1.7	1.2
Oxygen	wt.%	1.6	1.8	2.1
Total sulphur	wt.%	0.5	0.5	0.6

Table A.4: CO_2 adsorption results for coal and chars derived from 6 mm particles

		BC-5-53		AC-5-72		FC-2-21	
		Coal	**Char**	**Coal**	**Char**	**Coal**	**Char**
Parameter	**Unit**						
Coal micropore surface area D-R	m^2/g	134	104	210	182	122	60
Carbon micropore surface area D-R	m^2/g	191	125	293	216	185	82
Monolayer capacity D-R	cm^3/g	29.3	22.7	45.9	39.7	26.7	13.2
BET surface area	m^2/g	88	69	128	114	80	44
Langmuir surface area	m^2/g	96	73	152	122	87	47
Micropore volume x 10^{-2} H-K	cm^3/g	3.02	2.30	3.95	3.96	2.77	1.34
Median pore width H-K	Å	4.0	4.0	3.9	3.9	3.9	4.2
Micropore porosity	%	2.4	1.1	3.0	1.5	2.3	1.1

A.3 Vitrinite reflectance histograms

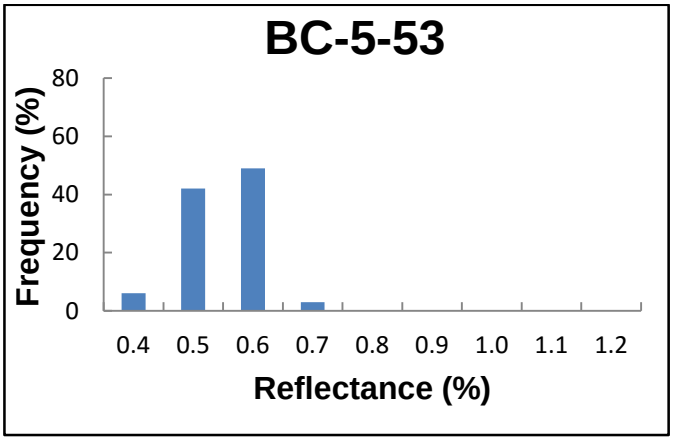

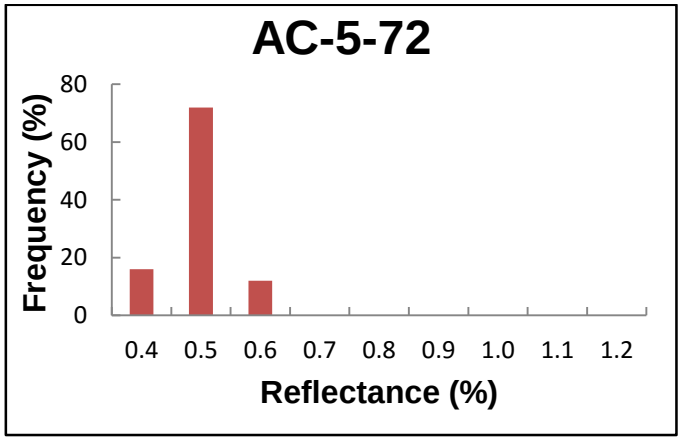

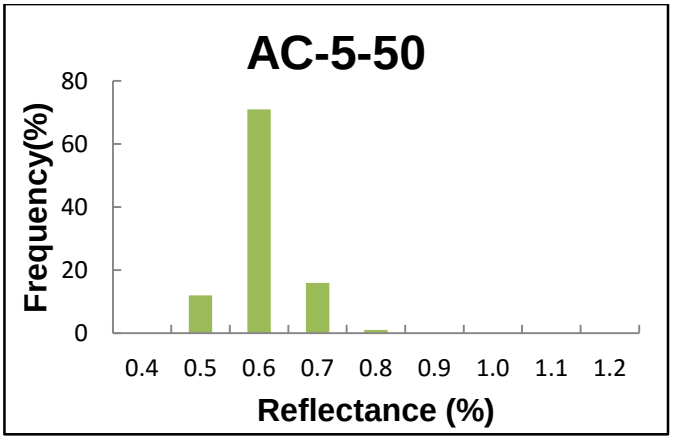
AC-5-50
Frequency(%)
80
60
40
20
0
0.4 0.5 0.6 0.7 0.8 0.9 1.0 1.1 1.2
Reflectance (%)

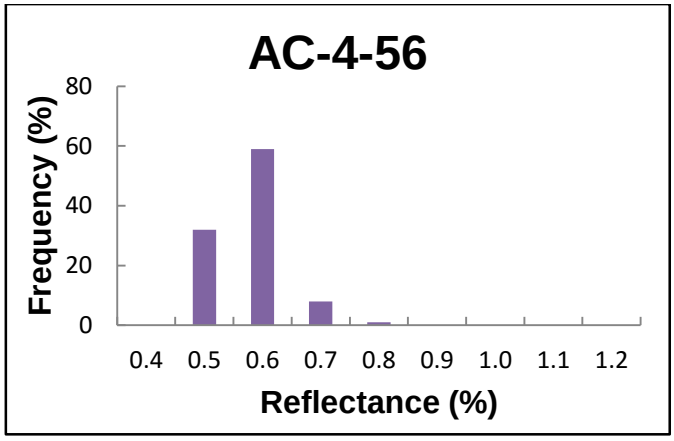
AC-4-56
Frequency (%)
80
60
40
20
0
0.4 0.5 0.6 0.7 0.8 0.9 1.0 1.1 1.2
Reflectance (%)

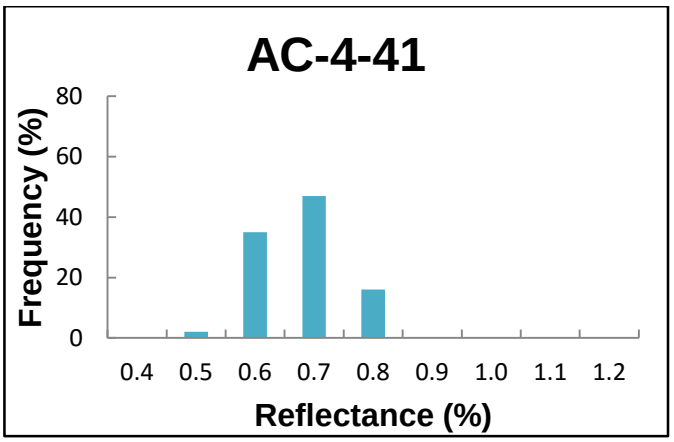
AC-4-41
Frequency (%)
80
60
40
20
0
0.4 0.5 0.6 0.7 0.8 0.9 1.0 1.1 1.2
Reflectance (%)

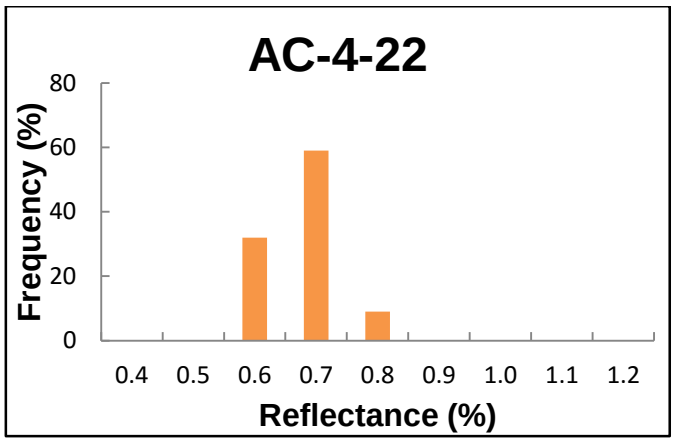
AC-4-22
Frequency (%)
80
60
40
20
0
0.4 0.5 0.6 0.7 0.8 0.9 1.0 1.1 1.2
Reflectance (%)

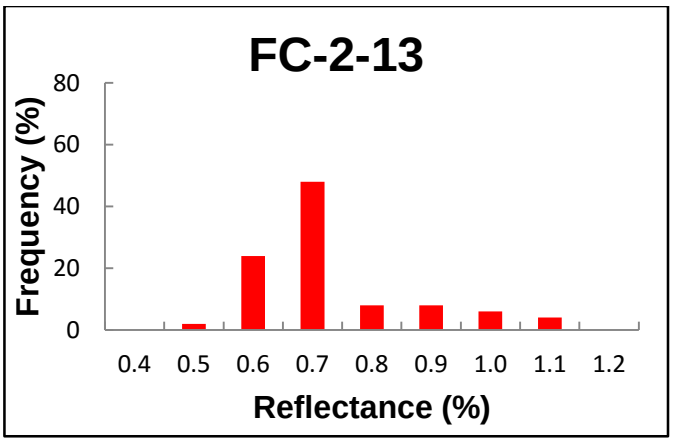
FC-2-13
Frequency (%)
80
60
40
20
0
0.4 0.5 0.6 0.7 0.8 0.9 1.0 1.1 1.2
Reflectance (%)

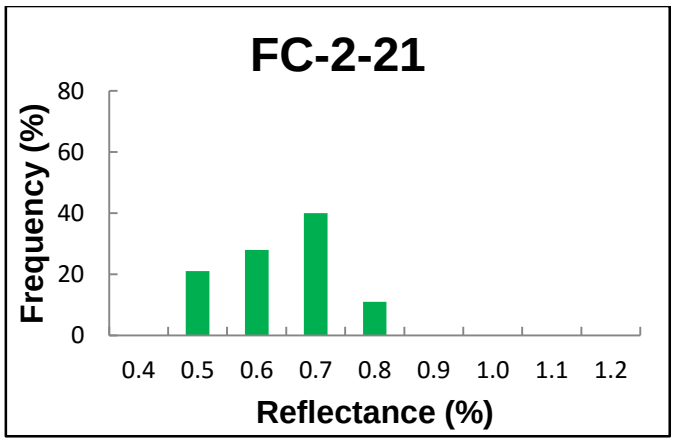
FC-2-21
Frequency (%)
80
60
40
20
0
0.4 0.5 0.6 0.7 0.8 0.9 1.0 1.1 1.2
Reflectance (%)

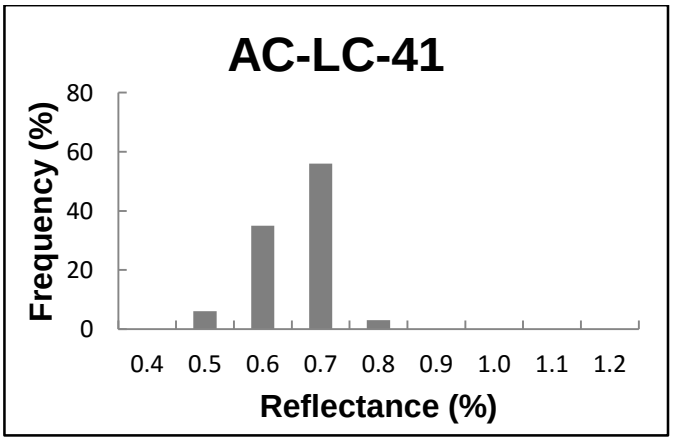
AC-LC-41
Frequency (%)
80
60
40
20
0
0.4 0.5 0.6 0.7 0.8 0.9 1.0 1.1 1.2
Reflectance (%)

A.4 Additional properties for statistical analysis

A.4.1 Coal properties

Table A.5: Additional coal properties for statistical analysis (a.d.b)

		BC-5-53	AC-5-72	AC-5-50	AC-4-56	AC-4-41	AC-4-22	FC-2-13	FC-2-21	AC-LC-41
Parameter	**Unit**									
Chemical										
Mineral matter	wt.%	14.3	11.2	15.8	15.1	18.2	28.1	17.9	21.4	21.0
PRN	-	7.0	4.8	7.5	8.8	10.1	6.6	9.0	9.0	12.7
Mineral										
Base-Acid ratio	-	0.13	0.13	0.09	0.30	0.77	0.17	0.04	0.04	0.14
Base-Acid ratio + phosphorus	wt.%	0.13	0.13	0.09	0.30	0.85	0.18	0.06	0.04	0.14
Bed agglomeration probability	-	5.30	2.25	1.00	2.58	52.00	0.02	1.25	1.87	0.25
Silica %	-	86.1	86.1	91.9	65.8	40.5	78.1	94.2	95.3	81.7
Slagging factor	wt.%	0.09	0.07	0.08	0.22	0.86	0.08	0.02	0.01	0.14
Fouling index	wt.%	0.02	0.02	0.02	0.04	0.03	0.09	0.00	0.01	0.01
Si_2O/Al_2O_3	-	2.7	2.8	3.5	1.2	1.2	1.2	1.6	1.4	1.6
Fe_2O_3/CaO	-	5.30	0.68	0.65	0.18	0.64	0.00	0.29	1.87	0.01
Fe_2O_3 + CaO	wt.%	1.2	0.8	0.7	2.1	5.3	2.7	0.5	0.4	1.7
Petrographic										
V/I	-	1.6	4.8	1.5	2.1	1.0	0.4	0.2	0.3	1.0
Thermal										
Slagging index – oxidising	°C	1521	1422	1452	1343	1334	1453	1550	1550	1397
Slagging index - reducing	°C	1550	1460	1492	1378	1328	1497	1550	1550	1507

A.4.2 Char properties

The mineral matter content of the char samples, is the only char property that was additionally added for the statistical analysis. The estimated mineral matter properties are given in Table A.6.

Table A.6: Additional char properties for statistical analysis (a.d.b)

Sample	Mineral matter (wt.%)	
	950 °C	1050 °C
BC-5-53	21.7	19.8
AC-5-72	24.8	21.3
AC-5-50	23.4	23.8
AC-4-56	22.9	26.2
AC-4-41	24.3	24.8
AC-4-22	36.8	37.6
FC-2-13	24.7	25.0
FC-2-21	24.2	25.1
AC-LC-41	31.5	32.5

A.5 Equations for derived properties

A.5.1 Chemical

The mineral matter content is derived using the Parr formula (Speight, 2005):

$$Mineral\ matter = 1.08\ Ash + 0.55\ Total\ Sulphur \quad \text{(A.1)}$$

PRN (Dakic *et al.,* 1989):

$$PRN = \frac{volatile\ content}{inherent\ moisture} \quad \text{(A.2)}$$

A.5.2 Mineral

Base – acid ratio (Coaltech, 2007):

$$\frac{CaO\ +\ K_2O + MgO +\ Na_2O +\ Fe_2O_3}{Al_2O_3 + SiO_2 + TiO_2} \quad \text{(A.3)}$$

Bed agglomeration probability (Gulyurtlu *et al.,* 2008):

$$\frac{Fe_2O_3}{K_2O +\ Na_2O} \quad \text{(A.4)}$$

Slagging factor (Coaltech, 2007):

$$\left(\frac{CaO\ +\ K_2O + MgO +\ Na_2O +\ Fe_2O_3}{Al_2O_3 + SiO_2 + TiO_2}\right) \times Total\ sulphur\ (d.b) \tag{A.5}$$

Silica % (Coaltech, 2007):

$$\frac{Si_2O\ \times 100}{Si_2O +\ Fe_2O_3 + CaO + MgO} \tag{A.6}$$

Fouling index (Coaltech, 2007):

$$\left(\frac{CaO\ +\ K_2O + MgO +\ Na_2O +\ Fe_2O_3}{Al_2O_3 + SiO_2 + TiO_2}\right) \times (K_2O +\ Na_2O) \tag{A.7}$$

A.5.3 Petrographic

Maceral index (Su *et al.,* 2001):

$$MI = (HVF)^{2.5}(RF) \tag{A.8}$$

With

$$RF = \frac{L + \frac{V}{RoV^2}}{I^{1.25}} \tag{A.9}$$

$$HVF = \frac{HV}{30} \tag{A.10}$$

Reactive maceral index (Helle *et al.,* 2003):

$$RMI = \frac{L + \frac{V}{RoV^2}}{Inr^{1.25}} \tag{A.11}$$

Petrofactor (Kizgut *et al.,* 2003):

$$\frac{Vitrinite\ reflectance}{Total\ reactives} \times 100 \tag{A.12}$$

A.5.4 Thermal

Slagging index (Coaltech, 2007):

$$\frac{(HT + 4\ \times IT)}{5} \tag{A.13}$$

A.6 XRD results

Table A.7: XRD results for minerals present in BC-5-53, including amorphous material

Parameter	Unit	Coal	Char (950 °C)	Ash (950 °C)	Ash (1050 °C)
Quartz	wt.%	4.5	8.3	42.7	43.3
Kaolinite	wt.%	7.2	0.5		
Illite	wt.%	0.1			
Microcline	wt.%	0.2			
Pyrrhotite	wt.%		0.2		
Dolomite	wt.%	0.3			
Anatase	wt.%	0.1	0.2		
Rutile	wt.%				0.2
Graphite 2H	wt.%	0.2	3.2		
Muscovite	wt.%	0.6			
Gypsum	wt.%		0.1		
Fluoroapatite	wt.%	0.2			
Anhydrite	wt.%		0.3	0.4	0.2
Lime	wt.%				0.1
Hematite	wt.%		0.1		
Anorthite	wt.%		2.8	0.8	1.6
Cristobalite	wt.%			0.1	0.3
Mullite	wt.%		0.2	16.1	24.7
Sillimanite	wt.%		0.3		
Periclase	wt.%		0.1	0.1	0.1
Portlandite	wt.%		0.1		
Diopside	wt.%			0.4	0.4
Total mineral matter	**wt.%**	**13.4**	**16.4**	**60.6**	**70.9**
Amorphous	**wt.%**	**86.6**	**83.6**	**39.4**	**29.1**
Total	**wt.%**	**100.0**	**100.0**	**100.0**	**100.0**

APPENDIX B: Experimental calibrations and results

B.1 Mass flow calibration curves

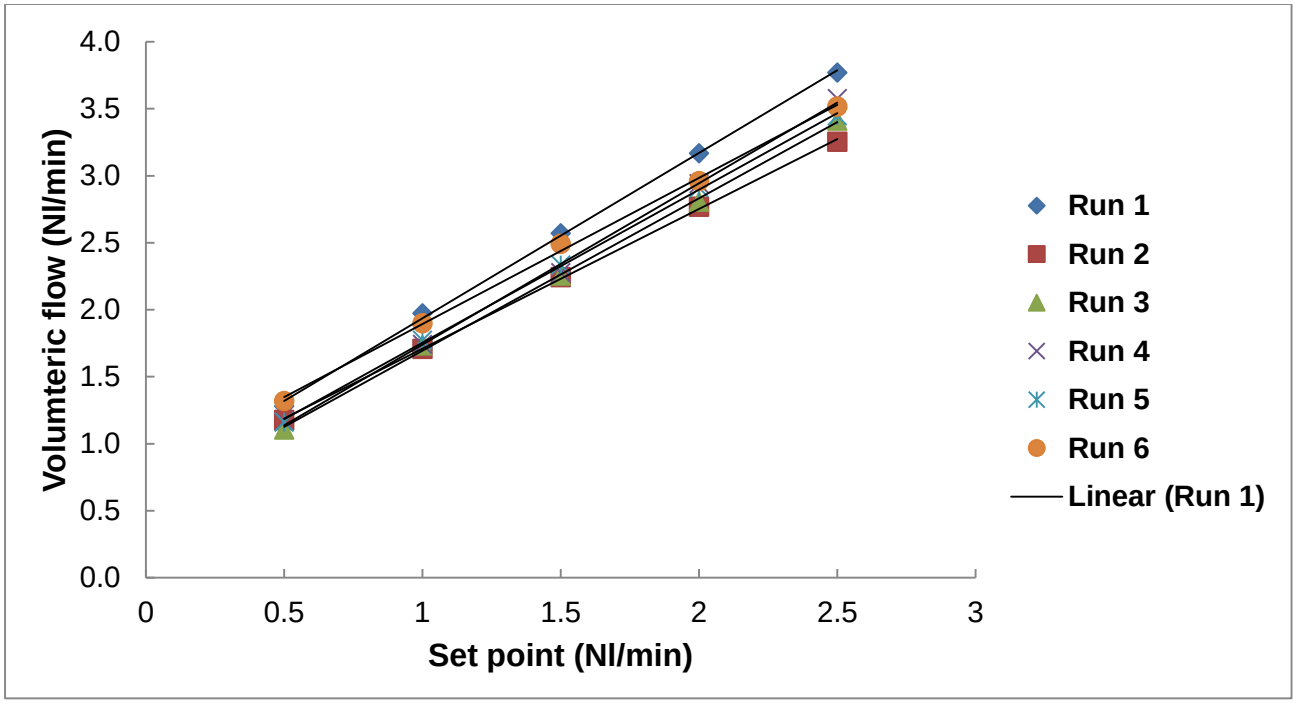

Figure B.1: Mass flow calibrations for nitrogen MFC

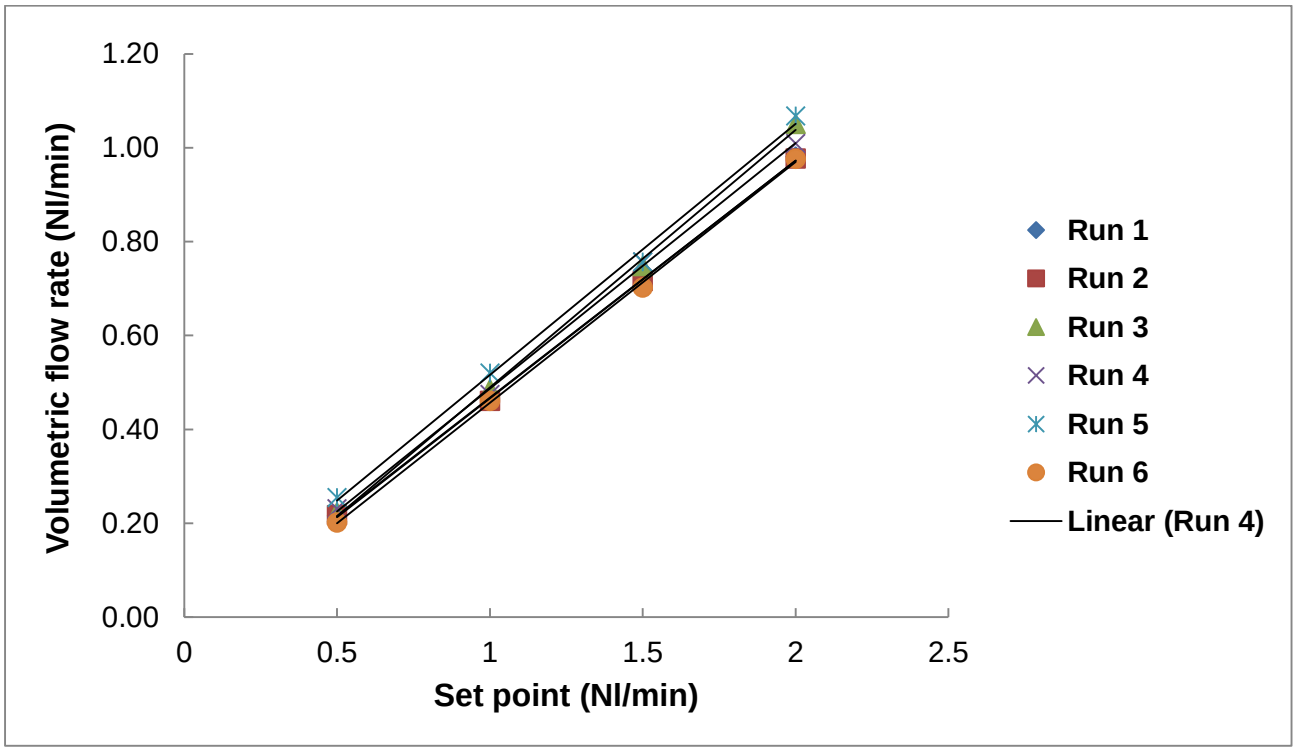

Figure B.2: Mass flow calibrations for carbon dioxide MFC

From Figure B.1 and B.2 it can be seen that there is a linear correlation between the set point and measured flow values and that the mass flow remained constant throughout the experiments, with the average error being 5.9% for the nitrogen and 5.2% for carbon dioxide. The calibration for the nitrogen rotameter used for the horizontal tube furnace is given in Figure B.3.

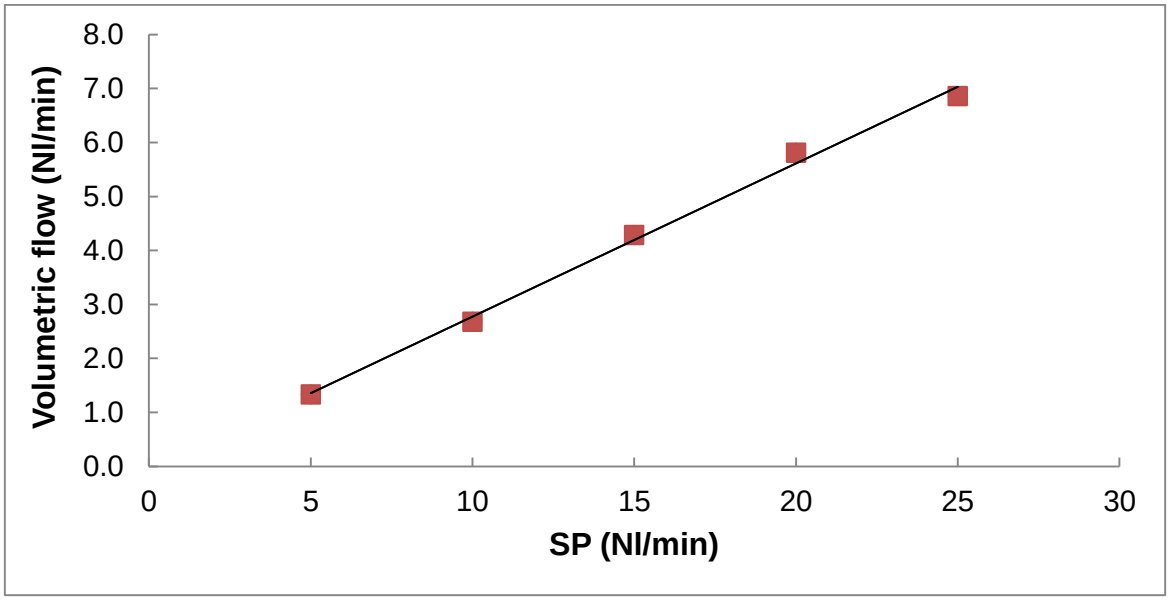

Figure B.3: Mass flow calibration for nitrogen rotameter

B.2 Temperature profiles

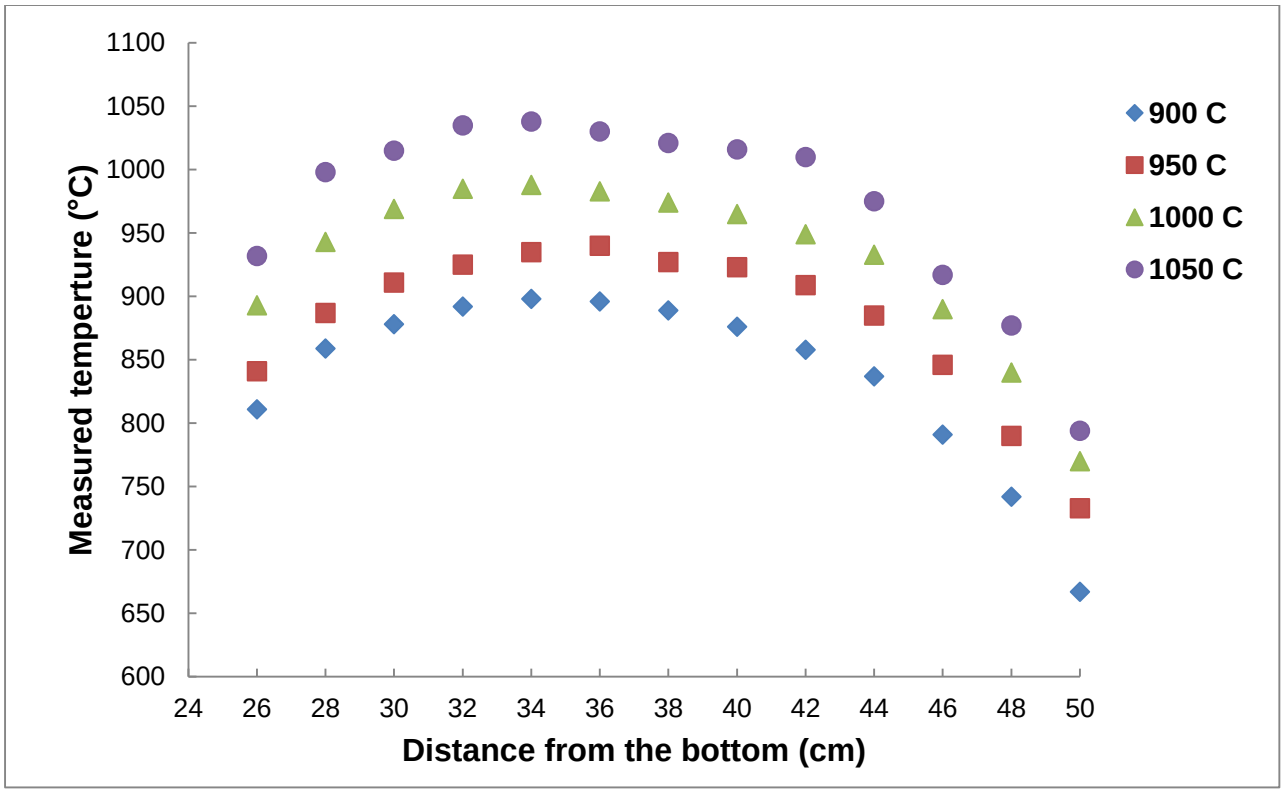

Figure B.4: TGA temperature profile with a nitrogen flow

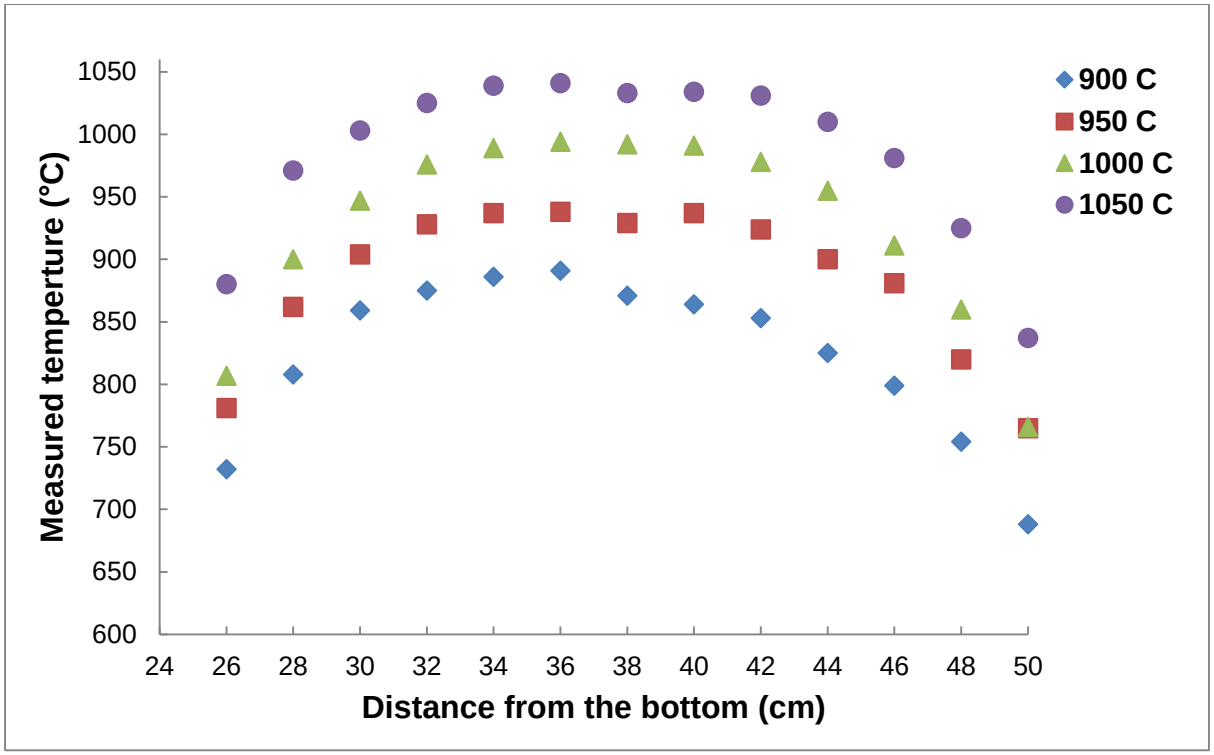

Figure B.5: TGA temperature profile with a nitrogen/carbon dioxide flow

From both Figure B.4 and B.5 it is seen that the heating zone is located 34 cm from the bottom of the tube furnace until ± 40 cm from the bottom. Additionally it is observed that there exists a difference of 10 °C between the measured temperature and the set point for both profiles.

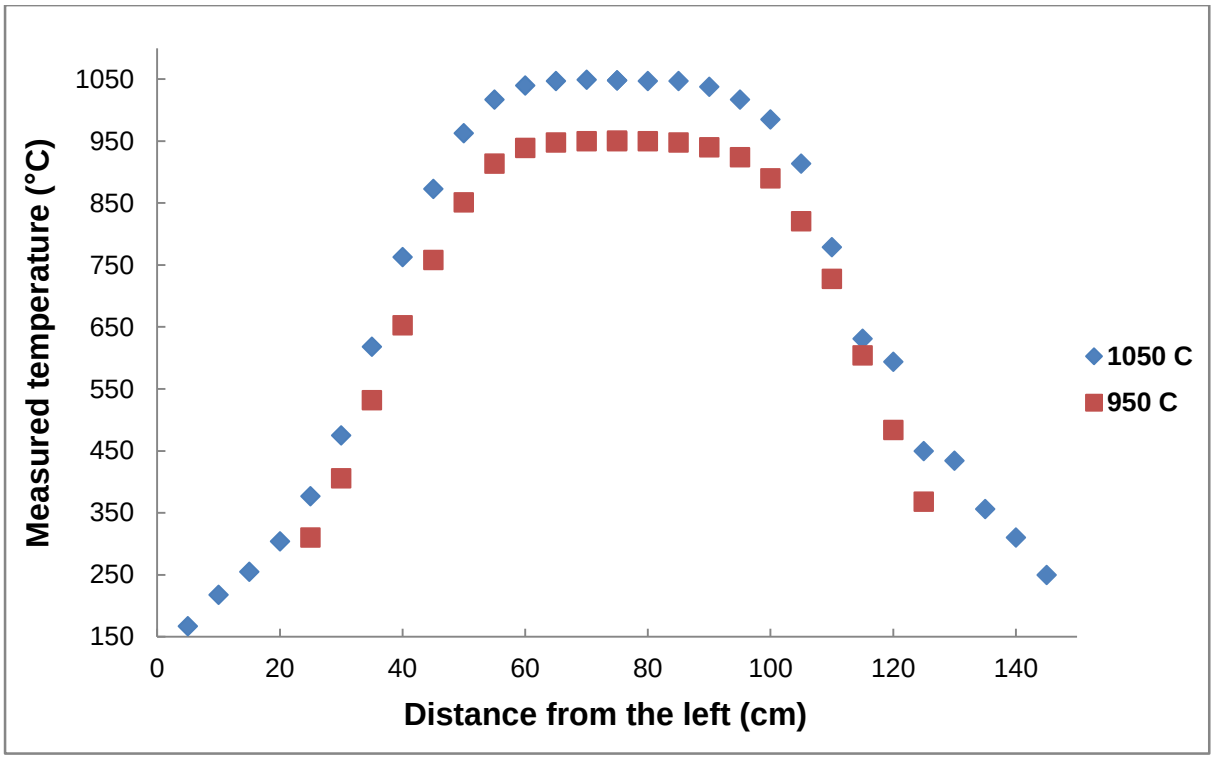

Figure B.6: Temperature profile of horizontal tube furnace without flow

The profile in Figure B.6 shows that the heating zone of the horizontal tube furnace is located 60 cm from the left side of the furnace and is stable for 30 cm. It is also seen that there is no temperature difference between the set point and measured temperature. The temperature profile was also determined for a nitrogen flow, but no difference was observed for the results.

B.3 Balance calibrations

Table B.1: Balance calibrations

Theoretical (g)	Measured (g)	Difference (%)
1.000	1.001	0.1
2.000	2.001	0.05
5.000	5.002	0.04
10.000	10.004	0.04
20.000	20.004	0.02
50.000	50.008	0.016
100.000	100.004	0.004
200.000	200.014	0.007

B.4 Sample holder

In Figure B.7 the sample holder configuration for the three different experiments are given.

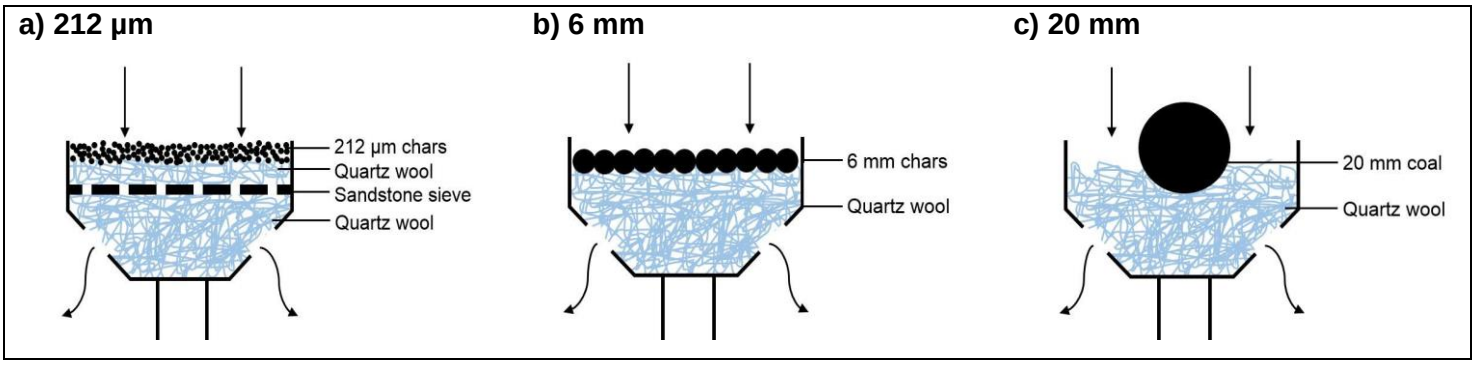

Figure B.7: Sample holder schematics

The first is for the pulverised chars and it can be seen that an additional sandstone sieve is added to, with 0.8 mm holes. A thin layer of quartz wool is then added on top of the sieve to prevent the particles from falling through the openings. The second picture represent sample holder of the 6 mm chars and it is seen that the particles are placed on top of the quartz wool in a single layer. The last schematic is that of 20 mm particles, were a single 20 mm coal particle is placed on top of the quartz wool. A burn profile test was also done, with the results showing a uniform conversion distribution in Figure B.8.

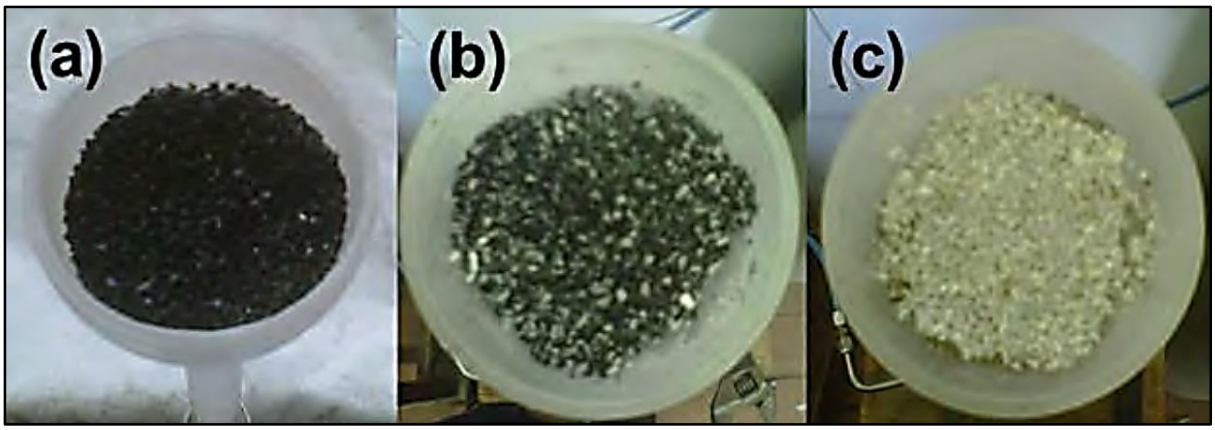

Figure B.8: Burn profile tests (Taken from Du Toit, 2013)

For Figure B.8 (a) is 0% conversion, (b) 50% conversion, (c) 100% conversion. For 50% conversion, it is seen that the sample is converted uniformly through the bucket.

B.5 Experimental error

The experimental error was first determined by estimating the average of the three different runs:

$$\bar{x} = \frac{1}{N}\sum_{i=1}^{N} x_i \tag{B.1}$$

Next the standard deviation was estimated:

$$\sigma = \sqrt{\frac{\sum_{i=1}^{N}(x_i - \bar{x})^2}{N-1}} \tag{B.2}$$

And the standard error (SE)

$$SE = \frac{\sigma}{\sqrt{N}} \tag{B.3}$$

The *t*-distribution value for a confidence level interval of 95%, was then determined. A confidence level of 95% was chosen as it is a reasonable compromise between the reliability and precision. A too high confidence level (99%) is reliable, but not very precise. A lower confidence level (90%) is precise, but not a reliable. A *t*-distribution had to be used, since the amount of data points were less than 30 (Devore & Farnum, 2005). The *t*-distribution was estimated as follow:

$$t = \frac{\overline{\bar{x} - \mu}}{\sigma/\sqrt{N}} \tag{B.4}$$

With μ being the mean value. The *t*-distribution value was 4.303 (degree of freedom = 2) for a 95% confidence level. The confidence level interval (CI) is as follow:

$$CI = \bar{x} \pm (SE \times t) \quad \text{(B.5)}$$

The experimental error was then as calculated:

$$Err\ (\%) = \frac{CI}{\bar{x}} \times 100 \quad \text{(B.6)}$$

The experimental errors of phase one and two are given in Table B.2 and B.3 respectively.

Table B.2: Experimental (%) error for phase one

Sample	950 °C	1050 °C	Average
BC-5-53	5	9	7
AC-5-72	7	6	6
AC-5-50	15	9	12
AC-4-56	19	4	11
AC-4-41	7	3	5
AC-4-22	21	18	19
FC-2-13	2	9	5
FC-2-21	13	15	14
AC-LC-41	2	5	3

Table B.3: Experimental error (%) for phase two

	BC-5-53		AC-5-72		FC-2-21	
	212 µm	**6 mm**	**212 µm**	**6 mm**	**212 µm**	**6 mm**
900 °C	10	14	8	6	7	17
950 °C	3	7	5	5	4	19
1000 °C	3	2	5	7	12	28
1050 °C	7	11	5	14	5	7
Average	**6**	**9**	**6**	**8**	**7**	**18**

APPENDIX C: Heat and mass transfer calculations

C.1 Heat transfer

C.1.1 Test isothermal conditions

In order to ensure that the coal samples were at isothermal conditions during the experiments, the criterion developed by Anderson (1963) was applied:

$$\frac{(r_A''')d_{coal}^2(\Delta H_r)}{4k_{coal}T} < 0.75\,\frac{T\,R}{E_a} \qquad \text{(C.1)}$$

The thermal conductivity (k_{coal}) is that of anthracite which is 0.26 W/m·K (Incropera *et al.,* 2007). Table C.1 and C.2 compares the calculated left- and right-hand sides for phase one and two.

Table C.1: Isothermal operation criteria for phase one at 1050 °C

Sample	Left	Right
BC-5-53	6.6×10^{-4}	42.0
AC-5-72	1.0×10^{-3}	68.0
AC-5-50	6.1×10^{-4}	102.4
AC-4-56	6.5×10^{-4}	92.4
AC-4-41	4.4×10^{-4}	82.6
AC-4-22	4.0×10^{-4}	346.8
FC-2-13	2.6×10^{-4}	63.5
FC-2-21	3.3×10^{-4}	53.0
AC-LC-41	4.7×10^{-4}	68.6

Table C.2: Isothermal operation criteria for phase two at 1050 °C

Sample	6 mm		212 µm	
	Left	Right	Left	Right
BC-5-53	1.1×10^{-4}	34.6	3.7×10^{-7}	36.4
AC-5-72	1.5×10^{-4}	38.3	4.1×10^{-7}	41.9
FC-2-21	7.7×10^{-5}	39.1	2.1×10^{-7}	47.4

From Table C.1 and C.2 it can be seen that for both phase one and two isothermal conditions existed for each sample.

C.1.2 Time to reach isothermal conditions

Although it was established that the samples were under isothermal conditions, the time for the particles to reach these conditions also needs to be considered. If the time necessary is in the same order than the total reaction time, the assumption of isothermal conditions is no longer valid. The time was estimated by utilising the approximate solution for transient conduction.

Initially the lumped capacitance method was used, however, the Biot numbers were greater than 0.1 indicating that assumption made regarding the negligibility of temperature gradients within the particle is invalid. The approximate solution was chosen as an alternative due to the fact that it considers the temperature distribution inside the particle as a function of particle geometry and time (Incropera *et al.,* 2007).

C.1.2.1 Assumptions

The following assumptions were made in order to determine the time of the particle to reach isothermal conditions:

- The particle has a spherical shape.
- The thermal properties used in the estimation are that of anthracite coal and remain constant.
- Radiation heat transfer from the furnace wall is negligible.
- Physical transformation during pyrolysis and gasification is not considered.
- Heat generation during pyrolysis and gasification is not considered.

C.1.2.2 Time estimation

The Biot number was firstly calculated in order to determine the one-term approximate coefficients C_1 and ξ_1 (Incropera *et al.,* 2007):

$$Bi = \frac{h\, r_{coal}}{k_{coal}} \tag{C.2}$$

h is the convection coefficient for heat transfer determined in Section C.1.2.3. Next the Fourier number was calculated as follow (Incropera *et al.,* 2007):

$$Fo = -\frac{1}{\xi_1^2}\ln\left(\frac{\theta_0^*}{C_1}\right) \tag{C.3}$$

With:

$$\theta_0^* = \frac{T - T_\infty}{T_i - T_\infty} \tag{C.4}$$

The Fourier number was greater than 0.2 for both phase one and two, indicating the validity of the approximate solution. Lastly the time to reach isothermal conditions was estimated (Incropera *et al.,* 2007):

$$t = Fo\frac{r_{coal}^2}{\alpha} \tag{C.5}$$

With the thermal diffusivity (α):

$$\alpha = \frac{k_{coal}}{\rho_{coal}\, c_{p,coal}} \tag{C.6}$$

The results are given in Table C.3 and C.4 .

Table C.3: Time to reach isothermal conditions for phase one at 1050 °C

Sample	Time (minutes)	Percentage of total time (%)
BC-5-53	47.6	13.0
AC-5-72	45.9	13.4
AC-5-50	47.6	11.5
AC-4-56	47.8	12.3
AC-4-41	47.8	5.3
AC-4-22	51.7	6.2
FC-2-13	48.7	3.2
FC-2-21	47.9	4.3
AC-LC-41	47.9	4.7

Table C.4: Time to reach isothermal conditions for phase two at 1050 °C

Sample	6 mm		212 µm	
	Time (minutes)	Percentage of total time (%)	Time (minutes)	Percentage of total time (%)
BC-5-53	2.6	0.4	0.022	0.015
AC-5-72	2.2	1.1	0.018	0.015
FC-2-21	4.2	0.5	0.035	0.008

It is important to note that the values given in Table C.3 and C.4 are only an approximate estimation of the time to reach isothermal conditions, as only transient conduction of the reagent gas is considered. Factors such as radiation from the furnace walls, heat generation during devolatilisation, swelling and fragmentation facilitates heating of the sample thereby reducing the time to reach isothermal conditions.

C.1.2.3 Convection coefficient

The convection coefficient for a single sphere was estimated as follow (Incropera *et al.,* 2007):

$$h = Nu_D \frac{k_{gas}}{d_{coal}} \tag{C.7}$$

The Nusselt number was estimated by utilising the correlation recommended by Whitaker (1972) for heat transfer in a sphere (Incropera *et al.,* 2007):

$$Nu_D = 2 + \left(0.4\, Re_D^{\frac{1}{2}} + 0.06 Re_D^{\frac{2}{3}}\right) Pr^{0.4} \left(\frac{\mu}{\mu_s}\right)^{\frac{1}{4}} \tag{C.8}$$

$$\begin{bmatrix} 0.71 \leq \mathrm{Pr} \leq 380 \\ 3.5 \leq Re_D \leq 7.6 \times 10^4 \\ 1.0 \leq \left(\frac{\mu}{\mu_s}\right) \leq 3.2 \end{bmatrix}$$

With the Prandlt number and Reynolds number calculated as follow (Incropera *et al.,* 2007):

$$\mathrm{Pr} = \frac{c_{p,gas}\,\mu}{k_{gas}} \tag{C.9}$$

$$Re_D = \frac{\dot{v}\, d_{coal}}{\mathrm{v}} \tag{C.10}$$

Normally the thermophysical property values such as the thermal conductivity, specific heat and dynamic viscosity can be retrieved from tables for pure gases; however, since the reagent gas is a mixture of 25 vol. % CO_2 and 75 vol. % N_2, the values must be estimated using various correlations and mixing rules. The calculated values were afterwards compared to Advanced System for Process Engineering (Aspen) generated properties, with the maximum difference being 2.4%.

The estimated convection coefficients were 16 and 41 W/m^{2}K for single 20 and 6 mm particles respectively.

The convection coefficient for a packed bed was estimated as follows (Incropera *et al.,* 2007):

$$h = St\, \rho_{gas} \dot{v}\, c_{p,gas} \tag{C.11}$$

The Stanton (*St*) number was estimated by utilising the modified Reynolds or Chilton-Cilburn analogies (Incropera *et al.,* 2007):

$$j_h = St\, Pr^{2/3} \tag{C.12}$$

$$[0.6 < \mathrm{Pr} < 60]$$

The Colburn *j*-factor for heat transfer of gases in a packed bed is calculated with the following correlation (Perry *et al*., 1997):

$$j_h = 0.91Re^{-0.51} \quad [0.01 < Re < 50] \tag{C.13}$$

The Prandlt number was determined with Equation C.12, while the Reynolds number for a packed bed is calculated as follows (Perry *et al*., 1997):

$$Re = \frac{\dot{v}\rho_{gas}d_{coal}}{6\mu(1-\varepsilon_v)} \tag{C.14}$$

The bed porosity was assumed to be 0.4 for both 6 mm and 212 µm packed bed (Dullien, 1979; Zhang *et al.,* 2006b). The estimated convection coefficients for the 6 mm and 212 µm packed beds were 43 and 167 W/m^{2}K respectively.

C.2 Mass transfer

C.2.1 Internal mass transfer

In order to determine if the pore resistance adversely affected the reactivity the Weisz-Prater criterion for an *n*-th order irreversible reaction was calculated (Figueiredo & Moulijn, 1986; Fogler, 2006):

$$M_w = L^2 \frac{\left(-\frac{r_A'''}{C_A}\right)_{obs}}{D_{eff}} \cdot \frac{n+1}{2} = L^2 \left(\frac{k'}{D_{eff}}\right) \cdot \frac{n+1}{2} \ll 1 \tag{C.15}$$

If the value of the Weisz-Prater criterion is less than one, the reactant fully infiltrates and bathes the entire surface. The particle is then in the diffusion free regime and the rate of pore diffusion can be neglected, thus the effectiveness factor can be assumed to be one (Fogler, 2006).

C.2.1.1 Assumptions

The following assumptions were made in order to estimate the internal resistance:

- The coal particle had a spherical shape and thus the characteristic length is calculated as follow:

$$L = \frac{r_{coal}}{3} \tag{C.16}$$

- The tortuosity of the coal particle was 1.414 (Eghlimi *et al.,* 1999; Kim *et al.,* 2014).

- The porosity calculated was that of the micropore surface area of the chars determined by CO_2 adsorption analysis.
- The average micropore diameter determined by the CO_2 gas adsorption analysis was used for the calculation purposes.
- The rate constants were taken as the initial specific reaction rate.
- The reaction order for 212 µm char CO_2 gasification was determined through regression of the Wen model.

C.2.1.2 Effective diffusion coefficient

Firstly the effective diffusion coefficient was estimated as follow (Eghlimi *et al.,* 1999; Huo *et al.,* 2014; Kim *et al.,* 2014; Johnsson & Jensen, 2000):

$$D_{eff} = \frac{\varepsilon}{\tau}\left[\frac{1}{D_{kn}} + \frac{1}{D_{AB}}\right]^{-1} \quad \text{(C.17)}$$

Where D_{kn} is the Knudsen diffusion coefficient (Huo *et al.,* 2014; Kim *et al.,* 2014):

$$D_{kn} = \frac{2}{3} r_{pore} \sqrt{\frac{8RT}{\pi\, M_{CO_2}}} \quad \text{(C.18)}$$

Where D_{AB} is the molecular diffusion coefficient, calculated by utilising the method described by Hirschfleder *et al.* (1949) which considers the influence of molecular forces (Kim *et al.,* 2014; Szekely *et al.,* 1976; Welty *et al.,* 2008):

$$D_{AB} = \frac{1.858 \times 10^{-27}\, T^{\frac{3}{2}}}{P\, \sigma_{AB}^2 \Omega_D}\left(\frac{1}{M_{CO_2}} + \frac{1}{M_{N_2}}\right)^{1/2} \quad \text{(C.19)}$$

Where σ_{AB}^2 is the collision diameter of the binary mixture and the Ω_D is the collision integral based on the Lennard-Jones potential. The Weisz-Prater of the phase two, 212 µm particles is given in Table C.5.

Table C.5: Weisz-Prater criteria for internal diffusion, phase two 212 µm chars

Sample	1050 °C	1000 °C	950 °C	900 °C
BC-5-53	1.2×10^{-2}	4.1×10^{-3}	3.0×10^{-3}	7.3×10^{-4}
AC-5-72	7.3×10^{-3}	5.0×10^{-3}	2.0×10^{-3}	9.2×10^{-4}
FC-2-21	9.3×10^{-3}	5.4×10^{-3}	3.1×10^{-3}	1.2×10^{-3}

From the above results it can be seen that the values are less than one for each sample at each temperature and therefore rate of internal mass transfer resistance is assumed to be negligible for phase two, 212 µm experiments from a theoretical standpoint.

C.2.2 External mass transfer

In order to determine if rate of external mass transfer is negligible the external effectiveness factor, which is the ratio of the partial pressure at the particle surface to the partial pressure of the ambient atmosphere, was estimated (Kim *et al.,* 2014):

$$\eta_{ex} = \frac{P_{CO_2,s}}{P_{CO_{2,}\infty}} \tag{C.20}$$

The partial pressure at the particle surface was estimated as follow (Fogler, 2006; Kim *et al.,* 2014):

$$P_{CO_{2,}s} = P_{CO_{2,}\infty} - \frac{q_{CO_2}}{h_m} \tag{C.21}$$

Where h_m is the mass transfer coefficient of CO_2 determined in Section C.2.2.1. The flux of CO_2 was calculated by performing a steady-state mole balance, with the results for a single particle (Fogler, 2006; Kim *et al.,* 2014):

$$q_{CO_2} = \frac{d_{coal}}{6} \rho_{coal} R_{s,0} \tag{C.22}$$

And for a packed bed:

$$q_{CO_2} = A_c a_c R_{s,0} \tag{C.23}$$

With:

$$a_c = \frac{6(1 - \varepsilon_v)}{d_{coal}} \tag{C.24}$$

The bed porosity was assumed to be 0.4 for both 6 mm and 212 µm. The results for phase one and two at 1050 °C are given in Table C.6 and C.7.

Table C.6: External effectiveness factor for phase one at 1050 °C

Sample	η_{ex}
BC-5-53	0.93
AC-5-72	0.90
AC-5-50	0.94
AC-4-56	0.93
AC-4-41	0.96
AC-4-22	0.96
FC-2-13	0.97
FC-2-21	0.97
AC-LC-41	0.95

Table C.7: External effectiveness factor for phase two at 1050 °C

Sample	η_{ex} – **6 mm**	η_{ex} – **212 µm**
BC-5-53	0.98	1.00
AC-5-72	0.98	1.00
FC-2-21	0.99	1.00

C.2.2.1 Mass transfer coefficient

The mass transfer coefficient was estimated analogous to the convection coefficient for both a single particle and a packed bed in Section C.1.2.3. The mass transfer coefficient for a single particle was determined as a function of the Sherwood number, molar diffusion coefficient and the diameter of the particle (Incropera *et al.,* 2007):

$$h_{m,CO_2} = Sh\frac{D_{AB}}{d_{coal}} \tag{C.25}$$

The Sherwood number for a single particle was estimated using the Frossling correlation (Fogler, 2006):

$$Sh = 2 + 0.6Re^{\frac{1}{2}}Sc^{\frac{1}{3}} \tag{C.26}$$

With:

$$Sc = \frac{\nu}{D_{AB}} \tag{C.27}$$

$$Re = \frac{\dot{v}\, d_{coal}}{\nu} \tag{C.28}$$

The molecular diffusion coefficient was calculated by utilising the method described by Hirschfleder *et al.* (1949) (Equation C.19). The mass transfer coefficient estimated for single 20 mm particle was 0.05 m/s.

The mass transfer coefficient for a packed bed was determined as follow (Incropera *et al.,* 2007):

$$h_{m,CO_2} = St_m\, V \tag{C.29}$$

The Stanton number for mass transfer was estimated through the use of the Chilton-Colburn analogy given below (Incropera *et al.,* 2007):

$$j_m = \ St_m Sc^{\frac{2}{3}} \qquad [0.6 < Sc < 3000] \tag{C.30}$$

The Schmidt number was determined using Equation C.27. The Colburn *j* – factor for the mass transfer inside a packed bed, assuming spherical particles, was estimated with the following correlation (Perry *et al*., 1997):

$$j_m = 0.91 Re^{-0.51} \qquad [0.01 < Re < 50] \tag{C.31}$$

The Reynolds number for a packed bed:

$$Re = \frac{\dot{v}\rho_{gas} d_{coal}}{6\mu(1-\varepsilon_v)} \tag{C.32}$$

The bed porosity was once more taken as 0.4 for both 6 mm and 212 µm. The estimated mass transfer coefficients for the 6 mm and 212 µm packed bed were 0.15 and 0.58 m/s respectively.

APPENDIX D: Statistical analysis

D.1 ANOVA

A two-way ANOVA was done to compare the mean differences between the two groups and to understand the interaction between the independent variables (temperature and coal) with the dependent variables (coal & char properties). Two-way ANOVA analysis was selected as two variables namely coal and temperature were investigated and the analysis was performed using SPSS. For the two-way ANOVA to be applicable the data must adhere to six assumptions made for this analysis. The first three assumptions are validity assumptions that cannot be tested using statistics, due to the fact that they relate to the manner in which the data was collected (Laerd Statistics, 2013b). The second group of assumptions are known as distributional assumptions made for parametric data and confirm the validity of the two-way ANOVA analysis (Field, 2009).

- Homogeneity of variance.
- Independence of variables – This assumption is related to the manner in which the data was generated and collected.
- Normally distributed data.

Levene's test for equality of Variances was performed in order to determine homogeneity of variance for each combination of the groups of the two independent variables. The results are given Table D.1.

Table D.1: Levene's Test of Equality of Error Variances

F-value	df1	df2	ρ
3.8	17	36	4.0×10^{-4}

From the results in Table D.1 it can be seen that the sigma-value (*p*) is less than .05 and therefore there are statistically significant differences between the coal and reactivity and temperature and reactivity. The null hypothesis of equal variance is therefore rejected with this analysis.

Tests Between-Subject Effects also investigates the homogeneity of the data, reports the main results of the two-way ANOVA analysis and indicates whether the independent variables or their interactions are statistically significant (Laerd Statistics, 2013b). The results are given in Table D.2.

Table D.2: Results of the Tests Between-Subjects Effects

Source	Type lll Sum of Squares	df	Mean square	F-value	ρ
Corrected model	.394*	17	.023	32	1.2×10^{-16}
Intercept	1.186	1	1.19	1623	1.5×10^{-31}
Coal	.176	8	.022	30	1.0×10^{-13}
Temperature	.171	1	.17	234	2.5×10^{-17}
Coal*Temp	.048	8	.006	8	3.2×10^{-6}
Error	.026	36	.001		
Total	1.607	54			
Corrected total	.421	53			

* R^2 = .937 (Adjusted R^2 = .908)

From the results in Table D.2 it can be seen F-value, which measures the systematic variation to the unsystematic variation, is greater than one for the coal, temperature and the interaction between the coal and temperature. This indicates that the experimental manipulations of these variables had an influence on the reactivity, with temperature having the greatest influence. The sigma-value (ρ) for both independent variables and their interaction is less than .05 and therefore the variables and the interaction of the variables have a statistically significant effect on reactivity. Therefore it can once again be concluded that the homogeneity of variance assumption is not valid.

The data was transformed using log-transformation in order to satisfy the homogeneity of variance assumption. The results of both the Levene's Test of Equality of Error Variances ($F(17, 36) = 2.4$, $p < .05$) and the Tests Between-Subjects Effect showed that there are statistically significant differences for the transformed data. Log transformation of the data was, therefore, not successful in increasing the homoscedasticity of the data.

Post hoc tests were also performed to report the simple main effects as reporting the main effects alone can be misleading. Only the effect of coal on reactivity is reported as this independent variable has more than two groups. The results are shown in Table D.3.

Table D.3: Results of Post hoc tests

Coal	N	Subset					
		1	2	3	4	5	6
FC-2-13	6	.069					
FC-2-21	6	.082	.082				
AC-4-41	6		.12	.12			
AC-LC-41	6		.13	.13			
AC-4-22	6			.14	.14		
BC-5-53	6			.16	.16	.16	
AC-5-50	6				.18	.18	
AC-4-56	6					.19	
AC-5-72	6						.27

* Turkey method was used

The results in Table D.3 indicate that coals that fall within the same subsets have similar reactivities. FC-2-13 and FC-2-21 fall within the same subset and therefore have similar reactivities, which corresponds with the results in Chapter 5 (Section 5.3). Similarly FC-2-21, AC-4-41 and AC-LC-41 also have similar reactivies and therefore they fall within the same subset.

The last analysis that was performed was the test of normality, which tests the assumption of normally distributed data. The results are given in a Q-Q plot in Figure D.1.

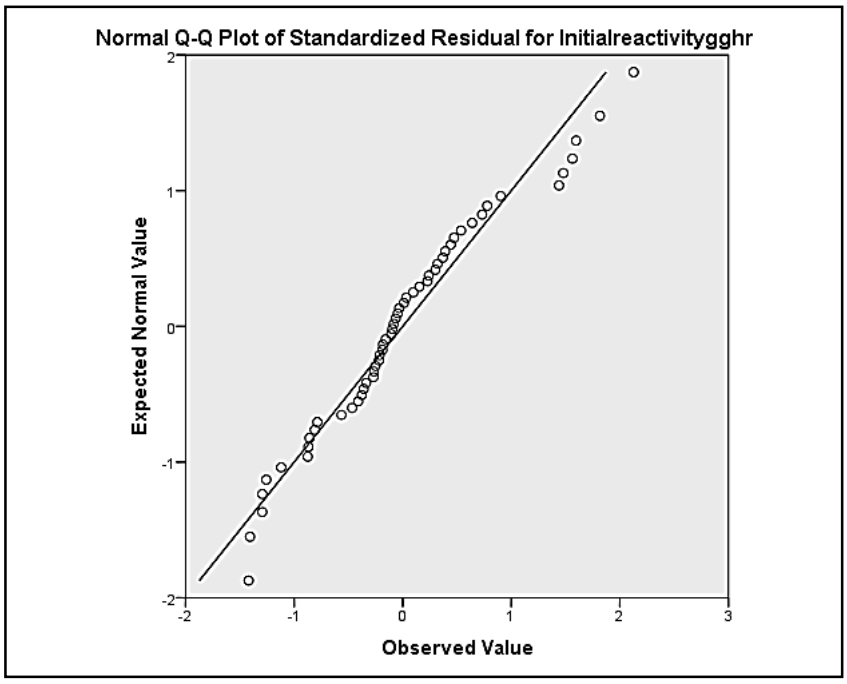

Figure D.1: Normal Q-Q Plot

From Figure D.1 it can be seen that most of the data points are located close to the diagonal line, with the exception of a few points. It can therefore be concluded that there exists a slight deviation from normality, but that overall the data is normally distributed. The assumption of normality for parametric data is therefore satisfied. The deviation from normal vs. the observed value is given in Figure D.2.

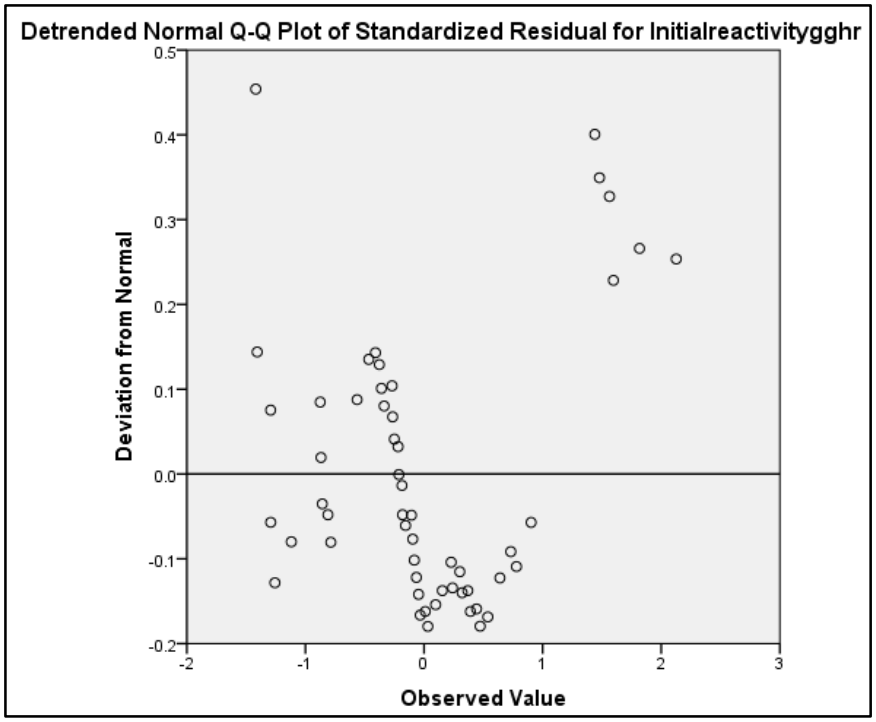

Figure D.2: Normal Q-Q Plot of standardised residual

The data is non-parametric in nature and for this reason Spearman's correlations coefficient was utilised to estimate the linear correlations between reactivity and coal/char properties.

D.2 Multiple linear regression

After the linear correlations were determined, multiple linear regressions were done to derive empirical equations from which the initial specific reaction rate could be determined. Before multiple linear regressions can be performed, certain assumptions must be satisfied. These assumptions are as follow (Laerd Statistics, 2013c):

- The dependent variables must be measured on a continuous scale.
- Must have two or more independent variables.
- Independence of observations (residuals)
- Linear relationships between the dependent and independent variables.
- Homoscedasticity.
- No too little multicollinearity.
- No significant outliers

- Residual (errors) must be approximately normally distributed.

Most of the assumptions are satisfied and also have been verified in Section D.1. For the third assumption, the Durbin-Watson statistic was ran for each empirical equation derived. If the values were close equal or close to two there exists no serial correlations. The results of the Durbin-Watson statistics are summarised in Table D.4.

Table D.4: Durbin-Watson statistics results

Equation description	Durbin-Watson statistics
Coal properties at 950°C	1.1 – 1.5
Coal properties at 1050°C	0.9 – 2.3
Char properties at 950°C	0.9
Char properties at 1050°C	1.3 – 1.9

From the results it is seen that the values fall between one and two, with a value of two indicting no serial correlation and therefore the independence of residuals assumption is verified.

Multicollinearity occurred between many of coal and char properties. Before regression, the correlation coefficients between the selected variables were estimated to ensure that there are no strong linear correlations between the selected variables. If a correlation coefficient greater than .70 existed between variables, the property with the smallest linear correlation coefficient with initial reaction rate was omitted and the regression was performed. Additionally the variance inflation factor (VIF) was also estimated for the different coefficients in order to quantify the extent of multicollinearity. The VIF of the estimated coefficient for all the reported empirical equations were below three, which indicates that multicollinearity is not a concern (Field, 2009).

Once the regression was performed, the equations were evaluated with regards to their coefficient of determination, F-values, significance values (p-values) of the entire equation as well as the individual coefficients. R^2, the F-values and *p*-values of the equations are reported in Section 5.7 and Appendix F. The significance values for all the determined equations as well as the individual coefficients were below .05 indicating that both the equation and individual coefficients have a statistically significant influence. The VIF was below three for all the determined coefficients.

APPENDIX E: Statistical correlations

E.1 Coal properties

Table E.1: Statistical parameters for chemical coal properties with CO_2 reactivity

Property	950°C		1050°C	
	r_s (two – tailed)	ρ	r_s (two – tailed)	ρ
Raw				
Oxygen content	.68	9.1×10^{-5}	.53	.004
Volatile matter	.55	.003	-	-
Inherent moisture	.54	.004	-	-
Hydrogen content	.53	.004	-	-
Nitrogen content	-	-	.65	2.7×10^{-4}
Pyrite	-	-	.60	.001
Gross calorific value	-	-	.59	.001
Organic sulphur	-	-	-.43	.024
Fixed carbon	-	-	-.51	.006
Derived				
Atomic O/C ratio	.67	1.2×10^{-4}	.54	.003
PRN	-.51	.007	-.52	.006

Table E.2: Statistical parameters for mineral properties with CO_2 reactivity

Property	950°C		1050°C	
	r_s (two – tailed)	ρ	r_s (two – tailed)	ρ
Mineral – coal properties				
Illite	.50	.008	-	-
Muscovite	.44	.023	-	-
Pyrite	-.44	.021	-	-
Goyazite	-	-	-.40	.041
Kaolinite	-	-	-.45	.018
Mineral – ash properties				
Hematite	.50	.009	-	-
Cristobalite	-.47	.014	-.49	.010
Anhydrite	-	-	-.41	.033
Lime	-	-	-.52	.006

Table E.3: Statistical parameters for ash properties with CO_2 reactivity

Property	950°C		1050°C	
	r_s (two – tailed)	ρ	r_s (two – tailed)	ρ
Raw				
MgO	.60	.001	-	-
CaO	.57	.002	-	-
SO_3	.54	.004	-	-
TiO_2	-.41	.034	-	-
Al_2O_3	-.42	.028	-	-
Cr_2O_3	-.53	.005	-.65	2.8×10^{-4}
Fe_2O_3	-	-	.45	.019
SiO_2	-	-	-.56	.003
P_2O_5	-	-	-.64	3.3×10^{-4}
Derived				
Fouling index	.61	.001	-	-
Base/ Acid ratio	.53	.005	-	-
Base/Acid ratio + phosphorus	.53	.005	-	-
Alkali index	.44	.022	-	-
Fe_2O_3 + CaO	.44	.023	-	-
SiO_2 percentage	-.44	.021	-	-
Si_2O/Al_2O_3	-	-	.45	.019

Table E.4: Statistical parameters for thermal coal properties with CO_2 reactivity

Property	950°C		1050°C	
	r_s (two – tailed)	ρ	r_s (two – tailed)	ρ
Raw				
FT - Reducing	-.45	.019	-	-
HT - Oxidising	-.47	.015	-	-
IT - Reducing	-.62	.001	-.48	.011
ST - Oxidising	-.62	.001	-	-
HT - Reducing	-.67	1.3×10^{-4}	-	-
ST - Reducing	-.69	7.5×10^{-5}	-.42	.027
IT - Oxidising	-	-	-.44	.024
Derived				
Slagging index - Reducing	-.58	.001	-.43	.027
Slagging index - Oxidising	-	-	-.44	.024

Table E.5: Statistical parameters for petrographic coal properties with CO_2 reactivity

Property	**950°C**		**1050°C**	
	r_s (two – tailed)	**ρ**	**r_s (two – tailed)**	**ρ**
Raw				
Vitrinite	.65	2.3×10^{-4}	-	-
Liptinite	.59	.001	-	-
Micrinite	.45	.019	-	-
Vitrinite reflectance	-.40	.039	-	-
Reactive Semi-fusinite	-.62	.001	-	-
Derived				
V/I	.64	3.0×10^{-4}	-	-
Reactive maceral index	.58	.002	-	-
Total reactives	.58	.002	-	-
Maceral index	.55	.003	-	-
Petrofactor	-.48	.010	-	-
Total inertinite	-.64	3.0×10^{-4}	-	-

Table E.6: Statistical parameters for structural coal properties with CO_2 reactivity

Property	**950°C**		**1050°C**	
	r_s (two – tailed)	**ρ**	**r_s (two – tailed)**	**ρ**
Raw				
Micropore volume (H-K)	.58	.002	-	-
Median pore width (H-K)	-	-	.53	.005
Derived				
Carbon surface area (D-R)	-	-	-.52	.006

E.2 Char properties

Table E.7: Statistical parameters for chemical char properties with CO_2 reactivity

Property	**950°C**		**1050°C**	
	r_s **(two – tailed)**	ρ	r_s **(two – tailed)**	ρ
Raw				
Nitrogen content	.55	.003	-	-
Gross calorific value	-	-	.62	.001
Carbon content	-	-	.58	.002
Fixed carbon	-	-	.49	.009
Ash value	-	-	-.51	.006
Derived				
Mineral matter	-	-	-.49	.009

Table E.8: Statistical parameters for raw mineral char properties with CO_2 reactivity

Property	**950°C**		**1050°C**	
	r_s **(two – tailed)**	ρ	r_s **(two – tailed)**	ρ
Gypsum	.50	.009	-	-
Pyrrhotite	.49	.009	-	-
Cristobalite	.44	.022	-	-
Microcline	-.46	-.015	-	-

Table E.9: Statistical parameters for structural char properties with CO_2 reactivity

Property	**950°C**		**1050°C**	
	r_s **(two – tailed)**	ρ	r_s **(two – tailed)**	ρ
Raw				
Micropore surface area (D-R)	.62	.001	-	-
Monolayer capacity (D-R)	.62	.001	-	-
Limiting micropore volume (D-R)	.62	.001	-	-
Median pore width (H-K)	-.50	.008	-.69	5.9×10^{-5}
Derived				
Carbon surface area (D-R)	.56	.002	-	-

APPENDIX F: Additional empirical equations

F.1 Coal properties

F.1.1 950 °C

Table F.1: Empirical equations for coal properties at 950 °C

Equation	R^2	F-value	ρ
$R_{s,0-950℃} = -0.009\ Fixed\ carbon + 0.56$	045	21	.000
$R_{s,0-950℃} = 0.11\ Micropore\ porosity - 0.002\ Inert\ semi - fusinite - 0.18$	0.44	9	.001
$R_{s,0-950℃} = -0.002\ Total\ inertinite + 0.17$	0.43	19	.000
$R_{s,0-950℃} = -0.002\ Inert\ semi - fusinite + 0.14$	0.33	13	.002

F.1.2 1050 °C

Table F.2: Empirical equations with for coal properties at 1050 °C (R^2 = 0.9)

Equation	R^2	F-value	ρ
$R_{s,0-1050℃} = 0.01\ Volatile\ matter + 0.034\ Inherent\ moisture - 0.21$	0.90	105	< .05
$R_{s,0-1050℃} = 0.58\ Atomic\ H/C\ ratio + 0.02\ MI - 0.27$	0.90	105	< .05
$R_{s,0-1050℃} = 0.032\ Inherent\ moisture - 0.088\ Fuel\ ratio - 0.004\ Ash\ yield + 0.30$	0.90	65	< .05

F.2 Char properties

F.2.1 950 °C

Table F.3: Empirical equations for char properties at 950 °C

Equation	R^2	F-value	ρ
$R_{s,0-950℃} = 0.001\ BET\ surface\ area - 0.047$	0.39	16	< .05
$R_{s,0-950℃} = 2.49\ Micropore\ volume - 0.042$	0.38	16	< .05

F.2.2 1050 °C

Table F.4: Empirical equations for char properties at 1050 °C

Equation	R^2	F-value	ρ
$R_{s,0\ -1050℃} = 0.28\ Nitrogen + 0.003\ Micropore\ surface\ area - 0.27$	0.81	53	< .05
$R_{s,0\ -1050℃} = 0.005\ Micropore\ surface\ area - 0.06$	0.68	53	< .05
$R_{s,0-1050℃} = 0.004\ CSA - 0.10$	0.67	51	< .05
$R_{s,0-1050℃} = 0.48\ Nitrogen - 0.31$	0.65	47	< .05

APPENDIX G: Conversion curves – Phase one

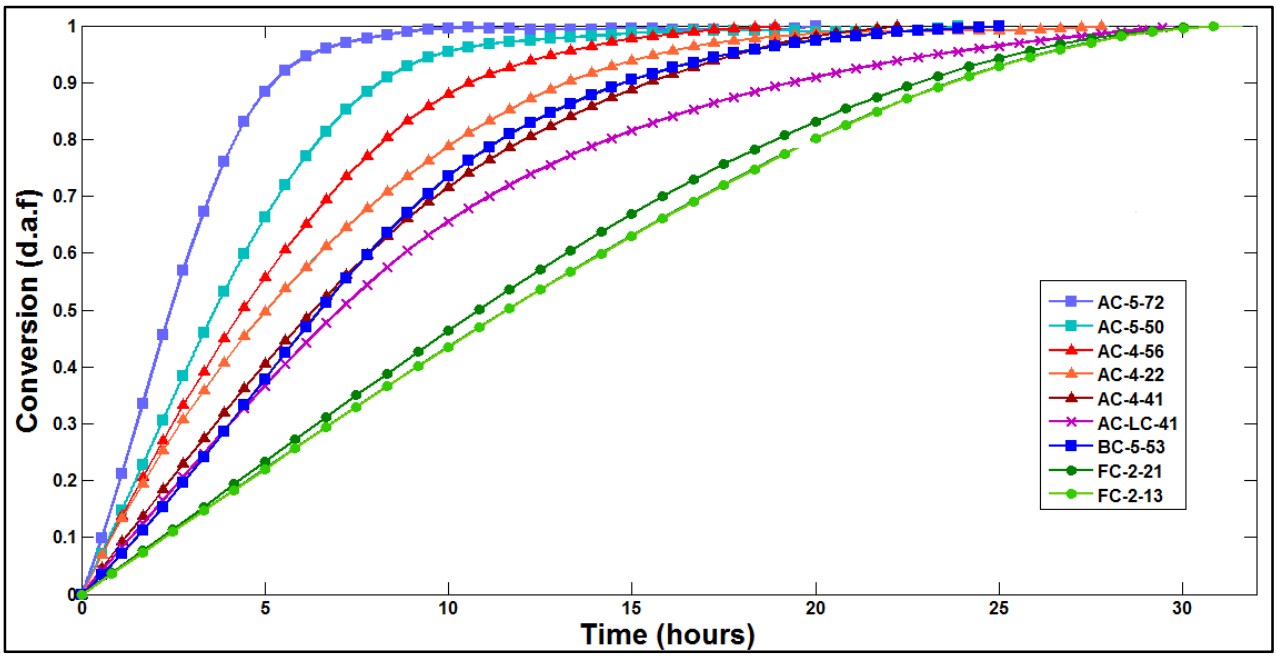

Figure G.1: Conversion curves at 950 °C

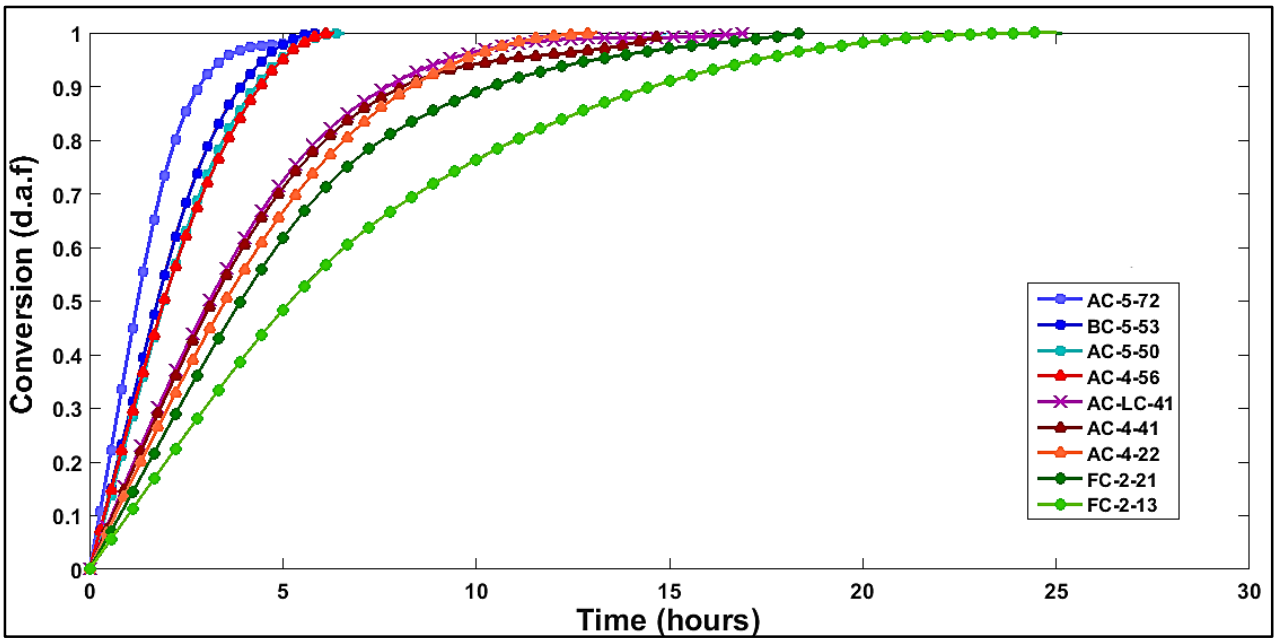

Figure G.2: Conversion curves at 1050 °C

APPENIDX H: Arrhenius plots

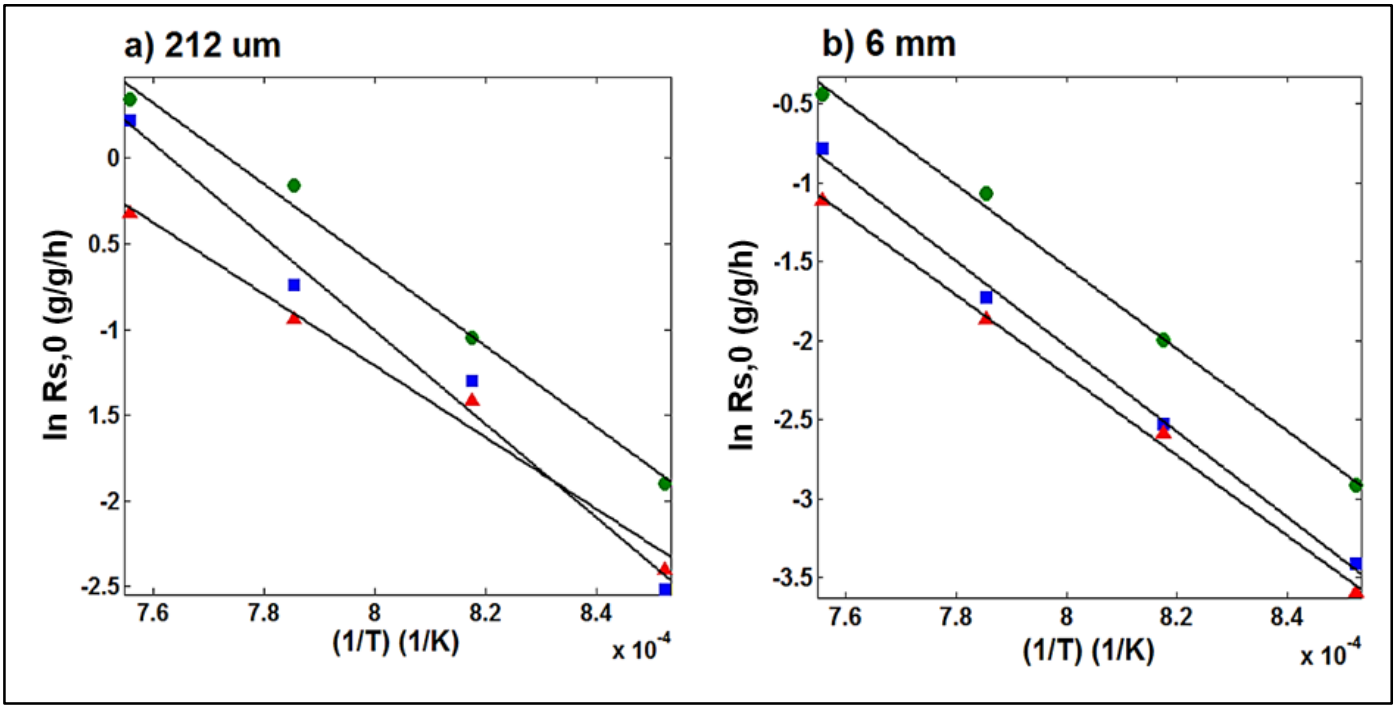

Figure H.1: Arrhenius plot for three coals at two particles sizes for experimental data (■ BC-5-53; ● AC-5-72; ▲FC-2-21; - Fit)

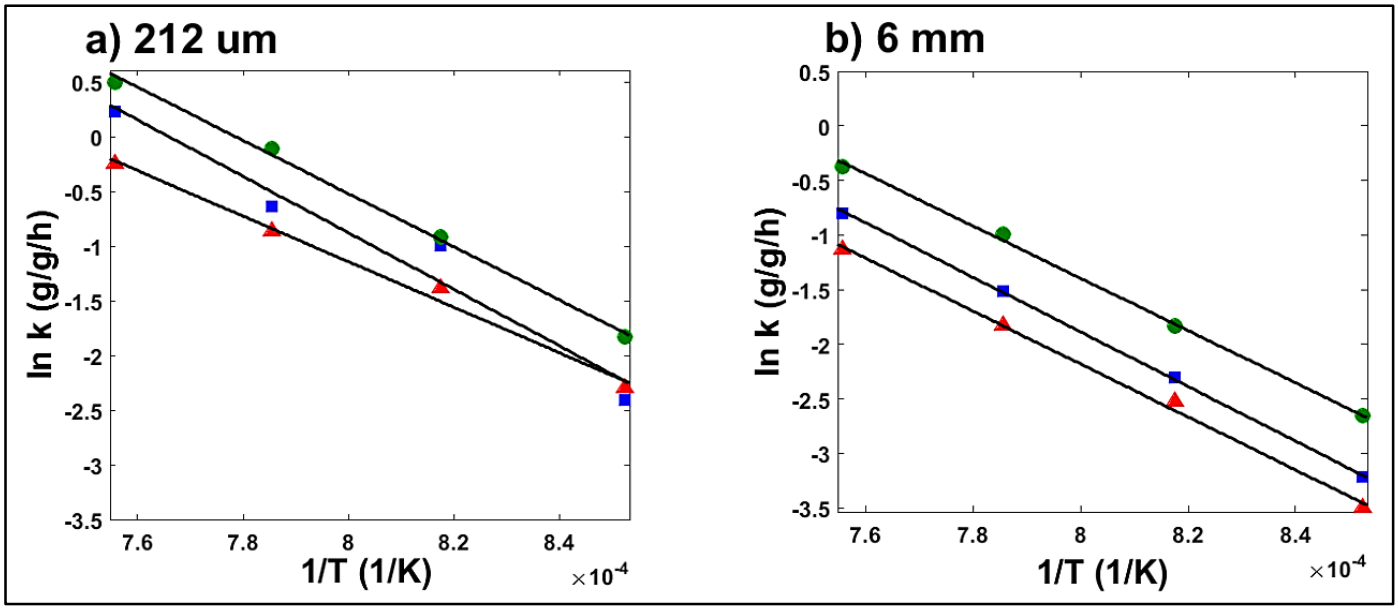

Figure H.2: Arrhenius plot for three coals at two particles sizes for model estimated data (■ BC-5-53; ● AC-5-72; ▲FC-2-21; - Fit)